Characterizing multiple roles of *pannier* during embryogenesis, as revealed with an augmented fluorescent live imaging toolkit, in the beetle *Tribolium castaneum*

Inaugural-Dissertation

zur

Erlangung des Doktorgrades

der Mathematisch-Naturwissenschaftlichen Fakultät

der Universität zu Köln

vorgelegt von

Jan Seibert

aus Speyer

Köln, 2017

Berichterstatter/in: **Dr. Kristen Panfilio**

Prof. Dr. Siegfried Roth

Tag der mündlichen Prüfung: 18.01.2017

Für Karolina

Contents

List of Tables

List of Figures

Abstract

Embryogenesis in the beetle *Tribolium castaneum* relies on the morphogenetic movements of the two extraembryonic membranes, amnion and serosa. It is due to their function and concerted development that the embryo is able to survive and hatch as a self-dependent organism. Remarkably, these extraembryonic tissues do not even contribute to the final form of the embryo. During formation of both membranes, their movements include tissue expansion, as well as intra-tissue fusion and inter-tissue separation. Thus, the amnion covers the embryo at its ventral and lateral sides, forming the amniotic cavity, while the serosa encloses the embryo and the amnion. Besides from serving as a yolk cover, the serosa provides the embryo with desiccation resistance and contributes to the innate immune response. In late development, the coordinated withdrawal and subsequent degeneration of both membranes facilitates embryonic dorsal closure, during which the amnion replaces the serosa as a transient yolk cover. In serosa-deficient embryos, the amnion adopts the serosa's function as an early yolk cover, enabling the embryo to hatch in a wild type manner.

To learn more about this highly adaptable tissue, the transcription factor *Tc pannier* (*Tc-pnr*), known to be expressed in the amnion at the very onset of blastoderm differentiation, was investigated. The wild type expression pattern of *Tc-pnr* was determined via *in situ* hybridization and the observed defects after parental RNA interference were analyzed. *Tc-pnr* deficient embryos display a pronounced hole in the dorsal cuticle and a characteristic bending of the abdomen and the head towards the dorsal side. This specific phenotype is the result of a defect during dorsal closure, when *Tc-pnr* is expressed in the cells of the dorsal most ectoderm and in the head. In *Drosophila melanogaster*, the dorsal hole is due to a loss of *Dm decapentaplegic* (*Dm-dpp*) expression in the dorsal most cells of the ectoderm. It could be shown that in *Tribolium*, *Tc-pnr* and *Tc-dpp* are co-expressed in corresponding cells of the dorsal ectoderm as well and that *Tc-pnr* regulates *Tc-dpp*

expression. This suggests that *Tc-pnr* has an essential function in dorsal closure and that its involvement is conserved in *Tribolium* and *Drosophila*. Conserved to *Drosophila* is also the involvement of *Tc-pnr* in *Tribolium* heart formation. Loss of *Tc-pnr* expression in the cardioblast cell row impairs its formation and negatively affects the expression of the heart marker gene *Tc midline* (*Tc-mid*). After loss of *Tc-pnr* expression in the amnion, where it was shown to be expressed at least until mid embryogenesis, the amnion displays various defects around the process of dorsal closure. Intriguingly, the amnion ruptures ectopically and withdraws independent from the serosa. This is in contradiction to a recent report that both membranes demonstrate bilayer adhesion during dorsal closure. Thus, it is assumed that *Tc-pnr* facilitates this adhesion, and that the adhesion is lost in the knock down. To investigate the disturbed interplay between the serosa and the amnion, an existing enhancer trap line expressing EGFP in the amnion was modified, by using a combination of CRISPR/Cas9 and homology directed repair, to express DsRed2 instead. The DsRed2 expressing amnion line can now be crossed to another line expressing EGFP in the serosa, to enable distinct visualization of both tissues and to finish the analysis on the ectopic amniotic rupture.

Concluding, the results indicate that *Tc-pnr* effects embryonic and extraembryonic development in diverse ways around the time of dorsal closure. As dorsal closure in *Tribolium* is a three-tissue system (amnion, serosa and embryo), investigation of the distinct regulatory effects of *Tc-pnr*, will promote the understanding of the concerted development of the two extraembryonic membranes and the embryo.

Chapter 1

Introduction

1.1 The new insect model organism *Tribolium castaneum*

With more than one million documented species, insects exhibit remarkable diversity and an outstanding species abundance in history [Engel, 2015]. 83% are holometabolous insects (insects with a complete metamorphosis), which are all winged insects (Pterygota). Within the Holometabola, 12% belong to the Diptera and 38% to the Coleoptera, the most diverse order [Engel, 2015]. The insect model species *Drosophila melanogaster* is a member of the former one, while the red flour beetle *Tribolium castaneum* belongs to the latter order. Besides from being a member of the most species rich insect order, *Tribolium* undergoes short germband development, which is within the Holometabola only seen in beetles [Roth and Hartenstein, 2008] and likewise observed in most arthropods [Schröder et al., 2008]. In short germ insects, only the most anterior head anlagen and the thorax are formed, while the rest emerges subsequently from a segment addition zone [Nakamoto et al., 2015]. This is in difference to the long germband development of *Drosophila*, in which all body segments are formed almost simultaneously at the blastoderm stage [Lynch et al., 2012]. The mechanism seen in *Tribolium* is considered to be the more ancestral one, similar to vertebrate embryogenesis [Schröder et al., 2008]. However, most important for the present study is that *Tribolium* has two distinct extraembryonic membranes, amnion and serosa. These are retained in most insects and in contrast to the reduced single complement in *Drosophila*, the amnioserosa [Panfilio, 2008]. The amnion and the serosa can also serve as models for epithelia movements in general. This would fit with *Tribolium's* already established role as a model for head development and DV/AP

axis-patterning, leading away from the *Drosophila* centric research in insects.

That *Tribolium* has developed into the new insect model organism next to *Drosophila* over the last two decades, would not have been possible without its published genome [Richards et al., 2008] and the by now exceeding toolkit. Transgenesis is well established [Berghammer et al., 1999b] and just recently extended by the new genome editing tool clustered regularly interspaced short palindromic repeats/CRISPR associated protein 9 (CRISPR/Cas9) [Gilles et al., 2015]. For manipulation of gene function, parental RNA interference (pRNAi) is the technique of choice, which works systemic in *Tribolium* [Bucher et al., 2002]. A genome-wide insertional mutagenesis and enhancer trapping screen contributed to the imaging possibilities, by yielding over 500 lines with new enhancer trap patterns [Trauner et al., 2009], as well as the development of a line expressing GFP in all nuclei [Sarrazin et al., 2012] and the development of a transient fluorescent labeling method [Benton et al., 2013]. Several of the enhancer trap lines, mostly showing enhanced green fluorescent protein (EGFP) expression in the amnion or the serosa, were already characterized by our group [Koelzer et al., 2014; Hilbrant et al., 2016]. How these two membranes develop and morphologically change throughout embryogenesis, will be discussed in the next section.

1.2 Embryonic and extraembryonic development in *Tribolium castaneum* and *Drosophila melanogaster*

In the last section, the difference between the two modes of germband development in *Drosophila* and *Tribolium* has been described. Besides this, basic embryonic movements are quite similar in both species (see Figure 1.1). Both undergo germband extension, in which the abdomen of the embryo extends over the posterior pole towards the dorsal side (Figure 1.1A2 and B3). Subsequently, germband retraction is initiated, when the extension of the germband has reached its maximum. During this period of development, the embryo shortens in anterior-posterior (AP) direction and thickens laterally in dorso-ventral (DV) direction. When the embryo has fully retracted (Figure 1.1B4), again having the same length as the egg in AP direction, dorsal closure starts (Figure 1.1A3 and B6). By extension of the flanks towards the dorsal side, the opening in the dorsal epidermis is closed and the embryo is ready to eclose after a while. Until then, the dorsal opening has been covered by the amnioserosa in *Drosophila*. Whereas the amnioserosa of *Drosophila* is

only covering the embryo's dorsal side from the late blastoderm on (Figure 1.1A1), until it has been replaced by the dorsal ectoderm during dorsal closure, development of the two extraembryonic membranes in *Tribolium* is much more sophisticated.

Starting with differentiation of the blastoderm, cell fates are determined in *Tribolium* (Figure 1.1B1). Cells in an oblique anterior-dorsal region will give rise to the serosa and the remaining cells in the larger ventral-posterior area of the egg, to the germ rudiment. The latter one is subdivided into cells giving rise to the amnion and into cells forming the embryo proper. Thereby, the presumptive amniotic cells are located in the anterior amniotic fold, which marks the border between serosa and embryo, as well as in a dorsal area extending into the posterior pole. Around the same time when this differentiation occurs, easily detectable by the larger and wider spaced nuclei of the serosa, cells at the posterior pole flatten before they are shifted into the yolk, forming the primitive pit. Subsequently, a fold is forming at the posterior, stretching ventrally over the involuting embryonic cells. This goes along with an extension of the serosa to the posterior. As morphogenesis proceeds, three distinct but at all-time connected tissue movements can be distinguished. First, involution of the embryo and its elongation emanating from a posterior segment addition zone. Secondly, extension of the amnion from posterior to anterior, while it starts to cover the embryo at its ventral and lateral sides. Thirdly, extension of the serosa from the posterior to the anterior ventral side, enveloping both embryo and amnion. When the serosa has extended roughly half of the ventral side of the embryo, the so-called serosal window emerges (Figure 1.1B2). Surrounded by the serosa, it is only inside this window that the embryo is still visible. The circumference of the serosal window are actually amniotic cells, which are not yet covered by the serosa. Eventually, the window closes and both membranes separate. After serosal window closure, the two extraembryonic membranes are for the first time discernible as two separate tissues. The tissue topology, with the serosa lining the inner eggshell and the amnion covering the embryo partially, persists throughout germband elongation (Figure 1.1B3) and retraction (Figure 1.1B4). Prior to dorsal closure both membranes rupture (Figure 1.1B4), enabling this last morphogenetic process. The serosa ruptures at the anterior ventral side, while the subjacent amnion ruptures in specialized cells of the rupture competence zone in the same area. Subsequent withdrawal of the serosa to the dorsal side, followed by the amnion (Figure 1.1B5), first over the head, then the abdomen, results in the formation of two

Drosophila

A1 late blastoderm

A2 extended germband

A3 dorsal closure

Embryo
Serosa
Amnion
Amnioserosa
Rupture

Tribolium

B1 differentiated blastoderm

B2 serosal window closure

B3 extended germband

B4 retracted germband

B5 amnion withdrawal and serosal degeneration

B6 dorsal closure
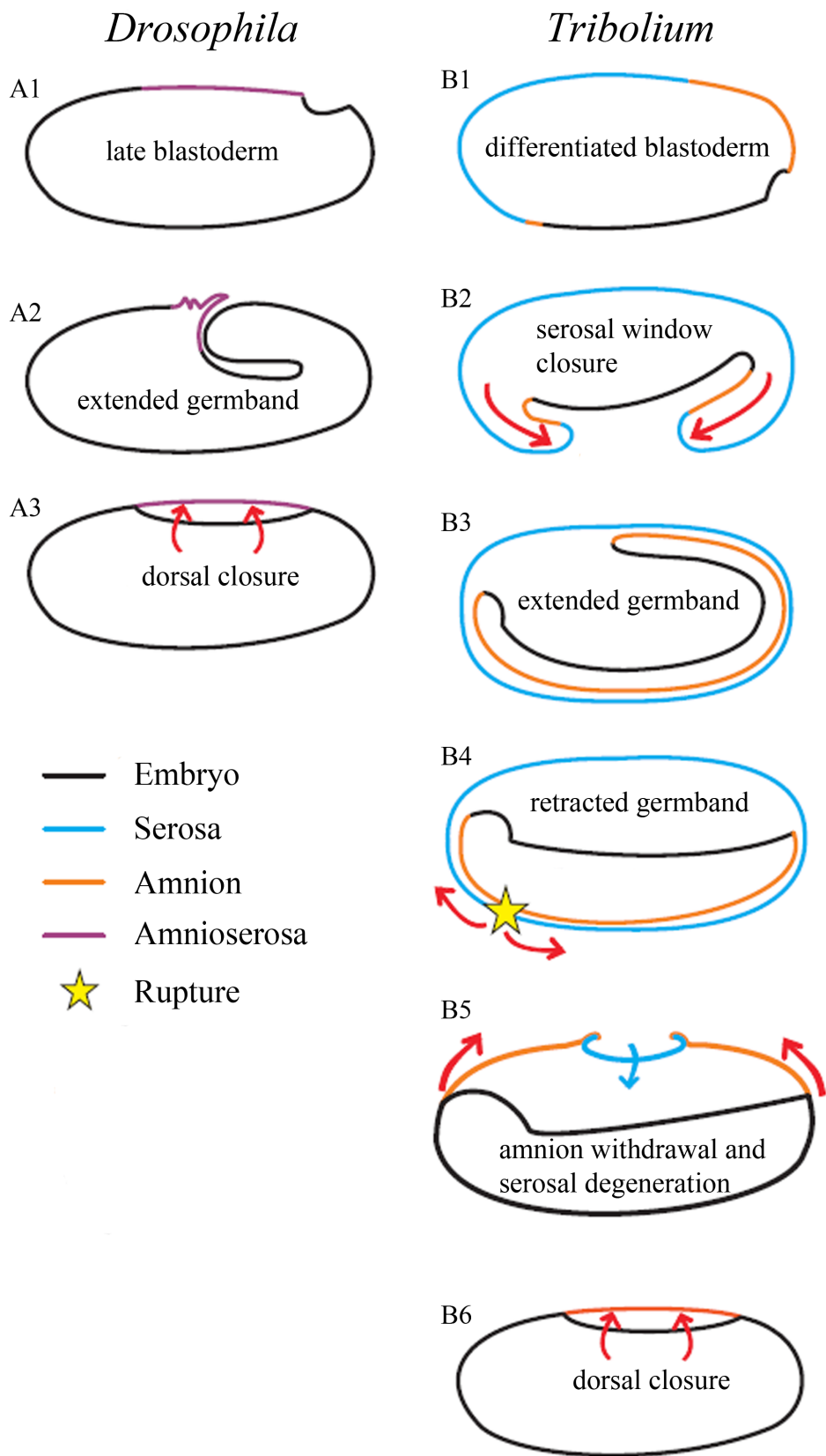
Figure 1.1: **Schematic of the extraembryonic and embryonic development in *Drosophila* and *Tribolium*.** (**A1-A3**) Development in *Drosophila*. (**B1-B6**) Development in *Tribolium*. (**A1**) At the late blastoderm stage, the extraembryonic amnioserosa is encompassing only a small region at the dorsal midline, while all other tissue is embryonic. The small indentation marks the site of pole cell invagination. (**A2**) The embryo has extended around the posterior pole. (**A3**) After retraction of the germband, the lateral flanks of the epidermis extend to the dorsal side (red arrows), while the amnioserosa degenerates. (**B1**) At the differentiated blastoderm stage, the anterior-ventral part gives rise to the serosa, while the posterior-dorsal part gives rise to the germ rudiment (amnion and embryo). The small indentation marks the primitive pit, where involution of the embryo starts. (**B2**) The embryo extends along with the amnion, while the serosa starts to encompass both by closing the serosal window (red arrows). (**B3**) The embryo is fully extended and lined at its ventral and lateral sides by the amnion. The serosa lines the inner eggshell. (**B4**) After retraction of the germband, both membranes rupture in an anterior-ventral region and withdraw first over the head and shortly after over the abdomen (red arrows). (**B5**) The serosa has withdrawn completely towards the dorsal side, forming the serosal dorsal organ, while the amnion is still underway, covering the yolk on the dorsal side. (**B6**) When the serosa has degenerated and the amnion has formed the 'second' dorsal organ, the embryo is closing its dorsal side, by extension of the lateral epidermis. Provided by T. Horn and modified from [Rafiqi et al., 2008].

distinct but connected dorsal organs, which are the densely folded extraembryonic membranes. Concomitantly, the lateral epidermis expands dorsally (Figure 1.1B6), following the retraction movement of the membranes. To facilitate closure of the embryo's back at the dorsal midline, both membranes sink down into the yolk (see Figure 1.1B5 for degeneration of the serosa only), degenerate and extraembryonic development is finished (the last two paragraphs are a summary with information out of the following papers: [Handel et al., 2000; Panfilio, 2008; Roth and Hartenstein, 2008; Schröder et al., 2008; Lynch et al., 2012; Strobl and Stelzer, 2014; Hilbrant et al., 2016]). Such complex movements are not found in *Drosophila* (see also [Rafiqi et al., 2008; Lynch et al., 2012; Schmidt-Ott and Kwan, 2016] for a comparison of membrane development in *Drosophila* and *Tribolium*). It is only during dorsal closure in *Tribolium*, when the serosa is degenerating and the amnion serves as a transient yolk cover that this organization is comparable to the one observed in *Tribolium* (compare Figure 1.1A3 and B6)

Although overall tissue movements during extraembryonic membrane development are well characterized in *Tribolium* and the serosa was shown to be involved in dessication resistance [Jacobs et al., 2013] and to contribute to the innate immune defense [Jacobs

and van der Zee, 2013; Jacobs et al., 2014], as well as the *Tribolium castaneum zerknüllt 1* (*Tc-zen1*) has been shown to be important for serosa specification [van der Zee et al., 2005; Jacobs et al., 2013; Jacobs and van der Zee, 2013; Panfilio et al., 2013; Koelzer et al., 2014; Jacobs et al., 2014], the amnion is not as well investigated. Albeit two more recent publications have shed some light on its function [Panfilio et al., 2013; Hilbrant et al., 2016] (see also [Panfilio, 2008] for potential functions of the amnion in insects) and consequently the amnion was identified as the initiator of rupture prior to the onset of dorsal closure [Hilbrant et al., 2016], genes specifiying the amnion early on are yet to be discovered. To initiate the search for such genes, in this study the role of the known amniotic marker gene *Tc pannier* (*Tc-pnr*), expressed in amniotic precursor cells in the anterior amniotic fold at the differentiated blastoderm stage [van der Zee et al., 2005, 2006], was interfered by pRNAi and the resulting phenotypes investigated via available tools (see 1.1). In *Drosophila* it is unclear if *Drosophila melanogaster pnr* (*Dm-pnr*) is important for the amnioserosa (see [Heitzler et al., 1996] contra [Herranz and Morata, 2001]), in which it is transiently expressed [Winick et al., 1993; Heitzler et al., 1996]. But due to the more static amnioserosa compared to the coordinated and complex morphogenetic movements the amnion is performing, *Dm-pnr* expression is not really meaningful, when it comes to the amnion in *Tribolium*, showing again the limitations of *Drosophila* centric research on extraembryonic membranes. Additionally, during this study it became clear that distinct visualization of the amnion as a separate tissue in tight interaction with the serosa is strongly impeded by currently available fluorescent lines. Therefore, a new transgenic line expressing Discosoma species red 2 (DsRed2) in the amnion was engineered.

Before introducing the amniotic marker gene *pnr* and the approach for generating the transgenic line, heart development and dorsal closure will be described. How these morphogenetic processes work genetically and biologically is important for the understanding of the data presented in this study.

1.3 The process of dorsal closure

1.3.1 Dorsal closure in *Drosophila melanogaster*

Dorsal closure is the morphogenetic movement by which a hole in the dorsal epidermis is closed by dorsally expanding lateral epithelium and concomitant retraction of the

amnioserosa. It starts shortly before germband retraction is complete, with an apical constriction of amnioserosal cells and slight dorso-ventral elongation of the leading edge cells (the dorsal-most epidermis cells). Subsequently, an actomyosin cable is formed in these leading edge cells, which stiffens the cells. This enables closing of the dorsal hole, as the cable contracts to the dorsal midline. When the two opposing leading edges come into approximate along the anterior-posterior axis, actin protrusions reach out to one another in a process called 'zippering'. At the same time, the amnioserosa continues with its dorsal-medial constriction and the tissue's surface area over the bulk is further reduced as individual amnioserosa cells withdraw beneath the surface and undergo apoptosis. Eventually, both leading edge cell rows come into physical contact, first forming a seam along the dorsal midline, before robust adherens junctions are formed, finishing closure of the dorsal epidermis [Jacinto et al., 2002; Fernández et al., 2007; Wada et al., 2007; Gorfinkiel et al., 2009; Heisenberg, 2009].

Genetically dorsal closure is initiated by *Dm* Jun N-terminal kinase (*Dm*-JNK) signaling. *Dm*-JNK is activated in the leading edge cells, where it activates *Dm decapentaplegic* (*Dm-dpp*) expression in the same cells. *Dm-dpp* gene expression in these cells is indispensable for dorsal closure, as it triggers downstream pathways, regulating the whole process [Harden, 2002]. Furthermore, in these most ectodermal cells, *Dm-pnr* is an upstream regulator of *Dm-dpp* [Herranz and Morata, 2001] and loss of *Dm-pnr* expression in these cells leads to the dorsal open phenotype, characterized by a hole in the dorsal cuticle [Jürgens et al., 1984], typically for mutations affecting *Dm-dpp* expression [Riesgo-Escovar and Hafen, 1997; Ricos et al., 1999].

1.3.2 Dorsal closure in *Tribolium castaneum*

Dorsal closure in *Tribolium* differs in its starting topography, as dorsal closure is a three-tissue system (amnion, serosa and embryo). At the retracted germband stage, prior to rupture, the amnion is connected to the dorsal epidermis and the serosa, forming a bilayer with the latter one. The epidermal border cells connected to the amnion display an indistinct and irregular border to the amnion, in difference to the regular arrangement of the leading edge cells in *Drosophila*. Following rupture of the serosa in an anterior-ventral area and of the amnion in the same area within a specialized cap region, the membranes withdraw to the dorsal side. It is assumed that the amnion thereby initiates rupture,

while the serosa drives the withdrawal, strengthened by the fact that both membranes are connected throughout the movement to the dorsal side. When the serosa contracts at the dorsal side, forming the serosal dorsal organ (a square-like, thick and folded structure), the amnion serves as a provisional yolk cover. It is around this time that the epidermal flanks of the embryo start to extend dorsally by slight elongation in DV direction. Subsequently, the serosal dorsal organ degenerates and sinks down into the yolk, with the amnion still attached. The amnion has by then folded over the serosa and a second, amniotic dorsal organ has formed. This more transient dorsal organ stretches in AP direction, as the serosa degenerates and the epidermis is closing in towards the midline. These processes are concomitant with a general stretching of the embryo in AP direction, as the embryo bends towards the ventral side. In the closing phase, when the amnion degenerates into the yolk, the two sides of the epidermis come together in a wavelike fashion, so that some regions meet before adjacent regions. This irregular closure at the midline is again different from the more regular zippering observed in *Drosophila* [Panfilio et al., 2013; Hilbrant et al., 2016]. Genes known to facilitate dorsal closure in *Tribolium* are not known.

Overall, dorsal closure in *Tribolium* and *Drosophila* display many distinct features, complicating a comparison between both modes of dorsal closure. As dorsal closure goes along with the movement of the cardioblast cell row to the dorsal midline, this event will be described in the next section.

1.4   Heart development in *Drosophila melanogaster*

The insect heart, known as the dorsal vessel, is a dorsomedial muscular tube that is best understood in *Drosophila* and will be described in the following paragraph, including the level of the underlying cardiac gene regulatory network [Cripps and Olson, 2002].

In *Drosophila* cardiac tissue arises from the mesoderm. The mesoderm itself is specified by an enrichment of *Dm* Dorsal (*Dm*-Dl) protein in the ventral-most region of the embryo. When the mesoderm subsequently spreads laterally during invagination, it comes into the range of *Dm*-Dpp signaling, a ligand of the bone morphogenetic protein (BMP) pathway that is secreted by the overlaying ectoderm. *Dm*-Dpp binds to its membrane receptor and activates a downstream signaling cascade, resulting in the restriction of *Dm tinman* (*Dm-tin*) expression in the so specified dorsal mesoderm. To further induce the cardiac mesoderm, *Dm* Wingless (*Dm*-Wg) signaling is needed. It is secreted from the
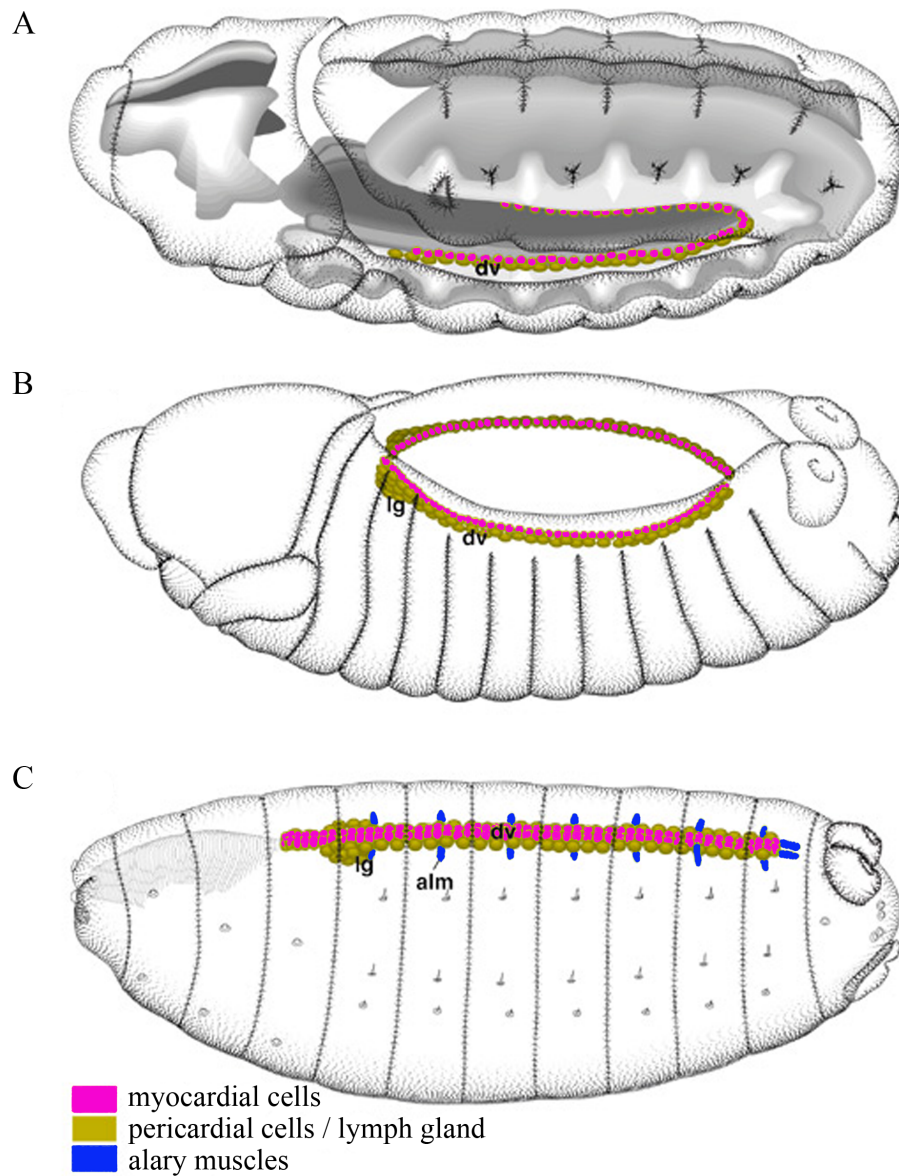
Figure 1.2: **Formation of the *Drosophila* heart**. (**A**) In the cardiac mesoderm, the progenitor cells of the dorsal vessel, the myocardial cells and the pericardial cells, are specified. Latter ones flank the myocardial cells. (**B**) During dorsal closure, the two rows of cells from each side of the embryo come together at the dorsal midline. At this time, the lymph gland is formed, which is later responsible for hematopoiesis (formation of blood cellular components). (**C**) When dorsal closure is finished, the two myocardial cell rows form a central lumen, through which the hemolymph circulates. The dorsal vessel is by than anchored to the dorsal epidermis via the alary muscles. (alm) alary muscles; (dv) dorsal vessel; (lg) lymph glands; Modified from [Hartenstein, 1993]

ectoderm and its downstream target genes act together with the BMP pathway in the dorsal mesoderm to specifiy the cardiac mesoderm. Thereafter, the three transcriptional effectors *Dm-tin*, *Dm Dorsocross* (*Dm-Doc*) and *Dm-pnr* become activated to specify two distinct subsets of cardiac progenitor cells (myocardial and pericardial cells). These precursor cells align in the dorsal mesoderm of both sides of the embryo and the cardioblasts (= myocardial cells) form two continuous cell rows, surrounded by pericardial cells (Figure 1.2A). Mediated by partially synergistic control of downstream target genes like *Dm midline* (*Dm-mid*) or *Dm even-skipped* (*Dm-eve*), expressed in specific subsets, individual cells are assigned to particular fates as the two rows migrate to the dorsal midline during dorsal closure of the embryonic flanks (Figure 1.2B). Here they come together and the dorsal vessel is formed (Figure 1.2C) [Cripps and Olson, 2002; Tao and Schulz, 2007; Bryantsev and Cripps, 2009]. The cardioblasts are thereby forming the inner contractile cardiac tube, while the pericardial cells, important for ultrafiltration and excretion of the haemolymph, form two loose rows at their outside [Rugendorff et al., 1994; Bodmer, 1995; Medioni et al., 2009].

With this last section the foundations for this study, regarding extraembryonic and embryonic development, the latter one with emphasis on heart formation and dorsal closure, have been explained. Therefore, the gene *pannier* will now be introduced in more detail, as it is the analysis of this gene that is the main part of this study.

1.5 The extraembryonic marker gene *pannier*

1.5.1 *pannier* in *Drosophila*

Dm-pnr is a GATA transcription factor with two C_4 zinc fingers, highly similar to the vertebrate GATA-1 transcription factor. Thus, it belongs to the family of zinc finger motif DNA-binding proteins [Ramain et al., 1993; Winick et al., 1993].

In the embryo, *Dm-pnr* is expressed early in the presumptive amnioserosa and dorsal epidermis right after cellularization [Winick et al., 1993; Heitzler et al., 1996; Herranz and Morata, 2001]. The latter expression domain persists throughout germband extension and retraction until dorsal closure is finished, whereas *Dm-pnr* expression in the amnioserosa is lost during germband retraction [Winick et al., 1993; Heitzler et al., 1996; Calleja et al., 2000; Herranz and Morata, 2001]. Around the time of heart cell specification, which

is after the germband fully extended, *Dm-pnr* is additionally expressed in the cardiac mesoderm [Gajewski et al., 1999]. Subsequently, when the embryo has shortened, *Dm-pnr* expression appears in the posterior spiracles [Winick et al., 1993].

Dm-pnr performs many functions during *Drosophila* embryogenesis. The most important ones for this study are its involvement in (1) dorsal closure and (2) heart development and its more general role in acting as a (3) dorsal-ventral (DV) selector like gene.

(1) The *pnr* phenotype (dorsal hole and bending of the head and posterior abdomen to the dorsal side) was first described in *Drosophila* in 1984, as part of a large-scale screen affecting larval cuticle [Jürgens et al., 1984]. The cause of the dorsal hole in the cuticle was traced back to the regulatory effect of *Dm-pnr* on *Dm-dpp*. *Dm-pnr* is expressed in the dorsal ectoderm, up-regulating *Dm-dpp* expression in the same area prior to dorsal closure [Herranz and Morata, 2001]. As *Dm-dpp* is known to be essential for dorsal closure [Affolter et al., 1994; Glise and Noselli, 1997], the dorsal hole is due to a missing activation of *Dm-dpp* in *Dm-pnr* mutants [Herranz and Morata, 2001]. This connects *Dm-pnr* to the signaling pathways mediating dorsal closure in *Drosophila* [Knust, 1997; Harden, 2002]. Another important factor in dorsal closure is the amnioserosa [Scuderi and Letsou, 2005]. As *Dm-pnr* is expressed in the amnioserosa only transiently during the early development [Heitzler et al., 1996; Herranz and Morata, 2001], a direct effect can be excluded. Although cell death was reported in the amnioserosa in *Dm-pnr* mutants [Heitzler et al., 1996], the membrane expresses the amnioserosal marker *Dm u-shaped* (*Dm-ush*) in the mutant (so the amnioserosa is not absent after loss of *Dm-pnr* expression) and none of the investigated *Dm-pnr* mutants so far adopted the u-shaped morphology, a characteristic phenotypic trait of genes important for amnioserosa development [Frank and Rushlow, 1996]. It is rather *Dm-pnr's* ectodermal expression in the late embryo regulating *Dm-dpp* expression [Herranz and Morata, 2001] that effects dorsal closure. *Dm-dpp* is involved in ensuring that the cell shape changes in the epidermis and in the amnioserosa proceed in a coordinated way, orchestrating dorsal closure [Fernández et al., 2007; Wada et al., 2007].

(2) Consistent with its expression in the cardiac mesoderm [Gajewski et al., 1999], *Dm-pnr* has an important function in heart development. It promotes the development of all heart cells [Alvarez et al., 2003] and specifies subsets of cells for pericardial or

myocardial cell fate [Gajewski et al., 1999; Reim and Frasch, 2005]. Accordingly, besides its effect on other heart genes, *Dm-pnr* is essential for expression of the myocardial marker gene *Dm-mid* [Reim and Frasch, 2005], while the pericardial marker gene *Dm-eve* is up-regulated in *Dm-pnr* mutants, suggesting an inhibitory effect in the latter case.

(3) The role of *Dm-pnr* as a DV selector like gene is not in connection with early DV patterning in the embryo but limited to specific compartments/tissues during later embryogenesis. At the retracted germband stage, *Dm-pnr* is expressed in the dorsalmost epidermis, sharing a border with the amnioserosa at the dorsal side and one with the *Dm iroquois* (*Dm-iro*) expression domain at the ventral side. Thus, the dorsal part of each segment can be subdivided into a medial region, where *Dm-pnr* is expressed and a lateral one, where *Dm-iro* is expressed [Calleja et al., 2000]. In the *Dm-pnr* null mutant [Ramain et al., 1993], the lateral region expands at the expense of the medial region, illustrated by an extension of *Dm-iro* expression into the former *Dm-pnr* domain [Calleja et al., 2000]. In wild type embryos at the extended germband stage, *Dm-dpp* is expressed in two stripes, extending from the head to the end of the abdomen [Herranz and Morata, 2001]. The dorsal stripe abuts the amnioserosa, while the more lateral stripe runs along the lateral side of the embryo. In the null mutant, the dorsal expression is lost, while *Dm-dpp* expression in the lateral stripe is unaffected. Measurements of the number of cells from the lateral *Dm-dpp* expression stripe to the border with the amnioserosa, showed no cell loss, supporting for a transformation of the medial into the lateral region. That *Dm-pnr* subdivides each segment into a medial and lateral region, is further strengthened by observations of larval cuticular features of the null mutant. Dorsal triangles, which can be found only in the medial region of the abdominal region, are replaced by spinules, which normally appear only in the lateral region [Herranz and Morata, 2001]. Thus, it is likely that *Dm-pnr* acts as a selector like gene (genes which function within distinct regions of the body, where they determine specific developmental pathways), partitioning the dorsal epidermis into a medial and lateral region through specification of the former [Mann and Morata, 2000; Herranz and Morata, 2001]. These findings can be expanded to a more general role in establishing the *Drosophila* body plan along the DV axis, if considering the function of *Dm-pnr* in defining the dorsal eye margin [Oros et al., 2010] and the dorsal eye fate [Singh et al., 2012]. Another example would be the subdivision into medial and lateral regions in the adult dorsal thoracic and abdominal segments [Calleja et al., 2000].

Interestingly, in the latter three publications, *Dm-iro* is reported as a downstream target of *Dm-pnr* regulation.

1.5.2 *pannier* in *Tribolium*

The function of *Tc-pnr* in *Tribolium* development is unclear. Until this time, *Tc-pnr* has been used only as a marker for different tissues throughout embryogenesis. Hence, its expression pattern is rudimentary known.

When the posterior fold has been formed shortly after differentiation of the blastoderm, *Tc-pnr* is expressed in the presumptive amniotic part of the fold as well as in the anterior amniotic fold, albeit considerably weaker. Both domains are connected by expression in the dorsal amnion [van der Zee et al., 2005, 2006]. At the extended germband stage, *Tc-pnr* is expressed in the dorsal ectoderm [van der Zee et al., 2006; Nunes da Fonseca et al., 2008]. Furthermore, expression in the heart at the retracted germband stage has been reported [Cande et al., 2009].

Genes regulated by *Tc-pnr* are not known. Only upstream regulators affecting *Tc-pnr* expression and ones which do not affect it have been identified.

Tc-zen1 RNAi does not effect *Tc-pnr* expression. In *Tc-zen1* knock down embryos, serosal tissue identity is lost and to a certain degree respecified as amnion. It is in the enlarged amniotic tissue that *Tc-pnr* is still expressed as well as in the head during germband extension [van der Zee et al., 2005]. At the onset of differentiation of the blastoderm, when *Tc-pnr* is expressed in the presumptive amniotic tissue, *Tc-dpp* RNAi abolishes its expression. This is caused by ventralization, indicated by a straight border between the serosa and the germ rudiment. Also later on, when the embryo has fully extended its germband, *Tc-dpp* RNAi leads to a complete loss of *Tc-pnr* expression in the ectoderm [van der Zee et al., 2006]. After *Tc short gastrulation* (*Tc-sog*) RNAi, the border has also lost its obliqueness. But in contrast to *Tc-dpp* RNAi, *Tc-pnr* is still expressed in the cells of the border, as well as in the primitive pit. It is only in the region of the former dorsal amnion, which was respecified to an ectodermal cell fate that the transcript is lost. It is assumed that this is a secondary effect caused by the effect of *Tc-sog* RNAi on *Tc-dpp*, due to a ventral to dorsal transport of *Tc-dpp* molecules by *Tc*-Sog in the wild type. When *Tc-pnr* is expressed in the ectoderm, *Tc-sog* RNAi does not lead to a loss of expression but a gain of expression in a ventral ectodermal stripe. As

Tc-dpp is expressed there ectopically as well, this is again assumed to be an indirect effect mediated by *Tc-dpp* [van der Zee et al., 2006]. The same is true after *Tc-Toll1* RNAi. Here, *Tc-pnr* is expressed in the exact same ring-like domains in the extended germband as *Tc-dpp*. The expression in the ectoderm along the dorsal side of the embryo is lost. A possible cause of this is that ectodermal patterning is initiated by activation of *Tc-sog* through *Tc-Toll1*, resulting in *Tc-dpp* expression along the dorsal midline. Since *Tc-dpp* is expressed in the straight border between germ rudiment and serosa after *Tc-Toll1* knock down, this process is started with an AP asymmetry, assumed to lead to the alternative expression pattern [Nunes da Fonseca et al., 2008].

The during this study generated DsRed2 expressing transgenic line was already used for the analyses of *pnr*. Therefore, the adopted CRISPR/Cas9 system will be introduced, as well as a brief outlook on the benefits of the new line will be provided.

1.6   Transgenesis in *Tribolium castaneum*

Visualization of amnion and serosa as two separate tissues is difficult throughout embryogenesis, as they are either forming a bilayer in close proximity or they are physically in contact. To build on the existing resource of two recently characterized extraembryonic marker lines expressing EGFP in the amnion and serosa respectively [Trauner et al., 2009; Koelzer et al., 2014; Hilbrant et al., 2016], the *EGFP* transgene in the line labeling the amnion was replaced by a *DsRed2* transgene, using the CRISPR/Cas9 system [Cong et al., 2013]. Transgenic beetles of the subsequently established new strain termed red HC079 (rHC079) could then be crossed to transgenic beetles expressing EGFP in various tissues, leading to offspring heterozygous for both markers. This greatly enhanced discrimination of the two tissues by fluorescent imaging.

In the following two sections a general introduction into the CRISPR/Cas9 system and how it is used for gene editing will be provided. In the concluding section, the motivation for the generation of the DsRed2 expressing line will be stated in more detail and in relation to possible applications for the research on extraembryonic membrane development.

1.6.1 The CRISPR/Cas9 system as an endogenous immune defense for Archaea

The CRISPR locus was first discovered in the *Escherichia coli* genome. The locus is organized as an alternating series of repeat sequences and spacer sequences [Ishino et al., 1987]. Almost 20 years later, it was discovered that CRISPR spacers have identical sequences to that of mobile genetic elements (MGEs) [Bolotin et al., 2005; Mojica et al., 2005; Pourcel et al., 2005] and in cooperation with Cas proteins act as part of the adaptive immune system in bacteria and archaea [Barrangou et al., 2007]. How the CRISPR/Cas9 system (type II of the five CRISPR/Cas types [Makarova et al., 2015]) works in prokaryotes, is thoroughly described in an array of publications [Kirchner and Schneider, 2015; van der Oost et al., 2014; Peng et al., 2015; Rath et al., 2015]. Below, the three main steps of the system are shortly summarized.

1) **Acquisition**: The DNA of an invading MGE is fragmented into individual spacer sequence stretches (26 bp - 72 bp in length) by Cas nucleases. Subsequently, those spacers are integrated into the CRISPR array (combination of CRISPR locus and Cas genes) within the host genome.

2) **Expression**: The CRISPR array is transcribed into precursor CRISPR RNA (pre-crRNA) and trans-activating crRNA (tracrRNA). The tracrRNA binds to a 25 nt long complementary sequence within the repeat sequence of the pre-crRNA. This binding results in a double-stranded region, which is cleaved by the ribonuclease RNase III. The now mature crRNA (the spacer was trimmmed to a ∼20 nt long stretch) still forms a duplex with the tracrRNA, the tracrRNA:crRNA complex, which is also called guide RNA (gRNA). Interaction of the gRNA with the endonuclease Cas9, leads to the formation of the Cas9 ribonucleoprotein (Cas9-RNP) complex, needed for target interference.

3) **Interference**: The gRNA guides the Cas9 to specific loci (protospacers; 20 nt long complementary sequences to the crRNA) on invading MGEs. This is facilitated by scanning the MGEs for a protospacer adjacent motif (PAM), a three nucleotide long binding motif, which is directly adjacent to the protospacer. Subsequently, first the PAM sequence binds to the gRNA and secondly, base pairing between the protospacer and the crRNA occurs. Triggered by these binding events, the Cas9 cleaves both strands of the bound DNA, leading to target degradation.

These three steps together form a strong defense mechanism of the immune sys-

tem against invading viruses like bacteriophages and other MGEs. In this regard, it is worth noting that viruses have developed sophisticated countermeasures against the CRISPR/Cas system in diverse ways [Bondy-Denomy et al., 2013; Deveau et al., 2008; Pawluk et al., 2014; Seed et al., 2013].

1.6.2   Gene editing via CRISPR/Cas9

In 2012 Jinek and colleagues published the first experimental evidence for applying CRIS-PR/Cas9 as a tool for gene editing [Jinek et al., 2012]. They showed that it is possible to combine crRNA and tracrRNA via an artificial tetraloop into a chimeric RNA that is necessary to direct Cas9 to specific DNA targets. This gRNA has a 20 nt sequence at its 5' end provided by the crRNA for DNA binding, whereas the tracrRNA provides stem-loops required for formation of a complex with Cas9 [Jinek et al., 2012; Nishimasu et al., 2014]. Additionally, the PAM sequence was identified as indispensable for specific target DNA binding by Cas9 [Jinek et al., 2012; Sternberg et al., 2014]. In CRISPR/Cas9 systems, the canonical sequence of the PAM is NGG (the sequence is specific to the CRISPR/Cas type, while the CRISPR/Cas types are grouped based on their individual set of Cas genes [Mojica et al., 2009; Makarova et al., 2015]) and located upstream (at the 5' end) of the protospacer [Anders et al., 2014].

This breakthrough in CRISPR research was accompanied by a wave of publications, improving not only our understanding of the underlying biology and mechanics [Makarova et al., 2015; Nishimasu et al., 2014] but also of the usability of CRISPR/Cas9 as a system for gene editing [Cong et al., 2013; Mans et al., 2015; Mali et al., 2013; Ran et al., 2013]. Hence, in the last years CRISPR/Cas9 has become the leading genome engineering tool, boosted by its easy and cost-efficient application, as well as by the availability of online tools for fast and easy design of specific gRNAs.

In the course of advancing CRISPR research and the accompanied spread of use of this new gene editing technique, the number of animal species in which the CRISPR/Cas9 system could successfully be implemented increased greatly. Not only organisms with an already huge set of tools for genome engineering like mouse [Zhou et al., 2014], *Drosophila* [Xue et al., 2014] or zebrafish [Auer et al., 2014] could benefit from this development, but also organisms with smaller research communities, like the mosquito *Aedes aegypti* [Kistler et al., 2015], the flea *Daphnia magna* [Nakanishi et al., 2014], the cricket *Gryllus*

bimaculatus [Awata et al., 2015], the nematode *Pristionchus pacificus* [Witte et al., 2015], the silkworm *Bombyx mori* [Ma et al., 2014], the crustacean *Parhyale hawaiensis* [Martin et al., 2016] and the beetle *Tribolium castaneum* [Gilles et al., 2015].

1.6.3 Application of CRISPR/Cas9 in *Tribolium castaneum*: advancing research on extraembryonic membranes

In 2015 M. Averof and his group showed that CRISPR/Cas9 is feasible in *T. castaneum* [Gilles et al., 2015]. By injection of either *in vitro* transcribed Cas9 and a specific gRNA or by injection of two plasmids harboring the corresponding sequences, they achieved considerable transgenesis efficiencies, both for knock-out (loss of gene expression) and knock-in (gain of foreign gene expression) experiments. Different promoters driving expression of the CRISPR toolkit in plasmids were tested regarding their efficiency. Endogenous loci were targeted via specific gRNAs and the resulting phenotypes compared to those obtained by RNAi. Altogether, they provided the *Tribolium* community with a good starter set for further gene editing.

Of special interest for the present study was the use of a gRNA designed for guiding Cas9 specifically to *EGFP* [Auer et al., 2014]. Injected in combination with a plasmid harboring a *DsRed2* transgene, replacement of *EGFP* via initiation of the homology directed repair mechanism was achieved [Gilles et al., 2015]. Considering that up to now all transgenic lines available in *Tribolium* are using GFPs [Sarrazin et al., 2012; Trauner et al., 2009] as fluorescent markers, this approach could easily change this by editing the existing lines.

The largest source of transgenic lines in *Tribolium* is a collection of enhancer trap lines, generated via insertional mutagenesis, known as the GEKU lines [Trauner et al., 2009]. Our lab already characterized some of these lines, leading amongst others to the discovery of two 'serosa lines' (G12424 and KT650) [Koelzer et al., 2014] and an 'amnion line' (HC079) [Hilbrant et al., 2016], expressing EGFP in the serosa and amnion, respectively. An enhancer trap line with EGFP expression in the cardioblast cell row (G04609) was characterized, too [Koelzer et al., 2014]. Via the use of the transgenic lines for both extraembryonic membranes (HC079, G12424 and KT650), it was actually just recently reported by our lab [Hilbrant et al., 2016] that both membranes have a distinct tissue identity during germband retraction and are not intercalating (contra [van der Zee

et al., 2005]) and are both still fully present (contra [Panfilio et al., 2013]). Now, to better understand the development of the two membranes during embryogenesis, it is not only necessary to look at them as separate tissues but also to examine how they interact. For the process of dorsal closure, this has been done in great detail [Panfilio et al., 2013]. Still, until the end of this highly dynamic morphogenetic process, both membranes stay connected as apposed epithelial sheets, hampering examinations of tissue borders or cell affiliation in those regions. To cite Panfilio et al. 2013 '...the exact structural nature of the relationship between the amnion and the serosa is difficult to visualize at these stages...' [Panfilio et al., 2013]. For an adequate investigation of these tissue regions, differential fluorescent labeling of the two membranes is necessary, which cannot be achieved with the current GEKU lines only expressing EGFP. By CRISPR/Cas9 mediated replacement of *EGFP* with *DsRed2* in the amnion line, amnion and serosa can be separately visualized by EGFP and DsRed2. This will enable us to not only investigate the morphogenetic movements and tissue changes of the separate membranes, but also their interplay during the highly dynamic phase of late *Tribolium* extraembryonic development.

1.7   Objectives

With this study two goals should be achieved: First, a detailed description of the wild type expression pattern of *Tc-pnr* and of the resulting phenotypes after parental RNA interference. Second, the replacement of an *EGFP* transgene in the amnion line HC079 with a *DsRed2* transgene, to enhance distinct visualization of both extraembryonic membranes in a heterozygous cross.

Chapter 2

Material & Methods

2.1 Fundamental beetle work

2.1.1 *Tribolium castaneum* husbandry

For experiments performed with *T. castaneum*, the following strains were used: the wild type San Bernardino strain [Brown et al., 2009], a transgenic line expressing GFP in all nuclei (nGFP line) [Sarrazin et al., 2012], three of the GEKU lines characterized by our lab [Koelzer et al., 2014; Hilbrant et al., 2016], the two GEKU lines characterized in this study (Figure 3.22), or the rHC079 line(s) generated during this project (see 3.1).

The beetles were kept at 30 °C and a relative humidity (RH) of 50% in the dark at all time. For stock keeping, a mixture of 2 kg "Weizenmehl Extra Type 405" (Diamant), 1 kg "Weizen Mehl Type 1050" (Goldkrone) and 1 g of the anti fungal powder "Fumagilin-B" (Medivet Pharmaceuticals Ltd.), termed "full flour", was used. On a weekly basis, adult beetles were separated from the flour via a 710 μm sieve and transferred back on full flour and a tablespoon of Springaline® inactive dried yeast (Biospringer) was added. Firstly this weekly stock keeping assured that populations did not overgrow, since the larvae are still small enough to fit through a 710 μm mesh and secondly it kept the flour from getting too dirty.

After a period of three months, an overnight egg lay (EL) was set up on "EL flour", which is "Instant Mehl Type 405" (Diamant) pre-sieved in a 300 μm sieve (discarding all particles with a diameter bigger than 300 μm). To do so, adult beetles were separated from full flour and transferred on EL flour. On the following day, beetles were again separated from EL flour and transferred back onto full flour. Subsequently eggs from this overnight collection were sieved out of EL flour via a 300 μm mesh and also transferred

on full flour. This procedure guaranteed that the used beetle populations were always very young and healthy and should therefore provide the experimenter with a consistently large amount of eggs.

2.1.2 Egg collection and fixation

To obtain embryos for experiments, adult beetles were put on EL flour for a specific time span. Depending on the desired developmental stage, eggs were either processed directly or transferred into EL baskets (self-made; approximately 3 cm tall piece of a plastic tube with an inner diameter of 22 mm and a wire gauze made from polyamide with a mesh size of 125 μm (Cat#510-9529, VWR) clued to one side of the open tube) on top of a flour filled petri dish (thereby preventing dessication of the eggs) and further incubated like this under normal culturing conditions. In the latter case, the minimum age of the embryos corresponds to the incubation time and the maximum age to the starting time of the EL plus the incubation time.

For techniques other than live imaging, embryos were fixed at specific times to preserve its tissue shape and molecular composition at the subcellular level. But first of all, the EL baskets were rinsed under gently flowing tap water to remove flour particles. Subsequent dechorionation and dissolving of residual yeast particles was achieved by putting the eggs in 100% DanKlorix (Colgate-Palmolive), which contains sodium hypochlorite, for 5 min with rinsing and agitation. Eggs were rinsed again in water and transferred with a paintbrush into a 1:2 phosphate-buffered saline (PBS):heptane solution in a glass vial, where they swim in the interphase. Remaining dirt particles were removed by exchanging the lower PBS phase once. For fixation, a 5% formaldehyde solution (4 ml heptane, 2 ml PBS and 2 ml 10% formaldehyde (Cat#04018, Polysciences, Inc.)) was used. The glass vial was strapped to a shaker and fixation was performed for 60 min at room temperature (RT) and shaking at $\sim$ 100 rpm. After this time, the lower phase was removed, 3 ml methanol was added and the whole glass vial was shaken for $\sim$ 1 min by hand. Due to the methanol shock (osmotic shock), the vitelline membrane bursts open and the eggs sink down to the bottom, from where they were transferred into a 1.5 ml tube. These steps were repeated several times, until all eggs were collected. Thereafter the eggs were washed three times with methanol and stored at -20 °C.

Tribolium embryos older than $\sim$ 20 h need a special treatment, since until $\sim$ 64 h,

the vitelline membrane cannot be removed by methanol shock and therefore needs to be dissected off of the embryo. This special fixation is only needed if an *in situ* hybridization or an antibody staining is planned. For nucleic acid stains like fuchsin, whose molecules are much smaller and can penetrate cracks in the vitelline membrane, it is not necessary. The special fixation used the same fixation solution as the normal one but fixation was performed for 2 h. Preparatory, a double-sided tape was stuck to the inner surface of a small petri dish lid and a Whatman® gel blotting paper (Cat#Z613916-25EA, Sigma-Aldrich®) of corresponding size was cut. After 2 h the eggs were pipetted onto the blotting paper and gently pressed on the double sided tape. 1 x PBS was used to submerge the eggs, to prevent dessication. Further processing can be delayed for several days by covering the petri dish and storage at 4 °C. Manual removal of the vitelline membrane was done by using a set of fine forceps (Cat#LH79.1, Carl Roth®). Devitellinized eggs were collected in a 1.5 ml tube containing 1 x PBS, postfixed for 20 min in 5% formaldehyde, washed two times in PBS plus 0.1% Tween®20 (PBT; Cat#P3563, Sigma-Aldrich®) and stored for up to four weeks in PBT at 4 °C. Longterm storage is possible in methanol at -20 °C.

2.2 Fundamental techniques of molecular biology

2.2.1 Isolation of genomic DNA

Three beetles were transferred into 200 μl HOM-buffer (80 mM ethylenediaminetetraacetic acid (EDTA) pH 8.0, 100 mM Tris(hydroxymethyl)aminomethane (Tris) pH 8.0, 0.5% sodium dodecyl sulphate (SDS), aseptic filtrated). 1 μl proteinase K (20 mg/ml) was added and digestion was conducted at 55 °C for 1 h. Every 20 min, the mixture was vortexed for 1 min. Phase separation at RT was achieved by addition of 200 μl 5M sodium chloride (NaCl) pH 5.2 and 300 μl chloroform and centrifugation for 15 min at 14k rpm. The DNA containing upper phase ($\sim$ 300 μl) was transferred by pipetting into a new tube. Precipitation was done by addition of 30 μl sodium acetate (NaOAc) and 600 μl 100% ethanol. After mixing and incubation at -20 °C for 1 h, the DNA was pelleted through 20 min centrifugation at 4 °C and 14k rpm. The supernatant was discarded, the pellet washed with 700 μl 70 % ethanol and centrifuged for 5 min. Subsequently the DNA was dried directly in the tube for $\sim$ 5 min after discarding the supernatant again. Resuspension was done in 20 μl nuclease-free water (Cat#AM9937, Ambion™). Prior

to storage at -20 °C, quality and concentration were determined using a NanoDrop 2000c (Thermo Scientific) spectrophotometer.

2.2.2 RNA extraction and cDNA synthesis

Eggs were handled according to 2.1.2. After bleaching and rinsing, the eggs were transferred with a paintbrush into a 1:1 PBS:heptane solution in a glass vial. The lower PBS phase was exchanged several times until it was clear and free of particles. All eggs were then transferred into a 1.5 ml tube, washed with PBS to get rid of any residual heptane, which evaporates while the embryos do not dry out in the lower PBS phase and washed again several times with distilled water. 300 μl TRIzol® reagent (Cat#15596-026, Invitrogen) was added, the eggs were smashed using a pestle (Cat#47747-358, VWR) and additional 200 μl TRIzol® reagent was added. If required, the homogenate can now be stored at -20 °C several days for short-term or at -80 °C for long-term. The aqueous phase was separated from the debris and transferred into a new tube after centrifugation for 10 min at 4 °C and 12k rcf. 100 μl chloroform was added and incubated for 10 min at RT. Phase separation was done by 15 min of centrifugation at 4 °C and 12k rcf (upper phase-RNA; middle phase-DNA; lower phase-protein). The RNA-containing upper phase was transferred into a new tube and mixed with 250 μl isopropanol by careful inversion of the tube. Another round of centrifugation for 10 min at 4 °C and 12k rcf lead to pelleting of the RNA. All supernatant was removed and 500 μl 75% ethanol was used for washing the pellet. Centrifugation for 5 min at 4 °C and 12k rcf was peformed, the supernatant discarded and the washing step repeated. Subsequently the RNA was dried directly in the tube for 5 to 10 min, resuspended in 30 μl nuclease-free water and incubated for 15 min at 60 °C to dissolve the RNA completely. After this the RNA concentration was measured using the NanoDrop 2000c spectrophotometer, aliquots were made and stored at -80 °C.

In order to synthesize copy DNA (cDNA) from RNA, the SuperScript® VILO cDNA Synthesis Kit (Cat#11754-050, Invitrogen) was used to reverse transcribe 2 μg of the isolated RNA via the enzyme reverse transcriptase into double stranded DNA, called cDNA. The procedure was executed as described in the manufacturer's protocol.

2.2.3 Design of primers

All primers were either designed using available coding sequence (CDS) data from the official gene set (OGS) of the *Tribolium* genome browser by M. Stanke (`http://bioinf.uni-greifswald.de/gb2/gbrowse/tribolium/`, last access: 24.08.2016), using sequence information obtained via the National Center for Biotechnology Information (NCBI) search page (`http://www.ncbi.nlm.nih.gov/`, last access: 24.08.2016) or using sequence information supplied by other research groups.

The web page Primer3Plus (`http://www.bioinformatics.nl/cgi-bin/primer3plus/primer3plus.cgi`, last access: 24.08.2016) was used for primer design with the default settings. If primers were designed in order to make probes for use in the *Tribolium in situ* hybridization protocol (see 2.4.2), the product size range was set to 700-850 bp (product sizes had to be reduced in some cases, if only shorter CDS were available). For all other applications this range was adapted to fit determining factors. Obtained primer sets were tested for potential self-complementarity via the web page Oligo Calc (`http://biotools.nubic.northwestern.edu/OligoCalc.html`, last access: 24.08.2016).

2.2.4 Polymerase chain reaction

The polymerase chain reaction (PCR) is a method to amplify stretches of DNA *in vitro* via denaturation of the double strand (ds), subsequent binding (annealing) of specific primers and elongation mediated by a DNA polymerase. The PCR product is the newly synthesized dsDNA strand identical to specific parts of the template DNA strand with the forward (fwd) primer and reverse (rev) primer as its border sequences.

All PCR reactions were conducted using the REDTaq® ReadyMix™ PCR Reaction Mix (Cat#R2523, Sigma-Aldrich®). In Table 2.1 the volumes for a standard 25 μl PCR reaction and in Table 2.2 the cycling parameters of a standard PCR are provided.

The elongation time depends on the size of the PCR product, where the rule of thumb is 1 min for 1 kb. Depending on the needed specificity, the second parameter to be adjusted is the annealing temperature, normally ranging from 50 °C to 60 °C, affecting the binding specificity of the primers to the DNA. Higher temperatures lead to an increased specificity, lower temperatures to a decrease in specificity.

Table 2.1: Standard PCR reaction

Volume	Reagent	Comment
12.5 μl	REDTaq ReadyMix	final concentration: 1 x
1 μl	fwd primer	working concentration: 10 μM
1 μl	rev primer	working concentration: 10 μM
x μl	template DNA	-
10.5 μl - x μl	nuclease free water	-

Table 2.2: Standard PCR cycling conditions

Step	Time	Temperature	Comment
1	95 °C	2 min	initial denaturation
2	95 °C	30 sec	denaturation
3	58 °C	30 sec	annealing
4	72 °C	1 min	elongation
5	-	-	repeat step 2-4 34 times
6	72 °C	7 min	final elongation

2.2.5 Agarose gel electrophoresis

To verify the correct product size after PCR, agarose gel electrophoresis was conducted. Due to the negative charge of DNA molecules and an applied electrical field in the gel chamber, all DNA fragments (PCR products) migrate toward the positively charged anode. Thus it is possible to separate DNA fragments by size only. Consequently, large fragments migrate more slowly through the gel matrix compared to small ones.

A 1% agarose gel was used for all runs and 1 x Tris-acetate-EDTA (TAE) buffer (50 x TAE: 2 M Tris, 0.05 M EDTA, pH 8.0, in water) was used as running buffer. Either 1 - 2 μl of PCR product was loaded (loading buffer is already included in the REDTaq® ReadyMix™) or 3 μl were loaded when mixed (15 μl total volume) with a pre-made loading buffer (5 x loading buffer: 5x TAE, 17.5% glycerol, in water, 0.01 g of Orange G (Cat#O3756-25G, Sigma-Aldrich®)). In both cases 100 V were applied for 20 min. By addition of one drop of an 0.025 % ethidium bromide solution (Cat#HP47.1, Carl Roth®) independent of the gel size, those different fragments were visualized at an

Molecular Imager® Gel Doc™ XR+ Imaging System (Bio-Rad Laboratories), where the large fragments showed up at the top of the gel and small ones more to its bottom. Either the SmartLadder (Cat#MW-1700-10, Eurogentec) or the Quick-Load® Low Molecular Weight DNA Ladder (Cat#N0474S, New England Biolabs) for small molecules served as size standards.

2.3   Cuticle preparation

For morphological analyses at the end of *Tribolium* embryonic development, cuticle preparation is the technique of choice. It dissolves all non-cuticle matter, leaving behind the epidermal cuticle and the outer eggshell. Therefore it is essential that the embryos can develop until the stage when the epidermis secretes this cuticle, which is for *Tribolium* around three days after deposition of the egg.

First, all dirt particles were dissolved by bleaching (see 2.1.2), next the EL basket harboring the embryos/larvae was transferred to a water filled petri dish, so that the embryos/larvae were floating on the water surface. Two drops of 1:1 Hoyer's medium (50 ml distilled water, 20 ml glycerol, 200 g chloral hydrate, 30 g gum arabic):lactic acid were dropped separately on a microscope slide (76 mm x 26 mm). The embryos/larvae were taken out of the baskets via a paintbrush, equally distributed between both drops and spaced out so the embryos/larvae were not laying on top of each other. This would have impaired inspection at the microscope later on. Next the two drops were covered with one cover slip (24 mm x 24 mm) each and the whole microscope slide was incubated at $50\,°C$ over night. Inspection was performed at a microscope with darkfield illumination.

2.4   Whole mount *in situ* hybridization

in situ hybridization is a staining method in molecular biology that utilizes nuclear acid hybridization to facilitate binding of a labeled single stranded nucleic acid molecule (probe) to a specific and complementary DNA/RNA sequence in a portion of a tissue. If the probe is applied to an entire tissue, in the present case the complete *Tribolium* embryo, this is called a whole mount *in situ* hybridization. Also, only RNA probes were used for hybridization to messenger RNA (mRNA) in the present case and all were labeled with digoxigenin (DIG) for subsequent visualization of the localized probe.

2.4.1 Probe synthesis

Primers were designed according to 2.2.3. A linker sequence was added to the 5' end of the gene specific forward primer (ggccgcgg) and to the 5' end of the gene specific reverse primer (cccggggc) (see Table 2.3 for a list of all used gene specific primer sequences without the linker sequence).

The first PCR was performed using both gene specific primers following Table 2.1 and Table 2.2. As template for this PCR served 1 μl cDNA originated from an *Tribolium* EL ranging from 0 - 72 h (see 2.1.2).

Table 2.3: Gene specific primers used for *in situ* hybridization

common name	*Tribolium* ID	fwd sequence (5' → 3')	rev sequence (5' → 3')
Tc-dpp	TC008426	GTGGCATGTTGTTGGGGTAA	TGTGGTCTGGAATGGGGTAC
Tc-eve	TC009469	CACACCGAAATACCCATTCC	TTTGAACAACTTGGGCTGCT
Tc-iro	TC003632	CCCGAAGTGTCGGTGTCTAC	TCCCGTTTGTCCTCTTCATC
Tc-mid	TC014296	AGTTCAACGAATTGGGAACG	TCAGAAACAACTGCGACCTG
Tc-mirr	TC003634	ACCAAGCCCCCTTCTACACT	TATAGCGAGGAGGCGGTAGA
Tc-pnr	TC010407	ATGCTTGTGGGCTTTACCAC	GCAGTAACGTGGTGTTGGTG
Tc-zen1	TC000921	TCCCAATTTGAAAACCAAGC	CGTTCCACCCTTCCTGATAA

Table 2.4: T7 universal primer sequences

primer	sequence
3' T7 universal primer	AGGGATCCTAATACGACTCACTATAGGGcccggggc
5' T7 universal primer	GAGAATTCTAATACGACTCACTATAGggccgcgg

For the second PCR, either the gene specific forward primer and a 3' T7 universal primer (template for antisense probe) or the gene specific reverse primer and a 5' T7 universal primer (template for sense probe) were used. These universal primers contain a complementary linker sequence and the sequence for the T7 promoter (see Table 2.4), which enabled *in vitro* synthesis of a RNA probe from the PCR product in the next step. PCR conditions were the same as before, with 1 μl of the first PCR as template. The PCR product of this second PCR was diluted with 25 μl nuclease free water. Both the

first and the second PCR were checked on an agarose gel (see 2.2.5) before the respective next step.

6 μl of the diluted template together with 8 μl nuclease free water, 2 μl transcription buffer, 2 μl T7 RNA polymerase (both Cat#10881767001, Roche) and 2 μl DIG RNA labeling mix (Cat#11277073910, Roche) were pipetted into a tube. The reaction was incubated for 4 h at 37 °C. For the last 10 min 1 μl DNAse was added and stopped by addition of 30 μl nuclease free water and 50 μl 2 x stop solution (0.2 M NaAc, 1% acetic acid, pH 6.0). 2 μl were extracted and stored to perform an agarose gel electrophoresis (see 2.2.5) later on. 5 μl transfer RNA (tRNA) were added to prevent degradation and facilitate the precipitation, which was started by addition 10 μl lithium chloride (MEGAscript® Kit, Ambion) and 300 μl 100% ethanol (carefully invert reaction tube 2 times). After precipitation for 30 min at -20 °C, the probe was pelleted by centrifugation for 20 min at 4 °C with 14k rpm. The supernatant was removed, 300 μl 70% ethanol was added and centifuged again for 10 min. Subsequently the supernatant was removed and the pellet was dried for up to 5 min. Finally the RNA probe was resuspended in 100 μl probe resuspension solution (50% formamid, 2 x saline-sodium citrate (SSC) (20 x SSC: 3 M sodium chloride and 300 mM trisodium citrate, pH 7.0)) and stored at -20 °C.

2.4.2 Protocol for *in situ* hybridization in *Tribolium castaneum*

Embryos were collected and fixed as described in 2.1.2 and transferred into 500 μl fresh methanol, prior to this three day protocol. The embryos were stepwise transferred into PBT ((1) 2:1 methanol:PBT, (2) 1:2 methanol:PBT). After the last step supernatant was removed and the embryos were washed two times in 500 μl PBT. Subsequently the embryos were first washed in 1:1 PBT:hybridization solution I (Hyb I) (25 ml formamide, 12.5 ml 20 x SSC pH 7.0, 50 μl heparin (50 mg/ml), filled up to 50 ml with millipore water) and secondly in Hyb I only, before the prehybridization in hybridization solution II (Hyb II) (Hyb I plus 500 μl salmon sperm DNA (100 μg/ml)) for 1 h at 63 °C. The salmon sperm DNA in Hyb II hybridizes to single strand nucleic acids in the embryo and therefore prevents unspecific binding of the probe. After removal of Hyb II, 100 μl Hyb II plus 1 - 2 μl probe were added to the embryos and incubated over night at 58 °C. During this hybridization period only specific binding should occur, as at the same time the probe will replace the salmon sperm DNA specifically bound during prehybridization. Note, all

steps until now were performed in tubes while rotating.

On the next day all embryos were transferred into handmade small baskets, deposited in a 24 well plate. The embryos were quickly washed four times in prewarmed (58 °C) Hyb I and another four times for 15 min each in Hyb I on a shaker (as all following steps) at 58 °C. Stepwise transfer into PBT was performed ((1) 2:1 Hyb I:PBT, (2) 1:2 Hyb I:PBT, each one for 10 min at 58 °C). After removal of the supernatant, embryos were washed once for 5 min in PBT at RT and three more times for 10 min each in PBT. Subsequently the embryos were washed two more times for 30 min each in blocking solution (100 μl 10% bovine serum albumin (BSA) in PBS, 30 μl normal goat serum (NGS; 60 mg/ml), filled up to 1 ml with PBT) to block all antibody binding sites and were incubated in 500 μl blocking solution plus 1 μl 1:10 in water prediluted Anti-DIG-AP Fab fragments (Cat#11093274910, Roche) over night at 4 °C. This antibody binds to the digoxigenin-11-uridine-5'-triphosphate (UTP) on the probe sequence, enabling the color reaction later on.

On the third and last day embryos were washed three times in PBT at RT, three more times for 15 min in PBT and additional three times in alkaline phosphatase (AP)-buffer (1 ml 1 M Tris hydrogen chloride (HCl) solution pH 9.5, 500 μl 1 M magnesium chloride (MgCl$_2$), 320 μl 5 M NaCl, 100 μl 20% Tween$^{®}$20, filled up to 10 ml with millipore water). Next the embryos were transferred with a glass pipette into 1 ml AP-buffer plus 20 μl NBT/BCIP stock solution (Cat#11681451001, Roche) in an glass bottom dish. In these dishes the progressing color reaction (triggered by the DIG antibody and the AP that converts nitro blue tetrazolium (NBT)/5-Bromo-4-chloro-3-indolyl phosphate (BCIP) into a purple dye) can easily be observed under a light microscope. During this the embryos should be covered, as the NBT/BCIP stock solution is sensitive to light. When the background started to increase (antisense and sense probe labeled embryos were always stopped at the same time as the 'unspecific' sense probe was used as background control, thereby the specific staining can be distinguished from the unspecific one), the color reaction was stopped by washing the embryos five times in PBT after the transfer into tubes. To reduce the background, which is the unspecific staining, embryos were stepwise transferred into ethanol while rotating ((1) 2:1 PBT:ethanol, (2) 1:2 PBT:ethanol) and after removal of the supernatant, the destaining was performed in 100% ethanol for up to 10 min and at all times observed under the microscope. After this the embryos were

stepwise transferred back to PBT ((1) 2:1 ethanol:PBT, (2) 1:2 ethanol:PBT) and washed three times in PBT. For lone time storage and to add a nuclear stain, the embryos were incubated for 1 h to equal parts in Vectashield antifade mounting medium with 4',6-diamidino-2-phenylindole (DAPI; Cat#H-1200, Vector Laboratories) and PBT to facilitate mixing and afterwards stored at 4 °C in this mixture.

2.5 Parental RNA interference

RNAi is a mechanism of gene silencing first identified in *Caenorhabditis elegans* and conserved throughout eukaryotic organisms. Triggered by double strand RNA (dsRNA) the RNAi pathway is initiated and subsequently complementary mRNA molecules are cleaved [Fire et al., 1998; Meister and Tuschl, 2004; Mello and Conte, 2004]. If injection of dsRNA into the female leads to a knock down of zygotic genes in its offspring, this is called parental RNAi (pRNAi). In *Tribolium* it was described to function in 2002 [Bucher et al., 2002].

In this work dsRNA complementary to a gene of interest was injected into virgin female beetles and by examination of knock down effects on their offspring, the gene was characterized.

2.5.1 Synthesis of dsRNA

To make template for the synthesis of dsRNA, two PCRs were performed according to 2.4.1. Instead of using any gene specific primer (see Table 2.5 for a complete list of all used primers for synthesis of dsRNA), both universal primers were used in the second PCR (see Table 2.4).

For synthesis of the dsRNA the MEGAscript T7 transcription kit (Cat#AM1334, Ambion) was used and the protocol was adapted from the manual. First, 2 μl of each nucleoside triphosphate (NTP), 2 μl 10 x reaction buffer, 2 μl enzyme mix and 8 μl product of the second PCR as DNA template were pipetted into a tube and incubated for at least 4 h at 37 °C. The reaction was stopped by adding 115 μl nuclease free water and 15 μl ammonium acetate stop solution (provided with the kit). Purification of the synthesized dsRNA was performed by addition of 150 μl Roti®-Phenol/Chloroform/Isoamylalcohol (Cat#A156.1, Carl Roth®), rigorous shaking for 1 min and subsequent centrifugation for 5 min at 5 k rpm. The upper phase containing the dsRNA was transferred into a new

Table 2.5: Gene specific primers used for pRNAi

common name	*Tribolium* ID	fwd sequence (5' → 3')	rev sequence (5' → 3')
Tc-iro	TC003632	CCCGAAGTGTCGGTGTCTAC	TCCCGTTTGTCCTCTTCATC
Tc-mirr	TC003634	ACCAAGCCCCCTTCTACACT	CGTCATCTTGTTCTCCTTCTTG
Tc-pnr	TC010407	ATGCTTGTGGGCTTTACCAC	GCAGTAACGTGGTGTTGGTG
Tc-pnr fragment 2	TC010407	GTTCCATACAAGCGGTGGTG	CCGAACTGAAACTCCATGCT
Tc-Toll1	TC000176	GCCGTTTCGCTCGTAACTCT	GTAGGGTCAAGTCGGGACATAA

tube. Precipitation was performed by adding 150 μl isopropanol, incubation at -20 °C
for 1 h and again centrifugation for 15 min at 14 k rcf and 4 °C. The supernatant was
removed and 300 μl 70% ethanol was added. The mixture was centrifuged for 5 min at
14 k rcf and 4 °C. Ethanol was removed and the pellet was dried on ice for up to 10
min. The dsRNA was resuspended in 50 μl nuclease free water and its concentration was
determined with a NanoDrop 2000c spectrophotometer. Before it was stored at -20 °C, 1
μl was checked on an agarose gel (see 2.2.5).

2.5.2   Obtaining virgin females and injection of dsRNA

A culture of the desired *Tribolium* line was put on EL flour for four to eight hours. The
eggs were collected as described in 2.1.1 and transferred into a 180 ml *Drosophila* vial
(Nerbe plus), filled with full flour and yeast and incubated at 30 °C. 27 days later a
mixture of mostly pupae and some adults and larvae were separated from the flour, the
pupae were sexed and both females and males put back on full flour separately. One
week later the now adult virgin females were anesthetized by incubation on ice until they
stopped moving. Numb beetles were than stuck to a double sided tape, the elytra and
one of the wings were spread and stuck to the tape. 2 μl of the specific dsRNA was
front-loaded into a borosilicate glass capillary (World Precision Instruments) (settings for
needle pulling at the laser-based micropipette puller P-2000 (Sutter Instruments): heat
= 700, filament = 4, velocity = 60, delay = 155 and pull = 175) and used to inject five
beetles ($\sim$ 0.4 μl each) into the exposed, soft, dorsal abdomen. As a positive control
served the injection of *Tc-Toll1* and as a negative one the injection of nuclease free water.
Injected beetles were transferred directly onto full flour with yeast. After two days of

recovery the surviving females were counted and crossed to the previously sorted males (4:1 females:males). Collection of eggs was performed for a period of one to two weeks, depending on when the knock down penetrance was decreasing.

2.6   Microscopy and image processing

Stained embryos from *in situ* hybridization (see 2.4.2) were directly mounted on microscope slides in a drop of Vectashield mounting medium using a fine brush. Two cover slips (22 mm x 22 mm) were cut in half using a diamond cutter and the two halves were stuck on top of each other via 70% glycerol in PBS at the ends of a microscope slide. A coverslip (24 mm x 50 mm) was carefully stuck on top of these cover slips, whereby the mounting medium gets in contact with it. By moving the cover glass slightly in one of four directions, this set up permits rotation of the embryos and inspection from different angles.

Embryos expressing one or more fluorescent proteins were either handled as described in 2.7 or fixed prior to inspection (see 2.1.2). In the latter case fixation was performed without subsequent cracking of the vitelline membrane, as methanol could degrade the fluorophores within hours or days. Instead, embryos were directly mounted in PBT or in Vectashield mounting medium. As DAPI within the mounting medium cannot pass the vitelline membrane, it had to be removed by hand (see 2.1.2) or at least partially cut open with a razor blade.

Embryos used for cuticle preparation could be inspected directly, as the embryos were already mounted on a microscope slide (see 2.3).

Microscopy was performed either with an AxioImager.Z2 with an Apotome.2 module for structured illumination (Zeiss), a SteREO Lumar.V12 (Zeiss) or a LSM710 scanning confocal microscope (Zeiss) and image acquisition was done using different versions of the imaging software Zen (Zeiss). Z-stacks were acquired with this software and merged applying the volume rendering method 'maximum intensity projection' (MIP; for all images but brightfield ones) or 'wavelets' (for brightfield images only). If structured illumination was used during acquisition, an 'ApoTome RAW convert' was performed before, to merge the individual images of this method again. Further image processing was done using the free image processing program ImageJ (version 1.50e) [Schneider et al., 2012] and the raster graphics editor Adobe® Photoshop® (version 12.1 x64). Brightfield images

acquired with the AxioImager.Z2 black and white camera were recolored using Adobe® Photoshop® (color balance set to: cyan - red: +20, magenta -green: -20, yellow - blue: +30).

2.7 Live imaging

Embryos used for time-lapse recordings were dechorionated as described in 2.1.2 but not fixed. Instead the embryos were transferred back into tepid water within the EL basket after removal of the chorion. Using a fine brush, the embryos were arranged on a high precision microscope coverslip (Cat#0107222, Marienfeld-Superior), either as pairs of two or in rows for single embryo imaging. Halocarbon oil 700 (Cat#H8898, Sigma-Aldrich®) was used to cover the embryos to prevent desiccation. Next four cover slips were cut in half with a diamond cutter. Four halves were stuck on top of each other via 70% glycerol on a microscope slide on both ends. On top of the fourth coverslip the cover glass with the embryos was stuck in such a way that the oil did not touch the microscope slide. This setup could be mounted on the microscope stage for live imaging.

Two different microscopes were used for time-lapse recordings, the DeltaVision™ RT widefield microscope (Applied Precision/GE Healthcare) and the AxioImager.Z2. All images were acquired as z-stacks, with an interval of 5 to 10 min. The imaging was either performed at 30 °C using the temperature controlled chamber of the DeltaVision™ microscope or at RT, as such a chamber was not available for the AxioImager.Z2. Processing was performed using the Zen software and ImageJ. Specifically for movies recorded at the DeltaVision™, an additional macro supplied by Thorsten Horn for z-stack merging and file conversion was used. This macro was modified to be used with two color movies by Maarten Hilbrant and myself (see 6.1).

Cell tracking was performed as described in [Koelzer et al., 2014].

2.8 Knock-in via CRISPR/Cas9 and homology directed repair

The enhancer trap line HC079, expressing EGFP under the control of an 3xP3 promoter in the amnion and in the eyes was targeted for knock-in [Trauner et al., 2009; Hilbrant et al., 2016]. Three components were co-injected as separate plasmids. Cas9 was *in*

vivo transcribed from the plasmid p(bshp68-Cas9) [Gilles et al., 2015] (Genbank accession number KR732918). gRNA targeting *EGFP* in the enhancer trap line HC079 was *in vivo* transcribed from p(U6b-eGFP1.gRNA) [Gilles et al., 2015] (Genbank accession number KR732920). Vector plasmid pBac[3xP3*DsRed*attP] [Yonemura et al., 2013] (Genbank accession number AB779766) served as template for homology directed repair, guided by the arms of the *piggyBac* transposon flanking the *DsRed2* transgene (see Figure 3.2). Injected beetles were crossed and the resulting offspring was screened for DsRed2 expression in the eyes. The plasmid pBac[3xP3DsRedattP] harbours an artificial 3xP3 promoter driving expression in the eyes [Sheng et al., 1997] and therefore could be used as marker for successful integration. After identification of those DsRed2 positive beetles, a series of crossings was performed to obtain homozygous red HC079 (rHC079) lines, each one originating from a single DsRed2 positive beetle (see Figure 3.3). Subsequently, all four like this generated rHC079 lines, namely #F, #W1, #W13 and #N, were analyzed by PCR and Sanger sequencing to validate the integration of the transgene. Further live imaging experiments were set up to compare the individual DsRed2 signal strength in the four lines.

2.8.1 Preparation of plasmids prior to injection

For replication purposes, all plasmids were transformed into One Shot® TOP10 Chemically Competent *E.coli* (Invitrogen) according to the manual. 1 μl of plasmid was added to the One Shot® cells, 10 μl and 50 μl were plated on lysogeny broth (LB) agar plates containing 100 μg/ml ampicillin. Cultures were picked from 10 μl plates and transferred into 50 ml LB medium containing 100 μg/ml ampicillin. This preparatory culture was incubated at 37 °C over night. Following the manual, purification of all plasmids was performed with NucleoBond PC 100 kit (Macherey-Nagel). In step 8 of the protocol (edition November 2011/Rev. 09), instead of using only isopropanol, also 0.1 volumes of ice cold 3 M NaAc were added, as isopropanol alone was not able to precipitate the plasmid DNA. Plasmid DNA was resuspended in 10 μl nuclease free water and concentration was determined with a NanoDrop 2000c spectrophotometer. The intact sequence was verified by Sanger sequencing (Lightrun™ sequencing service, GATC biotech; `https://www.gatc-biotech.com/de/produkte/sanger-services/lightrun-sequenzierung.html`, last access: 24.08.2016). Subsequently, all plasmids were diluted to a concentration of

1500 ng/μl and pooled, to achieve a final working concentration of 500 ng/μl. To further remove all particles from this aqueous solution, Ultrafree®-MC-HV centrifugal filter units with a Durapore® PVDF 0.45 μm membrane (Millipore) were used.

2.8.2 Production of needles for plasmid injection

Borosilicate glass capillaries with filiment (Warner Instruments) were pulled at the laser-based micropipette puller P-2000 with the following settings: heat = 400, filament = 4, velocity = 50, delay = 125 and pull = 30. Wrongly pulled needles (laser needs more than two laser pulses or tip of one the two pulled needles is shorter than the other one) were discarded, all other needles were polished on the microgrinder EG-44 (Narishige) for 15 min at an angle of 30 ° and speed set to 80.

2.8.3 Preparation of embryos and injection procedure
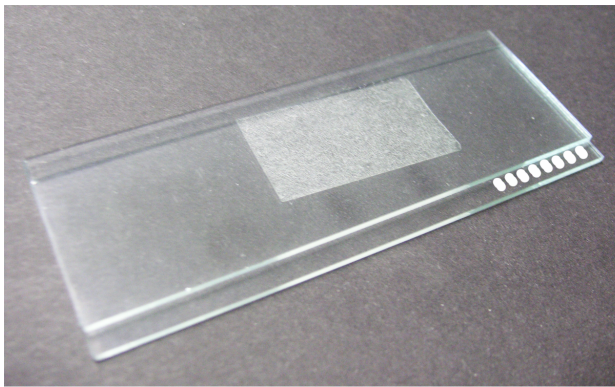
Adult beetles of the HC079 line were sieved, transferred on EL flour and put back to 30 °C. After an EL period of 1 h, freshly laid eggs were separated and transferred into an EL basket, embedded in a flour filled petri dish and incubated for one more hour at 30 °C. After this 2 h period, eggs were rinsed under warm, gently flowing tap water, removing most of the flour particles sticking to the eggs. Embryos were then mounted on a purpose-built set up (see Figure 2.1), with the anterior attached to the upper glass slide.

Figure 2.1: **Set up for lining up the eggs prior to embryonic injection.** Two glass slides were shifty attached to each other via a double sided tape, leaving enough space to line a single row of eggs (represented by white ovals) on top of the lower one. The anterior of each egg is in contact with the upper glass slide.

Normal drying of the before wet embryos was sufficient for adherens to the glass slide. The whole set up was fixed under a light microscope at RT. Prepared plasmid mix was shortly centrifuged prior to back loading into injection needles and connected to the FemtoJet® microinjector with pressure supply (Eppendorf). Injection at the posterior pole (next to the germ cells) was achieved by short pulses of pressure, triggered by the operator. After injection of all embryos ($\sim$ 120 per set up), the glass slides were transferred into a box filled with 15% NaCl, placed in an incubator at 30 °C and a RH of 50%. Placing the embryos in this environment should locally increase humidity, simulating conditions in the midst of flour in a normal culture box.

2.8.4 Crossing procedure and stock keeping

From the fourth to the sixth day after egg laying (AEL), hatched larvae were transferred twice daily with a fine brush into 30 ml *Drosophila* vials (Nerbe plus), filled with full flour. After pupariation, pupae were sexed, females and males were separated and incubated further until eclosion. Single crosses with uninjected adults of the HC079 line (P_1 cross) were set up (see Figure 3.3) in large blocks (built after [Berghammer et al., 1999a]). Eggs were collected in weekly intervals for three weeks, thereby increasing the number of potential heterozygous offspring. Embryos and larvae from those collections were left on EL flour plus added yeast until eclosion. Using a fluorescent microscope, adult beetles were screened for red fluorescence in the eyes, which served as a marker for proper integration of the *DsRed2* transgene into the germline. Heterozygous offspring expressing both DsRed2 and EGFP were subsequently sexed and single pair sibling crosses (F_1 cross) were set up in large blocks. Offspring of this F_1 cross were screened for homozygous DsRed2 expression. To verify on-target integration, embryos were additionally checked for expression of DsRed2 in the amniotic tissue, using a fluorescent microscope. Randomly picked beetles of these verified homozygous ones were sexed and single pair sibling crossed again (F_2 cross). Progeny of one these crosses was used to establish the transgenically modified rHC079 lines (#F, #W1, #W13, #N). As some of the offspring (in all cases only a small subset of the respective offspring is actually heterozygous for DsRed2 expression) of five of the P_1 crosses showed red fluorescence in the eyes, potentially five new lines could have established in the end. Due to the fact that one of these crosses lead to exactly one DsRed2 expressing beetle (the injected beetle already died after some days, leading to

an overall reduction in offspring), it was decided not to use this one further (another 'P$_1$ cross' would have to be set up), since after all just one successful integration event was needed to set up the new rHC079 line. So even with one loss the remaining four were assumed to be sufficient.

2.8.5 Verification of the exchanged transgene in the rHC079 lines

To verify the correct insertion of the transgene and simultaneously to test if the original transgene harboring EGFP was replaced by homology directed repair (original insertion took place at the piggyBac target site "TTAA" [Cary et al., 1989] at ChLG3:11827734..118 27737 (assembly 4.0 of the *Tribolium* genome; mapped by a former member of the lab)), various primers were designed to check the four rHC079 lines for different integration events. Primers are listed in Table 2.6 without product sizes, since these may vary depending on the *Tribolium* line and primer combination.

As template for PCR reactions, gDNA from the respective lines (wild type, HC079, #F, #W1, #W13, #N and a heterozygous cross between HC079 and #W13) was isolated as described in 2.2.1. PCR itself was performed according to 2.2.4. As product sizes up to ∼ 4 kb had to be expected when using the primers 'HC079 gDNA 5' fwd' and 'HC079 gDNA 3' rev' ('TTAA' site spanning primer set) to amplify the whole transgene, the extension time (step 4) (see Table 2.2) was increased to 5 min. Agarose gel electrophoresis (see 2.2.5) was performed to visualize the amplified PCR products. A 1% gel was used for the 'TTAA' site spanning primer set, for all others a 2% gel. Of the 25 μl total PCR reaction volume, 15 μl were applied onto the gels. The dye included in the REDTaq® ReadyMix™ PCR Reaction Mix was used to time the termination of the run.

As the presence of the whole construct at the expected location in the genome of all four rHC079 lines was now verified, the next step was to verify the sequences of different parts of the transgene by Sanger sequencing, to check for errors in the sequence introduced by the homology directed repair machinery. Most important was the transition from transgene to genome, as errors could be expected in this region. Primers 'iPCR#9' and 'HC079 gDNA 5' fwd' were used for the left border (defined by the left homology arm of the *piggyBac* transposon) and primers 'iPCR#14' and 'HC079 gDNA 3' rev' for the right border. Secondly, the attP site had to be checked using the primers 'attP gap

region fwd' and 'attP gap region rev', as its intact sequence is the prerequisite for future site-specific recombination via the ΦC31 integrase system. The last bit to be checked was the *DsRed2* transgene itself. Since red fluorescence was already used as the selection marker in the crossing procedure (see 2.8.4), an intact sequence was assumed. Because of this only two of the four rHC079 lines (#W13 and #N) were checked to verify this. Primers 'universal fwd' and 'universal rev' were used.

PCR reactions were performed according to the standard PCR cycling conditions in Table 2.2 and amplification of the product with the expected size was checked by gel electrophoresis (see 2.2.5). Still on the same day cloning of the PCR products into the pCR®II vector according to the manual of the TA Cloning® Kit Dual Promoter (pCR®II) (Invitrogen) was done. The *Thermus aquaticus Taq* polymerases adds a single deoxyadenosine (A) to the 3' ends of the PCR products, allowing the product to be ligated into the vector efficiently. As this 3' overhang degrades over time, thereby reducing ligation efficiency, cloning should be done on the same day as the initial PCR reaction. For each reaction 3 μl PCR product was used. Following the manual of One Shot® Mach1™-Ta^R Chemically Competent *E.coli* (Invitrogen), 2 μl ligation reaction were used for integration by transformation into *Escherichia coli* (*E. coli*) cells. 200 μl transformation mix were spread out on LB agar plates containing 100 μg/ml ampicillin and 40 μg/μl 5-bromo-4-chloro-3-indolyl-β-D-galactopyranoside (X-gal), in which X-gal was added to perform a blue-white screen. Selective plates were stored at 37 °C. On the next day five 'white' colonies from every plate were picked and each clone transferred into a separate bacterial culture tube, filled with 3 ml LB medium containing 100 μg/ml ampicillin. Before this transfer all clones were shortly dipped into a PCR premix (50 μl total volume (see Table 2.1), 1 μl of each 10 μM M13 fwd and rev primer (see TA Cloning® Kit Dual Promoter (pCR®II) manual for primer sequences)) and a colony-PCR was performed with an elongation time of 1 min 30 sec (see Table 2.2). Based on the resulting agarose gel electrophoresis (5 μl PCR product loaded (see 2.2.5)), those clones were chosen that showed a band of the expected size. All bacterial culture tubes containing a clone showing no band and therefore do not harbor any PCR insert, were dismissed. The remaining tissue culture tubes (two clones of each sample) were transferred to 37 °C and incubated while rotating over night. Plasmid purification was performed according to the manual of ZR Plasmid Miniprep™-Classic (Zymo Research), using 2.8 ml of the over

night culture as starting material. Plasmids were eluted in 20 μl nuclease free water and DNA concentration was determined with a NanoDrop 2000c spectrophotometer. Sanger sequencing was performed (see 2.8.1) and the resulting sequences were analyzed using the DNA sequence analysis software Sequencer™ (version 4.9, Gene Codes Corporation).

Table 2.6: Primers designed for detection of the transgene via PCR

PrimerID	Primers (5' → 3')	product size (HC079)	product size (rHC079)
attP gap region fwd	TGGTTTGTCCAAACTCATCAA	no product	405 bp
attP gap region rev	CCGAGTCTCTGCACTGAACA		
DsRed2 fwd	GAAGCTGAAGGTGACCAAGG	no product	506 bp
DsRed2 rev	GCTCCACGATGGTGTAGTCC		
EGFP A B fwd	CTTGTACAGCTCGTCCATGC		
EGFP A rev	ACGTAAACGGCCACAAGTTC	653 bp	no product
EGFP B rev	GCATCGACTTCAAGGAGGAC	335 bp	no product
HC079 gDNA 5' fwd	AGCTGGCGTGTTACTTCACC	3764 bp	3276 bp
HC079 gDNA 3' rev	ACGTTCCCTAACCCGAGAAT		
iPCR#9	CGCGCTATTTAGAAAGAGAGAG	563 bp	563 bp
iPCR#14	CGATAAAACACATGCGTCAATT		
universal fwd	TAAACAAGCGCAGCTGAACA	888 bp	858 bp
universal rev	GGGAGGTGTGGGAGGTTT		

2.8.6 Comparison of the relative DsRed2 signal in all four rHC079 lines

To test if the four rHC079 lines (#F, #W1, #W13 and #N) differ from each other in regard of their fluorescent signal strength, at what time in embryogenesis this signal is first detectable and how it progresses, live imaging experiments were performed.

First of all five individual ELs were set up, one for each of the rHC079 lines and one for the nGFP line, which served as a control in all experiments. After an EL period of 1 h, the eggs were transferred into EL baskets and incubated for 18 h at 30 °C (see also 2.1.2). Subsequently, eggs were prepared for live imaging as described in 2.7. Imaging

was started $\approx$ 20 - 21 h AEL, which is shortly before germ band extension has finished and the time when the fluorescent signal should rise over background levels [Hilbrant et al., 2016]. 12 images (z-stack thickness $\sim$ 88 μm, spacing = 8 μm) were taken every 10 min for 40 h at 30 °C, leading to a recording of 241 time-points. This means that embryogenesis was recorded from 20.5 h +/- 0.5 h to 60.5 h +/- 0.5 h AEL. The executed four discrete live imaging experiments (each one with all five lines) were performed with the DeltaVision™. As recommended in the manual for DsRed2, the 'mcherry' filter (part of the live cell filter set) was used and the exposure time was set to 200 ms. Image resolution was set to 640 x 480 and a binning of 2 x 2 used. After acquisition all image files were processed using ImageJ, executing a macro supplied by Thorsten Horn (see 6.1). This macro makes a z-projection of all images at each time-point and transforms the original file format into a tiff-file. All movies were surveyed and only those were used for further analyses, in which the embryo showed wild type development and was oriented in a complete lateral view. The latter restriction was chosen to preserve comparability between individual embryos. Next the new file was opened in ImageJ. Using 'polygon selections' the region of interest (ROI), which was the complete egg for this analysis, was defined and by 'fit spline' refined. The ROI was scanned using the 'ROI manager' and the preselected value 'integrated density', which is the sum of the values of the pixels in the selection, was displayed. The integrated density values were plotted as relative DsRed2 signal over the time-points to create the graph seen in Figure 3.7.

Chapter 3

Results

3.1 Targeted knock-in via CRISPR/Cas9 and homology directed repair

In order to enable distinct visualization of different tissues in heterozygous *Tribolium* embryos generated by crossing of two fluorescent lines, the enhancer trap line HC079 [Hilbrant et al., 2016] was modified by replacing the *EGFP* transgene (part of the plasmid pBac[3xP3-EGFPaf] [Trauner et al., 2009]) with *DsRed2*. This replacement was performed via a combination of the CRISPR/Cas9 gene editing technique, introducing a double strand break in the *EGFP* transgene, and the homology directed repair (HDR) mechanism triggered by homology between the *EGFP* transgene construct of the line HC079 [Trauner et al., 2009] and a donor plasmid harboring the *DsRed2* gene. The donor plasmid pBac[3xP3DsRedattP] [Yonemura et al., 2013] contains *DsRed2* under the control of an artificial 3xP3 promoter. This promoter drives expression in the eyes [Sheng et al., 1997], which was used as a transformation marker during screening of adult beetles in the process of establishing a homozygous DsRed2 line. 3xP3 is also responsive to nearby chromosomal enhancers [Lorenzen et al., 2003] and has been used for the original GEKU screen [Trauner et al., 2009]. Consequently, the newly introduced DsRed2 construct should drive the same amniotic expression in the red HC079 (rHC079) line as it did in the original HC079 line [Hilbrant et al., 2016]. Cas9 protein translated from an injected expression vector was used to create a double strand break in the *EGFP* sequence, guided there by an *EGFP*-specific gRNA. In zebrafish this gRNA achieved the highest efficiency in disrupting the *EGFP* open reading frame compared to other tested gRNAs [Auer et al., 2014]. By co-injection of the donor plasmid harboring only slightly

shorter homology arms than the original *piggyBac* transposon of the GEKU lines [Horn and Wimmer, 2000; Trauner et al., 2009], HDR was initiated and the *DsRed2* transgene was successfully integrated into the germ line.

3.1.1 Replacement of the *EGFP* transgene with a *DsRed2* transgene in the line HC079

To estimate how many embryos of the HC079 line would survive the stress caused by physical penetration of the egg and the subsequent treatment (see 2.8.3), eggs were mock injected with water. The enhancer trap line G12424 [Koelzer et al., 2014] served as a control, as it was originated from the same enhancer trap screen [Trauner et al., 2009]. For each line 400 eggs were injected and all larvae that hatched four to six days after injection were counted. The survival rate was 70% and 62% for the HC079 and G12424 lines, respectively (Figure 3.1).
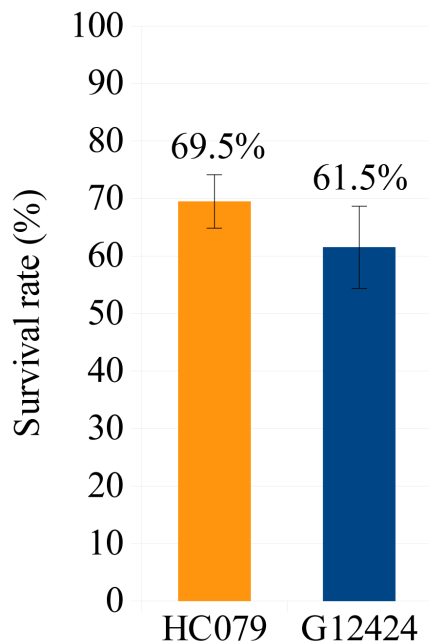
Figure 3.1: **Survival rate of mock injected embryos in the lines HC079 and G12424.** Eggs of both transgenic lines were handled as described in 2.8.3 but injected with water. The survival rate is the mean number of hatched larvae in four discrete experiments conducted on different days. Treated the same way, HC079 (n = 400) shows a 8% higher survival rate than G12424 (n = 400).

The replacement of *EGFP* with *DsRed2* is shown schematically in Figure 3.2. It

shows the double strand break induced by the Cas9 endonuclease, after it was guided to *EGFP* by the specific gRNA. Subsequently, the homology directed repair machinery starts to repair the broken DNA strand by searching for homologous sequences on other DNA strands. Normally this is the sister chromatid but it can also be a co-injected donor [Moehle et al., 2007]. In this case the homology is between the two *piggyBac* arms on each side of the respective construct (700 bp on the left side and 1300 bp on the right side of both constructs) and an internal 300 bp stretch within *piggyBac*. Thus, the homology directed repair machinery uses the part between the homology arms of the donor plasmid to repair the broken EGFP construct within the HC079 line, integrating the DsRed2 construct into the genome of the injected beetle.
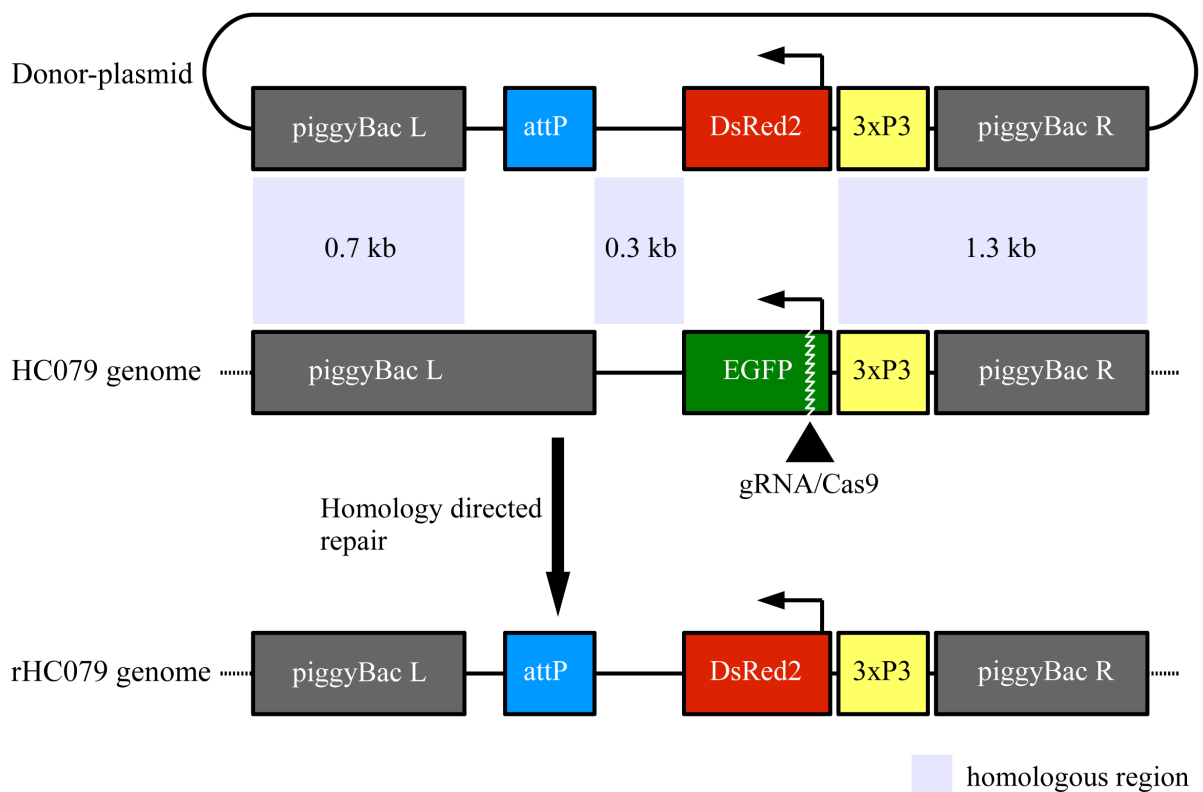
The donor plasmid pBac[3xP3DsRedattP] was modified from the fluorescent transformation marker pBac[3xP3DsRed afm] [Horn et al., 2002] by insertion of an attP sequence [Yonemura et al., 2013]. The attP sequence is part of the ΦC31 integrase system, used for site-specific integration [Bischof et al., 2007; Huang et al., 2009], providing a landing site for subsequent insertion of additional constructs. Another benefit of using this plasmid

Figure 3.2: **Schematic illustration for replacing the EGFP construct with the DsRed2 construct**. The donor plasmid harbors two *piggyBac* arms (left (L) and right (R)), an attP sequence, the 3xP3 promoter and the *DsRed2* transgene. The EGFP construct of the original HC079 line harbors somewhat longer *piggyBac* arms, a 3xP3 promoter and the *EGFP* transgene. Homology between the two constructs is supplied via 700 bp of the left *piggyBac* arm and 1300 bp on the right side of the construct by the 3xP3 promoter sequence and the complete right *piggyBac* arm. Additional 300 bp of homologous sequence are between the transgene and the attP sequence. The different homologous parts are the result of the fact that both constructs derived from the same source [Horn and Wimmer, 2000]. The double strand break, induced by co-operation of the gRNA and Cas9 (black arrowhead) is indicated by the jagged line. In the next step the homology directed repair machinery uses the donor plasmid as a template for the repair of the double strand break, thereby replacing the complete construct. Distances are not to scale.

is the homology of the *piggyBac* arms to the ones of the target construct. Slight differences in the size of the left *piggyBac* arm are due to the removal of approximately 800 bp in the transposase open reading frame via restriction enzymes, to inhibit any potential relocation of the transposon [Horn and Wimmer, 2000].

1992 embryos of the HC079 line were injected, of which 11.5% hatched but only 7.9% survived to adulthood (Figure 3.3A) and were back-crossed to beetles of the HC079 line (P_1 cross). The offspring of these crosses were examined for DsRed2 expression in their eyes, which is driven by the 3xP3 promoter [Sheng et al., 1997] and can therefore be used as a marker for successful integration of the transgene into the genome [Horn and Wimmer, 2000]. Offspring of 5 out of 157 embryos (3.2%) showed DsRed2 and EGFP expression in the eyes (Figure 3.3B), confirming that the DsRed2 construct was successfully integrated into the germ line of the injected P_0 embryos. However, one P_1 cross yielded only one single DsRed2 positive offspring before the parents prematurely died. To obtain homozygous beetles of the four remaining lines, an intercross between siblings was set up (F_1 cross). Consistent with the second law of Mendelian inherence (Law of Independent Assortment), roughly 25% of the offspring showed only DsRed2 expression in the eyes (Figure 3.3C). These homozygous embryos were again sibling crossed in an incross, to establish four individual rHC079 lines (named #F, #W1, #W13 and #N) (Figure 3.3D).

Already the heterozygous offspring of the P_1 cross was checked for on-target integration of the transgene under the control of the expected amniotic enhancer. This is necessary, although DsRed2 expression is not a reliable sign for on-target integration in

A **Embryonic injection**
of HC079
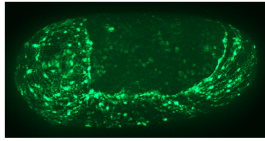
→survival rate: 7.9%
  (n = 1992)

B **P$_1$ cross**
injected   uninjected

X
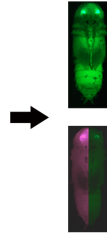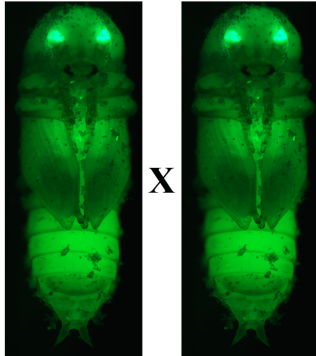
→homozygous offspring (EGFP): 96.8%
  (n = 157)

→**heterozygous offspring**: 3.2%
  (n = 157)

C **F$_1$ cross**
(sibling cross)

X
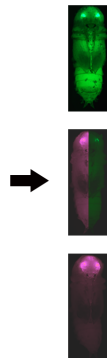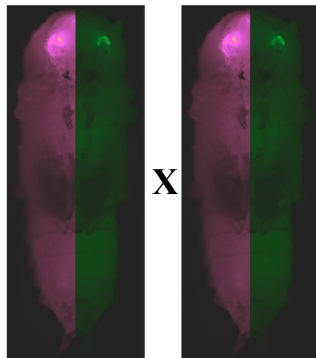
→homozygous offspring (EGFP): 24.5%
  (n = 1258)

→heterozygous offspring: 52.5%
  (n = 1258)

→**homozygous offspring** (DsRed2): 23.0%
  (n = 1258)

D **F$_2$ cross**
(sibling cross)

X
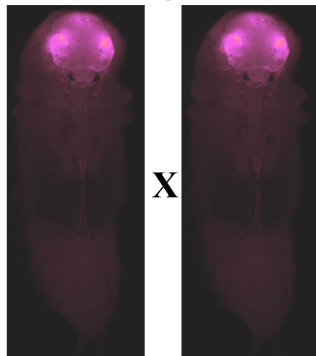
→four individual **rHC079** lines were
  established

Figure 3.3: **Screening procedure to establish homozygous lines, using DsRed2 expression in the eyes as a transformation marker.** (**A**) 1992 eggs of the amniotic line HC079 homozygous for EGFP expression in the amnion were injected at the posterior pole, next to the germ cells. 7.9% eclosed to become adult beetles. (**B**) All adult beetles were back-crossed into the original HC079 line in single pair matings. The offspring of this P_1 cross was screened for DsRed2 expression in the eyes, which served as a transformation marker. In total, five mate pairs (3.2%) produced offspring heterozygous for both markers in the eyes. (**C**) Single pair F_1 sibling crosses between heterozygote offspring were set up for four of the five lines (see main text). As expected, an approximate ratio of 1:2:1 (homozygous EGFP:heterozygous EGFP/DsRed2:homozygous DsRed2) was obtained. (**D**) In order to establish four independent lines homozygous for DsRed2 expression in the amnion, the F_2 cross between DsRed2 only beetles was set up as a series of single pair sibling crosses. All progeny were homozygous for DsRed2 and were used to establish the new rHC079 lines (named #F, #W1, #W13 and #N).
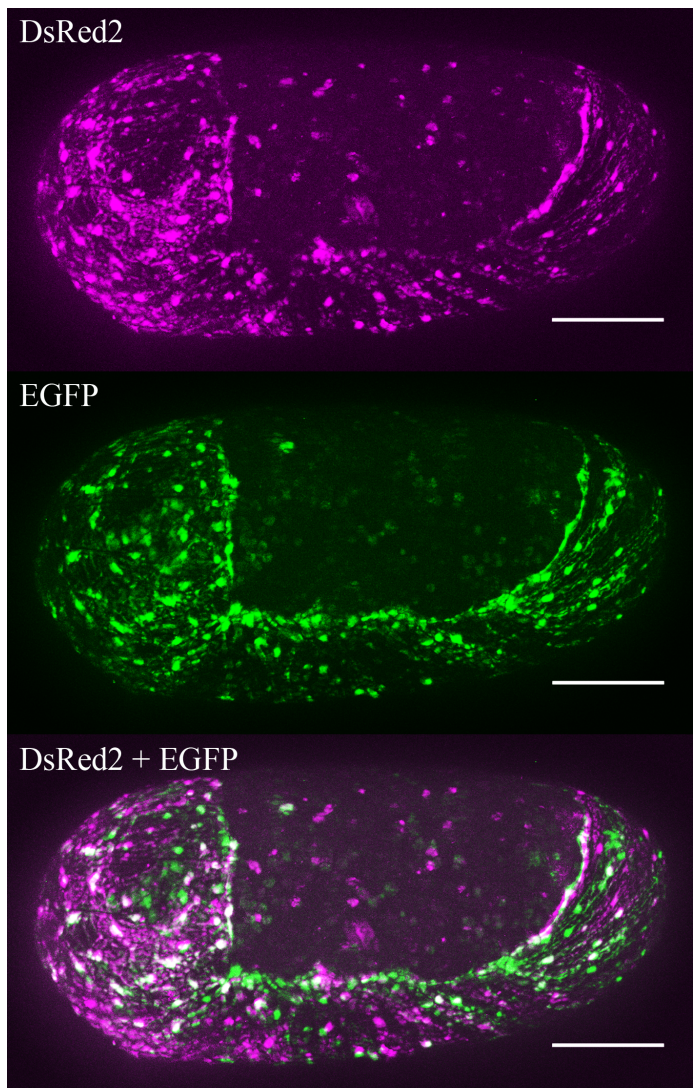
Figure 3.4: **EGFP and DsRed2 expression in the amnion of a heterozygous embryo.** Two images taken from the same embryo, which is an offspring derived from a cross of the HC079 line with the rHC079 line #W13. The one on top visualizes DsRed2 expression in the amnion and the one in the middle EGFP expression in the same amniotic tissue. The lowest picture is an overlay of DsRed2 and EGFP expression in the amnion, confirming that *DsRed2* is under control of the same amniotic enhancer as *EGFP*. Scale bars are 100 μm.

this step, as 3xP3 can drive eye expression even if integrated elsewhere, leading to a false-positive signal. For this, heterozygous beetles were crossed and their embryos investigated for DsRed2 expression in the amnion. Figure 3.4 shows an example embryo with successful on-target integration expressing both *EGFP* and *DsRed2*. In the upper picture DsRed2 is clearly expressed in the amnion, similar to EGFP in the middle picture, which represents the original expression in the line HC079. The overlay of both transgenes' expression patterns in the lower picture shows that DsRed2 truly is expressed in the amnion, as both expression patterns encompass the exact same area within the egg, with exactly the same border towards the yolk.

3.1.2   Verification of the newly integrated DsRed2 construct

Although in all four rHC079 lines DsRed2 was shown to be expressed in the amnion, it was tested if a complete replacement of the EGFP construct and also a complete insertion of the DsRed2 construct had taken place. To verify this, several distinct primer pairs (Figure 3.5) were applied in different PCR reactions using gDNA isolated from each line (Figure 3.6).

Figure 3.5 illustrates all primer pairs and their location within the genome/construct of each individual line used for the analyses. The wild type San Bernardino strain, as well as the original HC079 line were used as negative and positive controls.

In Figure 3.6A the two genomic primers spanning the original integration site of the EGFP construct (marked by the "TTAA" target motif of the *piggyBac* transposon [Cary et al., 1989]; see also black arrows in Figure 3.5) were used to test if the EGFP construct was replaced by the DsRed2 construct. This could be verified for three of the lines (#F, #W1 and #N) but not for #W13. However, genomic DNA isolated from a cross between the HC079 line and the #W13 line yielded bands for both inserts. Despite the results with genomic DNA from #W13 only, this indicated successful integration of the whole
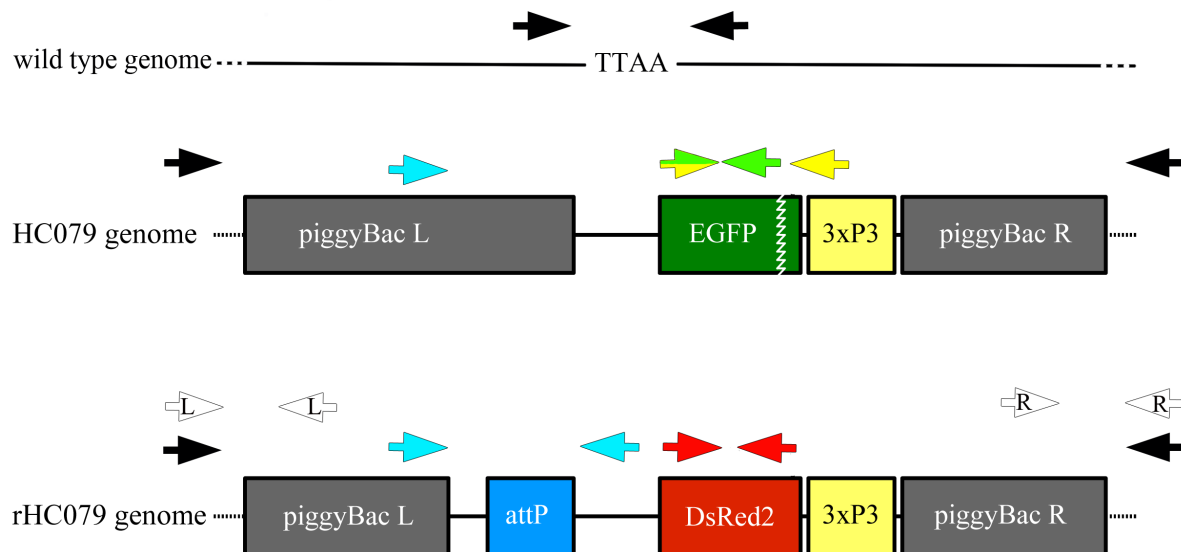
Figure 3.5: **Positions of the primers used for verification of the DsRed2 construct.** Illustrated are the wild type genome, the EGFP construct located in the original HC079 genome and the DsRed2 construct inserted in the rHC079 genome. The sequence 'TTAA' marks the genomic location in which the EGFP construct was inserted in the HC079 line [Trauner et al., 2009] (see main text). The black arrows are a genomic primer pair ('HC079 gDNA 5' fwd' and 'HC079 gDNA 3' rev') to test the integration of the whole insert (see Figure 3.6A). The two white arrow pairs are spanning the border between the genome and the DsRed2 construct on either the left (L; 'iPCR#9' and 'HC079 gDNA 5' fwd') or the right (R; 'iPCR#14' and 'HC079 gDNA 3' rev') side of the DsRed2 construct (see Figure 3.6B). The colored arrows directly correspond to the respective colors used in Figure 3.6C and were used for testing of individual sequences of the constructs. The green and yellow arrows are all three located within the *EGFP* sequence, in which the mixed arrow is associated with the both the green ('EGFP A B fwd' and 'EGFP B rev') and the yellow ('EGFP A B fwd' and 'EGFP A rev') primer. The red primer pair ('DsRed2 fwd' and 'DsRed2 rev') and the blue primer pair ('attP gap region fwd' and 'attP gap region rev') were used for verification of the *DsRed2* and attP sequence, respectively.

A
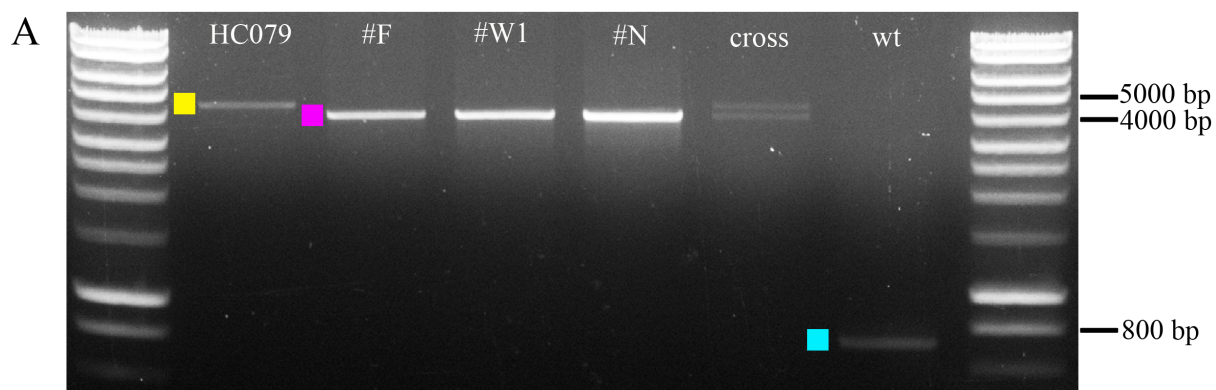
□ whole insert with EGFP construct: 4473 bp

□ whole insert with DsRed2 construct: 3985 bp

□ no insert: 713 bp (genomic sequence)

B
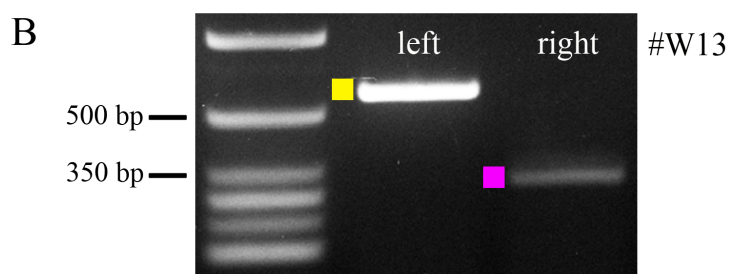
□ left insert border: 563 bp

□ right insert border: 318 bp

C
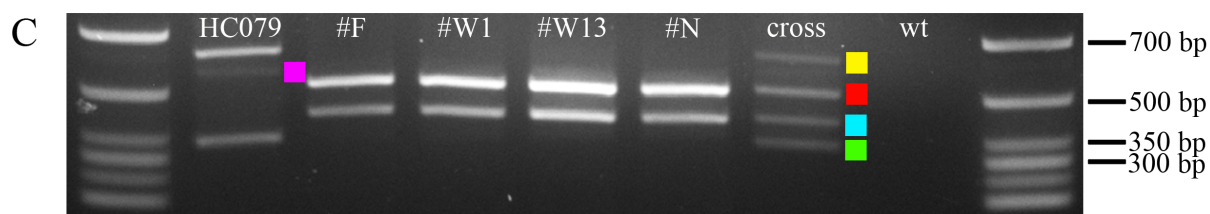
□ long EGFP: 653 bp

□ DsRed2: 506 bp

□ attP: 405 bp

□ short EGFP: 335 bp

□ inter primer pair binding: 573 bp

Figure 3.6: **Verification of all parts of the DsRed2 construct in the four rHC079 lines via PCR.** (**A**) Genomic primer pair (see also black arrows in Figure 3.5) encompassing the whole insert, to check for its complete integration. In the original HC079 line (4473 bp), in the three rHC079 lines #F, #W1 and #N (3985 bp), as well as in the cross (HC079 line x #W13 line) the respective construct(s) were detected. In the San Bernardino strain (wt), a band of the expected size is detected (no insert control). (**B**) In **A**, integration of the whole insert in the #W13 line could not be proven directly but indirectly in the cross. To verify the result, two primer pairs were used to check the integration of the insert at its left and right construct border (see also white arrows in Figure 3.5). In both cases bands of the expected size were yielded and integration of the insert in the #W13 line at the right genomic spot proven. (**C**) Single PCR reaction with four different primer pairs to verify the presence of the two transgenes and the attP sequence (see also colored arrows in Figure 3.5). The four rHC079 lines show two bands of corresponding size, one for DsRed2 and one for the attP sequence. In the HC079 control three bands are visible. One for long EGFP, stretching over the double strand break and short EGFP, which does not stretch over the break (see main text). The third band at 573 bp is due to binding between two primers of different primer pairs ('attP gap region fwd' and 'EGFP B rev'). In the cross all four (and weakly the fifth) bands are detected at the expected size, in contrast to the no insert control (wt).

DsRed2 construct. To verify the result, two primer pairs, each one spanning the border between the genome and the DsRed2 construct on either side (see also white arrows in Figure 3.5), were used for #W13 only (Figure 3.6B). The distinct bands confirmed the integration of the DsRed2 construct at the correct genomic location in the #W13 line. This leaves the possibility that the PCR performed in Figure 3.6A did not work well or at all with the line #W13, even though it was repeated several times. A possible reason for this could be degradation of the genomic DNA isolated from the #W13 line.

The results in Figure 3.6A and B already indicated that in all rHC079 lines the complete DsRed2 construct was inserted at the right genomic location, while replacing the EGFP construct (further supported by expression of DsRed2 under the control of the amniotic enhancer (see Figure 3.4)). To further confirm these results and specifically verify the insertion of the *DsRed2* sequence and the loss of the *EGFP* sequence, as well as the attP sequence, four distinct primer pairs were designed (see also the colored arrows in Figure 3.5). The two *EGFP* primer pairs were used to assess the possibility that during the process of homology directed repair *EGFP* was at least partially not replaced. Figure 3.6C illustrates that in the rHC079 lines indeed all expected sequences are present. Likewise, the *EGFP* sequences could not be detected in the rHC079 line but in the original

HC079 line and the cross.

To conclude this part of the analysis and check for possible errors done by the homology directed repair machinery, specific parts of the DsRed2 construct were amplified in PCR reactions and the products were sent for sequencing (see 2.8.5). The complete *DsRed2* sequence, the attP sequence and the transition from construct sequence to genomic sequence on both ends were sequenced. This was done for all four rHC079 lines (in the case of the genome - construct border the original HC079 line was sequenced as a control as well; the *DsRed2* sequence was sequenced in the lines #W13 and #N only). In none of the sequenced PCR products was any error in the DNA sequence detected (data not shown). This implies that perfect integration of the whole DsRed2 construct by concurrent removal of the EGFP construct in the rHC079 lines was achieved.

3.1.3 Comparison of the *DsRed2* signal strength between the four rHC079 lines

On the sequence level there is no difference between the four rHC079 lines, each one originating from a distinct knock-in event in a single embryo. As these lines were established for live imaging purposes, the signal strength of DsRed2 was tested in four discrete live imaging experiments (one recording of an embryo of the #W13 rHC079 line is included on the DVD; see 6.7 movie 1).

In each experiment all four lines have been imaged simultaneously, to control for inter-experiment variations. The integrated density (relative DsRed2 signal * region of interest; [Koelzer et al., 2014; Hilbrant et al., 2016]) was measured and plotted against the developmental age relative to amniotic rupture, which happens almost simultaneously with serosal rupture [Hilbrant et al., 2016]. The resulting curves are shown in Figure 3.7. All rHC079 lines display an overall similar progression of their signal intensity. It rises until rupture, after which it declines (more pronounced in #W1 and #N; the surface area of the amnion decreases after rupture, therefore the signal gets weaker), rises again until it reaches its maximum (formation of the amniotic dorsal organ goes along with an increase of the signal) and declines (when the amnion sinks down into the yolk and degenerates, the signal decreases again) in each of the lines. Except in the very onset of expression and after amniotic rupture, where #F becomes transiently stronger than #N, the order of the lines regarding the signal strength is very constant. #W1 exhibit
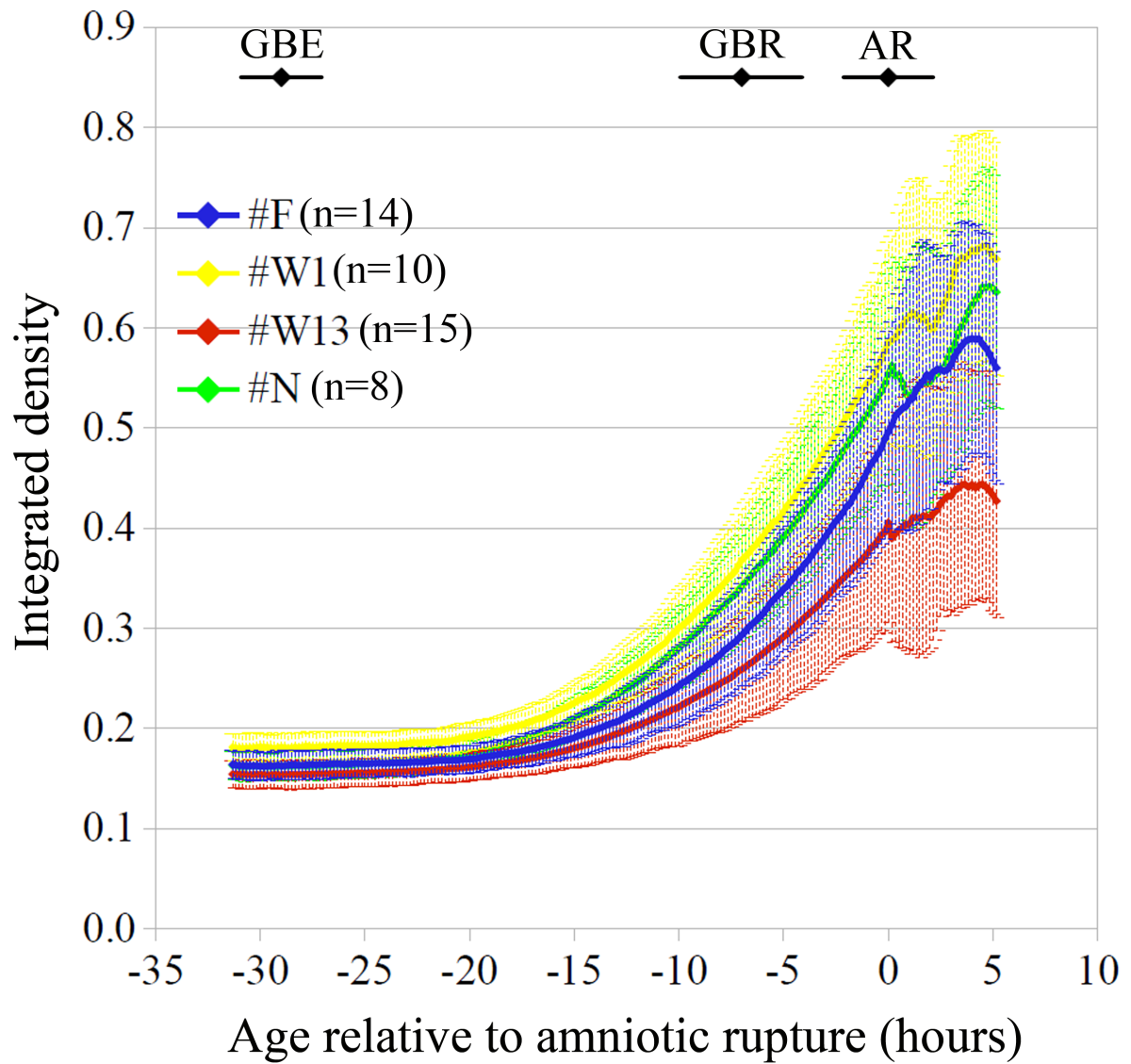
Figure 3.7: **Comparing the signal strength of DsRed2 in all four rHC079 lines.** In four discrete experiments, all lines were imaged simultaneously. The DsRed2 signal was recorded for 35 hours during development. Imaging started 20.5 h +/- 30 min after egg laying. The embryos were imaged at a constant temperature of 30 °C. All individual recordings were aligned by amniotic rupture. The integrated density (relative DsRed2 signal) was plotted against time. Error bars represent the mean standard deviation. GBE = germband extension; GBR = germband retraction; AR = amniotic rupture.

the strongest DsRed2 signal strength, followed by #N and #F. Only the weakest line, #W13, is considerably different, as the increase of the slope is slower throughout germband extension and retraction. Considering the intra- and inter-slide variation, these results indicate that lines #F, #W1 and #N possess similar expression strength, while line #W13 seems to be weaker.

3.1.4 Cross of the rHC079 line with different *EGFP* expressing lines

To show the potential of the new rHC079 lines for multiple-labeling experiments, the line #W13 was crossed to the *EGFP* expressing lines G12424, G04609 and G04910 (Figure 3.8).

In Figure 3.8A, the rHC079 line (red) is crossed with the line G12424 (green), which expresses *EGFP* in the serosa [Koelzer et al., 2014]. The images visualize both membranes at the start of extraembryonic membrane rupture (two movies of the heterozygous embryo expressing DsRed2 in the amnion and EGFP in the serosa are included on the DVD; see 6.7 movies 2A and 2B). In Figure 3.8B, the rHC079 line is crossed with the line G04609, which expresses *EGFP* amongst other in the cardioblast cell row [Koelzer et al., 2014] (white arrow; see also Figure 3.25 for a description of the other expression domains). As evident from the two cardioblast cell rows, which did come together at the dorsal midline and the residual *DsRed2* expression on top of them, the embryo is just finishing dorsal closure. Figure 3.8C is the same cross but a different embryo, where the amnion is withdrawing over the lateral flank of the embryo. In Figure 3.8D, the rHC079 line is crossed with the line G04910 (characterized in this study; see Figure 3.24). The amnion hast just withdrawn over the posterior pole and forms the amniotic dorsal organ.
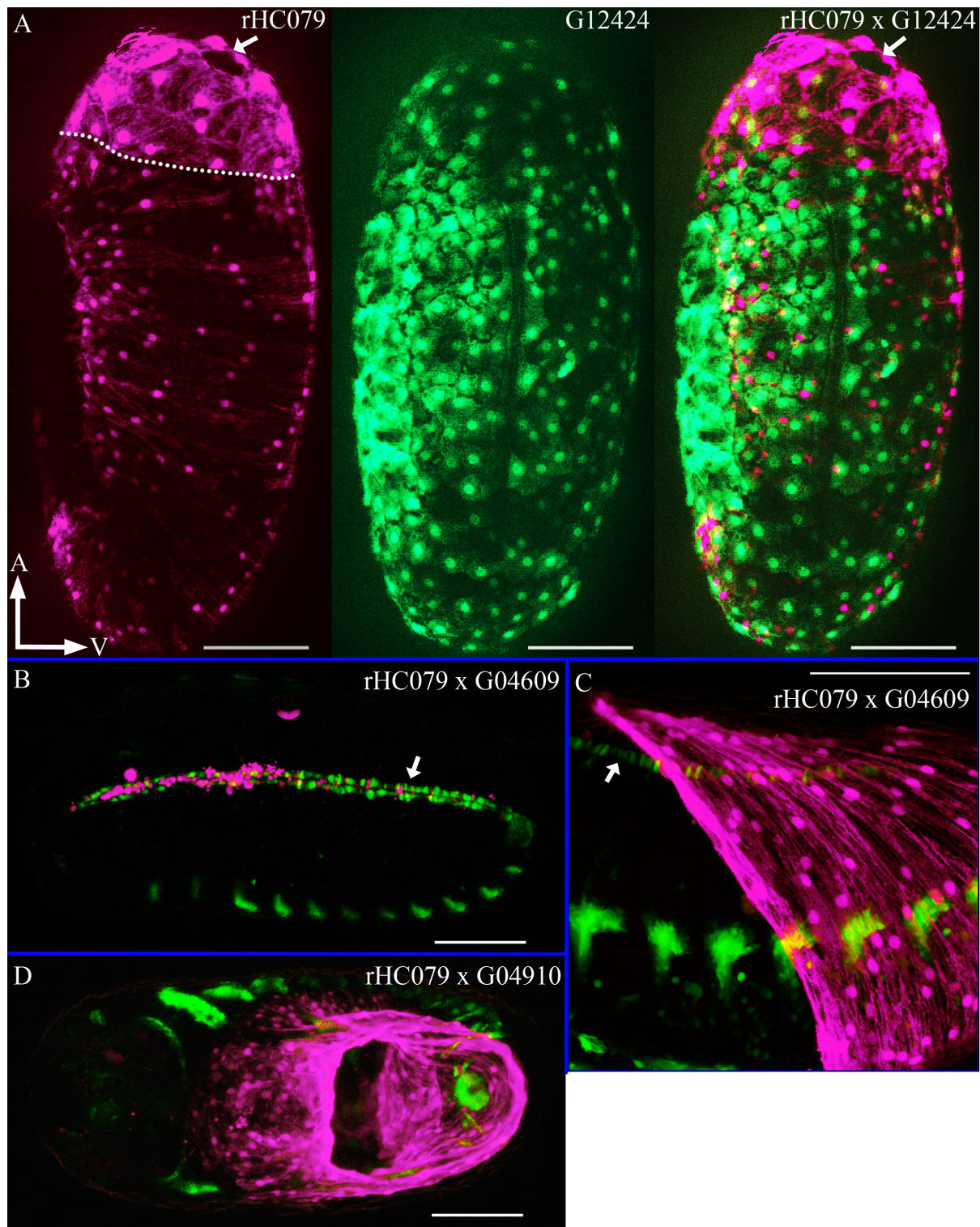
Figure 3.8: **Visualization of different crosses, using two fluorescent proteins.** (**A**) Cross of the rHC079 line with the G12424 line. The left image shows the DsRed2 channel only, the middle one the EGFP channel only and the right image is an overlay of both channels. The site of rupture in the amnion is marked by the white arrows (opening in tissue) and the anterior cap region is separated from the rest of the amniotic tissue via the white dashed line. (**B** and **C**) Cross of the rHC079 line with the G04609 line. *EGFP* expression within the cardioblast cell row(s) is marked by the white arrows. **C** was imaged at a higher magnification than **B**. (**D**) Cross of the rHC079 line with the G04910 line. The orientation of the embryo in **A** is as indicated in the image, while **B** is a dorso-lateral view, **C** a lateral view and **D** a dorsal view. Scale bars are 100 μm in **A, B** and **D** and 50 μm in **C**

3.2 Phenotypic analyses of the amniotic marker gene *Tc-pnr* after knock-down

The function of *Tc-pnr* in embryonic and extraembryonic development of *Tribolium* is not known. So far it has been used solely as a marker for the amnion [van der Zee et al., 2005, 2006; Nunes da Fonseca et al., 2008] and to a lesser extent as a marker for the heart [Cande et al., 2009]. However its expression in the early amnion makes it a promising target for the research on extraembryonic membrane formation of the amnion. This is especially true, as no other gene known to be expressed in the amnion was investigated functionally so far.

Therefore, the following analyses provide the first complete description of its expression pattern throughout embryonic development, as well as the description of its main phenotype after parental RNA interference (pRNAi). In depth functional analyses also revealed its impact on the morphological structure and integrity of the amnion. Furthermore conservation of its role during heart formation and dorsal closure compared to its *Drosophila* ortholog, as well as for its regulatory function on *Tc-iro*, was proven.

3.2.1 Expression pattern of *Tc-pnr* throughout *Tribolium* development

Tc-pnr was used mainly as a marker for the dorsal and the anterior amnion at the differentiated blastoderm stage [van der Zee et al., 2005, 2006; Nunes da Fonseca et al., 2008] and to stain the heart in retracted germband embryos. Additionally, *Tc-pnr* expression was reported in an unspecified extraembryonic tissue domain during germband extension

[Cande et al., 2009]. In order to complete the *Tc-pnr* expression pattern until early extraembryonic membrane formation and to verify the sparse information on subsequent development, *Tc-pnr* expression was investigated throughout the complete embryonic development of *Tribolium* (Figure 3.9 - Figure 3.12).

Tc-pnr is first expressed at the onset of the differentiated blastoderm stage in the dorsal part of the anterior amniotic fold, in the dorsal amnion and in amniotic cells around the developing primitive pit (Figure 3.9A and A`). At the onset of involution, *Tc-pnr* expression persists in the anterior amniotic fold (in some embryos weak *Tc-pnr* expression expands along the ventral part of the fold) and in the progressed posterior fold (Figure 3.9B and B`). When the serosal window has formed, *Tc-pnr* is expressed in amniotic cells around its edge and in the amnion over the segment addition zone (former growth zone; [Nakamoto et al., 2015]) (Figure 3.9C and C`). At this stage, the *Tc-pnr* expressing amniotic cells at the rim are not yet covered with serosal cells but are already mostly curving around the edge of the serosal window (Figure 3.9C``). The expression in the rim itself is discontinuous and consists out of two domains over the developing head lobes and one larger domain at its posterior border. As the serosal window is closing, the three domains come together except at the anterior (Figure 3.9D and D`). At the same time *Tc-pnr* expression expands in the amnion over the head lobes, as those start to develop. Just anterior of *Tc-pnr* expression in the amnion covering the segment addition zone, another expression domain within the amnion (see Figure 3.9D``) arises during constriction of the serosal window.

When the serosal window has almost closed, *Tc-pnr* is still expressed around its entire circumference, except its most anterior rim (Figure 3.10A and A`), most similar to Figure 3.9D and D`. Note that in Figure 3.10A fewer cells around the serosal window are stained compared to Figure 3.9D. The reason for this is that the number of stained cells is different in each embryo and that the shape of the serosal window is subject to minor variability. When the serosal window has closed, the *Tc-pnr* expressing cells then form a characteristic y-shape (Figure 3.10B and B`). From anterior to posterior, until the head has extended over the anterior pole, the middle part of this y is 17 +/- 1 *Tc-pnr* stained cells long (n=10; standard deviation = 0.84) (Figure 3.10B``). At this time *Tc-pnr* expression spreads greatly in the amnion covering the head lobes. This expansion continues throughout germband extension (Figure 3.10C-D and C`-D`). A new feature
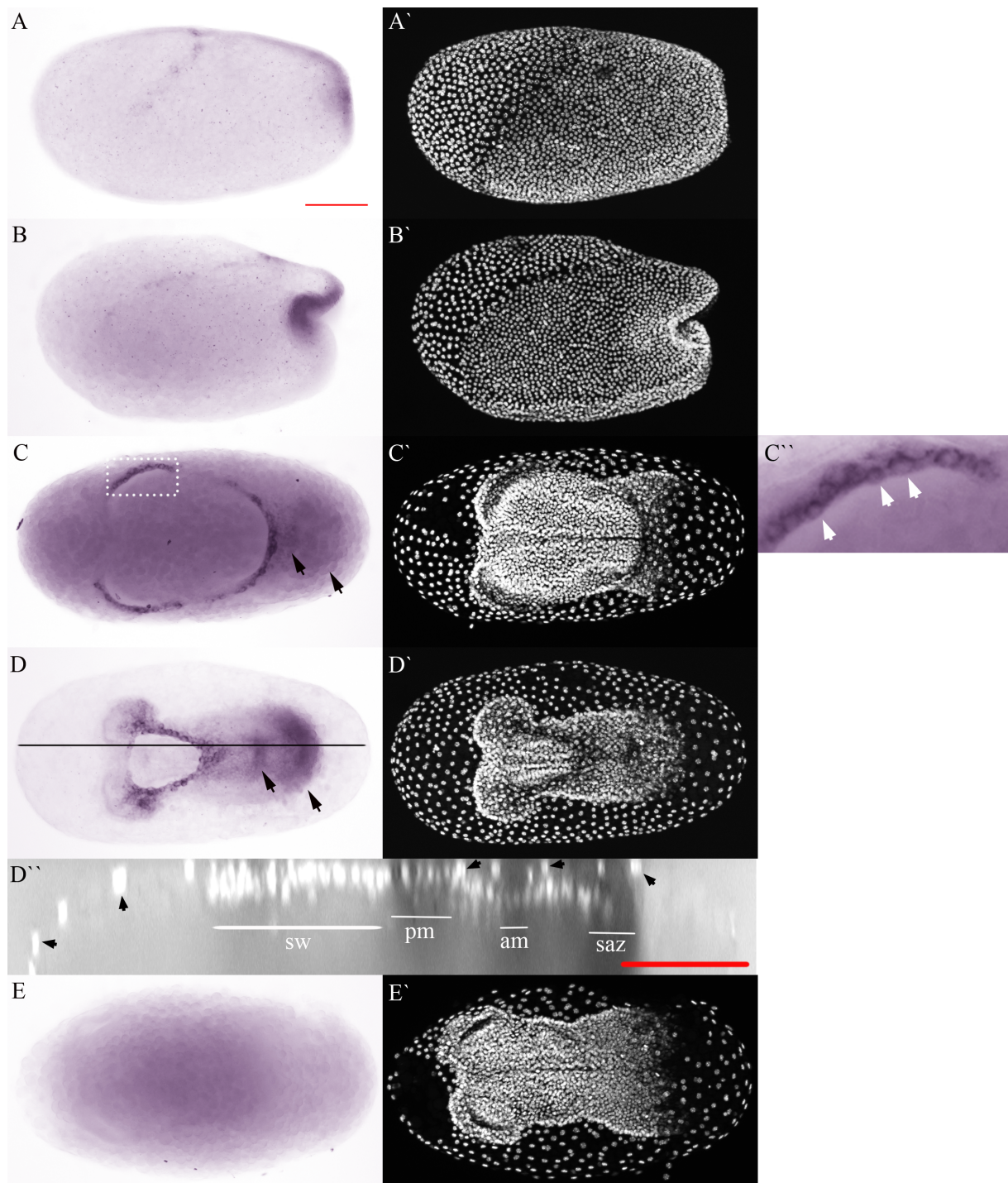
Figure 3.9: **Early dynamic expression pattern of *Tc-pnr***. (**A-E**) Embryos stained for *Tc-pnr* via *in situ* hybridization, in which (**E**) was the background control (using *Tc-pnr* sense probe). (**A`-E`**) Respective DAPI counterstain. (**D``**) Overlay of one optical slice of the images **D** and **D`** in black and white. (**A**) Embryo at the differentiated blastoderm stage, where *Tc-pnr* is expressed in the dorsal half of the anterior amniotic fold, in the dorsal amnion and in amniotic cells around the developing primitive pit. (**B**) Discontinuous expression of *Tc-pnr* persists in the anterior amniotic fold as the two other expression domains start to involute within the posterior fold. (**C**) After formation of the serosal window, *Tc-pnr* is strongly expressed in the rim of the serosal window in three distinct domains. *Tc-pnr* expression is also detected in the amnion covering the segment addition zone (right arrow) and weakly just anterior to this domain (left arrow). The area within the white rectangle is enlarged in **C``**. It shows three cells (marked by white arrows), which start to curve around the rim of the serosal window. (**D**) While the serosal window closes, *Tc-pnr* expression in its posterior rim extends slightly more into the posterior amnion and all three domains are now connected except in the anterior rim. As the head lobes develop, *Tc-pnr* starts to be expressed in the amnion covering those. Compared to **C**, the expression domain of *Tc-pnr* (left arrow) is now clearly distinct from the expression in the segment addition zone (right arrow). An orthogonal section along the whole egg length (black line) is enlarged in **D``**. It shows the expression of *Tc-pnr* in its three expression domains in the posterior margin of the serosal window (pm), in the segment addition zone (saz) and in amniotic cells (am) right between these two (sw = serosal window). Black arrows point to some serosal cells in the outermost cell layer. (**E**) The background control of an embryo at a developmental stage between **C** and **D** indicates that even the thick embryonic tissue does not lead to any unspecific staining. Scale bars are 100 μm. **A** and **B** are lateral views, **C-E** are ventral views.

of the amnion starting shortly after closure of the serosal window that was visualized via *Tc-pnr* staining, is the nuclei free spaces within the tissue (Figure 3.10E-E``and Figure 3.11A). This characteristic feature can be detected at least until full extension of the germband. Thus, the amnion looks perforated, although there are no actual holes in it. Neither are there unstained amniotic cells (see also Figure 3.11A-A```). In all investigated embryos these nuclei free spaces could be seen (n=15). Biological interpretation of this feature is difficult, as these 'holes' do not correspond to any obvious embryonic structure, nor are they solely located in areas of the amnion which are exposed to strong tension, as one could consider it is the case around the curved poles (see also Figure 3.10B-C). Expression of *Tc-pnr* in the amnion covering the segment addition zone is constant and is detected distinct from its anterior expression domain throughout germband extension (Figure 3.10A-D). The distinct small expression domain anterior to the segment addition zone is lost up to closure of the serosal window (compare Figure 3.9D and Figure 3.10A-B). Meanwhile, a new embryonic expression domain arises within cells of the head anlagen of the embryo (Figure 3.10A and C-D).

When the embryo has extended completely, *Tc-pnr* expression is seen in the whole amnion covering the embryo (Figure 3.11A and A`). *Tc-pnr* expression at this stage is clearly stronger in the most anterior part of the amnion, as compared to the rest of its expression throughout the amnion (Figure 3.11A``and A```). This is due to the larger cells in this region, which are known to have a bigger cytoplasmic volume and therefore, a higher amount of *Tc-pnr* transcript is found in these cells (see also Figure 3.11C; within an oblique domain of the anterior-ventral amnion, cells of the accordingly named anterior cap region mark the site of amniotic rupture prior to dorsal closure [Hilbrant et al., 2016]). During the following retraction of the germband, *Tc-pnr* gains expression in the cardioblast cell row, while expression in the amnion persists (Figure 3.11B-B``). Throughout these developmental stages, *Tc-pnr* is expressed in the tip of the legs, the initial appendages covering the pleuropodia and various head structures, namely the labrum, the labial appendages, the antennae and in a domain besides the latter one (Figure 3.11B-B`and D-D`).

After rupture and the subsequent withdrawal of both extraembryonic membranes, *Tc-pnr* is expressed in the dorsal most cells of the ectoderm and in a segmentally iterated fashion just ventral to the tracheal openings in all segments but T1 to T3 and in various
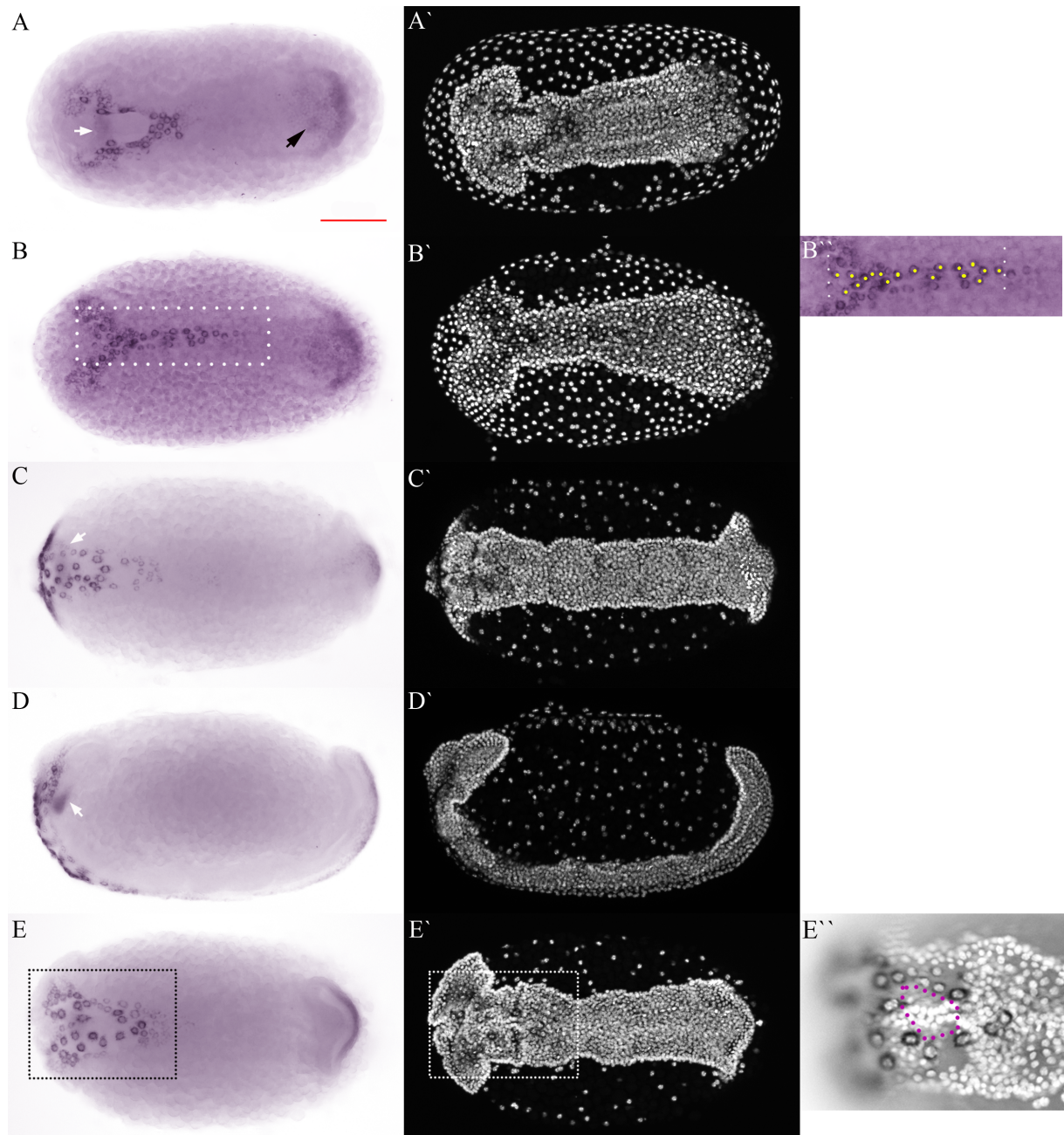
Figure 3.10: **Dynamic amniotic expression pattern of *Tc-pnr* during germband extension**. (**A-E**) Embryos stained for *Tc-pnr* via *in situ* hybridization. (**A`-E`**) Respective DAPI counterstain. (**E``**) Overlay of a single section of the projections in **E** and **E`**. (**A**) Embryo with an almost closed serosal window, similar to Figure 3.9D. *Tc-pnr* expression starts to expand in the amnion covering the head lobes. Expression in the amnion covering the segment addition zone is unchanged but the expression domain just anterior decreases to a small spot (black arrow). A new *Tc-pnr* expression domain arises in cells of the developing head (white arrow). (**B**) The small expression domain anterior to the segment addition zone is not visible as a distinct domain anymore at this stage, as the more posterior expression in the segment addition zone expanded anteriorly. Following closure of the serosal window *Tc-pnr* is expressed in an anterior amniotic stripe along the ventral midline of the embryo and expends greatly within the amnion covering the head lobes, forming a y-shape. The middle part of this y is around 17 *Tc-pnr* stained cells long (n=10; minimal cell count is 16, maximal cell count is 18), measured in an anterior-posterior direction. **B``** is an enlargement of the white rectangle in **B**, exemplarily showing yellow marked cells between two borders, which were used for the length measurement. Only fully stained cells were counted and only small overlaps in anterior-posterior direction were allowed. (**C-D**) Same embryo. The embryo extends over both poles and *Tc-pnr* expression broadens in the amnion covering the anterior embryo. In **D**, the embryo has an intact amnion but the serosa was removed manually, so that *Tc-pnr* expression towards the anterior and the posterior can be identified as of amniotic origin. A characteristic feature detected for the first time by *Tc-pnr* staining is the perforated looking amnion (see also Figure 3.11A), which becomes visible shortly after serosal window closure (**B-C** and **E**). The embryo in **E** shows the same perforation of the amnion as **C** but is a little bit younger, as apparent from the length of the germband. The region within the dashed rectangle is enlarged in **E``**, showing that within the purple area encompassing a 'hole', no nuclei are present. The white arrows in **C** and **D** point to the expression domain in the head. Scale bar is 100 μm. **A-C** and **E** are ventral views, **D** is a lateral view.
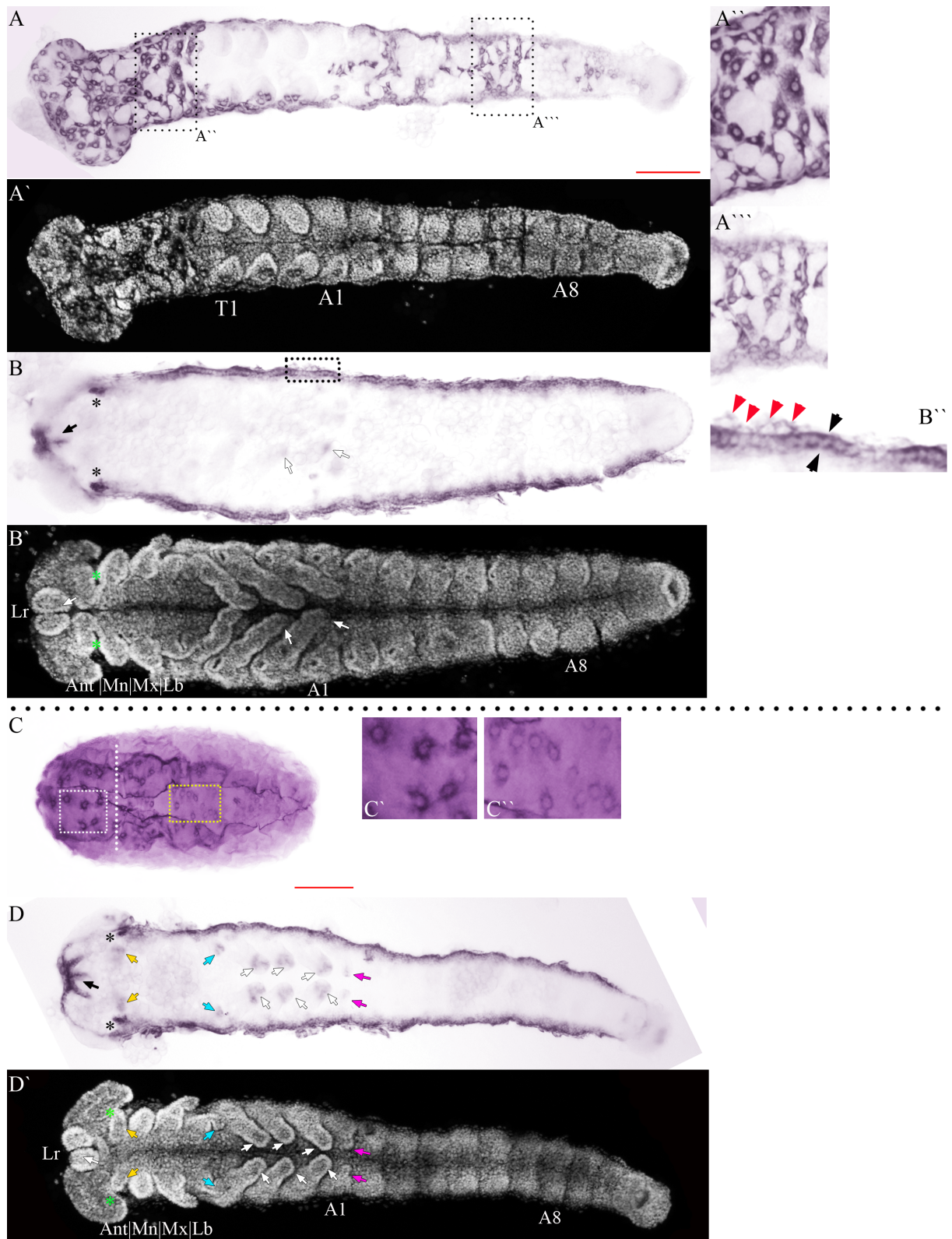
Figure 3.11: **Expression pattern of *Tc-pnr* at the fully extended germband stage and during germband retraction.** (**A**-**D**) Embryos stained for *Tc-pnr* via *in situ* hybridization. (**A`**-**B`** and **D`**) Respective DAPI counterstain. The images in **C**-**D** below the dashed black line contain supporting information for the images in **A**-**B**. (**A**) *Tc-pnr* is expressed in the whole amnion covering all but the dorsal side of the embryo at the fully extended germband stage. The amnion is partially ripped apart owing to the dissecting method used. **A``** and **A```** show enlargements of the respective areas as indicated in **A**, both at the same magnification. *Tc-pnr* is clearly stronger expressed in the most anterior amniotic cells (**A``**), whereas its expression is weaker in the rest of the amnion (**A```**). If looking at the embryo in **C**, which also has a fully extended germband but was stained without removing the vitelline membrane and the serosa, the stronger stain in the larger anterior cells compared to the smaller cells of the posterior amnion becomes more obvious. The dashed white line in **C**, approximately marks the border between the amniotic cells of the anterior cap region with strong *Tc-pnr* expression and the remaining cells with weaker expression. This distinction is further strengthened, if comparing the cell shapes. The cells left to the border have a more relaxed roundish shape, while the cells to its right are more stretched along the dorsal-ventral axis (see also the white and yellow dashed rectangles, which are enlarged in **C`** and **C``**, respectively). Both cell shapes are characteristic for the respective region within the amnion. (**B**) Embryo during germband retraction. *Tc-pnr* is expressed in the cardioblast cell row and the remaining amniotic tissue, which partially covers this expression (see also **B``** for an enlargement of the area within the dashed black rectangle in **B**; the two black arrows confine the cardioblast cell row; the four red arrows mark for individual cells of the amnion, covering the cardioblast cell row). For description of the embryonic expression domains, which are only weakly stained in **B**, the embryo in **D** is used. The embryo in **D** is slightly younger as the one in **B** but the head structures are already visibly developed (**D`**). Therefore, one can detect *Tc-pnr* expression in the labrum (black arrow), the antennae (yellow arrow), the labial appendages (blue arrow) and in two dot-like domains besides the antennae (asterisks). Further expression is seen in the tip of the legs (white arrows) and in the appendages still covering the pleuropodia (magenta arrows). Scale bars are 100 μm. **A** - **D** are ventral views.
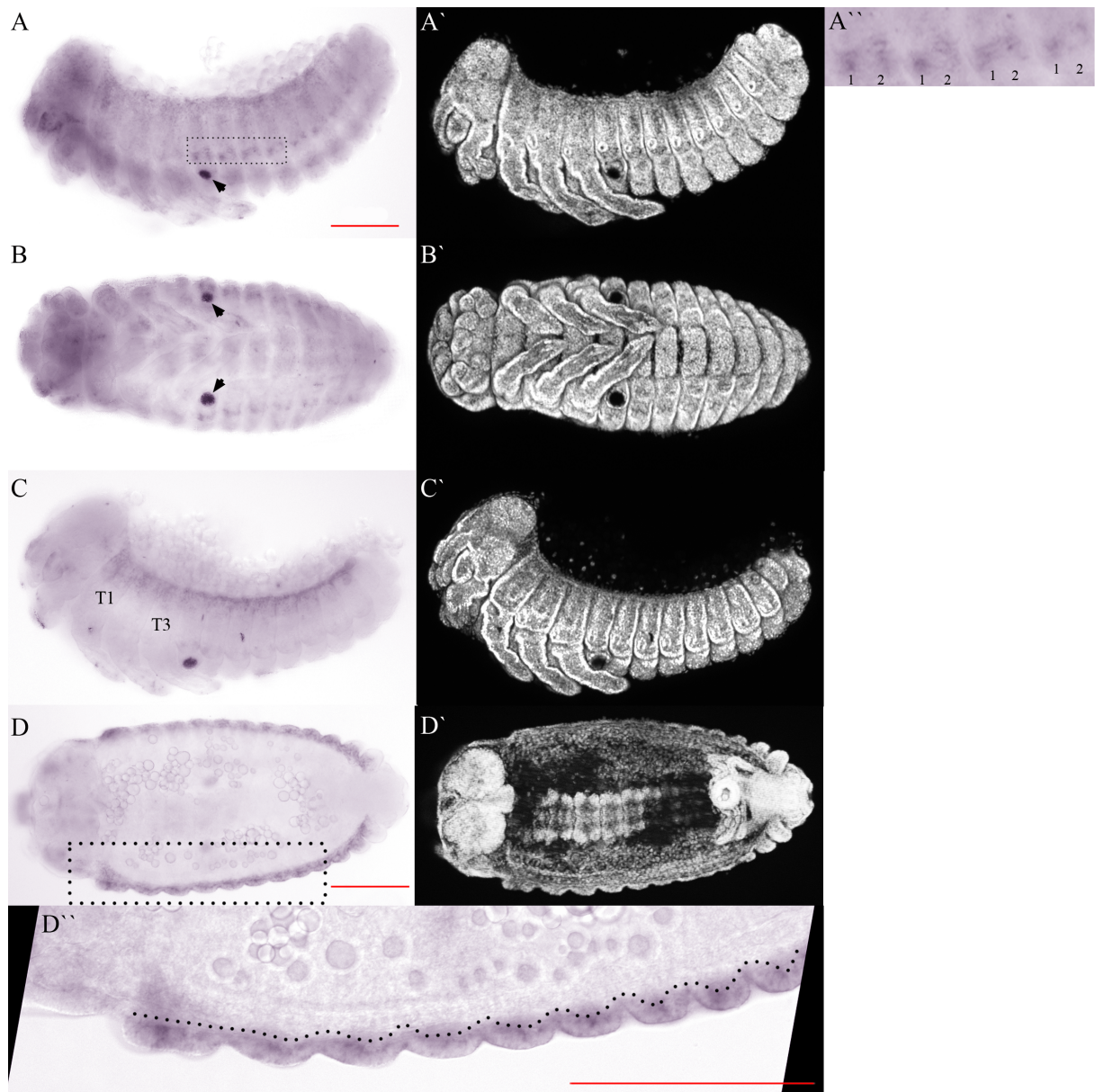
Figure 3.12: ***Tc-pnr* expression pattern around the period of membrane rupture and the onset of dorsal closure**. (**A-D**) Embryos stained for *Tc-pnr* via *in situ* hybridization. (**A`-D`**) Respective DAPI counterstain. (**A, B**) Same embryo. Prior to dorsal closure *Tc-pnr* is expressed in the most dorsal ectoderm and in a two patch pattern just ventral to the tracheal openings in all but the three most anterior segments (T1-T3). Expression in the head and in the legs persists (see main text). Black arrows point to unspecific staining within the pleuropodia. The black dashed rectangle encompasses four sets of the segmentally iterated *Tc-pnr* expression pattern, enlarged in **A``**. Thereby, the numbers 1 and 2 iterative label the two expression patches in each segment. (**C**) Slightly younger embryo as **A**, presumably just before rupture, where *Tc-pnr* expression is better visible in the dorsal ectoderm but all other expression is weaker compared to **A**, due to a reduced staining period. (**D**) Flat mounted embryo, comparative to **C**, in which *Tc-pnr* expression is shown in the outer most cell row, which corresponds to the dorsal most ectodermal cell row. Towards the posterior the expression pattern broadens, which is due to the bending of the embryo, so that more cells of the ectoderm come into view (compare to **C**). The area encompassed by the black dashed rectangle, is shown in **D``**, imaged with a higher magnification. (**D``**). Focus on the outer most cell row, which is delimited by the black dashed line to the inner mesoderm. Scale bars are 100 μm in **A-D** and 50 μm in **D``**. **A** and **C** are lateral views, **B** is a ventral view and **D** is a dorsal view.

domains in the head and the legs (Figure 3.12A-D and A`-D``). The latter two expression domains were confirmed by looking at other embryos stained for *Tc-pnr* and probably correspond in part to the expression pattern seen in extended germband embryos (see Figure 3.11D).

3.2.2 Knock down penetrance of *Tc-pnr*

As *Tc-pnr* has no reported gene function, pRNAi was used to assess the role of *Tc-pnr* in extraembryonic and embryonic development. Triggering pRNAi, injection of dsRNA into the abdomen of females leads to the knock down of zygotic *Tc-pnr* expression in the offspring, facilitating analyses of the resulting phenotypes [Bucher et al., 2002].

   Tc-pnr dsRNA was injected in concentrations ranging from 900 ng/μl to 1400 ng/μl, without major differences in the penetrance of the knock down phenotypes, in eight discrete experiments. The penetrance was assessed by cuticle preparation (Figure 3.13A) and live imaging (Figure 3.13B). In both cases injection of water served as a negative control. For the analysis by cuticle preparation additionally *Tc-Toll1* was used to confirm that this procedure is providing valid and reproducible data. Injection with *Tc-Toll1*

dsRNA resembled its specific phenotype in all embryos [Nunes da Fonseca et al., 2008]. Injection with water (control) resembled in 91.8% - 94.1% the wild type phenotype (Figure 3.14A). Knock down of *Tc-pnr* produced a strong dorsal open phenotype (82.4%), easily detectable by the characteristic bending of head and posterior abdomen towards its dorsal side and a hole in the dorsal cuticle (Figure 3.14B). Noteworthy, the penetrance of the two other phenotypes empty egg (intact egg shell but no embryonic cuticle inside; Figure 3.14C) and cuticle crumbs (intact or broken egg shell and partial cuticle detectable (mostly antenna or tip of the leg); Figure 3.14D) is doubled after *Tc-pnr* pRNAi compared to the control (from 5.1% to 10.0% in the case of empty egg and from 3.1% to 6.3% for cuticle crumbs). The wild type phenotype is constant at a low percentage (1.3% and 1.5% by cuticle preparation and live imaging, respectively) in the knock down.

To conclude that the phenotypes observed after injection of *Tc-pnr* dsRNA reflect the function of *Tc-pnr* and are not due to an off-target effect of the dsRNA on another gene, a second *Tc-pnr* dsRNA was made. The new primer pair used for it does not overlap with the original primer pair on the *Tc-pnr* coding sequence. Subsequently, the new dsRNA named *Tc-pnr* fragment 2 was injected at a concentration of 1000 ng/μl into beetles, which were used in a single pRNAi experiment. The knock down penetrance of *Tc-pnr* fragment 2 was assessed for about three weeks by cuticle preparation (Figure 3.13C). Four days after injection, *Tc-pnr* fragment 2 resembled in 46.8% the dorsal open phenotype from the original *Tc-pnr* fragment but in 52.7% the empty egg phenotype, while the cuticle crumbs phenotype was insignificant with only 0.7%. When comparing these results to the ones of the negative control, it becomes apparent that these values are not representative. The penetrance of the wild type phenotype (which is normally over 90%; see Figure 3.13A and B) is strongly reduced by roughly 35% to 57.6%. Like-wise the empty egg phenotype is increased to 36.4% (5.1% in Figure 3.13A), as well as the cuticle crumbs phenotype (3.1% in Figure 3.13A, compared to 6.1% in Figure 3.13C). 12 days and 19 days after injection the penetrance of the dorsal open phenotype in the *Tc-pnr* fragment 2 knock down rised to 77.2 and 68%, respectively. Accordingly, the empty egg phenotype declined to 22% and 31.1%, respectively. The cuticle crumbs is still insignificant at 0.4% and 0.8%, respectively. In the control, the wild type phenotype is 81.2% 12 days after injection and 71.1% 19 days after injection of the dsRNA. Empty egg phenotype and cuticle crumb phenotype are 7.6% and 11.2% 12 days after injection and 6.3% and 22.5% 19 days after

A

Knock down penetrance: cuticle preparation

B

Knock down penetrance: live imaging

C

Knock down penetrance of *Tc-pnr* fragment 2: cuticle preparation
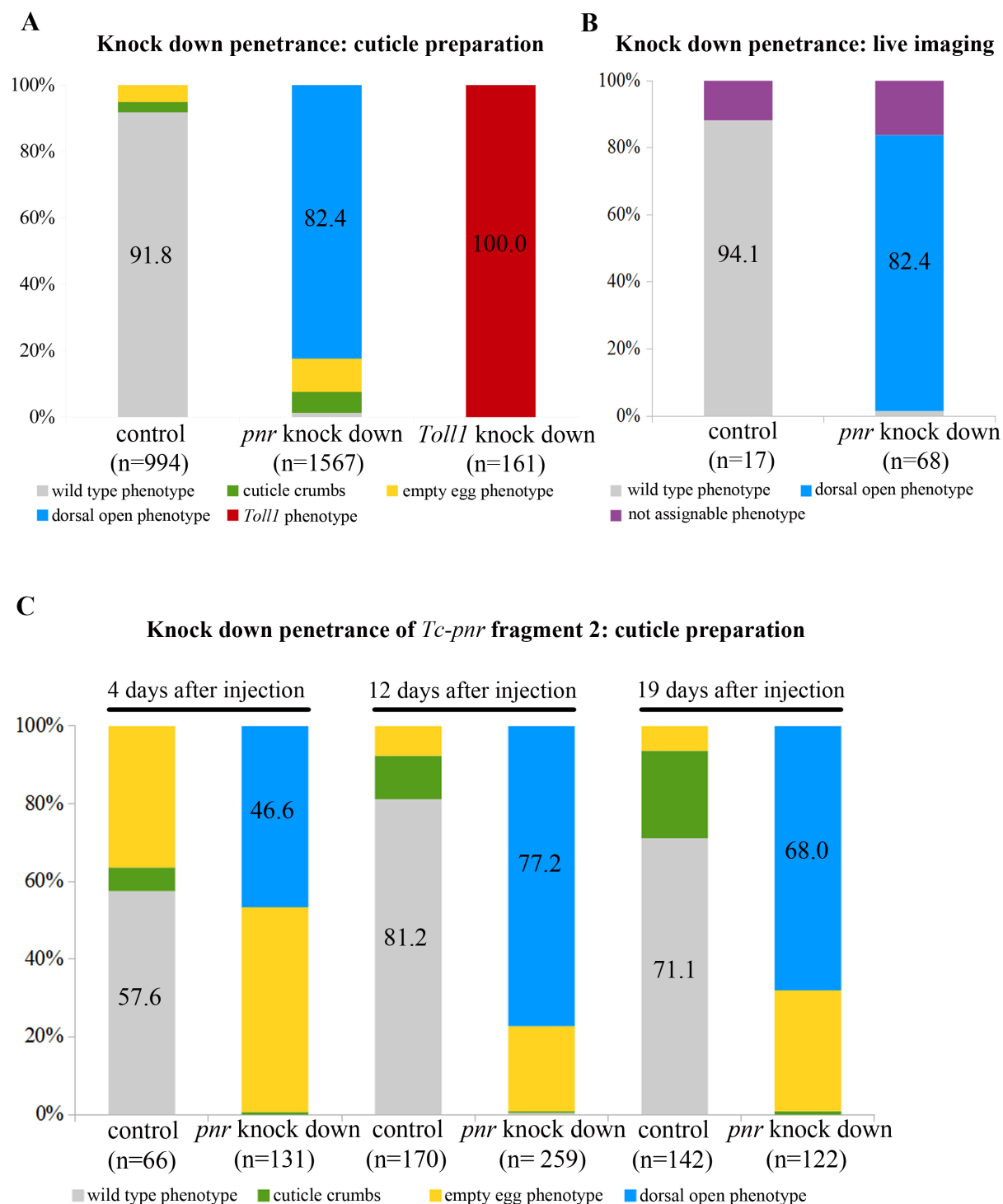
Figure 3.13: **Knock down penetrance of *Tc-pnr* pRNAi**. (**A**) Comparison of the penetrance after *Tc-pnr* and *Tc-Toll1* pRNAi with a water injection (control), assessed via cuticle preparation of three to six days old larvae. 91.8% of the controls offspring developed a wild type cuticle, which is in contrast to the 82.4% showing the dorsal open phenotype and 100% showing the *Tc-Toll1* specific phenotype of the respective knock down. Furthermore in the control 5.1% did not develop any embryonic cuticle (empty egg phenotype) and 3.1% showed some cuticle crumbs. In the *Tc-pnr* knock down this values were doubled (10.0% empty egg and 6.3% cuticle crumbs). 1.3% developed wild type like in this knock down. (**B**) Comparison of the penetrance between the control and *Tc-pnr* knock down, assessed by three separate live imaging recordings. Embryonic development was recorded for at least 25 hours starting shortly before rupture, thereby assuring that the dorsal open phenotype could be detected. Strikingly its penetrance was again 82.4%. Almost the same was the wild type phenotype with 1.5% and the not assignable phenotype added the remaining 16.2%. The latter phenotypic class includes all embryos which cannot be assigned to one of the other classes due to the limitations of live imaging. Presumably, it resembles the 16.3% of the empty egg and cuticle crumbs phenotype in **A**. The control produced 88.2% wild type phenotype, most similar to the result in **A**. (**C**) Knock down penetrance of the non-overlapping *Tc-pnr* fragment 2 and a control at three different time-points throughout a single experiment. In the control, the wild type phenotype fluctuated from 57.6% 4 days after injection, to 81.2% after 12 days and 71.1% after 19 days. The same was true for the dorsal open phenotype of the knock down (46.6%, 77.2% and 68%, respectively). The empty egg phenotype was highly increased in both the knock down and the control (36.4%, 7.6%, 6.3% and 52.7%, 22%, 31.1%, respectively), compared to Figure 3.13A. The same was true for the cuticle crumbs phenotype in the control (6.1%, 11.2% and 22.5%) but not for the knock down, in which it decreased (0.7%, 0.4% and 0.9%), compared to Figure 3.13A. General differences to Figure 3.13A are probably caused by seasonal fluctuations effecting the health of cultured *Tribolium* lines and the reduced robustness of the data set (see main text).
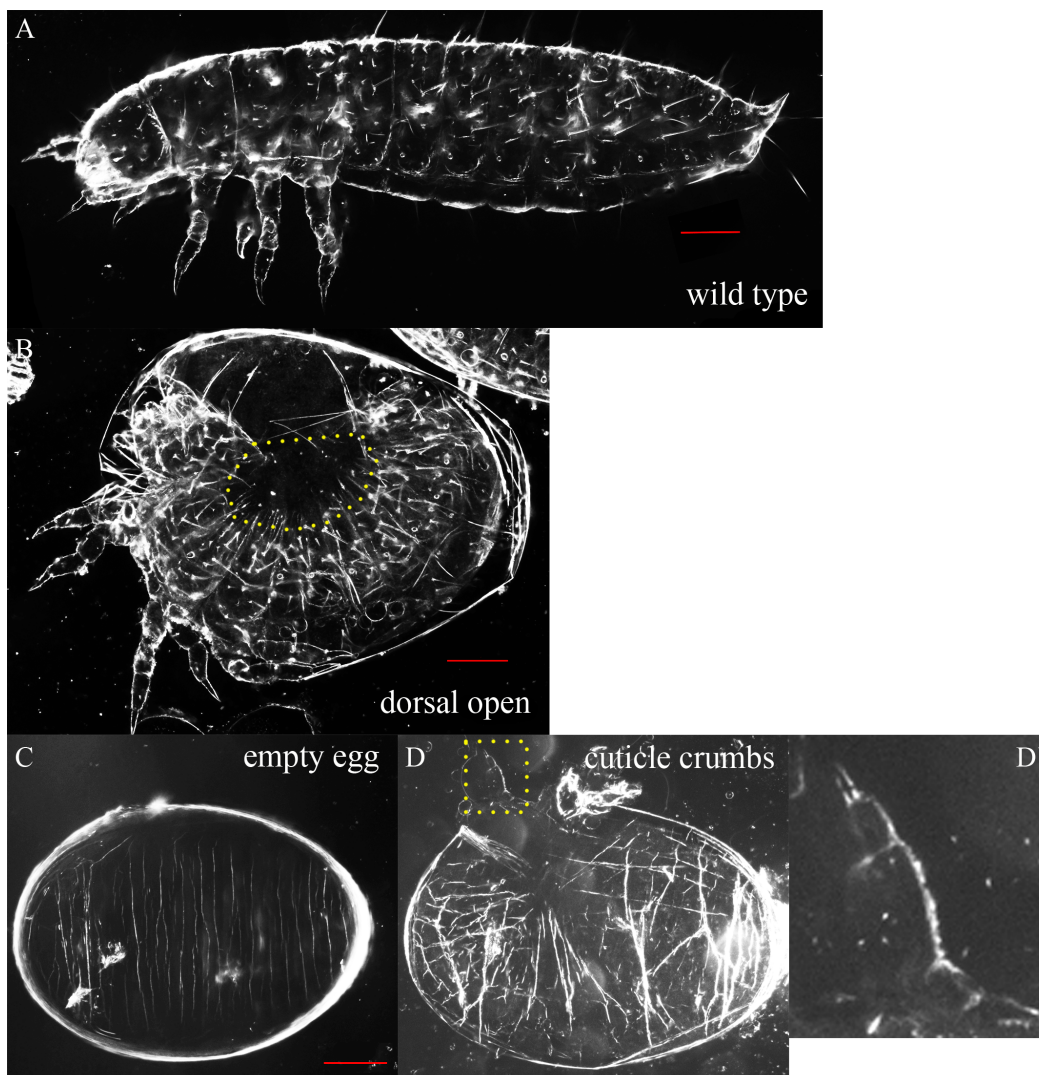
Figure 3.14: **Observed phenotypes after *Tc-pnr* pRNAi**. (**A-D**) Cuticle preparations of three to six days old larvae and eggs after *Tc-pnr* pRNAi, showing all four distinct phenotypic categories. (**A**) First instar larva with wild type cuticle. (**B**) Embryo showing the characteristic bending of the dorsal open phenotype, in which the head and the posterior abdomen almost come in touch on the dorsal side. The yellow dashed area encompasses the dorsal hole that is the actual eponym of this phenotype. Within this area no cuticle was produced. Although the eggshell is broken and it appears as if the embryo did at least try to hatch, this is an artifact due to the pressure applied on the egg during the mounting process. All embryos showing this phenotype die while they try to close their back. (**C**) The empty egg phenotype does not produce any cuticle but has an intact egg shell. (**D**) In the cuticle crumbs phenotype mostly the pretarsus or a tip of the antenna, as in the present picture, are the only visible cuticle remnants of the embryo. **D`** is an enlargement of the yellow rectangle in **D**, zooming in on an antenna, which is most likely still attached to some other cuticle. Scale bars are 100 μm.

injection, respectively.

One important consideration has to be taken into account when looking at the data from *Tc-pnr* fragment 2. The beetles used for the pRNAi experiment were taken from *Tribolium* lines with overall bad health (high mortality rate and reduced life span), as it was the case for most of all other *Tribolium* lines cultured in the lab at this time. This is a known phenomena within the *Tribolium* community, probably due to seasonal changes effecting the health of the population. This could explain the high rate of the empty egg and cuticle crumb phenotype, even in the wild type. In addition, as the data shown in Figure 3.13C was collected from a single experiment only, its informative value is limited.

3.2.3 Comparing the topography of a normal developing embryo to one going to show the dorsal open phenotype

It is only shortly after serosal rupture and prior to dorsal closure that measurable and visible differences between a wild type embryo and an embryo going to show the dorsal open phenotype after *Tc-pnr* RNAi can be detected (see Figure 3.15; one movie for showing the development of the wild type embryo and one movie showing the development of the *Tc-pnr* knock down embryo are included on the DVD; see 6.7 movies 3A and 3B, respectively)).

Therefore, embryos in Figure 3.15 are synchronized to the first time point during imaging when the serosa visibly withdraws from the anterior (Figure 3.15A1 and B1). While the serosa has fully withdrawn from the abdomen in wild type embryos after 30 min (n=7; standard deviation is 10 min) (Figure 3.15A2), this process is not as fast in *Tc-pnr* knock down embryos (Figure 3.15B2). In those the duration is doubled to 60 min (n=20; standard deviation is 30 min). When the serosa is then degenerating within the yolk and the flanks of the embryo are almost coming together in the wild type embryo (Figure 3.15A3), the knock down embryo has already started to bend towards its dorsal side (Figure 3.15B3). At this time the serosa starts degenerating in an atypical way so that even at the end of imaging of the here shown knock down embryo reminant serosal cells are still detectable (Figure 3.15B3-B5). While the flanks of the wild type embryo expand towards the dorsal midline in a more even anterior-to-posterior fashion (compare dashed light blue line in Figure 3.15A1-A3), this is not the case in the *Tc-pnr* knock down. Here the bending of the head and tail towards the dorsal side, forming the characteristic
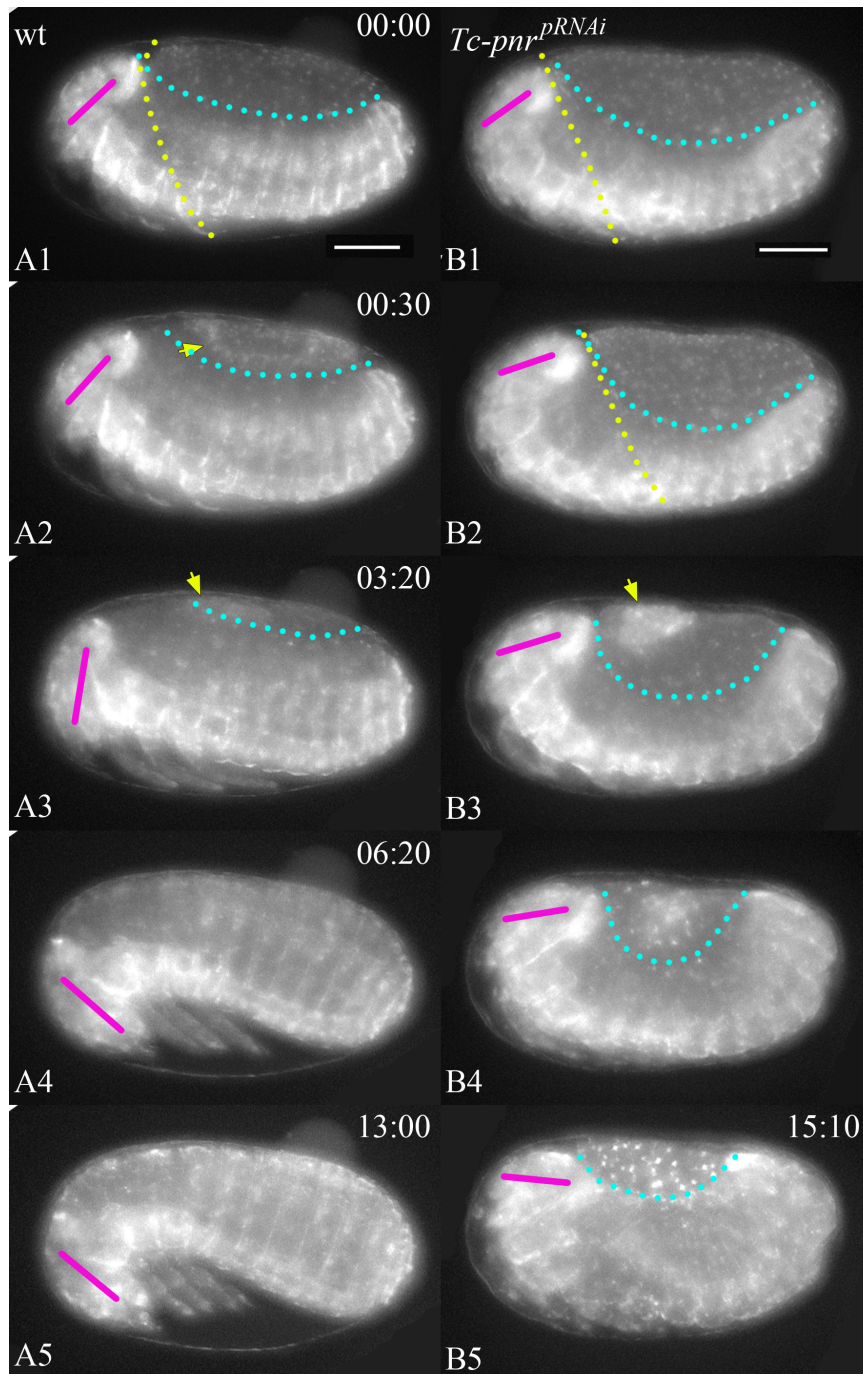
Figure 3.15: **Onset of the dorsal open phenotype after serosal rupture**. Live imaging of a wild type embryo (**A1-A5**) and a *Tc-pnr* knock down embryo (**B1-B5**) using the nuclear GFP (nGFP) line [Sarrazin et al., 2012]. In all pictures the orientation of the head is marked by a purple line, using two landmarks in the head. The light blue dashed line marks roughly the most dorsal tissue of the closing flanks. (**A1** and **B1**) Both embryos are synchronized to the first time point in which serosal rupture is visible. The dashed line separates the part of the embryo still encompassed by the serosa (to its right) and the part where the serosa has withdrawn (to its left). (**A2** and **B2**) In wild type the serosa has withdrawn towards the dorsal side, forming the dorsal organ (yellow arrow). After the same time in the knock down, the serosa still encompasses a large posterior part of the embryo. (**A3** and **B3**) The serosa has sunken into the yolk, while its knock down counterpart is partially still on top of the yolk (yellow arrows). In the knock down the bending of the head and the posterior abdomen towards the dorsal side has visibly proceeded. (**A4** and **B4**) The wild type embryo has finished dorsal closure and the head has reached its final orientation. On the contrary, the serosa is still undergoing degeneration in the knock down. **A5** and **B5** show the last imaged time point of the respective embryos. The wild type embryo has not changed its appearance but is performing periodic muscle twitching due to the activity of the longitudinal body muscles [Koelzer et al., 2014] (not visible in **A5**). The dorsal open phenotype is now apparent in the knock down and the extent of the dorsal opening can be seen. Even though dorsal closure has failed in the knock down, the embryo's flanks have extended significantly towards its dorsal side. The bright spots within the dorsal hole have been traced throughout the recording and could be identified as remaining serosal nuclei. In the *Tc-pnr* knock down the head is almost bent 180 ° clock wise compared to the orientation of the wild type's head. Scale bars are 100 μm. Time stamp is in h:min. The embryos have been imaged at a constant temperature of 30 °C.

basket shape, leads to a narrowing furrow, the dorsal hole. This narrowing is further increased, as the lateral sides of the embryo do not come up as much as in wild type (compare dashed light blue line in Figure 3.15B2-B4). It is only at the final dorsal open topography that it becomes best visible that the flanks do expand dorsally, while the embryo tries to close its back (Figure 3.15B5). The extent of the dorsal hole is quite variable at this stage. While the embryo in Figure 3.15B5 is a good representative for most other knock down embryos, in some embryos the dorsal opening is much smaller in anterior-posterior extent. This is due to an increased bending of both the head and the posterior abdomen. In Figure 3.15 the purple line indicates the orientation of the head, as introduced in Panfilio et al. 2013. Compared to the wild type, an almost 180 ° clock wise turnover has occurred (compare Figure 3.15A5 and B5), which can even extend 180 ° in knock down embryos with a more narrow dorsal hole.

3.2.4 *Tc-pnr* regulates *Tc-dpp* expression in the dorsal epidermis during dorsal closure

The cause of the dorsal hole in *Dm-pnr* mutants of *Drosophila* has been traced back to its regulatory role on *Dm-dpp* [Herranz and Morata, 2001], which is an essential signaling molecule during dorsal closure [Affolter et al., 1994; Glise and Noselli, 1997].

In *Tribolium* it is known that *Tc-dpp* is expressed in cells of the dorsal most ectoderm in extending germband embryos [Sanchez-Salazar et al., 1996; Giorgianni and Patel, 2004; Ober and Jockusch, 2006]. Figure 3.16A-B``shows that this expression persists in the dorsal most cells of the ectoderm in retracted germband embryos, resembling the expression in *Drosophila* [Arquier et al., 2001; Chen et al., 2002]. *Dm-pnr* expression in the ectoderm shares the same dorsal limit like *Dm-dpp* [Winick et al., 1993; Herranz and Morata, 2001]. The same applies for *Tc-pnr* (see Figure 3.12A and C), compared to *Tc-dpp*. These similarities led to the assumption that *Tc-pnr* may regulate *Tc-dpp*, like its ortholog in *Drosophila* [Herranz and Morata, 2001]. Indicated by the dorsal hole in *Tc-pnr* knock down embryos, which is a specific feature of dorsal closure mutants in *Drosophila* [Byars et al., 1999], this could help to clarify the role of *Tc-pnr* during dorsal closure. Experimentally, *Tc-pnr* knock down embryos were stained with a *Tc-dpp* probe (Figure 3.16).

In *Tc-pnr* knock down embryos, *Tc-dpp* expression is unaffected in the proctodeum,

wt

Tc-dpp

A

A`

wt

Tc-dpp

B

B`

yolk

ectoderm

B``

wt

Tc-dpp

C

C`

Tc-pnr^*pRNAi*^

Tc-dpp

D

D`

Tc-pnr^*pRNAi*^

Tc-dpp

E

E`

Tc-pnr^*pRNAi*^

Tc-dpp

F

F`
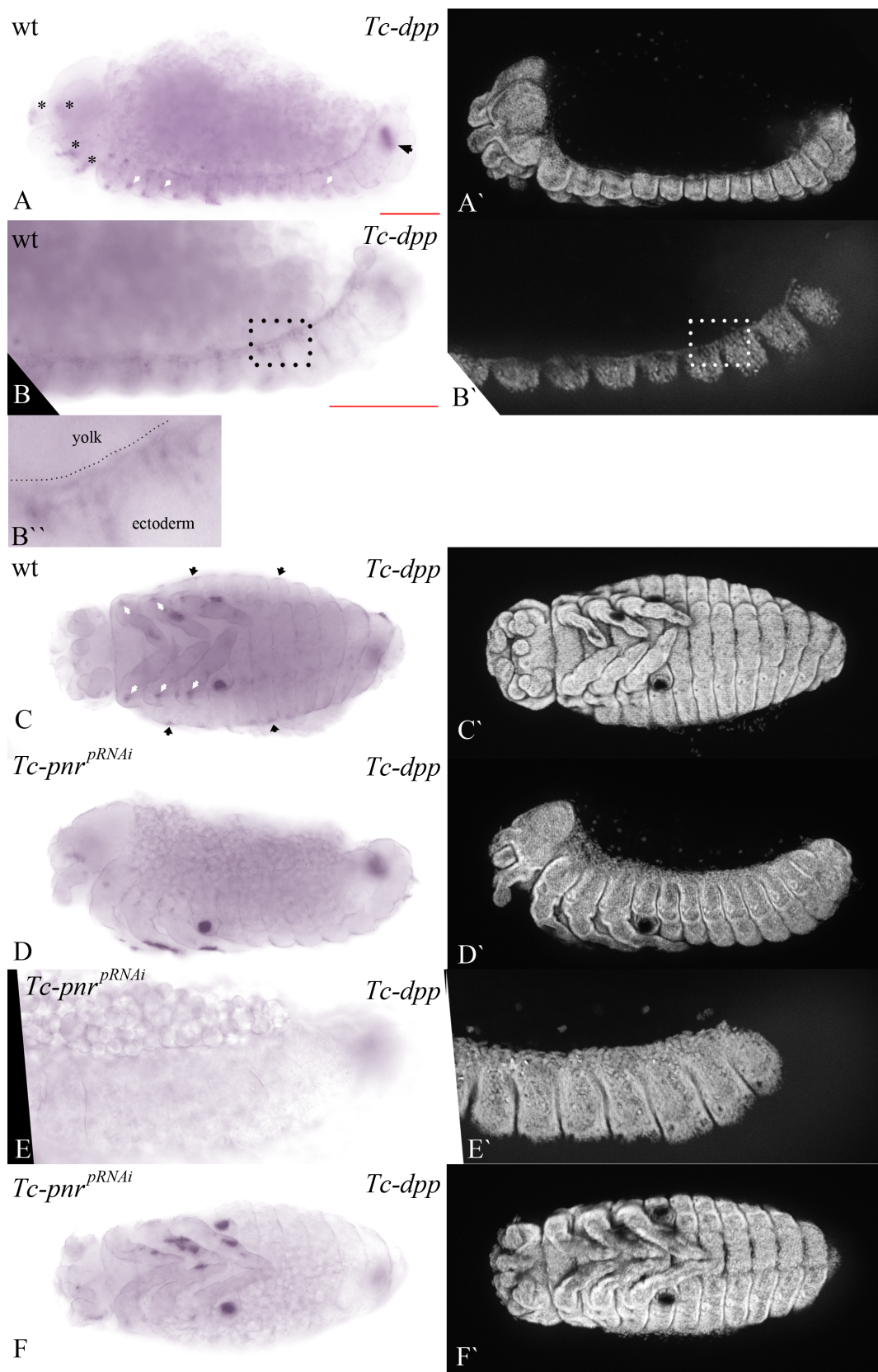
Figure 3.16: ***Tc-dpp* expression in the dorsal most ectoderm depends on *Tc-pnr*.** (**A-F**) Embryos stained for *Tc-dpp* via *in situ* hybridization. (**A`-F`**) Respective DAPI counterstain. (**B** and **E**) The same embryos as in **A** and **D**, respectively but imaged at a higher magnification. (**A**) *Tc-dpp* is in wild type expressed in cells along the dorsal most ectoderm. Additional expression domains are seen in the proctodeum (black arrow) and in various domains within the developing head (asteriks). Along the lateral flank weak expression within a patchy stripe is detectable (white arrows point to some of the its expression; the latter expression pattern is stronger in extending germband embryos [Giorgianni and Patel, 2004; Ober and Jockusch, 2006] but could be verified in the developmental stage seen in **A** by looking at other embryos stained for *Tc-dpp* as well). (**B**) The projection focuses on the dorsal most ectoderm of the posterior part of the embryo in **A**, where *Tc-dpp* is expressed in a row of cells, directly adjacent to the yolk. **B``** is an enlargement of the area within the rectangle seen in **B** and **B`**. The border between the yolk and the ectoderm is visualized by the dashed black line. Dorsal to the line is the yolk and ventral to it the ectoderm. *Tc-dpp* is expressed in the ectodermal border cells. (**C**) Different embryo stained for *Tc-dpp*, where its expression is seen in the patchy lateral stripe in T1-T3 (white arrows). The black arrows point to expression in the dorsal most ectoderm. (**D**) In the knock down, *Tc-dpp* expression is absent in the dorsal most row of cells in the ectoderm but still expressed in all other domains (this might not be apparent from this embryo, as all other expression domains beside in the proctodeum stain not very strong for *Tc-dpp* in general but it has been verified by looking at other embryos that only the *Tc-pnr* expression within the dorsal most ectoderm is consistently absent after *Tc-pnr* pRNAi). (**E**) The projection focuses on the dorsal most ectoderm of the posterior part of the embryo in **D**, where *Tc-dpp* is no longer expressed. (**F**) The same embryo as in **D**, showing the loss of *Tc-dpp* expression along the dorsal most cells in the ectoderm. **A, B, D** and **E** are lateral views, **C** and **F** are ventral views. Scale bars are 100 μm.

the head and along the lateral flank (Figure 3.16D and F; see figure legend). It is only the expression in the cells of the dorsal most cell row that is absent in the knock down (Figure 3.16D and E). This finding suggests that *Tc-dpp* is indeed a downstream target of *Tc-pnr* in these cells.

3.2.5 *Tc-pnr* regulates *Tc-iro* at the differentiated blastoderm stage and represses it in the dorsal epidermis during dorsal closure

In *Tribolium*, *Tc-iro* is primarily used as a marker for the amnion at the differentiated blastoderm stage [Nunes da Fonseca et al., 2008, 2010]. At this stage, both *Tc-iro* and *Tc-pnr* are expressed in the anterior amniotic fold, the dorsal amnion and in cells of the posterior fold, whereas *Tc-iro* expression extends more ventral in the latter one (Figure 3.17A and G). To check if *Tc-iro* is regulated by *Tc-pnr*, the expression of *Tc-iro* was investigated in *Tc-pnr* knock down embryos until germband extension (Figure 3.17).

When the posterior fold has formed and involution of the embryo has begun, *Tc-iro* is expressed in the anterior amniotic fold, the dorsal amnion stretching into the posterior fold and the posterior part of the involuting embryo (Figure 3.17A and A`). In the *Tc-pnr* knock down *Tc-iro* expression is lost, even in the embryonic part, where *Tc-pnr* is normally not expressed (Figure 3.17B and B` and compare to Figure 3.17G). By the time the serosal window has formed, *Tc-iro* is expressed in its margins, the amnion covering the segment addition zone, as well as the segment addition zone itself and in streaky domains within the ectoderm (Figure 3.17C and C`). Again, the complete *Tc-iro* expression is lost in the knock down except weakly in two separate domains in the amnion over the head lobes. Here its expression is diminished but faintly visible (Figure 3.17D and D` and compare to Figure 3.17H). The residual *Tc-iro* expression in the amnion was verified by repeated *in situ* stainings in different *Tc-pnr* knock down experiments. By the time the amnion and serosa separated and the embryo extended over both poles, *Tc-iro* is expressed in the amnion and in an segmental-like repeated pattern within the embryo (Figure 3.17E and E`). The knock down expression pattern could not be validated to 100%, even after repeating the staining with embryos from different experiments. Probably, *Tc-iro* expression in the embryo is not affected but its expression within the amnion is diminished (Figure 3.17F and F` and compare to Figure 3.17I and J). These results indicate that *Tc-*
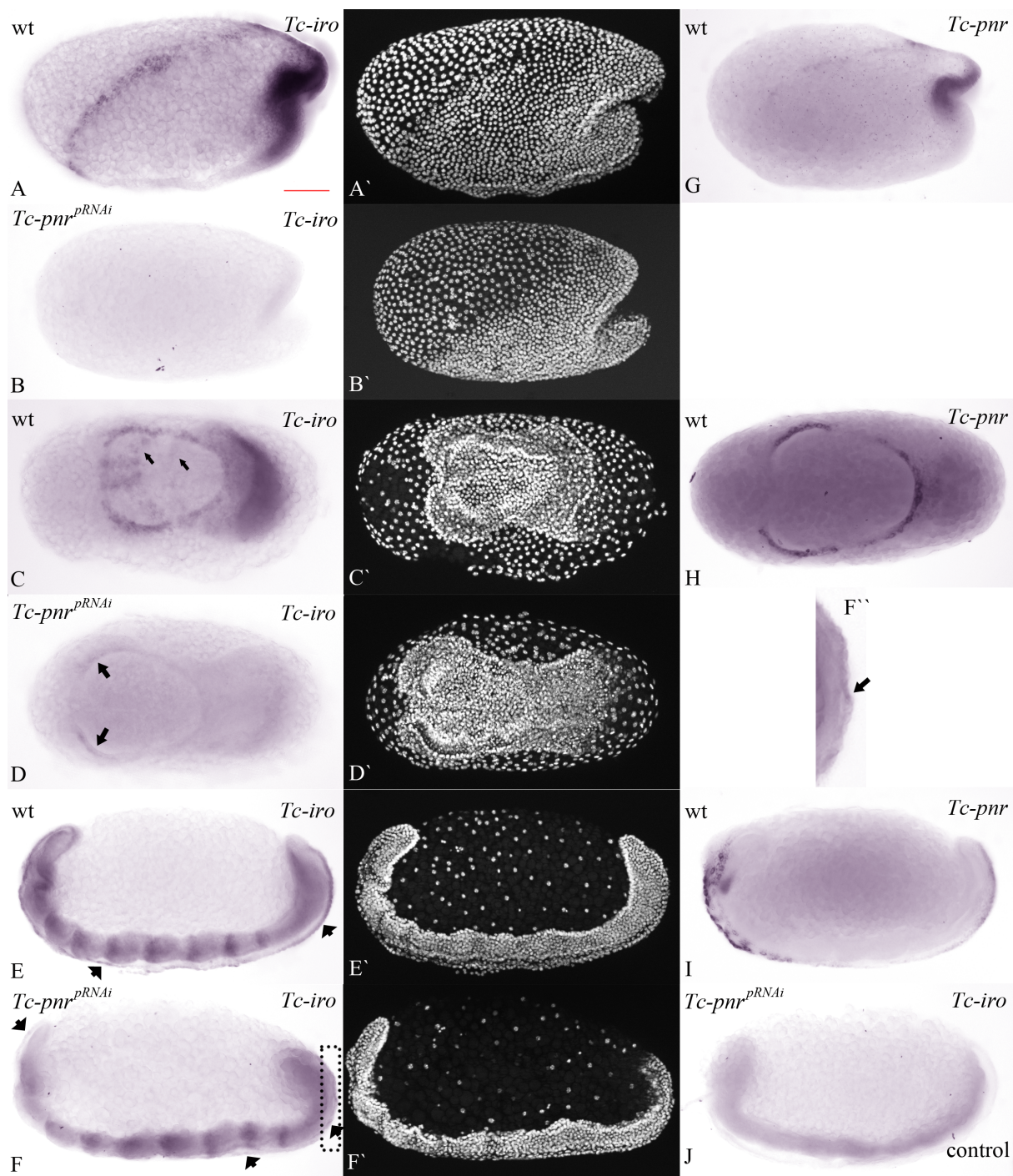
Figure 3.17: **Dynamic effect of *Tc-pnr* knock down on *Tc-iro* expression until mid germband extension**. (**A-F**) Embryos stained for *Tc-iro* via *in situ* hybridization. (**G-I**) Embryos stained for *Tc-pnr* via *in situ* hybridization (for details on the expression pattern, see Figure 3.9 and Figure 3.10). (**J**) Background control (using *Tc-iro* sense probe. (**A`-F`**) Respective DAPI counterstain. (**A, C, E, G, H** and **I**) Wild type embryos. (**B, D, F** and **J**) *Tc-pnr* knock down embryos. (**A**) *Tc-iro* is expressed in the anterior amniotic fold, the dorsal amnion and in cells around the posterior fold. (**B**) *Tc-iro* expression is absent in the *Tc-pnr* knock down embryo. (**C**) When the serosal window has formed, *Tc-iro* is expressed in the whole amnion at its circumference, in the segment addition zone and the overlaying amnion, as well as in the ectoderm (black arrows). (**D**) In the knock down, only weak expression in two domains in the amnion covering the head lobes is still present (black arrows). (**E**) During germband extension *Tc-iro* is expressed in segmental-like stripes and in the complete amnion (black arrowheads). (**F**) *Tc-iro* expression in the embryo is not affected in the knock down but its expression in the amnion is diminished (black arrowheads point to weak *Tc-iro* expression in the amnion). The area within the black rectangle is enlarged in **F``**. The black arrow points to weak expression in the outermost cell layer, which is the amnion. **A, B, E, F, G, I** and **J** are lateral views, **C, D** and **H** are ventral views. Scale bar is 100 μm.

pnr regulates *Tc-iro* expression to a certain degree not only in tissues where both genes are expressed both also in embryonic tissue, where *Tc-pnr* is not expressed. Additionally, this regulation of *Tc-iro* by *Tc-pnr* seems to weaken from differentiation of the blastoderm, until halfway through germband extension.

Interestingly, the knock down of *Tc-iro* does result in an early defect, which is not observed in *Tc-pnr* knock down embryos. In the severe occurrence of the *Tc-iro* phenotype after pRNAi, differentiation of the blastoderm is defective, as well as formation of the primitive pit. Still, a posterior fold like structure is able to form and cells of potential serosal origin try to envelope a tissue cluster with tentacle-protrusions, reminiscent of a kraken (Figure 3.18A1 and A2). In the mild occurence, the embryo is able to form but not completely in a wild type manner (Figure 3.18B). Nonetheless, the embryo does undergo a movement reminiscent of germband extension (inferred also by live imaging data; three movies are included on the DVD, showing wild type development and the mild and severe phenotype after *Tc-iro* pRNAi in the nGFP line genetic background (the latter one also shows the absence of proper primitive pit formation); see 6.7 movies 4A-4C, respectively). Investigation of the knock down penetrance (Figure 3.18D), showed that 66.4% (n=1895) of the embryos develop a wild type cuticle, which is in contrast to 91.7% (n=1975) in the control embryos. This indicates that the observed defects only affect a subset of the knock

D — Knock down penetrance: cuticle preparation
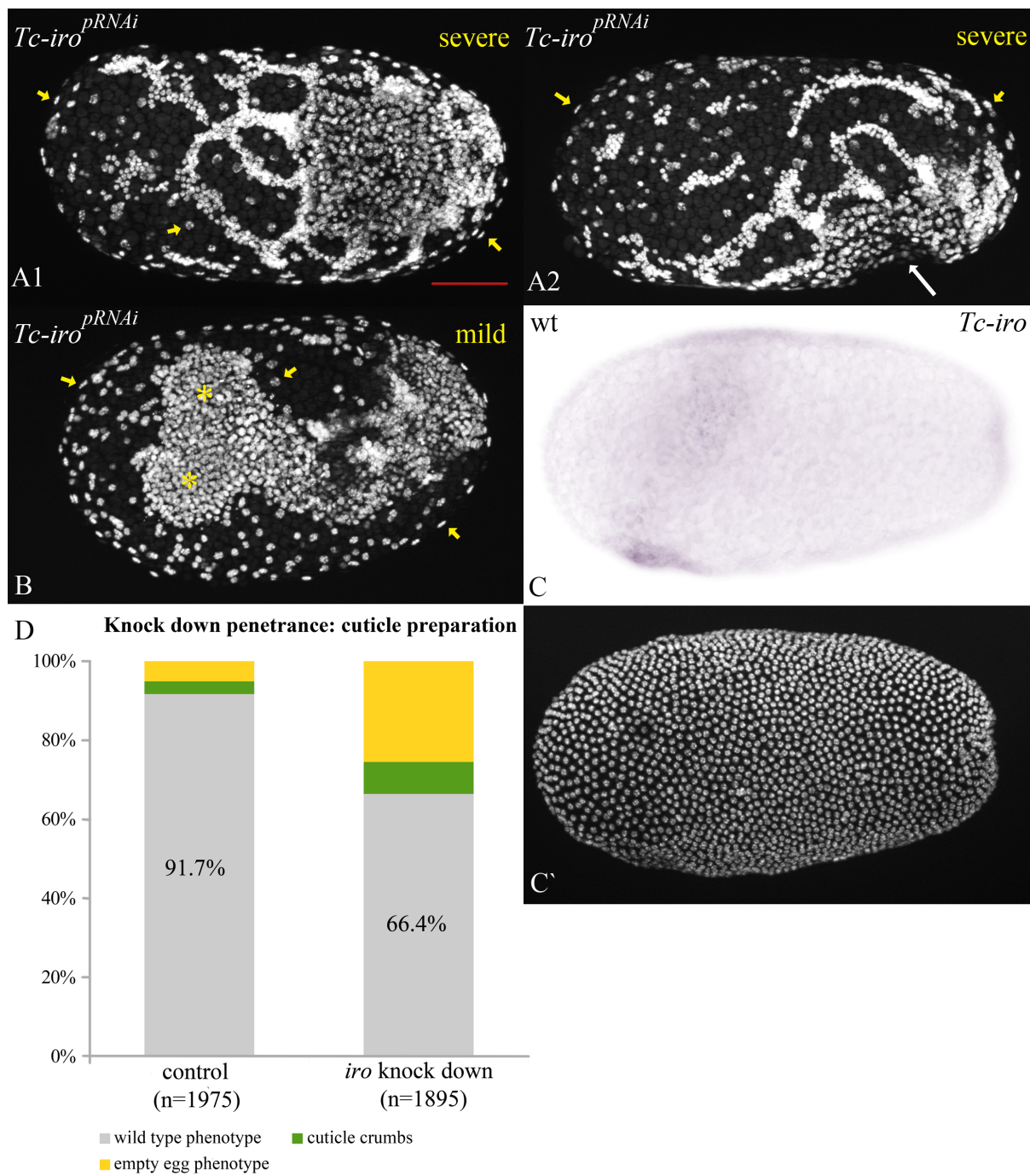
Figure 3.18: **Phenotypes after *Tc-iro* parental RNAi**. (**A-B**) After *Tc-iro* pRNAi, the observed phenotype can be divided into two main groups, depending on its severeness: In the severe phenotype, differentiation of the blastoderm fails and a single tissue cluster with tentacle-like cell protrusions forms (**A1**). A posterior fold like structure does form (white arrow in **A2**). The yellow arrows point to some of the presumptive serosal cells. In the mild phenotype, an embryonic structure with clearly distinct head lobes (marked by the two yellow asteriks) does form, reminiscent of a normal wild type embryo (**B**). (**C**) Embryo stained for *Tc-iro* via *in situ* hybridization. *Tc-iro* is expressed at the late undifferentiated blastoderm stage in a broad band in cells of the presumptive serosa and, towards the posterior, in the presumptive anterior amniotic fold. (**C`**) Respective DAPI counterstain. (**D**) Comparison of the penetrance after *Tc-iro* pRNAi with a water injection (control) derived from five discrete experiments, assessed by cuticle preparation. In the control, 91.7% of the controls offspring develop a wild type cuticle. In the knock down, 66.4% develop wild type like. The empty egg phenotype is increased from 5.1% in the wild type, to 25.5% in the knock down. The cuticle crumbs phenotype is increased from 3.2% to 8.1%, respectively. The embryo in **A1** is a potential ventral view and the same embryo as in **A2**, which is a potential lateral view. The embryo in **B** is a potential ventral view. Scale bar is 100 μm.

down embryos, which is in accordance with overall observations during the experiments. The main phenotype is the empty egg phenotype, which is quintupled in the knock down (25.5%) compared to the wild type (5.1%). The cuticle crumbs phenotype is increased to 8.1% from 3.2%, respectively.

These findings indicate that *Tc-iro* is important for processes before differentiation of the blastoderm, when *Tc-pnr* is not yet expressed but *Tc-iro* already is (Figure 3.18C) [Sharma et al., 2013a]. The observed impaired formation of the primitive pit could point to a need for *Tc-iro* for its formation, even though the subsequent movement arising from the posterior fold does happen in the knock down. As a defect in the formation of the primitive pit is not observed in *Tc-pnr* knock down embryos, it could be due to *Tc-iro* expression around the posterior fold, where its expression extends more ventral than *Tc-pnr* expression (compare Figure 3.17A and G).

In accordance with previous findings in *Drosophila* that the dorsal epidermis at the retracted germband stage is divided into a medial and lateral region, marked by *Dm-pnr* and *Dm-iro* expression, respectively [Calleja et al., 2000], it was reported that loss of *Dm-pnr* expression leads to a transformation of the medial region into the lateral one [Herranz and Morata, 2001]. This is accompanied by an expansion of the *Dm-iro* expression domain into the dorsal medial region [Calleja et al., 2000].
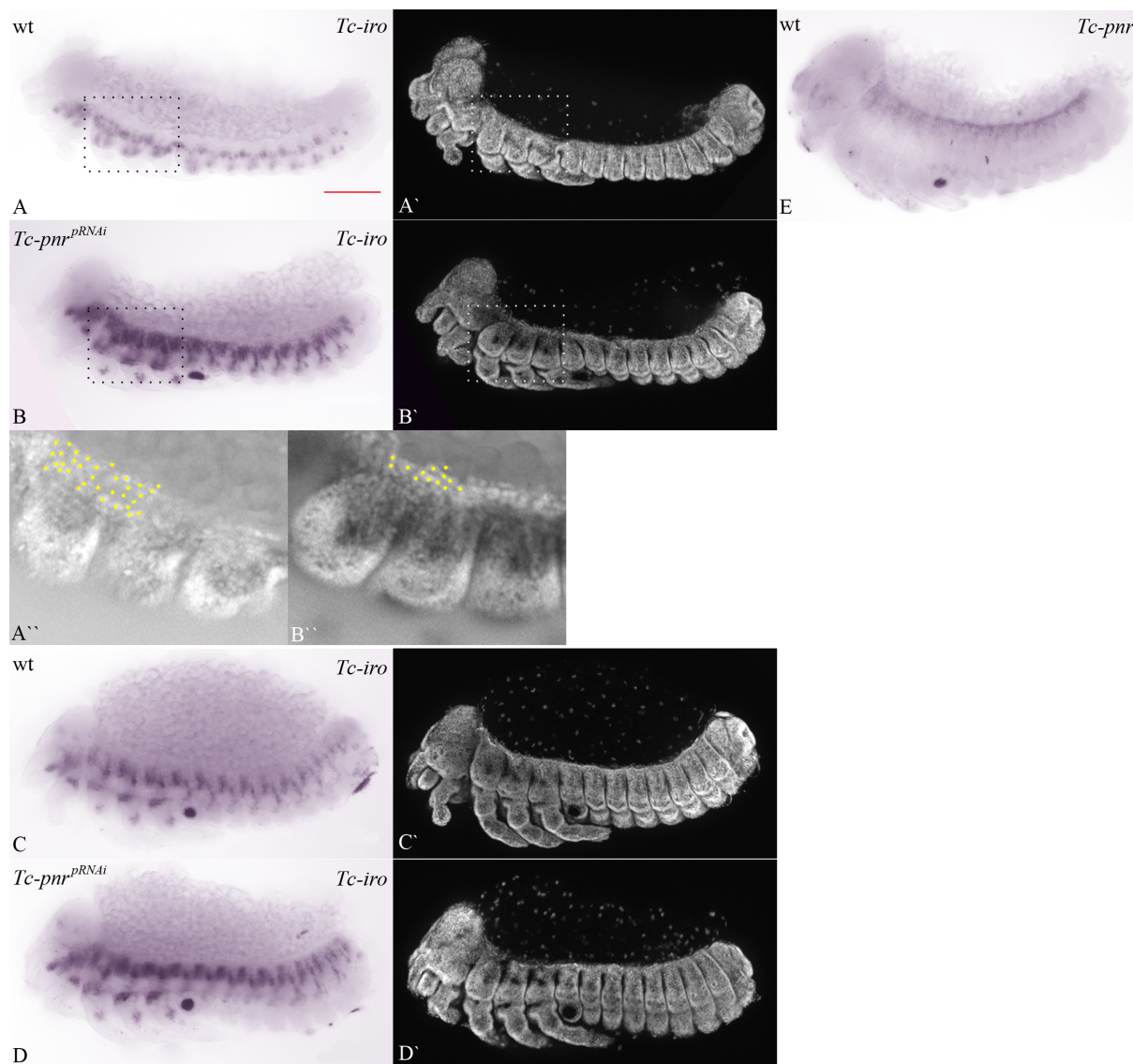
Figure 3.19: **_Tc-pnr_ represses _Tc-iro_ expression in the dorsal ectoderm at the retracted germband stage**. (**A-D**) Embryos stained for _Tc-iro_ via _in situ_ hybridization. (**E**) Embryo stained for _Tc-pnr_ via _in situ_ hybridization. (**A`-D`**) Respective DAPI counterstain. (**A``** and **B``**) Overlay of a single section of the projections in **A, A`** and **B, B`**. (**A, C** and **E**) Wild type embryos. (**B** and **D**) _Tc-pnr_ knock down embryos. (**A** and **C**) _Tc-iro_ is expressed in the lateral ectoderm (investigated by relating the DAPI counterstain to the specific _Tc-iro_ stain in the single sections of the projection, which is in the outermost cell layer, the ectoderm) in a segmental repeated pattern that extends into the head region and ventral to this expression in a similar pattern in embryonic tissue. Small areas of expression are also seen in the legs in **C**. (**B** and **D**) The two latter expression domains persist in the _Tc-pnr_ knock down, whereas _Tc-iro_ expression in the lateral ectoderm is extended dorsally. **A``** and **B``** are enlargements of the respective areas in **A, A`** and **B, B`**, which illustrate this extension more clearly. The yellow dots roughly indicate unstained cells from the most dorsal _Tc-iro_ expression to the dorsal margin of the embryo. In the knock down, this _Tc-iro_ expression free area is approximately halved compared to the wild type. (**E**) Same embryo as in Figure 3.12. Scale bar is 100 μm.

To check if _Tc-iro_ expression in the lateral ectoderm expands more dorsally in _Tc-pnr_ knock down embryos and therefore would be conserved to _Drosophila_, wild type and knock down embryos were stained for _Tc-iro_ expression (Figure 3.19).

Figure 3.19A, A`and C, C`show that _Tc-iro_ is expressed in the lateral ectoderm, as well as in other embryonic domains. Furthermore, expression of _Tc-iro_ expands in the _Tc-pnr_ knock down towards the dorsal ectoderm (Figure 3.19B and D and B`and D`), where _Tc-pnr_ is normally expressed (compare to Figure 3.19E). Albeit the expansion of the _Dm-iro_ expression domain is more pronounced in the _Dm-pnr_ mutant [Calleja et al., 2000], the tendency of _Tc-iro_ to extend more dorsally could be shown. This indicates that the expression of _Tc-iro_ in the ectoderm dorsal to its normal expression pattern is due to _Tc-pnr_ induced repression in this domain in wild type, what seems to be conserved to a certain degree in both _Tribolium_ and _Drosophila_.

3.2.6 Different defects in the amnion after _Tc-pnr_ pRNAi

Tc-pnr is a consistent marker of the amnion throughout most of _Tribolium_ embryonic development. Its expression starts at the differentiation of the blastoderm (see Figure 3.9A) and persists until the embryo finishs germband extension (see Figure 3.11A). At the retracted germband stage, it is still expressed in the amnion (see Figure 3.11B). In later

stages accessibility of the extraembryonic membranes by *in situ* hybridization is profoundly impeded by the vitelline membrane and resulting dissecting methods, so that reliable statements about its expression are not possible anymore with whole mount staining procedures.

In *Drosophila*, *Dm-pnr* is expressed starting at the cellular blastoderm in the precursor cells of the amnioserosa. Expression in the amnioserosa is constant until mid germband extension. Afterwards, it starts to weaken until it is no longer detectable at the end of germband extension [Winick et al., 1993; Heitzler et al., 1996].

That *Tc-pnr* is permanently expressed in the extraembryonic tissue, suggests a more important function in *Tribolium* than in *Drosophila*, where only a potential early cell death was reported (compare [Heitzler et al., 1996] and [Herranz and Morata, 2001]).

To check if the amnion is affected in *Tribolium*, *Tc-pnr* pRNAi was performed and the resulting phenotype visualized by the HC079 line, in which EGFP is expressed in the amnion starting shortly after germband extension [Hilbrant et al., 2016]. The development of 15 *Tc-pnr* knock down embryos was recorded. 10 showed the dorsal open phenotype and eight of this subset of embryos (80%) displayed different defects in the amnion directly or passively during the process of rupture (Figure 3.20; five movies showing the respective defect in the amnion of the embryos in Figure 3.20A-E are included on the DVD; see 6.7 movies 5A-5E, respectively). The other five embryos belong to the 'not assignable phenotype', introduced in Figure 3.13. In Figure 3.20A the most frequent defect is seen (three out of eight; 38%). The amnion withdraws significantly more slowly over the posterior abdomen (ranging from 2h40min in the first, up to 5h10min in the second embryo; in the third embryo the extraembryonic tissue is not able to withdraw over the abdomen) than in control embryos (compare to 3.2.3). This leads to a constriction of the embryo, as indicated by the area between the blue dashed line and the purple dashed line. The amnion in Figure 3.20B has several small holes (one out of eight; 13%), even though only one is visualized in the figure. All holes which are visible in the amniotic dorsal organ, are already seen prior to rupture. Consequently, these holes neither impair rupture, nor the following withdrawal. Ectopic amniotic rupture of the amnion (two out of eight; 25%) in Figure 3.20C, is initiated within the hole enclosed by the yellow dashed line. Interestingly, the hole is getting smaller prior to rupture. In another embryo, ectopic rupture was recorded at the posterior (not shown). Normal rupture together with
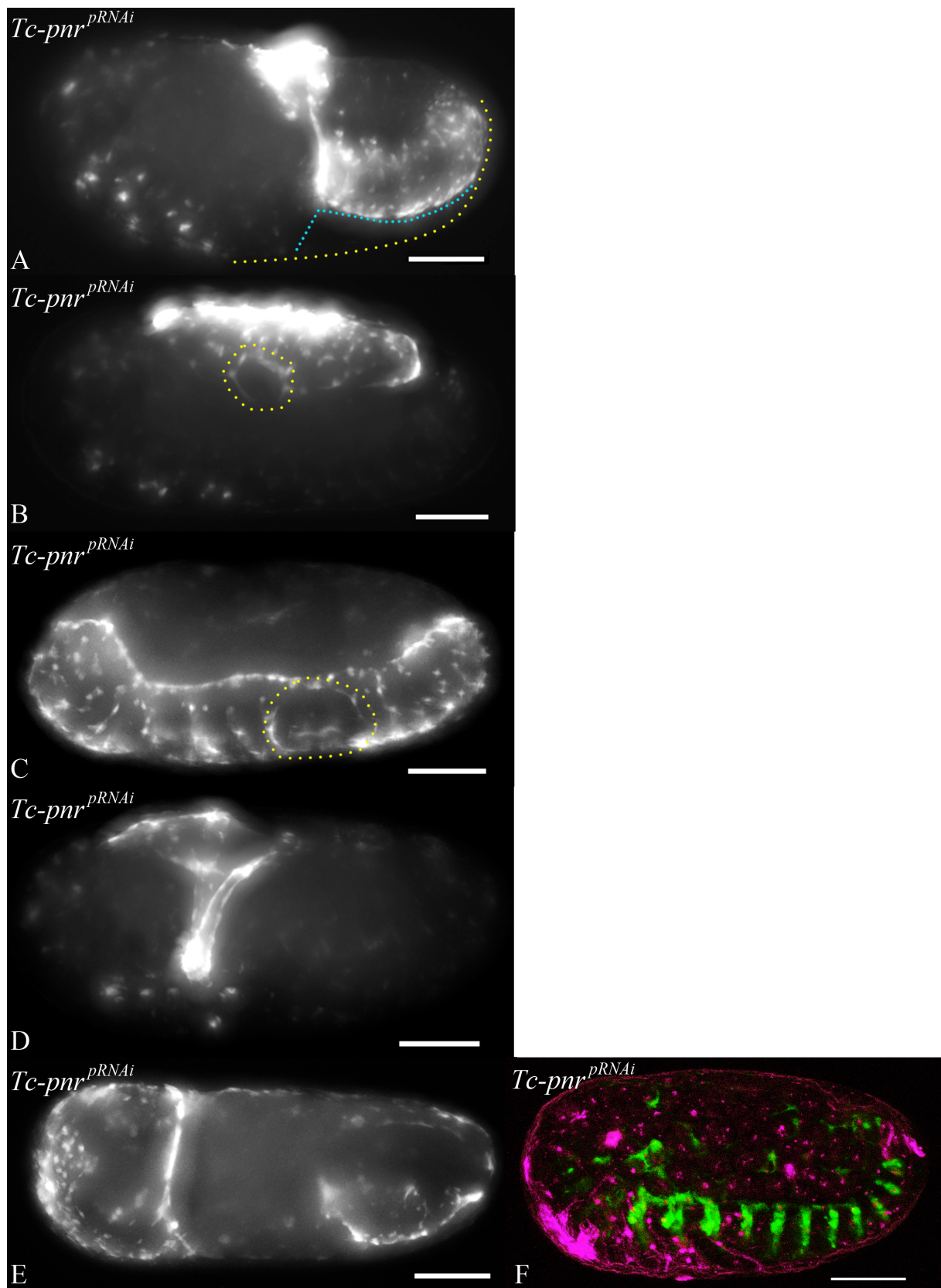
Figure 3.20: **Different amniotic defects after *Tc-pnr* pRNAi**. (**A-E**) Embryos of the HC079 line, showing defects during amniotic rupture or in the amnion itself after *Tc-pnr* pRNAi. (**F**) Cross of the rHC079 line (magenta) and the enhancer trap line G04910 (green) (see Figure 3.22). (**A**) The amnion retracts very slow over the abdomen, squeezing the abdomen during this time strongly. The dashed yellow line follows the shape of the eggshell and the blue one the embryo, visualizing the constriction caused by the slow propagation of amniotic withdrawal over the abdomen. (**B**) The amnion has withdrawn to the dorsal side. At its lateral flank a hole is visible, outlined by the dashed yellow line. (**C**) The dashed yellow line reconstructs a large hole in the amnion, where ectopic rupture will take place. (**D**) The amnion does not withdraw over the abdomen but due to an additional ectopic rupture at the posterior, a constriction has formed in the middle of the embryo. Here the amnion will start to degenerate and subsequently withdraw to the dorsal side. (**E**) The outline of the amnion is visible to a certain degree, while the organization of amniotic nuclei is abnormal. Expression in the amnion is partially lost. (**F**) Similar defect to the embryo in **E**. After *Tc-pnr* knock down, the amnion is not recognizable in its normal form and only in the more ventral anterior cap region as well as slightly posterior, the red fluorescence can be assigned to its amniotic origin. Its normal outlines separating it at the dorsal side towards the yolk are completely gone. The embryo itself has at least formed an extending germband and seems rather wild type like. **A-D** and **F** are lateral views, **E** is a dorsal view. Scale bars are 100 μm.

ectopic rupture at the posterior pole (one out of eight; 13%) lead to the constriction in Figure 3.20D. The last recorded defect is the one seen in Figure 3.20E. In this dorsal view the normal cell arrangement in the amnion is disordered (one out of eight; 13%). While there is cell accumulation in the anterior cap region, other areas look rather cell free. Another single *Tc-pnr* knock down embryo imaged in a separate experiment, showed a similar defect (Figure 3.20F). Again, there is an accumulation of cells, this time in the ventral part of the anterior cap region. It is only directly posterior of these cells that additional cells bear a strong enough signal to be identified as of amniotic origin. The rest of the 'amniotic region' (if it exists) is indistinguishable from the background. A clear border between the amnion and the yolk cannot be identified.

In all eight recorded embryos, the amnion is always able to rupture and in six of them the amnion is able to withdraw to the dorsal side, where it degenerates as described in Figure 3.15. It is only in an embryo exhibiting slow withdrawal of the amnion and in the embryo shown in Figure 3.20E that complete withdrawal is not happening. In case of the first embryo, the amnion is not able to withdraw over the abdomen. Still, amnion withdrawal is slowed down already before. In the second embryo, imaging was stopped
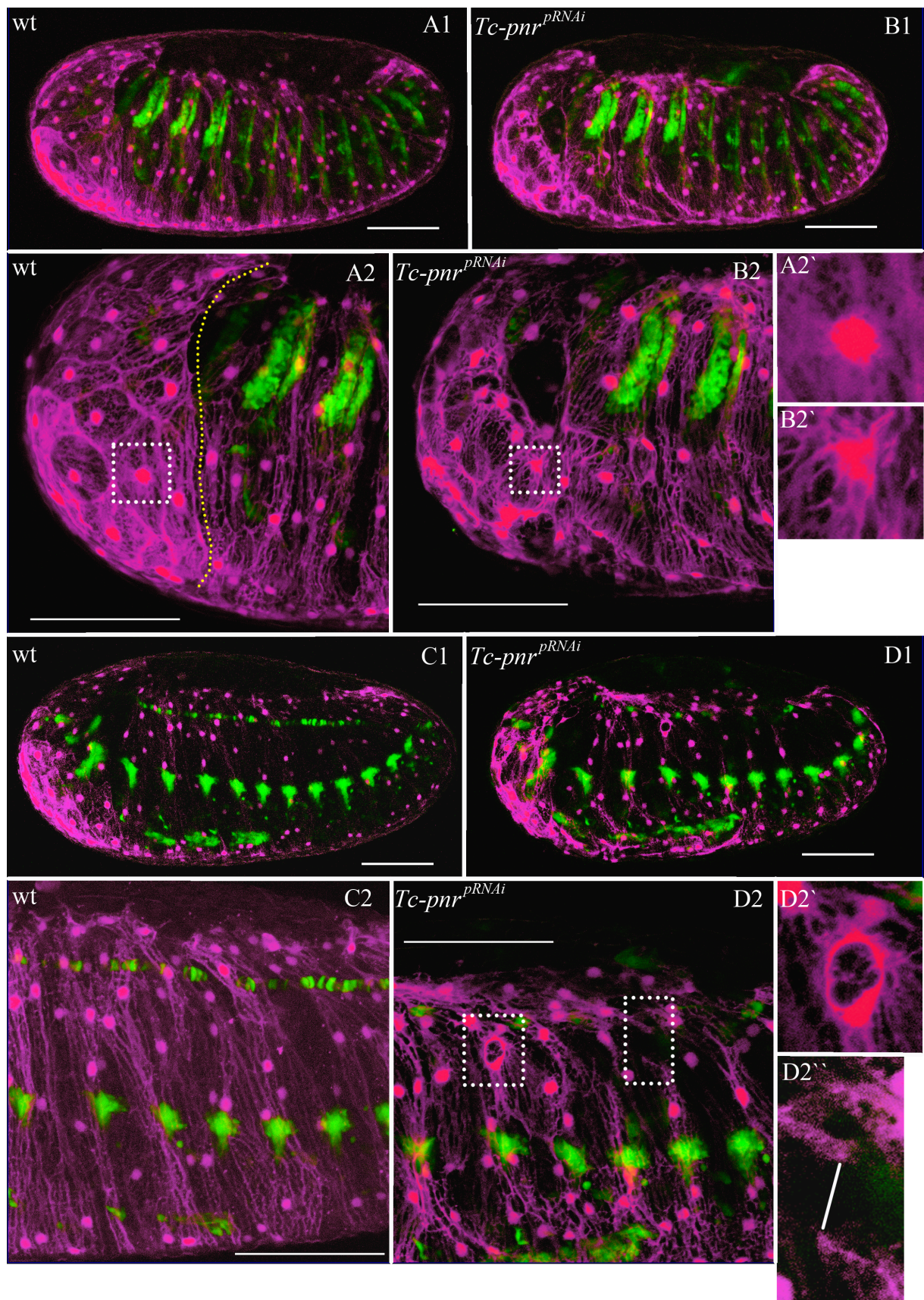
Figure 3.21: **Normal morphology of the amnion is disturbed in *Tc-pnr* knock down embryos**. Cross of the rHC079 line (magenta) with the line G04910 (**A1, B1**) and G04609 (**C1, D1**) (both in green). Embryos in **A2-D2** are the same embryos as in **A1-D1** respectively but imaged at higher magnification. (**A1, C1**) Wild type embryos. (**B1, D1**) *Tc-pnr* knock down embryos. (**A2**) Focus on the anterior cap region (anterior to the dashed yellow line), for comparison with **B2**. (**B2**) The cell shapes of the normally large cells of the anterior cap are disturbed and the borders between individual cells cannot be identified easily. Visualized by DsRed2 expression, the nuclei look different from the wild type (compare **A2`** and **B2`**, which are enlargements of the respective white dashed rectangles). The border between the anterior cap region and other amniotic tissue as drawn in **A2**, can not be found. (**C2**) Focus on the amnion in the middle of the embryo, for comparison with **D2**. (**D2**) The overall organization is disturbed and the expression shows dark gaps with no expression (more pronounced towards the posterior), if compared to the wild type. Hole-like structures are visible (**D2`**) and connections between the DsRed2 labeled 'protrusions' seem to be broken (**D2``**; normal connection is indicated by the white line). Scale bars in **A2-D2** are 50 μm and 100 μm in **A1-D1**.

shortly after rupture, so that it can not be assessed if the amnion withdraws over the abdomen.

To investigate the observed amniotic defects in more detail, the rHC079 line was crossed either to the line G04609 [Koelzer et al., 2014] or the in this study characterized enhancer trap line G04910 [Trauner et al., 2009] (Figure 3.21; see also Figure 3.22A1-A3; one movie showing the progression of the EGFP signal in the line G04910 and one showing the progression of the EGFP signal in the line G09423 are included on the DVD; see 6.7 movies 6A and 6B, respectively). The two EGFP expressing lines were used to provide positional information, by using the specific expression in the cardioblast cell row in the line G04609 (therefore also referred to as the 'heart' line) and the segmentally repeated expression in the line G04910 as embryonic landmarks. After *Tc-pnr* pRNAi, the anterior cap region, where the amnion will rupture prior to dorsal closure [Hilbrant et al., 2016], is not distinguishable from other regions within the amnion (Figure 3.21). The nuclei have changed their morphology from roundish to a blob-like shape (compare Figure 3.21A2`and B2`). Cells within the specialized cap region seem to be more often affected than other cells. Dark areas in between individual cells are visible. These can be either actual holes in the tissue or they are due to a localized reduction in the DsRed2 signal. In the non-cap region, these dark areas are also apparent (Figure 3.21D2). Additionally, small hole-like structures are visible (Figure 3.21D2`). Protrusion, which seem to connect different nuclei
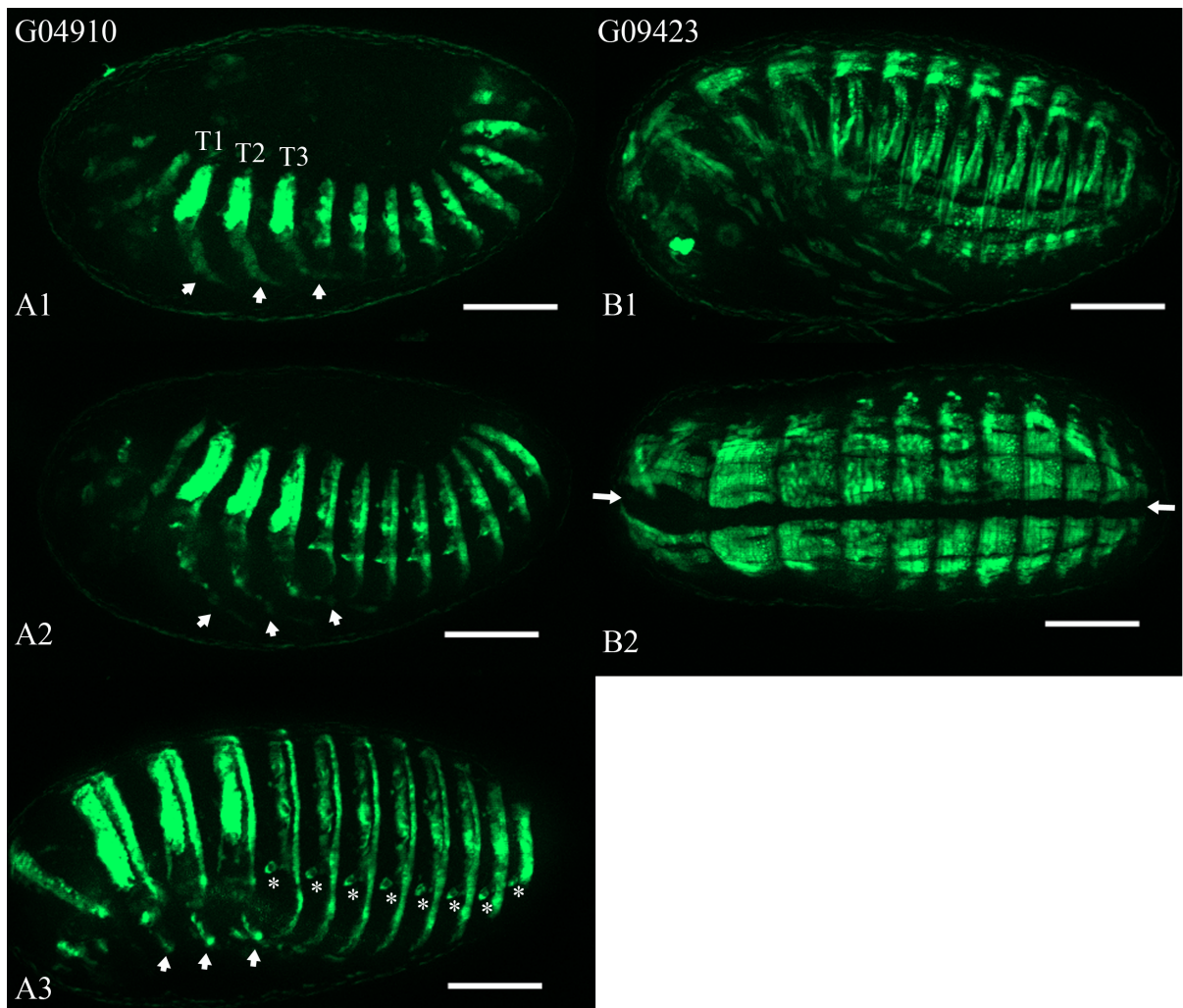
Figure 3.22: **Expression pattern of the enhancer trap lines G04910 and G09423**. (**A1-B2**) Embryos of the two GEKU lines G04910 and G09423 [Trauner et al., 2009], characterized during this study. (**A1-A3**) Embryos of the enhancer trap line G04910. EGFP expression in a segmentally repeated fashion from the head towards the abdomen, in the openings of the tracheal system (white asteriks) and in the legs (white arrows). The EGFP signal is stronger in the upper half of T1-T3. During embryogenesis, the EGFP signal comes up around mid germband retraction. (**B1-B2**) Embryos of the enhancer trap line G09423. EGFP expression in somatic muscles, similar to the transgenic line pBA19 [Lorenzen et al., 2003; Stappert et al., 2016]. No expression is visible in the heart and in the brain (black longitudinal space in the dorsal view in **B2**, marked by white arrows). The EGFP signal in this lines comes up very late during embryogenesis, approximately towards the end of dorsal closure. **A1-A3** and **B1** are lateral views, **B2** is a dorsal view. Scale bars are 100 μm.

and/or marking cell borders and which are visualized by DsRed2 expression, are normally running in a relatively straight DV direction (Figure 3.21C2). In the knock down however, these connections are either rippled or absent, indicated by the loss of DsRed2 expression. Some of these protrusions seem also broken (Figure 3.21D2``). If looking at the different defects within the amniotic tissue, it becomes apparent that the overall morphology of the amnion is disturbed in *Tc-pnr* knock down embryos. This indicates that *Tc-pnr* expression in the amnion is normally needed for maintaining this morphology.

3.2.7 *Tc-pnr* knock down does not effect the serosa and does not cause a defect during early embryogenesis

In order to check if the early *Tc-pnr* expression in the anterior amniotic fold effects the serosa, the expression of *Tc-zen1* in *Tc-pnr* knock down embryos was investigated (Figure 3.23).
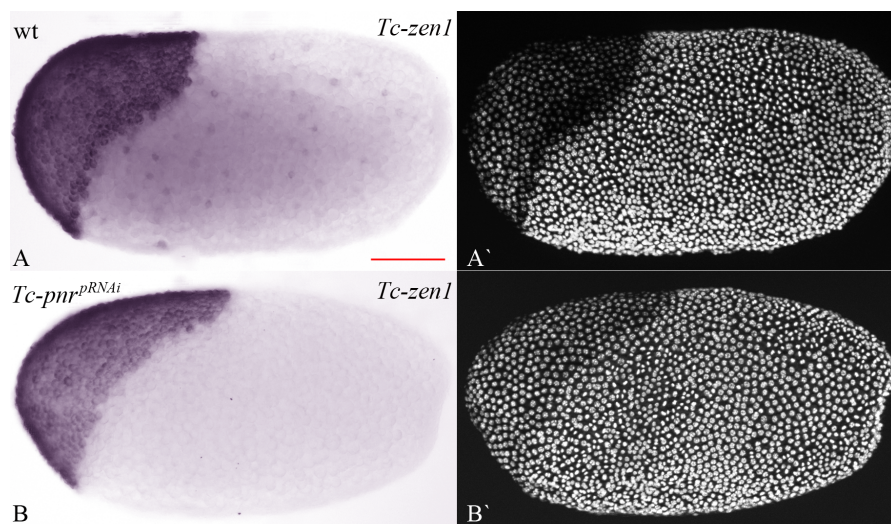
Tc-zen1 is expressed in the prospective cells of the serosa in an oblique anterior domain, just before the onset of the first visible differentiation of the blastoderm into

Figure 3.23: ***Tc-zen1* expression at the late undifferentiated blastoderm stage is not affected in *Tc-pnr* knock down embryos**. (**A, B**) Embryos stained for *Tc-zen1* via *in situ* hybridization. (**A`, B`**) Respective DAPI counterstain. (**A**) In the wild type, *Tc-zen1* is expressed in cells of the prospective serosa. (**B**) After knock down of *Tc-pnr*, *Tc-zen1* expression is not altered. Scale bar is 100 μm.

germ rudiment and serosa (Figure 3.23A and A`). That the distinction between cells giving rise to the serosa and cells of the presumptive amnion is not completely accessible, was shown by a double *in situ* hybridization analysis of *Tc-zen1* and *Tc-iro* [Sharma et al., 2013a]. The authors showed that at the late undifferentiated blastoderm, as well as at the very beginning of the differentiated blastoderm stage, both genes are partially expressed in the same cells [Sharma et al., 2013a]. As the knock down of *Tc-pnr* resulted in a loss of *Tc-iro* expression in domains where *Tc-pnr* is expressed and in some where it is not expressed (see Figure 3.17), *Tc-zen1* expression in the *Tc-pnr* knock down was checked. Figure 3.23B shows that *Tc-zen1* expression is not altered. However, a partial loss of *Tc-zen1* expression at its posterior border towards the germ rudiment, can not be excluded.

To test if loss of *Tc-pnr* expression does effect early embryogenesis (late undifferentiated blastoderm until extended germband) at all, 18 knock down embryos were imaged using the nGFP line. None of them exhibited any detectable defect (data not shown).

To conclude the analysis of the serosa during late embryogenesis (retracting germband until completion of dorsal closure), *Tc-pnr* knock down embryos were imaged in a cross of the 'serosa' line G12424 (EGFP expression in the serosa starting before germband extension [Koelzer et al., 2014]) and the 'heart' line G04609 (EGFP expression in the cardioblast cell row starting during retraction of the germband [Koelzer et al., 2014]). 27 *Tc-pnr* knock down embryos were imaged, of which 21 showed the dorsal open phenotype (77.8%). In three embryos serosal rupture was greatly delayed (11.1%) but probably it did happen after the recording was stopped, as the serosa started to contract, a typical movement prior to rupture. In comparison, the withdrawal of the serosa in the embryos exhibiting the dorsal open phenotype, serosal withdrawal was not delayed (*Tc-pnr* knock down embryos: 30 min; n = 21; standard deviation is 20 min; control embryos: 30 min; n = 6; standard deviation is 20 min; time in minutes is the mean value it takes the serosa to withdraw over the abdomen after rupture), which is in opposition to 3.2.3. In the three remaining embryos, embryonic tissue was present, although development did not proceed (11.1%). Interestingly, in none of the embryos exhibiting the dorsal open phenotype, the serosa did rupture ectopically, despite the reported physical connection of both tissues [Hilbrant et al., 2016].

3.2.8 The amnion and the serosa withdraw partially independent from each other after rupture of both extraembryonic membranes

In the last two sections it was shown that the amnion ruptures ectopically after *Tc-pnr* pRNAi, while the serosa seems to be mostly unaffected (see also Figure 3.15 for slow withdrawal of the serosa). To investigate this further, knock down embryos of the nGFP line were used for live imaging. In the nGFP line, GFP is localized to the nuclei [Sarrazin et al., 2012] and therefore should illuminate both serosal and amniotic nuclei. Unfortunately, the GFP signal in the amnion was very hard to distinguish from any other signal, whereas the serosa was at all time easily discernible.

27 *Tc-pnr* knock down embryos were imaged, of which 24 show the dorsal open phenotype (88.9%). The remaining three embryos are counted as not assignable phenotype (11.1%). From the 24 embryos, only one embryo shows ectopic rupture of the amnion at the posterior, while the serosa ruptures and withdraws wild type like (Figure 3.24; the movie showing the *Tc-pnr* knock down embryo exhibiting ectopic amniotic rupture is included on the DVD; see 6.7 movie 7). In this embryo, the serosa ruptures normally at the anterior side and withdraws to form the dorsal organ, before it sinks down into the yolk and degenerates (Figure 3.24; blue dashed lines/areas). A small opening in a tissue at the ventral side becomes apparent in the movie, approximately 140 min after rupture of the serosa (Figure 3.24A4). This tissue is believed to be the amnion, which did not rupture together with the serosa. As visualization of the amnion is very difficult, not to mention the small opening, the expanding opening in the amnion is encircled by an orange dashed line (Figure 3.24A4-A10). This hole in the amnion increases over time towards the anterior and dorsal side, until it adopts a triangular shape (Figure 3.24A10). Than, approximately 300 min after rupture of the serosa, the hole rips open in a rupture like movement and the amnion withdraws over the abdomen (Figure 3.24A11; direction of withdrawal is indicated by the orange arrow). Withdrawal over the anterior part of the amnion seems not to take place, rather the amnion gets stuck next to the original opening, which is presumably just over the tip of the T3 leg (Figure 3.24A11; amnion withdrawal does not exceed the orange dashed line). This could provide a sufficient barrier, especially if the force to facilitate amniotic rupture is not strong enough anymore after amnion withdrawal over the abdomen. In this case the amnion would still cover the
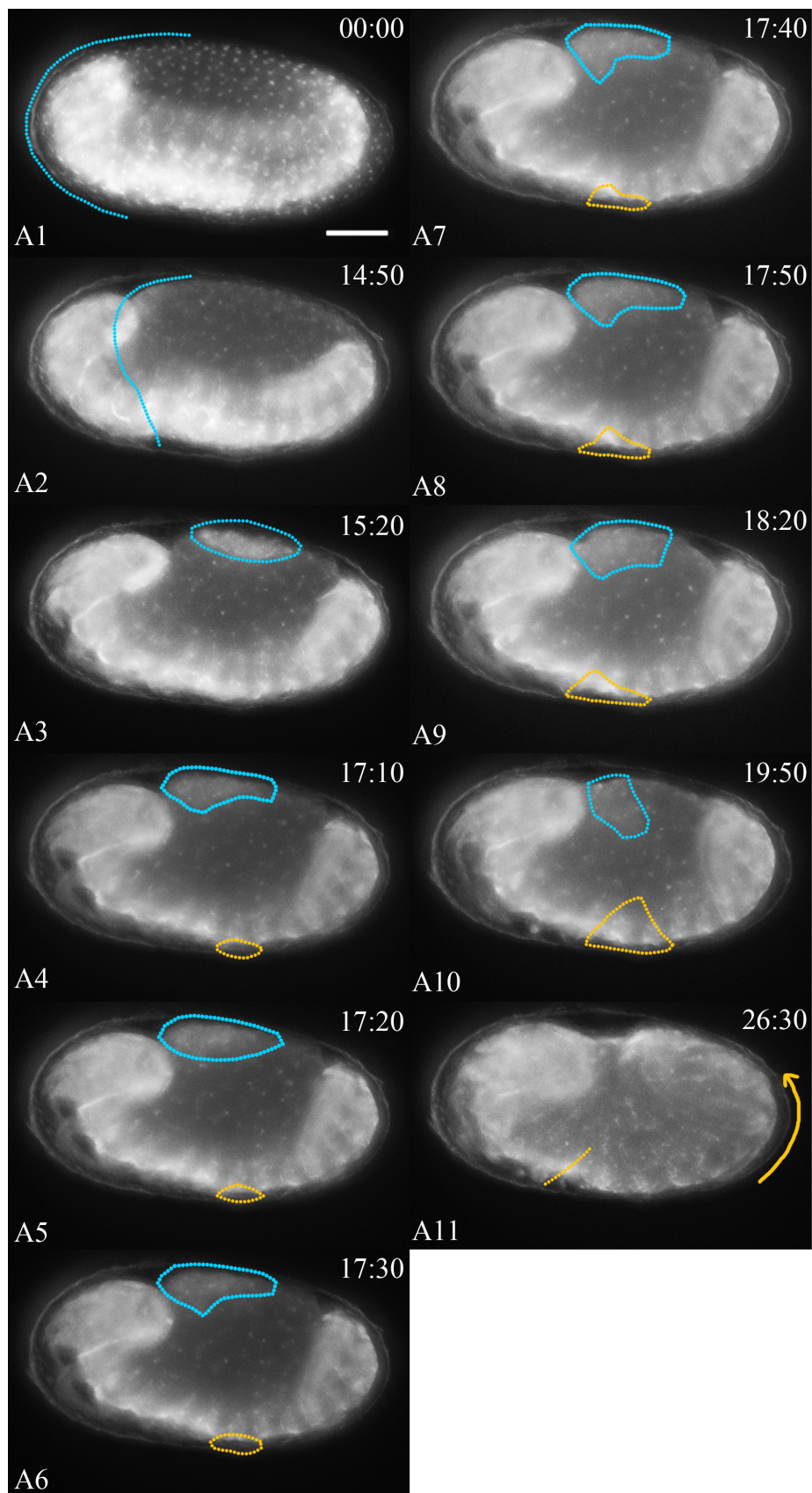
Figure 3.24: **The site of rupture of the amnion and the serosa differ after *Tc-pnr* parental RNAi**. *Tc-pnr* knock down embryo of the nGFP line. Live imaging was started 40.5 h +/- 2 h after egg laying, which corresponds to the time stamp 00:00 in **A1**. (**A1**) . The embryo has fully retracted and the serosa encloses embryo and yolk (indicated by the blue dashed line for the anterior part). (**A2**) The serosa has ruptured wild type like at the anterior (indicated by the blue dashed line). (**A3**) The serosa has withdrawn to the dorsal side, forming the serosal dorsal organ (encircled by the blue dashed line). (**A4**) The orange dashed line roughly encircles a hole in the amniotic tissue. (**A5-A9**) The hole has increased in size towards the anterior and slightly towards the dorsal side. (**A10**) The hole has widened to the dorsal side, now forming a triangle, while the serosa sinks down into the yolk. (**A11**) The amnion has ripped wide open and has withdrawn over the abdomen (indicate by orange arrow). Towards the anterior ventral side, the amnion got stuck (this position is marked by the orange dashed line). Time stamp is in h:min. The embryo has been imaged at a constant temperature of 30 °C. Scale bar is 100 μm.

embryo over the head and the thorax region.

Although only one embryo out of 24 (4.2%) embryos, which showed the dorsal open phenotype, showed ectopic rupture of the amnion, it is believed to occur more often, as in another live image experiment, 80% of the affected embryos exhibited ectopic rupture (see 3.2.6). One reason for this could be that visualization of the amnion is very difficult in the nGFP line. Therefore, it could well be that defects in the amnion were overlooked.

3.2.9 The severeness of different defects after *Tc-pnr* parental RNAi is affected by the strength of the knock down

The images in Figure 3.20F and Figure 3.21 were taken from knock down embryos, which were injected with degraded dsRNA. This resulted in a reduced concentration, which in turn lead to a more mild dorsal open phenotype as reported (see Figure 3.15). The penetrance of the phenotype, which is the percentage of all embryos showing the dorsal open phenotype (here 82.4%), was not affected. However, the dorsal open phenotype is not as pronounced as in the severe (normal) dorsal open phenotype. Figure 3.25 compares the mild and severe dorsal open phenotype, to one showing wild type development (One movie for of each of the three embryos showing their development, is included on the DVD; see 6.7 movies 8B, 8C and 8A, respectively). All imaged embryos resulted from a cross of the rHC079 line (DsRed2) with the 'heart' line G04609 (EGFP) but only the EGFP channel is visualized (and leakage from the DsRed2 signal into the EGFP channel; see yellow arrows), as DsRed2 expression in the amnion would have impeded the view on
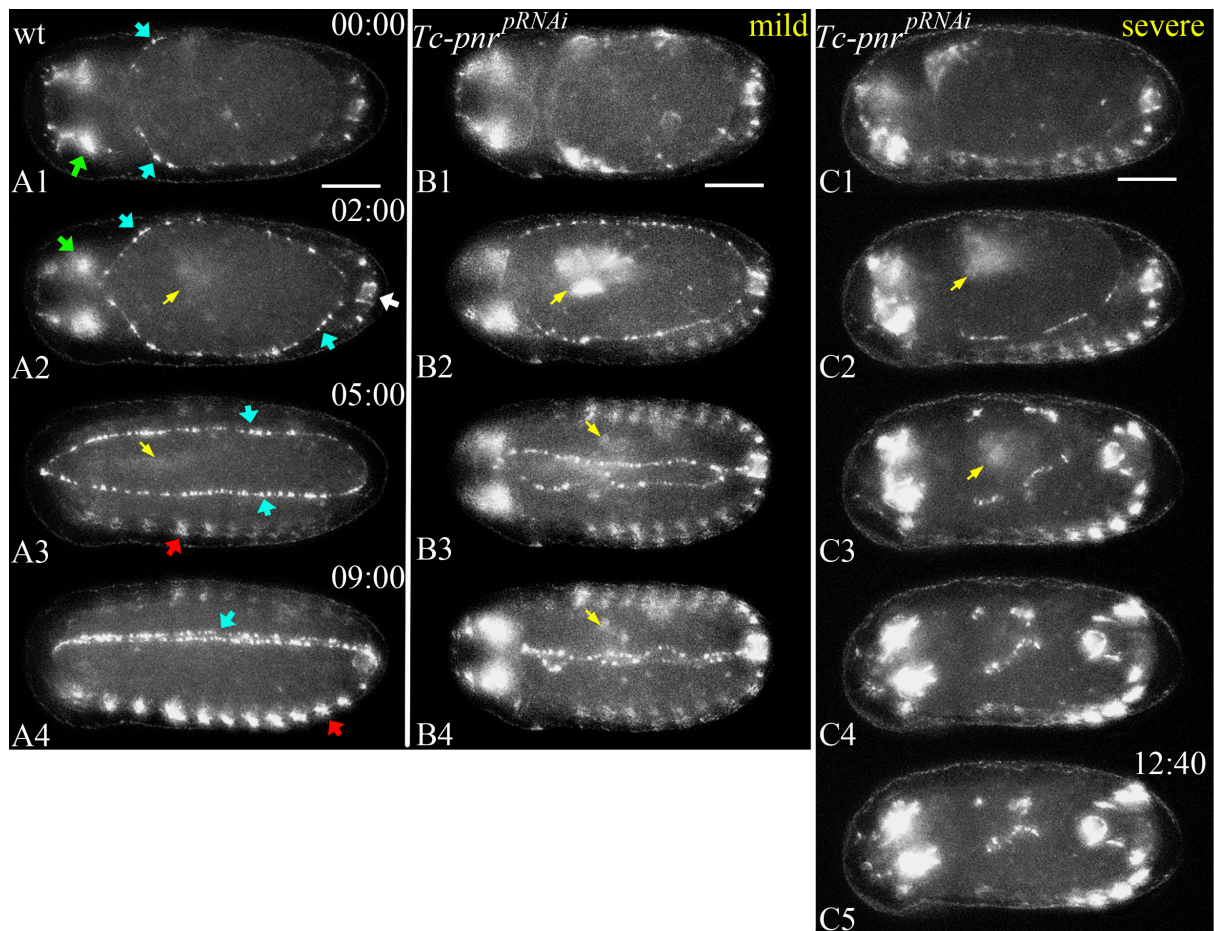
Figure 3.25: **Comparing the mild and severe phenotype after *Tc-pnr* pRNAi, while introducing normal heart formation using the 'heart' line G04609**. Live imaging of a wild type embryo (**A1-A4**) and two *Tc-pnr* knock down embryos (**B1-D4**), using a cross of the heart line (EGFP) and the rHC079 (DsRed2) line. Visualized is only the EGFP channel. The yellow arrows point to (weak) DsRed2 signal emitting from the amnion, due to a crosstalk between the EGFP and DsRed2 channel. All three embryos are synchronized to the first time point in which amniotic rupture is visible. (**A1-A4**) Normal developing embryo, where the two cardioblast cell rows (blue arrows) come together at the dorsal midline, as the embryo completes dorsal closure. The green arrows mark the EGFP expression in the head/eyes, the white arrow marks the proctodeum and the red arrows point to the segmental muscle blocks. (**B1-B4**) Mild dorsal open phenotype, in which the cardioblast cell rows come together rather wild type like at the midline but are unable to form a straight bicellular heart row. Notably, the head and abdomen bend only slightly towards the dorsal side. (**B1-B5**) Severe dorsal open phenotype, which shows the characteristic bending of the head and the abdomen towards the dorsal side. The two heart rows do not come together at the midline but seem to get drawn to the dorsal center of the embryo. All embryos are dorsal views. Time stamp is in h:min. The embryos have been imaged at a constant temperature of 30 °C. Scale bars are 100 μm.

the cardioblasts (blue arrows). What becomes apparent, besides from the characteristic bending (visualized by EGFP expression in segmental muscle blocks (red arrows), in the proctodeum (white arrow) and in the head/eyes (green arrows) [Koelzer et al., 2014]), is the effect on the cardioblast cell row (investigated in more detail in the following section), in which *Tc-pnr* is expressed (see Figure 3.11B). The normal formation of the heart row is shown in Figure 3.25A1-A4. In the mild phenotype (Figure 3.25B1-B4), the two cardioblast cell rows almost come together and the expression is only slightly affected. Additionally, the bending of the head and tail towards the dorsal side is not as severe. The severely affected embryo (Figure 3.25C1-C5) shows the characteristic strong bending, while heart formation is heavily impaired. These results point to the assumption that the effect of *Tc-pnr* may be dosage dependent.

3.2.10   *Tc-pnr* is involved in heart development in *Tribolium*

The 'heart' line G04609 was used to provide positional information in *Tc-pnr* knock down embryos. By doing so, it became apparent that EGFP expression in some cardioblasts (= myocardial cells) is lost and that the overall expression in the cardioblasts is diminished, compared to the wild type (Figure 3.26). If this visible loss of EGFP expression in some cardioblasts is really due to a loss of expression or if the cardioblasts itself are lost, is not known, as in both cases no EGFP expression would be detectable. EGFP expression in the segmental muscle blocks and in the head is not affected. Note that in the wild type embryo shown in Figure 3.26 (left image), the EGFP expression within the cardioblast cell row is not continuous. This specific feature of the G04609 line was already reported and is because not all cardioblasts are labeled in this line [Koelzer et al., 2014].
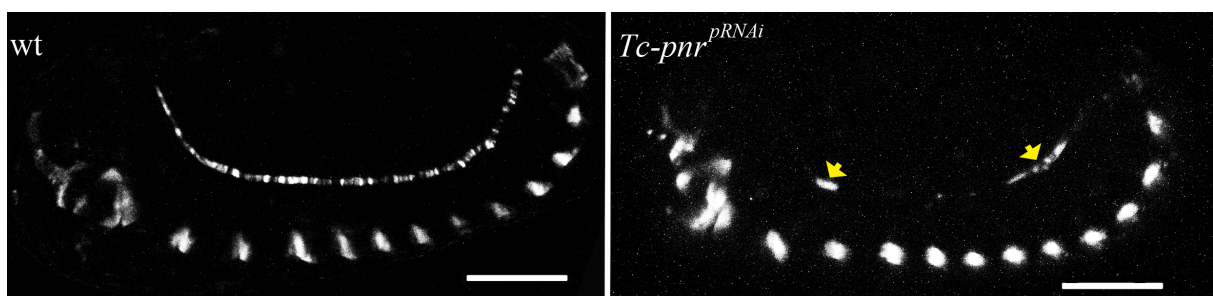
To identify the cause for the loss of EGFP expression in the G04609 line, a knock down embryo was imaged on the cell level and compared to a wild type embryo (Figure 3.27).

Figure 3.26: **EGFP expression is partially lost in the cardioblast cell row of *Tc-pnr* knock down embryos of the G04609 line**. Comparison of a wild type embryo (left image) and a *Tc-pnr* knock down embryo (right image) from the G04609 line. In the image to the right, the two yellow arrows point to some of the residual EGFP expression within cells of the cardioblast cell row. The exposure time of EGFP was increased to achieve better visualization of the remaining EGFP expression in the cardioblasts. Therefore, the expression in the segmental muscle blocks and in the head is stronger compared to the wild type and due to the resulting overexposure in these expression domains, the shape of the domains appears different (compare roundish segmental muscle blocks in the right image, to the more slender ones in the left image). Scale bars are 100 μm.
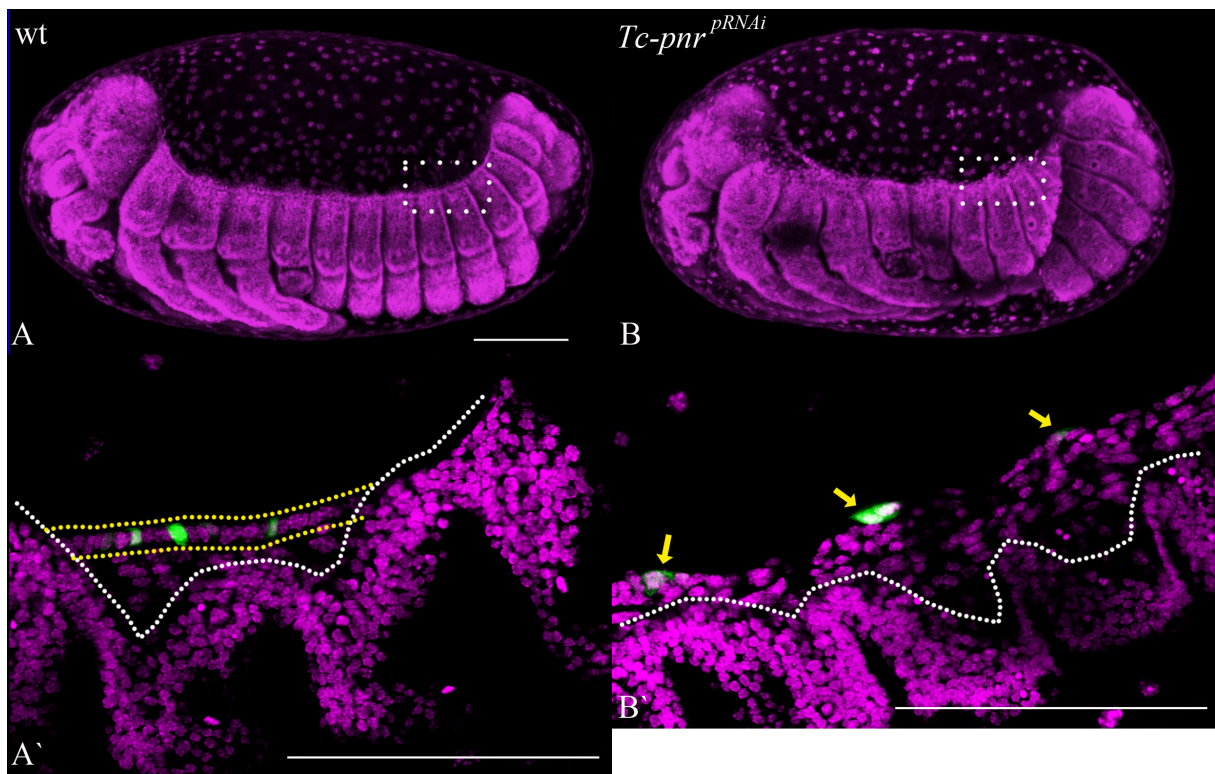
Figure 3.27: **The normal organization of the cardioblast cell row is impaired after _Tc-pnr_ pRNAi**. Comparison of a wild type embryo (**A**) and a _Tc-pnr_ knock down embryo (**B**), using the G04609 line as a marker for the cardioblasts (green) and the DAPI counterstain to label all nuclei (magenta). **A`** is a single section of the area within the white dashed rectangle of the projection in **A** but imaged with a higher magnification. **B`** is a single section of the area within the white dashed rectangle of the projection in **B** but imaged with a higher magnification. (**A**) Wild type embryo, stained with DAPI. (**B**) Knock down embryo, stained with DAPI. The cut at the posterior of this embryo was artificially introduced and is not in relation to any phenotype. (**A`**) The white dashed line separates the small roundish ectodermal cells (below the line), from the bigger and cell shape wise more variable mesodermal cells (above the line). Within the two yellow dashed lines, the cardioblast cell row is discernible as a well structured row of cells. (**B`**) The three yellow arrows point to residual EGFP expression in cells with potential cardioblast identity. The cardioblast cell row is not discernible anymore from other mesodermal cells. The white dashed line separates the mesoderm from the ectoderm. Scale bars are 100 μm in **A** and **B** and 50 μm in **A`** and **B`**.

Figure 3.27A`shows a wild type embryo of the G04609 line, expressing EGFP in some of the cardioblasts (less cardioblasts express EGFP, as the embryo was exposed to methanol for too long, negatively effecting the expression of the fluorescent protein). Distinctive to other cells in Figure 3.27A`, is the cardioblast cell row (between the two yellow dashed lines). It is the dorsal most row of cells of the mesoderm, located slidely ventral to the dorsal most ecotdermal cell row and 'behind' the ectoderm, if looking from the lateral side. The cardioblasts are evenly organized and therefore well distinguishable from the adjacent mesodermal cells. In the _Tc-pnr_ knock down embryo, the cardioblast cell row is no longer visible as a well structured row of cells (Figure 3.27B`). However, the cells which still do express EGFP, are located in the dorsal most mesoderm, as it would be expected for cells within the cardioblast cell row. Interestingly, the 'shape' of the EGFP expression is rather atypically stretched in AP direction in the knock down, compared to the slightly in DV orientation stretched EGFP expression of the wild type cardioblasts (compare EGFP expression in Figure 3.27A`, to the EGFP expression in Figure 3.27B`, marked by the middle yellow arrow). By careful investigation of each individual section of the knock down embryo, it is assumed that this atypical AP stretched EGFP expression is due to an accumulation of three to five cells, which is typically not observed in a normal structured cardioblast cell row. The _Tc-pnr_ knock down embryo in Figure 3.26 (right image) supports this assumption, as the AP stretched 'shape' of EGFP expression can be

observed there as well.

The loss of EGFP expression could be traced back to the lack of normal organization of the cardioblast cell row after *Tc-pnr* pRNAi. If the cardioblasts are degraded subsequently to the knock down of *Tc-pnr* or if the gene driving the EGFP expression in the G04609 line is affected, remains unclear.

It was reported that the EGFP expression in the cardioblast cell row in the enhancer trap line G04609 is due to a partial trapping of the enhancer driving *Tc-midline* (*Tc-mid*) expression [Koelzer et al., 2014]. Partial, as in contrast to the EGFP expression in the cardioblasts in G04609, *Tc-mid* is expressed in all cardioblasts (Figure 3.28A, A``and B). *Tc-mid* is also expressed in segmentally repeated muscle blocks, in a similar pattern along the ventral midline and in the head and the legs. In *Tc-pnr* knock down embryos, the expression of *Tc-mid* in the cardioblast cell row is mostly lost, while all other expression domains remain unaffected (Figure 3.28C and D). This suggests that *Tc-mid* is a regulatory target of *Tc-pnr* for this subset of heart cells (the cardioblast cell row consists out of myocardial cells (cardioblasts) only, whereas the heart consists out of myocardial and pericardial cells). Interestingly, in some cells of the cardioblast cell row *Tc-mid* expression persists, meaning that the knock down does not effect all cardioblasts. This is also true for the EGFP expression in the G04609 line, after *Tc-pnr* pRNAi. Based on the assumption that G04609 traps partially the *Tc-mid* enhancer [Koelzer et al., 2014], these results may emphasize this assumption.

To further investigate the effects on heart development caused by *Tc-pnr* pRNAi, individual cardioblasts within the cardioblast cell row were tracked in a normal developing embryo and a *Tc-pnr* knock down embryo (Figure 3.29; the movie showing the development of the *Tc-pnr* knock down embryo is included on the DVD; see 6.7 movie 9; the wild type embryo is the same as in the movie 8A). The line G04609 was used for this analysis (the knock down embryo is a cross of the line G04609 with the line G12424).

Tracking of the cardioblasts starts, when both cardioblast cell rows are first visible in dorsal aspect (Figure 3.29'Start') and stops, when the cardioblasts do not move significantly anymore (Figure 3.29'End'). The track of each individual cardioblast during this time is retained in the image (Figure 3.29'End-tracked'). In the wild type embryo, cardioblasts located at different starting positions, have specific routes to cover. Cardioblasts located most anterior next to the head (tracks: light green, red and orange), move signif-
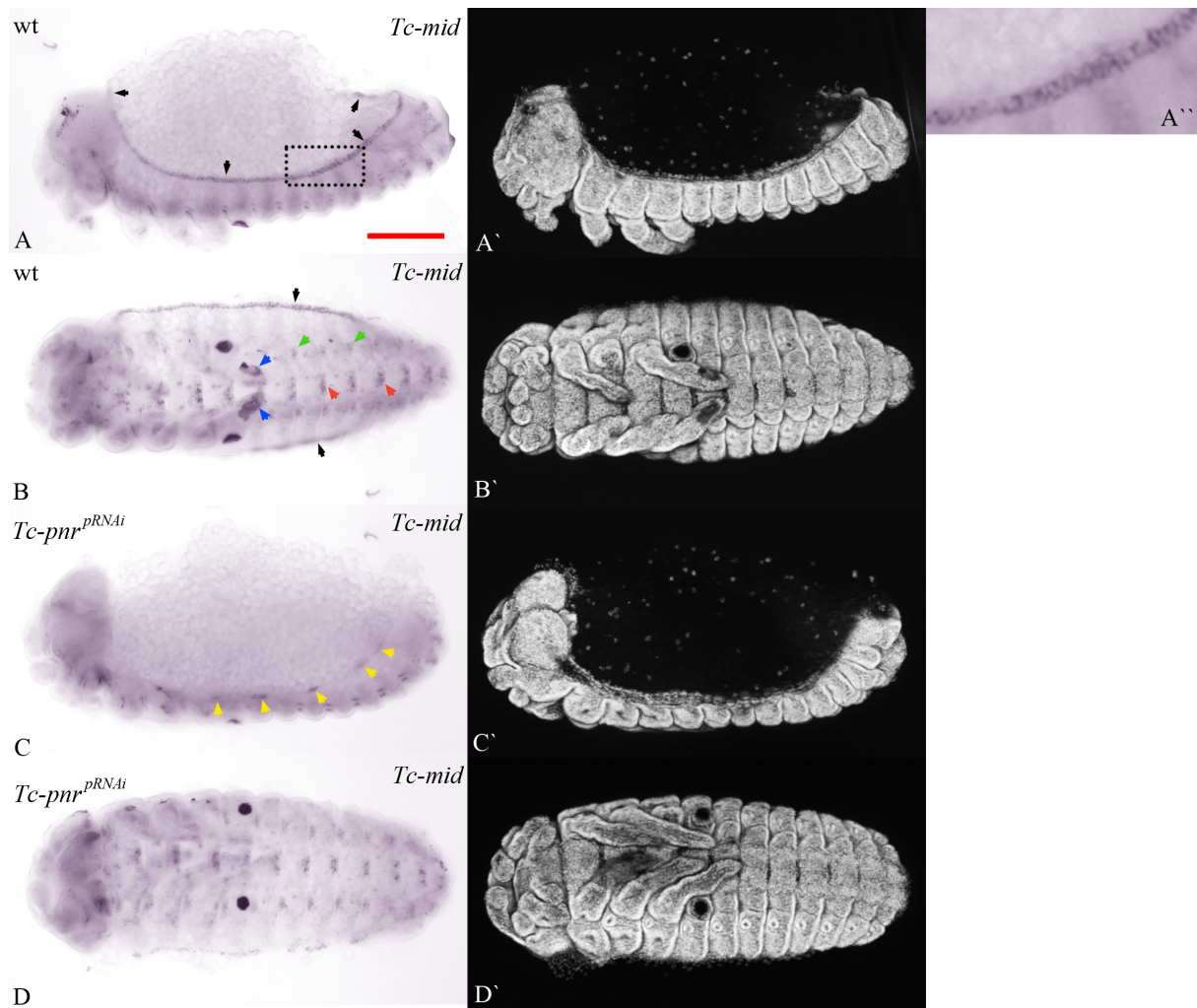
Figure 3.28: ***Tc-mid* expression in the cardioblast cell row is affected after *Tc-pnr* pRNAi**. (**A-D**) Embryos at the late retracted germband stage stained for *Tc-mid* via *in situ* hybridization. (**A`-D`**) Respective DAPI counterstain. (**A, B**) Wild type embryo in lateral (**A**) and ventral (**B**) orientation. (**C, D**) *Tc-pnr* knock down embryo in lateral (**C**) and ventral (**D**) orientation. (**A, B**) *Tc-mid* is expressed in the cardioblast cell row (the black arrows mark the cardioblast cell row) in the dorsal most mesoderm of the embryo, in an segmentally repeated pattern along the ventral midline (the two red arrows point to some of this expression) and in segmental muscle blocks (the two green arrows point to some of this expression). The blue arrows point to dirt particles, resulting in unspecific staining in both tips of the T3 legs. *Tc-mid* is also expressed in the legs and in the head. The area encompassed by the black dashed rectangle in **A** is enlarged in **A``**, showing localized *Tc-mid* expression in cells of the cardioblast cell row, in the dorsal most region of the dorsal mesoderm. (**C, D**) Most of the *Tc-mid* expression in the cardioblast cell row is lost after *Tc-pnr* pRNAi. Residual expression is marked by the yellow arrows. Comparison of the two ventral views shows that *Tc-mid* expression in other tissue domains is unaffected by *Tc-pnr* pRNAi. Scale bar is 100 μm.

wt
Start
Tc-pnr^{pRNAi}
00:00
00:00
End - tracked
End
13:50
13:10
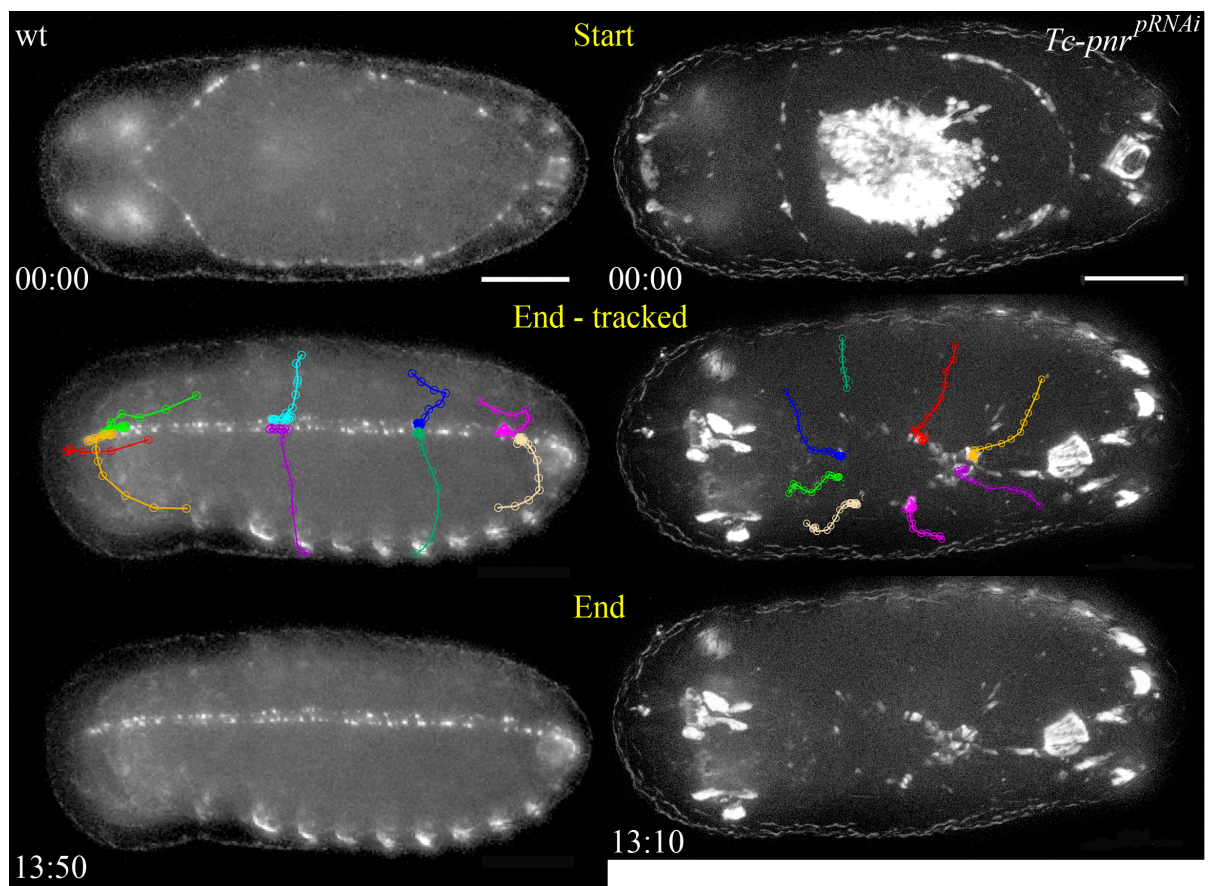
Figure 3.29: **Cardioblast cell tracking in a wild type embryo and a *Tc-pnr* knock down embryo**. Live imaging in a wild type embryo (left row; start of recording (00:00) is approximately 57h +/- 2h after egg laying) and a *Tc-pnr* knock down embryo (right row; start of recording (00:00) is approximately 62h +/- 2h after egg laying) of the G04609 line. Cardioblast tracking in both embryos was started as the cardioblast cell row ascended visibly ('Start') and was stopped approximately as the embryos head reached its final position ('End'). In the wild type, the cardioblasts located most anterior are moving towards the anterior pole, while the embryo closes its back. Expression of the 'red' marked cardioblast was lost when the head bent to the ventral side and could not be tracked further. Cardioblasts located posterior within the cell row move transiently towards the posterior pole, before the two cardioblast cell rows come together at the midline. Cardioblasts located more in the middle of the embryo, show overall a reduced movement in AP direction. In the *Tc-pnr* knock down, the anterior cells move only towards the posterior, whereas this movement is reversed for the posterior cardioblasts. The overall covered path by the posterior cardioblasts is slightly longer than the one of the anterior located cardioblasts. Movement of the 'light green', the 'dark green' and the 'beige' cells could not be tracked until the end, as the expression of all three cells faded away during imaging. Both embryos are dorsal views. The wild type embryo has been imaged at room temperature and the knock down embryo at a constant temperature of 30 °C. Scale bars are 100 μm.

icantly in an anterior direction, as the head bends towards the ventral side at the same time. Cardioblasts located more in the middle of the embryo, do not change their position much, if at all, in AP direction (tracks: purple, light blue, green and blue). Apparent is the slight transient shift towards the posterior of the two more posterior cardioblasts (tracks: green and blue). This movement is even more pronounced in the two most posterior cardioblasts (tracks: pink and beige), before both cells do a complete u-turn and move back anteriorly towards their original position. In the *Tc-pnr* knock down embryo, no such diverse set of movements could be identified. All cardioblasts move more or less straight to the same area in the middle of the dorsum. This implies that the movement of the cardioblast cell row is secondary caused by the bending of the embryo towards the ventral side, to achieve its final form at the dorsal midline. Strengthened is this, by the finding that the head of the embryos reaches its final position (see Figure 3.15) approximately at the same time, when the cardioblast cell rows come together at the dorsal midline.

An important finding of this analysis is as well that three of the eight tracked cardioblasts could not be tracked as long as the other five cardioblasts. This is due to a

decrease in the EGFP signal below trackable values. By checking other *Tc-pnr* knock down embryos (data not shown), it became obvious that this is a conserved feature after *Tc-pnr* pRNAi. This could indicate degeneration of cardioblasts or a delayed effect of the loss of *Tc-mid* expression on the EGFP signal, as a result of the loss of *Tc-pnr* expression in the cardioblast cell row, where *Tc-pnr* is expressed before dorsal closure starts.

Chapter 4

Discussion

4.1 The rHC079 line(s): Benefits and implications for their use

The original enhancer trap line HC079 was shown to express EGFP in the amnion, starting shortly before the onset of germ band extension [Hilbrant et al., 2016]. By investigating this line and another line expressing EGFP in the serosa (G12424), the amnion was identified as the 'initiator' of rupture of both extraembryonic membranes, while the serosa was identified as the 'driver' of the subsequent membrane withdrawal [Hilbrant et al., 2016]. However, these findings were only based on live imaging data of both lines recorded separately, as only *EGFP* was available in both lines. To continue this analysis, with emphasis on the interactions between the two extraembryonic membranes, we need to be able to observe both tissues separately within one embryo. Unfortunately, this was not possible with the existing lines, both expressing EGFP, as both membranes are either physically connected or in very close proximity to each other during later development [Hilbrant et al., 2016]. Therefore, the *EGFP* transgene in the line HC079 was replaced by a *DsRed2* transgene. This enabled distinct visualization of both amnion and serosa in a heterozygous cross of the respective lines.

Methodically, the replacement of *EGFP* with *DsRed2* in the original HC079 line was achieved by using a combination of CRISPR/Cas9 [Cong et al., 2013], targeting the *EGFP* transgene and homology directed repair (HDR). By injection of a donor plasmid, harboring the *DsRed2* transgene, into embryos prior to cellularization, successful integration of the transgene into the germ line was achieved in 5 (3.2%) of the 157 eclosed beetles, which is 0.3% of the initial 1992 injected embryos. Subsequently, four lines (#F, #W1, #W13

and #N) homozygous for the *DsRed2* transgene were established. To distinguish the new lines from the original HC079 line, the lines were termed red HC079 (rHC079) lines, in which 'red' is the synonym for red fluorescence.

All rHC079 lines were subsequently validated for seamless integration of the complete donor-plasmid and their DsRed2 signal strength was characterized.

4.1.1 Factors influencing the efficiency of transgenesis

The efficiency of transgenesis (here, the integration of the transgene into the germline) is not only influenced by the general uptake of the transgene into pre-blastoderm cells, the efficiency of the CRISPR/Cas9 system and the subsequently activated HDR mechanism, which are all factors which could not be determinded in this study but also by other factors. Those will be discussed in the following paragraphs.

While 69.5% (n = 400) of mock (water) injected embryos of the original HC079 line hatched, only 11.5% (n = 1992) did when injected with the plasmid mix (donor-plasmid, Cas9-plasmid and gRNA-plasmid). This can be explained by two possibilities. First, the plasmid solution itself was toxic [Wei-Ti et al., 2016], enhanced by undesired impurities, such as bacterial genomic DNA, a well known problem after plasmid purification [Tietze, 2009]. Secondly, the induced double strand break itself can cause cell death, if left unrepaired [Bennett et al., 1993; Mehta and Haber, 2014].

In a recent study, exactly the same plasmids for *Cas9* and the gRNA for targeting *EGFP* in the enhancer trap line Pig-19 but a different donor-plasmid for recombination were used to knock-in a *DsRed2* transgene [Gilles et al., 2015]. The authors reported a survival rate of injected larvae of 24% (n = 1866), more than two times the one I achieved (11.5%; n = 1992). This may be due to differences in injection parameters, like the speed of injection (reduced amount of dried-out eggs) or the handling of the needle (reduced back-flow when pulling out the needle from the egg).

The use of different lines targeted for injection could also make a difference, as indicated by the initial comparison of mock injected embryos of the G12424 and HC079 line. 61.5% (n = 400) and 68.5% (n = 400) of injected embryos hatched as larvae, respectively. Albeit it is not a significant difference, it is in so far interesting, as both lines originated from the same enhancer trap screen and should only differ in the genomic location of the *EGFP* transgene [Trauner et al., 2009]. This could point to effects caused by the initial

insertion of the *EGFP* transgene (for example that an enhancer can not 'reach' its target gene anymore), which do not cause lethality per se but lead to a reduced tolerance to influences from the outside (injection procedure), secondarily effecting the survival rate. Unfortunately, the authors of the study mentioned in the last paragraph, did not provide any data on mock injected embryos, to detect such differences [Gilles et al., 2015]. Of the 24% (= 444 of 1866) surviving larvae in their study, 70.9 % (= 315; n = 444) survived and eclosed. Of the 11.5% (= 230 of 1992) surviving larvae in this study, only 68.2% (= 157, n = 230) eclosed. The authors and I did follow the same protocol [Berghammer et al., 2009] but they cultured the beetles at all time at 32 °C, whereas I cultured the beetles at 30 °C. It was reported that at 32.5 °C, compared to 30 °C, the mortality rate of the larvae is 4% higher (see [Bucher, 2009]). This may point to others, unknown factors that effected the reduced survival rate.

The number of knock-in events obtained by this group was 6% (n = 315) [Gilles et al., 2015], which is two times higher than the one I obtained (3.2%; n = 157). This difference in knock-in efficiency may be caused by the different donor-plasmids used, effecting the efficiency of the HDR mechanism. The length of their homology arms flanking the double strand break is 0.7 kb and 1.0 kb [Gilles et al., 2015], while the homology arms used in this study are 0.3 kb and 1.3 kb, respectively. A third homology arm of 0.7 kb length is approximately 300 bp farther away from the double strand break than the 0.3 kb homology arm. How this second homology arm on one side of the transgene effects the HDR mechanism, is not known. However, a decrease in the length of at least one of the homology arms is known to negatively effect the frequency of insertion of a transgene [Pfander et al., 2011; Li et al., 2014]. Available guidelines for improving insertion frequency by using CRISPR/Cas9 and HDR, recommend the use of at least 0.8 kb long homology arms, if the insert is larger than 100 bp [Shen, 2016; Cong, 2016]. This difference in the size of one of the homology arms could account for the reduced knock-in efficiency in this study.

4.1.2 The four rHC079 lines may not be interchangeable

All four established rHC079 lines harbor the complete DsRed2 construct without any errors, integrated at the correct position within the genome, as validated by PCR and sequencing. Therefore, it is surprising that the relative DsRed2 signal strength varies

between the four lines. The line #W13 shows the weakest signal of all lines during embryogenesis. This is especially pronounced after germ band retraction. Likewise, the lines #W1 and #N show a much more pronounced decrease in their relative signal intensity right after amniotic rupture, before it aligns again with the intensities of the lines #W13 and #F. Based on the genetics, these different intensities of the DsRed2 signal cannot be explained. The high degree of variation within each line (see the mean standard deviation) on the other hand, is probably caused by inter-embryonic variation, which was already described for two other extraembryonic GEKU lines [Koelzer et al., 2014].

During one year of stock keeping, three lines (#F, #W1 and #N) displayed random periods of larval and pupal lethality, usually affecting all individuals of a given egg lay collection. Only #W13 did not show any of these defects and therefore was used for all subsequent experiments. The survival defects seen in the other lines, could be due to potential off-target cutting of the Cas9, since it is a general feature of engineered gRNAs that they can tolerate several mismatches in the target sequence [Peng et al., 2015]. Off-target cutting was found to occur in *zebrafish*, using the same EGFP targeting gRNA used in this study [Auer et al., 2014]. In *Tribolium*, off-target effects of the gRNA were not investigated but are believed to take place [Gilles et al., 2015].

Interestingly, the #W13 yields the weakest DsRed2 signal intensity but is the healthiest line. If considering that fluorophores are toxic [Jensen, 2012], weak expression of DsRed2 would directly lead to an increased health and account for this relation. However, why DsRed2 expression in this line is weaker in the first place, cannot be explained.

These results indicate that there are differences between the individual rHC079 lines. Interestingly, these can be expanded to the original HC079 line. The EGFP expression time course for this line is published and shows a steady increase of the relative EGFP signal after germband extension [Hilbrant et al., 2016], compared to the rHC079 lines. The relative DsRed2 signal in the rHC079 lines rather shows a plateau for several hours after germband extension. This is probably caused by the longer maturation time of DsRed2 (approximately six hours), compared to the maturation time of EGFP (approximately one hour) [Day and Davidson, 2009]. This would mean that after the enhancer activates expression of DsRed2 in the amnion, it takes several hours before the fluorescent protein matures, meaning that it is not fluorescent, even if expressed. This relates back to the fact that the maturation time is important for multiple-labeling experiments. In this regard it

would be a drawback, if one tissue can already be visualized, while another tissue cannot be visualized at the same time. This would decrease the time window for imaging of both tissues and should be avoided by choosing the appropriate fluorescent proteins.

4.1.3 DsRed2 and EGFP expression in the same embryo generates undesired crosstalk

The red fluorescent protein DsRed is the commercial variant of the wild type DsRed (drFP583), which was edited by insertion of a valine after the start codon [Matz et al., 1999; Bevis and Glick, 2002]. DsRed2, which was used in this study, is a mutant of the wild type DsRed (E57 mutant) [Terskikh et al., 2002; Yanushevich et al., 2002] and commercially available since 2001 [Living Colors™ DsRed2, 2001]. Compared to DsRed, it has a reduced maturation time of about six hours, making it more useful for multiple-labeling experiments [Day and Davidson, 2009], as performed in this study. Originally, DsRed2 was suggested to be well suitable for two-color detection in combination with EGFP [Living Colors™ DsRed2, 2001], the fluorescent protein expressed in all GEKU lines [Trauner et al., 2009]. Albeit it was known that the emission spectra of EGFP and DsRed2 overlap (see Figure 4.1), it became more clear during image analyses that the emission of DsRed2 'leaks' into the EGFP channel. This crosstalk of the DsRed2 signal can be advantageous when imaging at low resolution, as for example the DsRed2 expression in the amniotic dorsal organ can be used as a topographical landmark, not interferring in a cross with the G04609 line with the 'real' EGFP signal. However, in high resolution imaging the undesired crosstalk of the red and green fluorescent protein can become a problem. This is especially true, when distinct visualization of the amnion and serosa in tight connection is needed for a proper analysis [Hilbrant et al., 2016].

As an alternative to DsRed2, the red fluorescent protein monomer cherry (mCherry) could be employed. It possesses a superior photostability, critical for long-term imaging [Shaner et al., 2005]. Its intrinsic brightness level is approximately 50% that of EGFP [Day and Davidson, 2009], whereas DsRed2 is several times weaker compared to EGFP, as indicated by the performed imaging experiments (to achieve equal brightness levels when imaging at the AxioImager.Z2, the exposure time of DsRed2 was set to an approximately seven times higher value than the one of EGFP). Most important for multiple-labeling experiments however, is the reduction of crosstalk between the excitation and emission
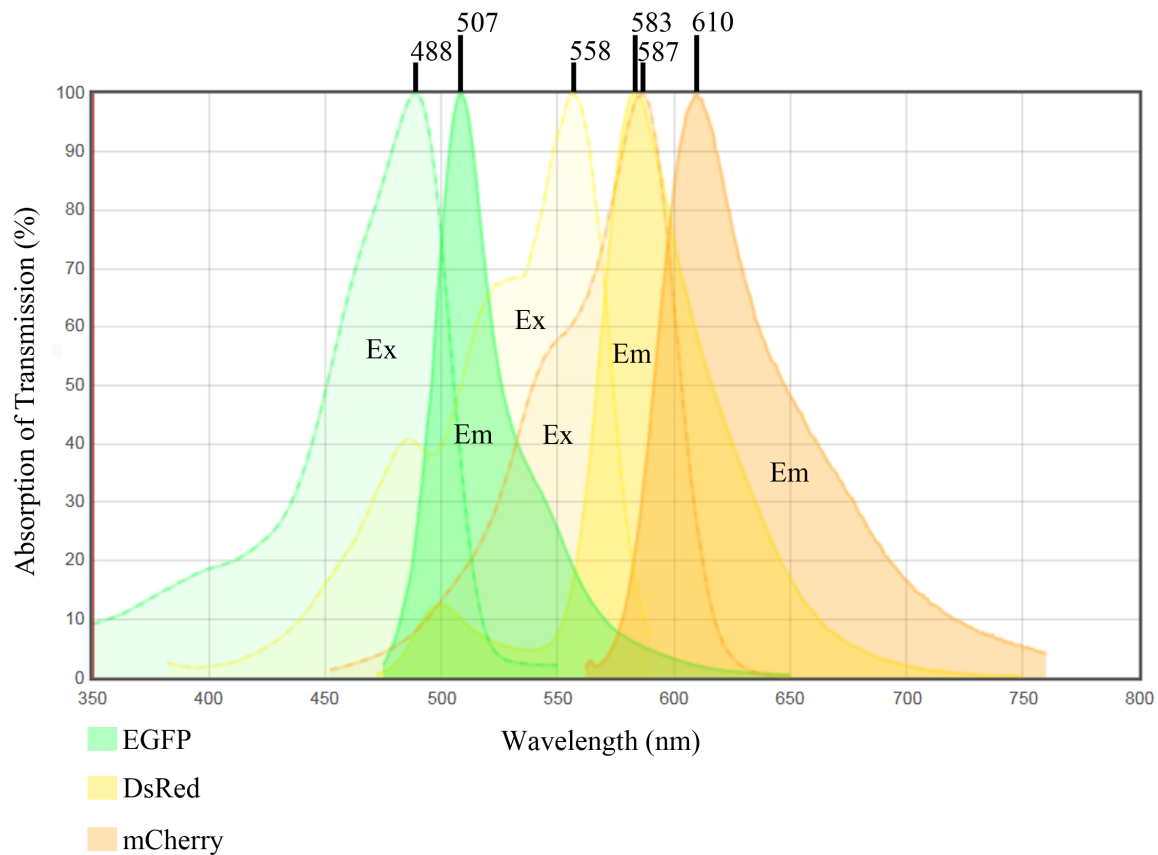
Figure 4.1: **Excitation and emission spectra of the three fluorescent proteins EGFP, DsRed and mCherry**. Visualization of the spectral overlap of the excitation and emission of the fluorescent proteins EGFP, DsRed2 (DsRed is visualized in default of the ones for DsRed2 in this spectral viewer) and mCherry. DsRed has an excitation and emission maxima of 558 nm and 583 nm, respectively. This is highly similar to the ones of DsRed2 (563 nm and 582 nm, respectively). The short bar on top of a peak belongs in all cases to the excitation maxima and the long bar to the emission maxima. The faint color represents the excitation area, while the more intense color the emission area, respectively of EGFP, DsRed and mCherry. (Ex) Excitation, (Em) Emission. Modified from [Chroma, 2016].

channels [Shaner et al., 2005] (Figure 4.1). EGFP has an excitation maximum of 488 nm and an emission maximum of 507 nm. The ones of DsRed2 are 563 nm and 582 nm, respectively (please note that in Figure 4.1, the spectra of DsRed and not DsRed2 is shown, due to the unavailability of all three spectra (EGFP, DsRed2 and mCherry) in this or any other spectra viewer). The maxima of mCherry are shifted more towards the red spectra of the visible light (587 nm and 610 nm, respectively) [Day and Davidson, 2009]. Hence, mCherry is presumably the best choice, as an alternative for DsRed2 in multiple-labeling experiments.

4.1.4 Use of the rHC079 line in this study and an outlook on its further application

In the first place, the rHC079 line was generated to be used in a cross with the serosa line G12424 [Koelzer et al., 2014]. Due to the nature of their connection during embryogenesis, both extraembryonic membranes were hard to visualize as distinct tissues in a heterozygous cross, with EGFP as the only fluorescent marker [Hilbrant et al., 2016]. This problem was solved, by generation of the DsRed2 expressing rHC079 lines. How these lines already have contributed to research on extraembryonic membrane development in *Tribolium* and how this will proceed, will be discussed in the following paragraphs.

In a recently published study, it was shown that the amnion ruptures before the serosa, acting as the initiator of rupture [Hilbrant et al., 2016]. Besides from the distinct morphology of the anterior cap region of the amnion, this result was based on a set of measurements, using homozygous beetles of the amnion line HC079 and the serosa line G12424 [Hilbrant et al., 2016]. The direct validation of this result is now possible using the line rHC079 in a cross with the line G12424.

In general, a heterozygous cross between both extraembryonic lines, will permit to simultaneously examine any effect on their development and on their interaction, caused by the knock down of extraembryonic marker genes or other target genes. Beneficial in this regard is that the fluorescent signal is not localized to the nuclei [Trauner et al., 2009; Koelzer et al., 2014], so that effects on cell shapes can be detected as well.

For the investigation of the knock down phenotypes after *Tc-pnr* pRNAi, the rHC079 line was crossed to enhancer trap lines with non-extraembryonic expression patterns. Thereby, the effects on the amnion and the cardioblast cell row (by using the GEKU

line G04609 [Trauner et al., 2009; Koelzer et al., 2014]) could be investigated, likewise taking advantage of multiple-labeling imaging. Similarly, the in this study characterized enhancer trap lines G04910 and G09423 were used in single crosses with rHC079, to distinctly visualize embryonic and extraembryonic defects. Even if the EGFP-expressing tissues in these other lines did not show any defect, their expression could still be useful as a landmark, as it was already reported for the G04609 line [Koelzer et al., 2014].

A drawback of the rHC079 is the crosstalk of DsRed2 and EGFP that was discussed in a previous section. As indicated in that section, the red fluorescent protein mCherry would be a better partner in multiple-labeling imaging. To study the interaction between the serosa and amnion on the level of individual cells in more detail, it will be necessary to minimize that crosstalk. Therefore, the next step will be to replace *DsRed2* with *mCherry*. This could be done either by generation of a completely new rHC079 line via injection of a donor-plasmid harboring a mCherry transgene into the initial HC079 line or via insertion of mCherry into the rHC079 line using the attP site and simultaneously removing the DsRed2 transgene via CRISPR/Cas9.

In general, the attP site enables site-specific recombination, mediated by the serine integrase ΦC31, between itself and a donor, harboring the attB site [Groth and Calos, 2004]. Via a 'cut-and-paste' approach, both sites attach to each other in such a way that the donor construct is integrated precisely into the attP site, thereby interrupting its sequence, as well as the attB sequence [Groth and Calos, 2004]. As this recombination event generates a stable integration, the ΦC31 integrase system is frequently used in insect transgenics [Huang et al., 2009; Long et al., 2013]. Therefore, future applications using the attP side include also the insertion of fluorescent markers labeling specific cell structures like nuclei, membranes or actin [Benton et al., 2013]. This will help to locate and characterize defects after the knock down of specific genes in more detail, than it is possible with the original GEKU lines alone.

In light of the analyses of the extraembryonic membranes in *Tc-pnr* knock down embryos, the cross of the G12424 serosa line and the rHC079 amnion line, will be an important tool here, too. Given that ectopic rupture of the amnion and normal rupture of the serosa in the same embryo was only shown in the nGFP line, which lacks the properties for distinct visualization of the two membranes, the cross provides these properties. The described defects in the amnion can be directly related to secondary derived effects within

the serosa, if such have been missed on the level of individual cells so far. Likewise, the potential delayed (ectopic) rupture of the amnion can be visualized and the effects of the subsequent withdrawal on serosa organization can be characterized in the same embryo. How the knock down of *Tc-pnr* then affects the interplay between the two normally connected dorsal organs, will be interesting to investigate as well.

In this sense, the rHC079 line already contributed to the live imaging possibillities of *Tribolium* but as the research questions are changing, the rHC079 line in particular and the live imaging toolkit in general, have to be adopted to these questions.

4.2   The wild type expression pattern of *Tc-pnr*

In this section the wild type expression pattern of *Tc-pnr* will be presented. It will help to bring the different defects after parental RNAi into context and will serve as a guideline for the discussion of these defects in the following sections.

The transcription factor *Tc-pnr* starts to be expressed in extraembryonic tissue at the differentiation of the blastoderm. It is expressed in the dorsal part of the anterior amniotic fold and the dorsal amnion, from where its expression extends into the primitive pit. During formation of the posterior fold and its subsequent progression towards the ventral posterior side, the two latter expression domains involute together with the embryo, as the amnion starts to cover the embryo on its ventral side. When the serosal window has formed, *Tc-pnr* is expressed in separate domains in its margin, which have arisen from its expression in the anterior amniotic fold. During closure of the serosal window, *Tc-pnr* expression extends into the amnion covering the head lobes. The most posterior amniotic expression covers the segment addition zone, while a transient expression domain arises in the amnion just posterior to the serosal window. Accompanied by the final closure of the serosal window, the *Tc-pnr* expression domains in its margins come together, forming a characteristic y-shape. During germband extension, *Tc-pnr* expression spreads in the complete amnion covering the anterior part of the embryo, before it extends to the posterior. It is shortly before the embryo has fully extended that *Tc-pnr* is expressed in the whole amnion. When the embryo has started to retract, *Tc-pnr* is additionally expressed in the cardioblast cell row and in separate domains within the head and the legs. In difference to its expression in the head and the legs, *Tc-pnr* expression in the cardioblast cell row does not persist, when the embryo is fully retracted. Potential amniotic expression

can not be verified at this late stages, due to limitations in staining [Koelzer et al., 2014]. Prior to dorsal closure, *Tc-pnr* expression arises in the dorsalmost ectoderm. Expression in the cardioblast cell row is absent.

4.3 *Tc-pnr* is not important for early processes during extraembryonic membrane formation

Tc-pnr and *Tc-iro* are both expressed in the early amnion at the differentiated blastoderm stage, which makes them potential interaction partners. To test this prediction, *Tc-pnr* knock down embryos were stained for *Tc-iro* via *in situ* hybridization. Amniotic *Tc-iro* expression is completely lost at the differentiated blastoderm stage and is only weakly detected in the amnion at the margins of the serosal window and in the amnion during germband extension, where *Tc-iro* is expressed in the wild type. Interestingly, although *Tc-pnr* itself is not normally expressed in embryonic tissue, early embryonic *Tc-iro* expression is also lost. During germband extension, this downregulation of *Tc-iro* expression in embryonic tissue is not observed anymore. This indicates that *Tc-iro* expression depends on the activation by *Tc-pnr* in all tissues throughout the early differentiated blastoderm stage but later on, *Tc-iro* is co-regulated by another gene in the amnion, whereas *Tc-iro* does not rely on *Tc-pnr* regulation in the embryo after closure of the serosal window.

To test if *Tc-pnr* knock down embryos show any defect during early embryogenesis, live imaging was performed. Unexpectedly, based on the expression pattern of *Tc-pnr* and its regulatory role on *Tc-iro*, no defect was observed through the completion of germband extension (which is the time the recording was stopped). Indirectly, this finding could imply that *Tc-iro* is also not needed for early embryogenesis and membrane formation. To verify this, *Tc-iro* pRNAi was performed. Albeit not at high penetrance (only 33.6% of the embryos show any defect and when considering that 8.3% of the wild type embryos show defects of the same categories, this value decreases to 25.3%), the knock down of *Tc-iro* does affect early embryogenesis and formation of the amnion, while the serosa seems to be largely unaffected. As none of the defects is seen in the *Tc-pnr* knock down, these defects are likely due to *Tc-iro*'s early expression in the region of the presumptive serosa (which refines over time into *Tc-iro* expression only in the anterior amniotic fold [Sharma et al., 2013a]) at the undifferentiated blastoderm stage. Therefore, loss of *Tc-iro*

expression after blastoderm differentiation is potentially compensated by other genes, or subtle knock down phenotypes could not be detected with the used methods. The via live imaging observed defect in the formation of the primitive pit in *Tc-iro* knock down embryos, cannot easily be explained. *Tc-pnr* is expressed in the same region around the primitive pit as *Tc-iro*, whose expression extends also into more ventral cells. As the knock down of *Tc-pnr* results in a loss of this complete expression pattern, it is more likely that an early Tc-iro signal affects downstream target genes, triggering a signaling pathway involved in formation of the primitive pit. Otherwise, the *Tc-pnr* knock down acting on *Tc-iro* expression may not be a complete one and the residual *Tc-iro* expression may be below detection rate via *in situ* hybridization staining. The direct and probably more complete knock down of *Tc-iro* on the other hand, could then explain the impaired formation of the primitive pit.

When the serosal window forms, *Tc-pnr* is expressed in the amnion at its margin. During subsequent closure of the window, *Tc-pnr* expression spreads in a distinct pattern around the site of closure. This could indicate a potential function of *Tc-pnr* for the detachment of the serosa and the amnion or serosal window closure in general. Such a function was recently reported for *Tc-Doc* [Horn and Panfilio, 2016]. *Tc-Doc* is also expressed in the amnion at the margin of the serosal window and was shown to be a key regulator of its closure, as its knock down impaired closure of the serosal window [Horn and Panfilio, 2016]. However, the loss of *Tc-pnr* expression did not cause any defect. The same is true after *Tc-iro* pRNAi [Horn and Panfilio, 2016], even though *Tc-iro* expression in the margin of the serosal window is affected after *Tc-pnr* knock down and *Tc-Doc* knock down [Horn and Panfilio, 2016]. The two genes *Tc-dpp* and *Tc hindsight* (*Tc-hnt*) on the other hand did show similar defects to the ones induced by *Tc-Doc* pRNAi, after embryonic RNAi, which was used to circumvent the earlier defects caused by the loss of these two genes, which may have masked their involvement in serosal window closure [Horn and Panfilio, 2016]. This could indicate that in the case of *Tc-iro*, a potential function in serosal window closure is as well concealed by the earlier defects shown in this study. In the case of *Tc-pnr*, it could be that a different gene, such as *Tc-dpp*, known to affect early *Tc-pnr* expression [van der Zee et al., 2006], compensates for the loss of *Tc-pnr* expression. In this regard, *Tc-Doc* is a rather unlikely direct upstream regulator of *Tc-pnr*, as *Tc-pnr* expression is unaffected after *Tc-Doc* pRNAi [Horn and Panfilio,

2016].

4.4 The specialized anterior amniotic cap region is specified early in development

It was recently reported that the amnion ruptures in a rupture competence zone in a specialized anterior amniotic cap region [Hilbrant et al., 2016]. *Tc-pnr* staining at the extended germband stage revealed that this anterior cap region is specified at least during germband extension. The shown stronger staining by a *Tc-pnr* probe in these cells, compared to more posterior ones in the amnion, is probably due to a higher concentration of is transcript. Thus, *Tc-pnr* expression would be higher expressed in cells of the anterior amniotic cap. That the increased stain by a *Tc-pnr* probe is due to the reported larger cells with a higher volume of cytoplasm [Hilbrant et al., 2016], can probably be neglected. A larger volume does not necessarily lead to a stronger staining, rather it should lead to an equal intense staining in a larger area of the cell, when assuming proportional expression. This finding suggests that *Tc-pnr* is indeed stronger expressed in the cells of the anterior amniotic cap region. Together with the shown defects in the whole amnion and the loss of a distinct cap region in retracted germband embryos after *Tc-pnr* pRNAi (discussed in a later section), it is likely that *Tc-pnr* is involved in the specification of the amniotic cap region. That a defect in this rupture competence zone [Hilbrant et al., 2016] leads to ectopic rupture within the amnion, further strengthens this assumption.

4.5 *Tc-pnr* is involved in the formation of the cardioblast cell row

The enhancer trap line G04609 was characterized and shown to express EGFP in the cardioblast cell row, therefore also referred to as the 'heart line' [Koelzer et al., 2014]. In this study, the heart line was used to examine a potential defect of the heart, as *Tc-pnr* is expressed in the cardioblast cell row during germband retraction.

Knock down of *Tc-pnr* in the heart line genetic background, resulted in a loss of most of the cardioblast-specific EGFP expression. Other EGFP expressing domains of the G04609 line were not affected. A consistent pattern, regarding in which cardioblasts EGFP expression is lost, could not be identified. The analysis of the role of *Tc-pnr*

was extended on *Tc-mid*, which is expressed in all cardioblasts and was reported to be partially trapped by the enhancer driving EGFP expression in the G04609 line [Koelzer et al., 2014]. *Tc-mid* expression was partially lost, again without observing a specific pattern. This result boosts the conclusion that *Tc-mid* is indeed partially trapped in the heart line.

In *Drosophila*, *Dm-pnr* is important for specification of the cardiac mesoderm, where it is expressed [Alvarez et al., 2003; Reim and Frasch, 2005]. The loss of heart cells in *Dm-pnr* mutant embryos is therefore indirectly via an earlier defect in the specification of the cardiac mesoderm [Alvarez et al., 2003]. As a consequence, the majority of cardiac progenitor cells are not specified and the dorsal vessel fails to form [Tao and Schulz, 2007]. To test if the formation of the cardioblast cell row in *Tribolium* is impaired due to the loss of *Tc-pnr* expression in these cells, *Tc-pnr* knock down embryos were investigated on the individual cell level, using the heart line as a marker for the cardioblast cell row and DAPI as an ubiquitous nuclear stain. The results clearly showed that the cardioblast cell row is lost as a morphologically distinct row of cells after *Tc-pnr* pRNAi. This result indicates that *Tc-pnr* is necessary for the specification of the cardioblast cell row. Similar to *Drosophila*, it may be that this function of *Tc-pnr* is achieved in cooperation with other genes like *Tc-tin* or *Tc-Doc*. Such an interaction of different genes for the specification of the cardioblasts would explain that some cardioblasts still express *Tc-mid*. Thus, it cannot be stated with certainty that *Tc-pnr* regulates *Tc-mid* expression or that *Tc-mid* is not expressed in the cardioblasts as these cells lost their cardioblast identity. If the line G04609 trapped the *Tc-mid* enhancer partially, this conclusion would also apply for the loss of EGFP expression in the heart line.

Interestingly, by cell tracking of individual cardioblasts in *Tc-pnr* knock down embryos of the heart line, it was shown that EGFP expression is lost over time in some of these cells. This may result from the loss of normal organization of the cardioblast cell row, so that cell adhesion and therefore vital signaling is lost and individual cardioblasts degenerate. Another explanation may be that the gradual loss of EGFP expression is then again a secondary cause but due to the loss of *Tc-mid* expression. Assuming that the *Tc-mid* enhancer is trapped in the heart line. If the enhancer in the G04609 line is activated and starts expression of *Tc-mid*, then EGFP expression will start not at the same time but it is delayed, depending on its maturation time. The same is true when

Tc-mid is no longer transcribed, as EGFP will still be expressed for some time, while its fluorescence decreases. To determine which of the two potential explanations is true, the nuclear GFP line (nGFP), which expresses GFP localized to the nuclei [Sarrazin et al., 2012], could be crossed to the G04609 line. By this, cardioblasts can be tracked and it can be monitored if individual cardioblasts loose their EGFP expression due to degeneration, which would result in a loss of the nGFP expression. Thus, it could be easily answered, if only the gene driving its expression is affected or if individual cardioblasts are absent.

In *Drosophila* it was reported that *Dm-pnr* specifies the pericardial cells [Alvarez et al., 2003; Reim and Frasch, 2005] and negatively regulates *Dm-eve* [Gajewski et al., 1999], which is expressed in a subset of these cells [Gajewski et al., 1999; Alvarez et al., 2003; Klinedinst and Bodmer, 2003]. In *Tribolium*, Tc-Eve has been used as a marker for a subset of the pericardial cells [Cande et al., 2009]. However, during this study performed *in situ* hybridizations for visualization of its transcript in wild type and in *Tc-pnr* knock down embryos, resulted in an unclear expression pattern (data not shown). This was mainly caused by an overall weak staining, interfering with the identification of *Tc-eve* positive cells within the dorsal mesoderm. Making a new *Tc-eve* probe or trying different primers for making these probes will help to handle this problem. Subsequently, it can be tested if the effect of *Tc-pnr* is conserved in *Tribolium*, compared to *Drosophila*.

A starting point for the more detailed investigation of heart development in *Tribolium* are certainly four publications, which deal with heart aspects in a broader sense. In the first one to name, the G04609 line was characterized and *Tc-mid* and *Tc-H15* expression in the cardioblast cell row described [Koelzer et al., 2014]. A more recent publication already presents data on the genes *Tc heartless* (*Tc-htl*) and *Tc down of FGF receptor* (*Tc-dof*) that shows that the knock down of each gene individually impairs EGFP expression in the heart line [Stappert et al., 2016]. The remaining two publications provide a source for more genes expressed in different subsets of heart cells [Janssen and Damen, 2008; Cande et al., 2009]. These resources and available literature from *Drosophila* (the gene regulatory network of heart formation is strikingly well conserved in distinct phyla [Cripps and Olson, 2002]), will provide sufficient starting material for an investigation of *Tribolium* heart development.

4.6 The amnion and the serosa rupture and withdraw independently after *Tc-pnr* parental RNAi

Based on the continuous expression of *Tc-pnr* in the amnion, it is likely that *Tc-pnr* is important for extraembryonic membrane development at some point during embryogenesis. Given that the knock down of *Tc-pnr* did not show any early defects, the later development advanced into focus, as *Tc-pnr* is still expressed in the amnion of retracting germband embryos. During late development, the accessibility of the extraembryonic membranes is strongly impaired by the secretion of the serosal cuticle and subsequent secretion of the larval cuticle [Koelzer et al., 2014]. Therefore, the characterization of the enhancer trap line HC079, which expresses EGFP in the amnion shortly before the onset of germband extension until its degeneration [Hilbrant et al., 2016], was published at the right time to circumvent this problem.

In order to investigate potential defects within the amnion, its morphology was examined using a cross of the subsequently established rHC079 line and either one of two GEKU lines (G04609 and G04910; to visualize embryonic landmarks) for distinct visualization of the DsRed2 and EGFP signal, respectively.

In *Tc-pnr* knock down embryos of a cross of the 'amnion' line rHC079, the morphology of the amnion is clearly abnormal. The anterior cap region cannot easily be distinguished from other amniotic tissue anymore. Still, DsRed2 expression in the nuclei of this specialized region seems to be stronger, as compared to control embryos. Nuclei in the cap region display an abnormal shape and borders between individual cells cannot be identified as such anymore. More general, cell outlines, labeled by DsRed2 expression in the wild type, display gaps (in the DsRed2 expression), small holes and black areas in the amnion (potentially also due to a loss of DsRed2 expression) arise.

In order to survey how and if these defects in amnion morphology are reflected in general tissue movements of the amnion, live imaging was performed.

Using the HC079 line, 15 *Tc-pnr* knock down embryos were recorded around the time of dorsal closure and different defects could be observed. 10 embryos exhibited the characteristic bending of the dorsal open phenotype after *Tc-pnr* pRNAi (66.7%; n = 15). In three of these embryos the amnion did withdraw very slow over the abdomen (30%; n = 10; ranging from 2h40min to 5h10min), compared to control embryos (deduced from the

withdrawal of the serosa, as both membranes are connected; serosal withdrawal over the abdomen takes around 30 min (n = 7)). Another three embryos showed ectopic rupture of the amnion (30%). One single embryo displayed several holes in the amnion (or only the EGFP expression was affected, so it would look like a hole to the investigator), which did not impair amnion rupture or withdrawal. In the last affected embryo, the normal morphogenesis of the amnion was severely affected. This last defect could partially reflect the unhatched phenotype or the cuticle crumbs phenotype (together 17.6%), obtained by cuticle preparation. These phenotypes will be discussed in more detail in the next section. The two remaining embryos, which did display the dorsal open phenotype, showed no amniotic defect (20%).

The ectopic rupture of the amnion was a very intriguing finding. It was recently reported that the amnion and the serosa form a bilayer during membrane withdrawal, tightly connected everywhere but in the anterior rupture competence zone [Hilbrant et al., 2016]. This would imply that the serosa ruptures ectopically as well. To test this, the development of *Tc-pnr* knock down embryos in a cross of the serosa line G12424 with the heart line G04609 was imaged during dorsal closure. 21 of the 27 knock down embryos displayed the dorsal open phenotype (78%). Of these 21 embryos, none showed an affected serosa. From the six embroys which did not display the characteristic bending, three exhibited slow serosal withdrawal (11%), while embryonic development in the remaining three embryos did not proceed visibly (11%; possibly contributing to the empty egg and cuticle crumbs phenotype). Withdrawal of the serosa was not delayed in embryos showing the dorsal open phenotype (withdrawal in 30 min (n = 21), compared to withdrawal in 30 min (n = 6) in control embryos).

The observed ectopic rupture of the amnion and the normal rupture of the serosa, may point to the conclusion that the serosa and the amnion are no longer connected after *Tc-pnr* pRNAi. However, such a conclusion based on separate experiments is limited in its significance. Defects occurring at low precentages could be artifacts, due to the preparation of the embryos prior to imaging or may represent normal occurring variations in the highly complex morphogenetic movements during extraembryonic membrane withdrawal and subsequent degeneration. Furthermore, each live imaging experiment was performed only once and should be repeated for validation of the results.

In this regard and to verify that the ectopic and normal rupture of the respective

extraembryonic membrane can be observed in the same embryo, live imaging with *Tc-pnr* knock down embryos in the genetic background of the nGFP line was performed. 27 embryos were imaged, whereby 24 displayed the dorsal open phenotype (89%). The three remaining embryos died during filming and probably represent the normal loss rate during imaging. The serosa could be visualized well but unfortunately the amnion could not. However, it was possible to identify one embryo (4%, n=24), in which ectopic rupture of the amnion at a ventral position in the center of the embryo and normal rupture of the serosa at the anterior side occurred. In contrast to the live imaging experiment performed using a cross of the serosa and the heart line, withdrawal of the serosa in *Tc-pnr* knock down embryos was delayed, compared to control embryos. In embryos showing the dorsal open phenotype, withdrawal of the serosa over the abdomen took 60 min (n = 20), while it took only 30 min (n = 7) in the control embryos. Albeit this results are contradictory to the results obtained with the cross (here, 30 min for each set of embryos), the standard deviation of the *Tc-pnr* knock down embryos in the nGFP genetic background is 30 min, compared to 20 min in the cross. This indicates that assumptions about the speed of extraembryonic membrane withdrawal are not easy to make. In order to find such differences between *Tc-pnr* knock down and wild type withdrawal, rather the time interval of image acquisition during live imaging should be narrowed down to 1-3 min, from the so far used 10 min interval in all recordings. This should provide enough temporal resolution for valid statements about a potential delay in membrane withdrawal.

To obtain more meaningful data regarding the potential uncoupled rupture of the amnion and the serosa, while at the same time reducing the imaging interval, the next step in this analysis would be to repeat the live imaging experiments in *Tc-pnr* knock down embryos, with a cross of the rHC079 and the G12424 line. Distinct visualization of both membranes could confirm the previous findings and the potential impaired interaction of the amnion and the serosa could be investigated in more detail. Unfortunately, due to time constrictions, I was not able to perform this concluding experiment anymore. A cross of the nGFP line with the rHC079 line will also be of potential use, to resolve if the observed gaps and holes in the DsRed2 expression of *Tc-pnr* knock down embryos are due to an actual loss of the nuclei. Otherwise an apoptosis stain could be used [Panfilio et al., 2013].

The provided results for the effects of *Tc-pnr* on amnion morphology are intriguing,

as it is the first gene in *Tribolium* that causes such changes in the amnion. However, further analyses on the cell level will be needed, to confirm that the amnion and the serosa are no longer attached during membrane withdrawal. That both extraembryonic membranes are attached is based on a rupture analysis using either the amnion and the serosa line individually in a cross with the G04609 line, limiting its informative value. For this analysis, the rHC079 line in a cross with the G12424 line will also be beneficial, connecting the analyses of *Tc-pnr* once more to the newly generated red HC079 line. To investigate how the dorsal hole effects the amnion and how the connection between the dorsal ectoderm and the amnion is affected after *Tc-pnr* pRNAi, the in the last paragraph recommended cross of the nGFP line with the rHC079 line will provide additional information.

Concluding, it should be mentioned that despite of the in this study described ectopic rupture of the amnion after *Tc-pnr* pRNAi, withdrawal of the amnion to the dorsal side mostly takes place. This suggests high plasticity of extraembryonic membrane rupture/withdrawal during late embryogenesis, which was also reported after *Tc-zen1* pRNAi [Panfilio et al., 2013] and *Tc-Doc* pRNAi [Horn and Panfilio, 2016].

4.7 The empty egg and cuticle crumbs phenotype

The dorsal hole in the cuticle is the main phenotype after *Tc-pnr* pRNAi and goes along with a characteristic dorsal bending of the embryo. However, two other phenotypes can be observed after the knock down as well. No cuticle is produced in the empty egg phenotype (10%), leaving an empty eggshell. In the cuticle crumbs phenotype (6.3%), only partial cuticle is produced. This means that in the latter case at least partial tissue is produced. Based on the embryonic body parts still covered by cuticle (antennae, pretarsus), it is also very likely that embryogenesis proceeds for a long time, before tissue degeneration starts. In turn, this could indicate that the embryos which produce no cuticle, likewise die late in embryogenesis but before any cuticle secretion starts. This assumption is strengthened by the data obtained by live imaging. The not assignable phenotype is mainly a collection of embryos which die during imaging, but in all cases embryogenesis proceeds at least until full germ band extension and often until the onset of dorsal closure (data not shown). Strikingly, the penetrance of the not assignable phenotype, resembles almost entirely the penetrance of empty egg phenotype and cuticle crumbs phenotype together (17.6% and

16.3%, respectively).

These observations may point to an effect of *Tc-pnr* on embryogenesis, before it is functioning in the process of dorsal closure. The cause of the dorsal hole in the cuticle, will be discussed in the following section.

4.8 The dorsal open phenotype occurs in *Drosophila* and *Tribolium*

Dorsal closure, the process in which a hole in the dorsal epidermis is closed by extension of the lateral ectoderm, [Panfilio et al., 2013], is impaired in *Tc-pnr* knock down embryos and becomes apparent by a hole in the dorsal cuticle. This dorsal open phenotype also occurs in *Dm-pnr* mutants of *Drosophila* embryos [Jürgens et al., 1984; Herranz and Morata, 2001], where *Dm-pnr* expression is lost in the dorsal ectoderm [Herranz and Morata, 2001]. In *Drosophila*, this loss of ectodermal *Dm-pnr* expression results in a loss of *Dm-dpp* expression in the leading edge cells of the ectoderm [Herranz and Morata, 2001], which then causes the defect in dorsal closure [Jacinto et al., 2002]. These data from *Drosophila* provided the motivation to undertake similar analyses in *Tribolium*. *Tc-dpp* expression in the dorsalmost ectoderm of extended germband embryos was already reported [Sanchez-Salazar et al., 1996; Giorgianni and Patel, 2004; Ober and Jockusch, 2006] and it was shown in this study that this very same expression pattern persists in retracted germband embryos and that this expression is lost after *Tc-pnr* pRNAi. Albeit efficient *Tc-dpp* pRNAi leads to a ventralization of the blastoderm [van der Zee et al., 2006], it was already shown in another publication that *Tc-dpp* pRNAi leads in 85% (n = not known, see [Ober and Jockusch, 2006]) of the affected embryos, to a defect in dorsal closure [Ober and Jockusch, 2006]. It is assumed by me that this is due to a reduced efficiency, so that this late phenotype is no longer masked by the early defect in DV patterning. On the level of individual cells, the reason of the dorsal hole, triggered by *Tc-dpp* pRNAi, was reported to be a loss of the dorsalmost cell row in the ectoderm [Ober and Jockusch, 2006]. This was discovered by more narrow extended germband embryos, compared to control embryos and a loss of the distinct morphology of the most dorsal cells of the ectoderm. Also, the expression of *Tc-wg* in *Tc-dpp* knock down embryos is no longer one cell row apart from the dorsal edge of the embryo but directly adjacent to it [Ober and Jockusch, 2006]. This could be a result from the loss of the dorsal most cell row as well. If cells are lost in

Tc-pnr knock down embryos or if the expression of genes directly adjacent to the dorsal most cell row is absent, was not tested. However, in *Drosophila* such a cell loss in *Dm-pnr* and *Dm-dpp* mutants was not reported. This could indicate that *Tc-dpp* is necessary for the formation of the dorsal most cell row, whereas in *Drosophila*, *Dm-dpp* specifies the leading edge cells. Even when acting differently in both species, in either case, *dpp* is indispensible for dorsal closure.

Based on the available data in this study and published data, it is assumed that the loss of *Tc-pnr* expression in the dorsal most ectoderm results in a loss *Tc-dpp* expression in these cells and causes the dorsal open phenotype. In *Drosophila Dm-pnr* mutants only the dorsal most *Dm-dpp* expression is affected, while the more lateral one persists. This is probably also the case in *Tribolium*, albeit due to the weak *Tc-dpp* staining in this region this cannot be stated with 100% certainty and has to be repeated. Alternatively, an antibody against *Tc* phosphorylated mothers against dpp (*Tc*-pMAD), which is the downstream effector of *Tc-dpp* [Horn and Panfilio, 2016], could be used to verify the effect of the loss of *Tc-pnr* expression on *Tc-dpp* expression. This is important, as *Dm-pnr* was reported to act as a DV selector like gene [Mann and Morata, 2000; Herranz and Morata, 2001], what will be discussed in the following section.

4.9 *Tc-pnr* interacts with *Tc-iro* during embryogenesis and might have a function in determining dorsal fates

In *Drosophila*, *Dm-pnr* is assumed to act as a DV selector like gene, which is a gene that functions within distinct regions of the body, where it determines specific developmental pathways. In the case of *Dm-pnr*, this is the determination of dorsal fates [Mann and Morata, 2000; Herranz and Morata, 2001].

The involvement of *Tc-pnr* during embryogenesis has been well conserved in the process of dorsal closure and during heart formation so far, compared to *Drosophila*. Therefore, it was investigated if *Tc-pnr* specifies dorsal fates as well. Based on the experiment performed in *Drosophila* that loss of *Dm-pnr* expression in the dorsal ectoderm leads to a dorsal expansion of the *Dm-iro* expression domain [Calleja et al., 2000] and encouraged that both genes interact during early embryogenesis in *Tribolium* [van der Zee

et al., 2006], the experiment was repeated in *Tribolium*. Wild type expression of *Tc-iro* was found to be conserved in a dorsal-lateral domain within the ectoderm at the late retracted germband stage. After *Tc-pnr* pRNAi, this expression domain extended dorsally, albeit not as pronounced as in *Drosophila* [Calleja et al., 2000]. This finding indicates that *Tc-pnr* normally supresses *Tc-iro* in the dorsal epidermis, which is in contrast to the loss of *Tc-iro* expression after *Tc-pnr* knock down in early development. Thus, both genes seem to interact throughout embryogenesis and *Tc-pnr* may actually be important for dorsal fates, by restricting gene expression or promoting gene expression in dorsal domains. The latter case might apply for its regulatory role on *Tc-dpp*, as it was discussed in the previous section. In the dorsalmost ectoderm, *Tc-pnr* might promote *Tc-dpp* expression, while a yet unknown gene restricts *Tc-dpp* expression to the dorsalmost cell row, as *Tc-pnr* expression expands more ventral than *Tc-dpp*. Thus, it could well be that without *Tc-pnr* expression, the dorsalmost ectoderm is not specified due to a loss of *Tc-dpp* expression, resulting in a dorsal hole. To verify this assumption, an antibody stain for *Tc*-pMAD will be needed. Performed in wild type embryos, the *Tc*-pMAD stain will resolve the question if the BMP ligand *Tc-dpp* is actually effecting the dorsal most cells via its effector *Tc*-pMAD. Similarly, in *Tc-pnr* knock down embryos, loss of *Tc*-pMAD will clearly show, if *Tc-pnr* effects the *Tc*-Dpp signalling cascade in the dorsal most cell row. That *Tc-pnr* might be important for dorsal bristle patterning (bristles along the larval body are arranged in a precise pattern in *Tribolium* [Schinko et al., 2008]), could strengthen its role as a DV selector gene further. In the supplements of this study (6.4), it is reported that the dorsal most macrochaetes of the A1-A8 segments are missing (assuming that this is not a secondary effect due to the dorsal hole in the cuticle), which was similarly reported in *Drosophila* [Heitzler et al., 1996; Calleja et al., 2000]. In the fly, it is concluded that this relates to the establishment of dorsal fates by *Dm-pnr* [Calleja et al., 2000]. Although the analysis performed in *Tribolium* was very rudimentary, it is yet another example that could point to the role of *Tc-pnr* as a DV selector like gene, but this will need further verification. Either, embryos exhibiting the mild phenotype could be used for such a continuing analysis, as the extend of the dorsal hole is not as pronounced in these embryos or the potential loss of dorsal cells could be investigated by cell counting or similar approaches. With both analyses it could be verified, if the loss of the dorsal most macrochaetes is due to ventralization of the dorsal tissue after loss of

Tc-pnr expression or if the cells developing these bristles are missing. It will be interesting to see in the future, if such effects can be observed in other tissues as well. Therefore, genes with expression ventral to *Tc-pnr's* expression could be the starting point (possible restriction of the gene's expression) or genes expressed in the same cells (promoting the gene's expression). For the latter case, *Tc-tin* might be an interesting target gene, as it is expressed in the cardiac mesoderm [Cande et al., 2009], connecting it directly to a possible future investigation of genes interacting with *Tc-pnr* during heart formation. In *Drosophila*, loss of *Dm-pnr* expression results in a loss of *Dm-tin* expression in the cardiac mesoderm, while a more ventral expression domain of *Dm-tin* in the visceral mesoderm is unaffected [Klinedinst and Bodmer, 2003]. Albeit this approach is very *Drosophila* centric, at least for the investigation of the role of *Tc-pnr* during embryogenesis it might be the right method, in light of the possible strong conservation between *Drosophila* and *Tribolium*.

4.10 Possible explanations for the dorsal bending of *Tc-pnr* knock down embryos

The cause of the dorsal bending of the embryo after *Tc-pnr* pRNAi was not directly investigated in this study. However, it is an intriguing movement of the embryo, which was reported before in *Tribolium*. None or only weak bending of the embryo (a valid statement about the degree of the bending cannot made, as the provided pictures in the respective publications do not provide enough information but the bending is clearly not as pronounced as in *Tc-pnr* knock down embryos) is observed in *Tc fibroblast growth factor 1b* (*Tc-fgf1b*) and *Tc-dpp* knock down embryos, which in both cases display a dorsal hole [Sharma et al., 2013b; Ober and Jockusch, 2006]. However, if the dorsal hole is also smaller compared to less bended *Tc-fgf1b* and *Tc-dpp* knock down embryos and if therefore a correlation between both defects exists, is unclear. A hint for such a correlation may be the observation that in less affected *Tc-pnr* knock down embryos, the dorsal bending and the extent of the dorsal hole is not as pronounced (deduced from the almost straight and complete cardioblast cell rows at the dorsal midline) as in stronger affected embryos. A possible explanation for such a correlation may be that the embryo tries to attenuate the extent of the dorsal hole by the dorsal bending. The embryo would thereby potentially also try to prevent yolk to ooze out of the hole, after the two

extraembryonic membranes degenerated, which normally serve as transient yolk covers until the completion of dorsal closure. This assumption is reflected by the observation that only in a few *Tc-pnr* knock down embryos (8.3%; n=24; data from a single live imaging experiment), the yolk oozes out. In the embryos where the yolk oozes out, this happens in all cases around the time when the embryo reached its maximum bending, which is at a time when the extraembryonic membranes do not cover the yolk anymore.

Another explanation for the bending could well be that the amnion is still attached to embryonic tissue at the anterior and posterior dorsal edges of the embryo. In these regions the amnion does not form a bilayer with the serosa (see [Hilbrant et al., 2016] for images visualizing the partial bilayer configuration of the amnion and the serosa). The amnion would then pull the embryo towards the dorsal side. This model would also fit with a possible role of the amnion in providing the properties for the adhesion to the serosa, which is presumably the case in *Tc-pnr* knock down embryos. If such adhesion properties are disturbed, it may be that the amnion is not able to separate from the embryo when dorsal closure proceeds.

Of course, both explanations for the dorsal bending are intellectual games only. It could well be that none of the explanations applies and a yet unknown mechanism is regulating the dorsal bending (whereas it is known that a dorsal closure in the head region does contribute to the normal ventral bending [Posnien et al., 2010; Panfilio et al., 2013]), which is affected after *Tc-pnr* pRNAi or that it is an interplay of both provided models.

4.11   Conclusion

The analysis of the function of the transcription factor *Tc-pnr* revealed that it is necessary to combine different tools for the investigation of a given gene, to obtain a more complete picture of its function. Albeit the rather simple cuticle preparation technique provided the first hint for the *Tc-pnr* dorsal open phenotype, it was the augmented set of live imaging tools, which enabled a more sophisticated analysis of its function. Investigation of the morphogenetic movements of the three-tissue system (amnion, serosa and embryo) during dorsal closure, affected by *Tc-pnr* pRNAi, would have been not possible without the combined use of different fluorescent lines. Each of the fluorescent lines provided information about a different aspect of *Tc-pnr* gene function. Linking these aspects, revealed then the

real complexity of the interplay between the three tissues. The like this obtained information provided the initial clue of what are the functions of *Tc-pnr*, guiding to the question of how *Tc-pnr* is facilitating these functions. Thus, on the level of genes, potential interaction partners of *Tc-pnr* were investigated, to start the analysis on the level of gene regulation. The gene level is the starting level of different levels of biological organization [Horn et al., 2015]. Genes then effect individual cells, the next level of biological organization. On this level it will be important to understand which cell properties of the amnion and the heart precursor cells were affected. The loss of cell identities lead in the case of the amnion to ectopic rupture and other defects affecting the morphogenetic movements of the amniotic tissue. Likewise, heart tissue formation was impaired. Thus, the level of tissue organization is affected. Given that two tissues of the three-tissue system were directly affected by *Tc-pnr* pRNAi, it is then necessary to start thinking globally. How does loss of tissue integrity influence the serosa and how is inter-tissue adhesion affected. With this the asked questions reached the last level of organization, which is the global egg level. Interestingly, on this level the embryo showed a high degree of plasticity. The embryo was able to maintain overall tissue movements, enabling withdrawal and degeneration of the two extraembryonic membranes during dorsal closure, while exhibiting a hole in the dorsal embryonic tissue. It is this combination of information on different levels of biological organization that is important for a developmental biologist, as he tries to understand developmental processes in its whole.

By looking into other organisms, in the present case mainly *Drosophila*, it is then also possible to add the evolutionary component. Despite the differences in extraembryonic and embryonic development in *Tribolium* and *Drosophila*, which are due to the fact that both species adapted to inhabit distinct environments, the respective *pnr* gene is involved in heart development and dorsal closure in both species and likely shares the same interaction partners. Thus, there seems to be a certain degree of conservation between the gene regulatory networks regulating these complex processes, even if the particular function of the respective *pnr* gene may differ.

4.12   Outlook

The provided data in this study opens up the possibility for more detailed analyses in several distinct directions. One is to continue research on the development of the heart.

Studying the *Tribolium* heart will enable a comparison with the gene regulatory network necessary for formation of the well studied *Drosophila* heart and thereby offer a glimpse into potential evolutionary changes in regulation of heart development in insects. This will lead away from the insect heart model organism *Drosophila* and potentially verify that heart development is strongly conserved between insects and vertebrates, as it is assumed [Medioni et al., 2009]. The process of dorsal closure will be another intriguing research topic. As dorsal closure in *Tribolium* is a three-tissue system (amnion, serosa and embryo), which is in difference to *Drosophila* (amnioserosa and embryo only), research on the system of dorsal closure in *Tribolium* will provide new insights into tissue movements and epithelial reorganization in general. Connected with this research direction is the further investigation of the amnion. It is known that the amnion and serosa are connected throughout their withdrawal to the dorsal side [Hilbrant et al., 2016] and the observed defects within the amnion in *Tc-pnr* knock down embryos permit now to investigate the function of the amnion in more detail. Especially if and how the amnion is potentially facilitating the adhesion between both membranes. The last major research direction regards the potential function of *Tc-pnr* as a DV selector gene, which seems to be conserved to *Drosophila*. So it is now up to following researchers, to built up on the provided foundation and choose one of these research questions, as in depth analysis on each of them is a major task for itself. In the preceding sections of the discussion, individual approaches for such investigations were already provided.

What was not discussed so far is that research on *Tc-pnr* can also be a starting point for a more evolutionary perspective. In the non-drosophilid species [Wotton et al., 2014], the scuttle fly *Megaselia abdita* (Diptera), the expression pattern of *Megaselia abdita pnr* (*Ma-pnr*) is already published and similar to *Tribolium*, *Ma-pnr* is expressed in the amnion [Rafiqi et al., 2008]. This is in so far interesting in an evolutionary perspective of extraembryonic membrane development, as *Megaselia* has two extraembryonic membranes, amnion and serosa. The development of the serosa is thereby similar to the one observed in *Tribolium*, while the amniotic tissue is reduced, similar to its *Drosophila* complement [Rafiqi et al., 2008; Wotton et al., 2014]. Another species for evolutionary comparisons of *pnr* function is the milkweed bug *Oncopeltus fasciatus* (Hemiptera). It shows a sophisticated set of movements during extraembryonic development, while having two complete extraembryonic membranes [Panfilio, 2008]. A resource which will contribute

more general to the analysis of gene evolution is the i5K project for genome sequencing [i5K Consortium, 2013]. 703 Hexapoda, 63 Chelicerata, 20 Crustacea and 6 Myriapoda were initially nominated for sequencing [i5K Consortium, 2013]. With those genomes, a comparative analyses of the properties of individual genomes can be conducted (genome size, overall gene number or gene lengths) but also synteny analyses (see 6.6) and it is an easy way for an initial check if homologous genes exist in different species.

Besides from the investigation of the function of *Tc-pnr* in this study, the two genes *Tc-iro* (see 3.2.5 and 6.5) and *Tc mirror* (*Tc-mirr*; data not shown) were investigated as well. Their wild type expression pattern in *Tribolium* was described and pRNAi experiments were performed to investigate their function. Although the analyses on both genes needs to be continued, especially *Tc-iro* seems to be a promising target for the investigation of extraembryonic membrane development. *Tc-iro* knock down embryos showed an early defect during differentiation of the blastoderm, which may result in the loss of proper amnion and serosa formation. Defects which arised during later development were also observed (amongst others an impaired heart formation) but not investigated further. *Tc-mirr* on the other hand is potentially functioning before the egg is leaving the ovaries of the female, as indicated by a reduction in the number of deposited eggs. Thereby, both genes offer the possibility to investigate different aspects during *Tribolium* embryogenesis. Analyses on both genes can also be expanded to *Oncopeltus*, in which initial experiments in wild type embryos were already performed.

Chapter 5

References

[Affolter et al. 1994]   AFFOLTER, M. ; NELLEN, D. ; NUSSBAUMER, U. ; BASLER, K.: Multiple requirements for the receptor serine/threonine kinase *thick veins* reveal novel functions of TGF beta homologs during *Drosophila* embryogenesis. *Development* 120 (1994), Nr. 11, P. 3105–3117

[Alvarez et al. 2003]   ALVAREZ, A. D. ; SHI, W. ; WILSON, B. A. ; SKEATH, J. B.: *pannier* and *pointedP2* act sequentially to regulate *Drosophila* heart development. *Development* 130 (2003), Nr. 13, P. 3015–3026

[Anders et al. 2014]   ANDERS, C. ; NIEWOEHNER, O. ; DUERST, A. ; JINEK, M.: Structural basis of PAM-dependent target DNA recognition by the Cas9 endonuclease. *Nature* 513 (2014), Nr. 7519, P. 569–573

[Arquier et al. 2001]   ARQUIER, N. ; PERRIN, L. ; MANFRUELLI, P. ; SÉMÉRIVA, M.: The *Drosophila* tumor suppressor gene *lethal(2)giant larvae* is required for the emission of the Decapentaplegic signal. *Development* 128 (2001), Nr. 12, P. 2209–2220

[Auer et al. 2014]   AUER, T. O. ; DUROURE, K. ; DE CIAN, A. ; CONCORDET, J. P. ; DEL BENE, F.: Highly efficient CRISPR/Cas9-mediated knock-in in zebrafish by homology-independent DNA repair. *Genome Research* 24 (2014), Nr. 1, P. 142–153

[Awata et al. 2015]   AWATA, H. ; WATANABE, T. ; HAMANAKA, Y. ; MITO, T. ; NOJI, S. ; MIZUNAMI, M.: Knockout crickets for the study of learning and memory: Dopamine receptor Dop1 mediates aversive but not appetitive reinforcement in crickets. *Scientific Reports* 5 (2015), P. 15885

[Barrangou et al. 2007]   BARRANGOU, R. ; FREMAUX, C. ; DEVEAU, H. ; RICHARDS, M. ; BOYAVAL, P. ; MOINEAU, S. ; ROMERO, D. A. ; HORVATH, P.: CRISPR Provides Acquired Resistance Against Viruses in Prokaryotes. *Science* 315 (2007), Nr. 5819, P. 1709–1712

[Bennett et al. 1993]   BENNETT, C. B. ; LEWIS, A. L. ; BALDWIN, K. K. ; RESNICK, M. A.: Lethality induced by a single site-specific double-strand break in a dispensable yeast plasmid. *Proc. Natl. Acad. Sci. U.S.A.* 90 (1993), Nr. 12, P. 5613–5617

[Benton et al. 2013]   BENTON, M. A. ; AKAM, M. ; PAVLOPOULOS, A.: Cell and tissue dynamics during *Tribolium* embryogenesis revealed by versatile fluorescence labeling approaches. *Development* 140 (2013), Nr. 15, P. 3210–3220

[Berghammer et al. 1999a]   BERGHAMMER, A. ; BUCHER, G. ; MADERSPACHER, F. ; KLINGLER, M.: A system to efficiently maintain embryonic lethal mutations in the flour beetle *Tribolium castaneum. Development Genes and Evolution* 209 (1999), Nr. 6, P. 382–389

[Berghammer et al. 1999b]   BERGHAMMER, A. J. ; KLINGLER, M. ; WIMMER, E. A.: A universal marker for transgenic insects. *Nature* 402 (1999), Nr. 6760, P. 370–371

[Berghammer et al. 2009]   BERGHAMMER, A. J. ; WEBER, M. ; TRAUNER, J. ; KLINGLER, M.: Red flour beetle (*Tribolium*) germline transformation and insertional mutagenesis. *Cold Spring Harbor Protocols* 2009 (2009), Nr. 8, P. pdb.prot5259

[Bevis and Glick 2002]   BEVIS, B. J. ; GLICK, B. S.: Rapidly maturing variants of the Discosoma red fluorescent protein (DsRed). *Nature Biotechnology* 20 (2002), Nr. 1, P. 83–87

[Bischof et al. 2007]   BISCHOF, J. ; MAEDA, R. K. ; HEDIGER, M. ; KARCH, F. ; BASLER, K.: An optimized transgenesis system for *Drosophila* using germ-line-specific phiC31 integrases. *Proc. Natl. Acad. Sci. U.S.A.* 104 (2007), Nr. 9, P. 3312–3317

[Bodmer 1995]   BODMER, R.: Migration of leukocytes across the vascular intima heart development in *Drosophila* and its relationship to vertebrates. *Trends in Cardiovascular Medicine* 5 (1995), Nr. 1, P. 21–28

[Bolotin et al. 2005]   BOLOTIN, A. ; QUINQUIS, B. ; SOROKIN, A. ; EHRLICH, S. D.: Clustered regularly interspaced short palindrome repeats (CRISPRs) have spacers of extrachromosomal origin. *Microbiology* 151 (2005), Nr. 8, P. 2551–2561

[Bondy-Denomy et al. 2013]   BONDY-DENOMY, J. ; PAWLUK, A. ; MAXWELL, K. L. ; DAVIDSON, A. R.: Bacteriophage genes that inactivate the CRISPR/Cas bacterial immune system. *Nature* 493 (2013), Nr. 7432, P. 429–432

[Brown et al. 2009]   BROWN, S. J. ; SHIPPY, T. D. ; MILLER, S. ; BOLOGNESI, R. ; BEEMAN, R. W. ; LORENZEN, M. D. ; BUCHER, G. ; WIMMER, E. A. ; KLINGLER, M.: The red flour beetle, *Tribolium castaneum* (coleoptera): A model for studies of development and pest biology. *Cold Spring Harbor Protocols* 2009 (2009), Nr. 8, P. pdb.emo126

[Bryantsev and Cripps 2009]   BRYANTSEV, A. L. ; CRIPPS, R. M.: Cardiac gene regulatory networks in *Drosophila. Biochimica et Biophysica Acta (BBA) - Gene Regulatory Mechanisms* 1789 (2009), Nr. 4, P. 343–353

[Bucher   2009]   BUCHER,   G.:   The   beetle   book. *http://wwwuser.gwdg.de/ gbucher1/tribolium-castaneum-beetle-book1.pdf*   (2009). – last access: 25.09.2016

[Bucher et al. 2002]   BUCHER, G. ; SCHOLTEN, J. ; KLINGLER, M.: Parental RNAi in *Tribolium* (coleoptera). *Current Biology* 12 (2002), Nr. 3, P. R85–R86

[Burglin 1997]   BURGLIN, T. R.: Analysis of TALE superclass homeobox genes (MEIS, PBC, KNOX, Iroquois, TGIF) reveals a novel domain conserved between plants and animals. *Nucleic Acids Research* 25 (1997), Nr. 21, P. 4173–4180

[Byars et al. 1999]   BYARS, C.L. ; BATES, K.L. ; LETSOU, A.: The dorsal-open group gene *raw* is required for restricted DJNK signaling during closure. *Development* 126 (1999), Nr. 21, P. 4913–4923

[Calleja et al. 2000]   CALLEJA, M. ; HERRANZ, H. ; ESTELLA, C. ; CASAL, J. ; LAWRENCE, P. ; SIMPSON, P. ; MORATA, G.: Generation of medial and lateral dorsal body domains by the *pannier* gene of *Drosophila. Development* 127 (2000), Nr. 18, P. 3971–3980

[Cande et al. 2009]   CANDE, J. D. ; CHOPRA, V. S. ; LEVINE, M.: Evolving enhancer-promoter interactions within the tinman complex of the flour beetle, *Tribolium castaneum. Development* 136 (2009), Nr. 18, P. 3153–3160

[Cary et al. 1989]   CARY, L. C. ; GOEBEL, M. ; CORSARO, B. G. ; WANG, H. ; ROSEN, E. ; FRASER, M. J.: Transposon mutagenesis of baculoviruses: Analysis of *Trichoplusia ni* transposon IFP2 insertions within the FP-locus of nuclear polyhedrosis viruses. *Virology* 172 (1989), Nr. 1, P. 156–169

[Cavodeassi et al. 2001]   CAVODEASSI, F. ; MODOLELL, J. ; GOMEZ-SKARMETA, J.L.: The Iroquois family of genes: From body building to neural patterning. *Development* 128 (2001), Nr. 15, P. 2847–2855

[Chen et al. 2002]   CHEN, H. ; MARINISSEN, M. J. ; OH, S. ; CHEN, X. ; MELNICK, M. ; PERRIMON, N. ; GUTKIND, J. S. ; HOU, S. X.: CKA, a novel multidomain protein, regulates the JUN N-Terminal kinase signal transduction pathway in *Drosophila. Molecular and Cellular Biology* 22 (2002), Nr. 6, P. 1792–1803

[Chroma 2016]   CHROMA: Chroma Spectra Viewer. *https://www.chroma.com/spectra-viewer?fluorochromes=10419,10392,10424* (2016). – last access: 13.10.2016

[Cong 2016]   CONG, L.:   Zhang lab's CRISPR frequently asked questions. *https://www.addgene.org/crispr/zhang/faq/* (2016). – last access: 13.10.2016

[Cong et al. 2013]   CONG, L. ; RAN, F. A. ; COX, D. ; LIN, S. ; BARRETTO, R. ; HABIB, N. ; HSU, P. D. ; WU, X. ; JIANG, W. ; MARRAFFINI, L. A. ; ZHANG, F.: Multiplex genome engineering using CRISPR/Cas systems. *Science* 339 (2013), Nr. 6121, P. 819–823

[i5K Consortium 2013]   CONSORTIUM i5K: The i5K initiative: Advancing arthropod genomics for knowledge, human health, agriculture, and the environment. *Journal of Heredity* 104 (2013), Nr. 5, P. 595–600

[Cripps and Olson 2002] Cripps, Richard M. ; Olson, Eric N.: Control of cardiac development by an evolutionarily conserved transcriptional network. *Developmental Biology* 246 (2002), Nr. 1, P. 14–28

[Day and Davidson 2009] Day, R. N. ; Davidson, M. W.: The fluorescent protein palette: tools for cellular imaging. *Chemical Society Reviews* 38 (2009), Nr. 10, P. 2887–2921

[Deveau et al. 2008] Deveau, H. ; Barrangou, R. ; Garneau, J. E. ; Labont, J. ; Fremaux, C. ; Boyaval, P. ; Romero, D. A. ; Horvath, P. ; Moineau, S.: Phage response to CRISPR-encoded resistance in *Streptococcus thermophilus*. *Journal of Bacteriology* 190 (2008), Nr. 4, P. 1390–1400

[Engel 2015] Engel, M. S.: Insect evolution. *Current Biology* 25 (2015), Nr. 19, P. R868–R872

[Fernández et al. 2007] Fernández, B. G. ; Arias, A. M. ; Jacinto, A.: Dpp signalling orchestrates dorsal closure by regulating cell shape changes both in the amnioserosa and in the epidermis. *Mechanisms of Development* 124 (2007), Nr. 1112, P. 884–897

[Fire et al. 1998] Fire, A. ; Xu, S. ; Montgomery, M. K. ; Kostas, S. A. ; Driver, S. E. ; Mello, C. C.: Potent and specific genetic interference by double-stranded RNA in *Caenorhabditis elegans*. *Nature* 391 (1998), Nr. 6669, P. 806–811

[Frank and Rushlow 1996] Frank, L. H. ; Rushlow, C.: A group of genes required for maintenance of the amnioserosa tissue in *Drosophila*. *Development* 122 (1996), Nr. 5, P. 1343–1352

[Gajewski et al. 1999] Gajewski, K. ; Fossett, N. ; Molkentin, J. D. ; Schulz, R. A.: The zinc finger proteins pannier and GATA4 function as cardiogenic factors in *Drosophila*. *Development* 126 (1999), Nr. 24, P. 5679–5688

[Gilles et al. 2015] Gilles, A. F. ; Schinko, J. B. ; Averof, M.: Efficient CRISPR-mediated gene targeting and transgene replacement in the beetle *Tribolium castaneum*. *Development* 142 (2015), Nr. 16, P. 2832–2839

[Giorgianni and Patel 2004] Giorgianni, M. W. ; Patel, N. H.: Patterning of the branched head appendages in *Schistocerca americana* and *Tribolium castaneum*. *Evolution & Development* 6 (2004), Nr. 6, P. 402–410

[Glise and Noselli 1997] Glise, B ; Noselli, S: Coupling of Jun amino-terminal kinase and decapentaplegic signaling pathways in *Drosophila* morphogenesis. *Genes & Development* 11 (1997), Nr. 13, P. 1738–1747

[Gomez-Skarmeta et al. 1996] Gomez-Skarmeta, J. L. ; Diez del Corral, R. ; de la Calle-Mustienes, E. ; Ferre-Marco, D. ; Modolell, J.: *araucan* and *caupolican*, two members of the novel Iroquois complex, encode homeoproteins that control proneural and vein-forming genes. *Cell* 85 (1996), Nr. 1, P. 95–105

[Gomez-Skarmeta and Modolell 2002] Gomez-Skarmeta, J. L. ; Modolell, J.: Iroquois genes: genomic organization and function in vertebrate neural development. *Current Opinion in Genetics & Development* 12 (2002), Nr. 4, P. 403–408

[Gorfinkiel et al. 2009] Gorfinkiel, N. ; Blanchard, G. B. ; Adams, R. J. ; Martinez Arias, A.: Mechanical control of global cell behaviour during dorsal closure in *Drosophila. Development* 136 (2009), Nr. 11, P. 1889–1898

[Groth and Calos 2004] Groth, A. C. ; Calos, M. P.: Phage Integrases: Biology and Applications. *Journal of Molecular Biology* 335 (2004), Nr. 3, P. 667–678

[Handel et al. 2000] Handel, K. ; Grünfelder, C.G. ; Roth, S ; Sander, K.: *Tribolium* embryogenesis: A SEM study of cell shapes and movements from blastoderm to serosal closure. *Development Genes and Evolution* 210 (2000), Nr. 4, P. 167–179

[Harden 2002] Harden, N.: Signaling pathways directing the movement and fusion of epithelial sheets: lessons from dorsal closure in *Drosophila. Differentiation* 70 (2002), Nr. 4, P. 181–203

[Hartenstein 1993] Hartenstein, V.: *Atlas of* Drosophila *Development.* Cold Spring Harbor Laboratory Press, 1993. – ISBN 9780879694722

[Heisenberg 2009] Heisenberg, C. P.: Dorsal closure in *Drosophila*: cells cannot get out of the tight spot. *BioEssays* 31 (2009), Nr. 12, P. 1284–1287

[Heitzler et al. 1996] Heitzler, P. ; Haenlin, M. ; Ramain, P. ; Calleja, M. ; Simpson, P.: A genetic analysis of *pannier*, a gene necessary for viability of dorsal tissues and bristle positioning in *Drosophila. Genetics* 143 (1996), Nr. 3, P. 1271–1286

[Herranz and Morata 2001] Herranz, H ; Morata, G: The functions of *pannier* during *Drosophila* embryogenesis. *Development* 128 (2001), Nr. 23, P. 4837–4846

[Hilbrant et al. 2016] Hilbrant, M. ; Horn, T. ; Koelzer, S. ; Panfilio, K. A.: The beetle amnion and serosa functionally interact as apposed epithelia. *eLife* 5 (2016), P. e13834

[Horn et al. 2002] Horn, C. ; Schmid, B. G. M. ; Pogoda, F. S. ; Wimmer, E. A.: Fluorescent transformation markers for insect transgenesis. *Insect Biochemistry and Molecular Biology* 32 (2002), Nr. 10, P. 1221–1235

[Horn and Wimmer 2000] Horn, C. ; Wimmer, E. A.: A versatile vector set for animal transgenesis. *Development Genes and Evolution* 210 (2000), Nr. 12, P. 630–637

[Horn et al. 2015] Horn, T ; Hilbrant, M. ; Panfilio, K. A.: Evolution of epithelial morphogenesis: phenotypic integration across multiple levels of biological organization. *Frontiers in Genetics* 6 (2015), Nr. 303, P. 86–92

[Horn and Panfilio 2016]   HORN, T. ; PANFILIO, K. A.: Novel functions for *Dorsocross* in epithelial morphogenesis in the beetle *Tribolium castaneum. Development* 143 (2016), Nr. 16, P. 3002–3011

[Huang et al. 2009]   HUANG, J. ; ZHOU, W. ; DONG, W. ; WATSON, A. M. ; HONG, Y.: Directed, efficient, and versatile modifications of the *Drosophila* genome by genomic engineering. *Proc. Natl. Acad. Sci. U.S.A.* 106 (2009), Nr. 20, P. 8284–8289

[Irimia et al. 2008]   IRIMIA, M. ; MAESO, I. ; GARCIA-FERNÁNDEZ, J.: Convergent evolution of clustering of Iroquois homeobox genes across metazoans. *Molecular Biology and Evolution* 25 (2008), Nr. 8, P. 1521–1525

[Ishino et al. 1987]   ISHINO, Y ; SHINAGAWA, H ; MAKINO, K ; AMEMURA, M ; NAKATA, A: Nucleotide sequence of the *iap* gene, responsible for alkaline phosphatase isozyme conversion in *Escherichia coli*, and identification of the gene product. *Journal of Bacteriology* 169 (1987), Nr. 12, P. 5429–5433

[Jacinto et al. 2002]   JACINTO, A. ; WOOLNER, S. ; MARTIN, P.: Dynamic analysis of dorsal closure in *Drosophila*: From genetics to cell biology. *Developmental Cell* 3 (2002), Nr. 1, P. 9–19

[Jacobs et al. 2014]   JACOBS, C. G. ; SPAINK, H. P. ; ZEE, M. van der: The extraembryonic serosa is a frontier epithelium providing the insect egg with a full-range innate immune response. *eLife* 3 (2014), P. e04111

[Jacobs et al. 2013]   JACOBS, C. G. C. ; REZENDE, G. L. ; LAMERS, G. E. M. ; ZEE, M. van der: The extraembryonic serosa protects the insect egg against desiccation. *Proceedings of the royal society B - biological sciences* 280 (2013), Nr. 1764, P. 20131082

[Jacobs and van der Zee 2013]   JACOBS, C. G. C. ; ZEE, M. van der: Immune competence in insect eggs depends on the extraembryonic serosa. *Developmental and comparative Immunology* 41 (2013), Nr. 2, P. 263–269

[Janssen and Damen 2008]   JANSSEN, R. ; DAMEN, W. G.: Diverged and conserved aspects of heart formation in a spider. *Evolution & Development* 10 (2008), Nr. 2, P. 155–165

[Jensen 2012]   JENSEN, E. C.: Use of fluorescent probes: their effect on cell biology and limitations. *The Anatomical Record (Hoboken)* 295 (2012), Nr. 12, P. 2031–2036

[Jinek et al. 2012]   JINEK, M. ; CHYLINSKI, K. ; FONFARA, I. ; HAUER, M. ; DOUDNA, J. A. ; CHARPENTIER, E.: A programmable dual-RNA-guided DNA endonuclease in adaptive bacterial immunity. *Science* 337 (2012), Nr. 6096, P. 816–821

[Jürgens et al. 1984]   JÜRGENS, G. ; WIESCHAUS, E. ; NÜSSLEIN-VOLHARD, C. ; KLUDING, H.: Mutations affecting the pattern of the larval cuticle in *Drosophila melanogaster. Wilhelm Roux's archives of developmental biology* 193 (1984), Nr. 5, P. 283–295

[Kerner et al. 2009]   KERNER, P. ; IKMI, A. ; COEN, D. ; VERVOORT, M.: Evolutionary history of the iroquois/Irx genes in metazoans. *BMC Evolutionary Biology* 9 (2009), P. 74

[Kirchner and Schneider 2015]   KIRCHNER, M. ; SCHNEIDER, S.: CRISPR-Cas: From the bacterial adaptive immune system to a versatile tool for genome engineering. *Angewandte Chemie International Edition* 54 (2015), Nr. 46, P. 13508–13514

[Kistler et al. 2015]   KISTLER, K. E. ; VOSSHALL, L. B. ; MATTHEWS, B. J.: Genome engineering with CRISPR-Cas9 in the mosquito *Aedes aegypti. Cell Reports* 11 (2015), Nr. 1, P. 51–60

[Klinedinst and Bodmer 2003]   KLINEDINST, S. L. ; BODMER, R.: Gata factor *pannier* is required to establish competence for heart progenitor formation. *Development* 130 (2003), Nr. 13, P. 3027–3038

[Knust 1997]   KNUST, E.: *Drosophila* morphogenesis: Movements behind the edge. *Current Biology* 7 (1997), Nr. 9, P. R558–R561

[Koelzer et al. 2014]   KOELZER, S. ; KÖLSCH, Y. ; PANFILIO, K. A.: Visualizing late insect embryogenesis: Extraembryonic and mesodermal enhancer trap expression in the beetle *Tribolium castaneum. PLOS ONE* 9 (2014), Nr. 7, P. 1–17

[Li et al. 2014]   LI, K. ; WANG, G. ; ANDERSEN, T. ; ZHOU, P. ; PU, W. T.: Optimization of genome engineering approaches with the CRISPR/Cas9 system. *PLOS ONE* 9 (2014), Nr. 8, P. 1–10

[Liu and Kaufman 2009]   LIU, P. ; KAUFMAN, T. C.: Morphology and husbandry of the large milkweed bug, *Oncopeltus fasciatus. Cold Spring Harbor Protocols* 2009 (2009), Nr. 8, P. pdb.emo127

[Liu and Kaufman 2004]   LIU, P. Z. ; KAUFMAN, T. C.: *hunchback* is required for suppression of abdominal identity, and for proper germband growth and segmentation in the intermediate germband insect *Oncopeltus fasciatus. Development* 131 (2004), Nr. 7, P. 1515–1527

[Living Colors™ DsRed2 2001]   LIVING COLORS™ DSRED2: *CLONTECHniques* XVI (2001), 2–3 P

[Long et al. 2013]   LONG, D. ; ZHAO, A. ; XU, L. ; LU, W. ; GUO, Q. ; ZHANG, Y. ; XIANG, Z.: In vivo site-specific integration of transgene in silkworm via PhiC31 integrase-mediated cassette exchange. *Insect Biochemistry and Molecular Biology* 43 (2013), Nr. 11, P. 997–1008

[Lorenzen et al. 2003]   LORENZEN, M. D. ; BERGHAMMER, A. J. ; BROWN, S. J. ; DENELL, R. E. ; KLINGLER, M. ; BEEMAN, R. W.: *piggyBac*-mediated germline transformation in the beetle *Tribolium castaneum. Insect Molecular Biology* 12 (2003), Nr. 5, P. 433–440

[Lynch et al. 2012]   LYNCH, J. A. ; EL-SHERIF, E. ; BROWN, S. J.: Comparisons of the embryonic development of *Drosophila*, *Nasonia*, and *Tribolium*. *Wiley Interdiscip. Rev. Dev. Biol.* 1 (2012), Nr. 1, P. 16–39

[Ma et al. 2014]   MA, S. ; CHANG, J. ; WANG, X. ; LIU, Y. ; ZHANG, J. ; LU, W. ; GAO, J. ; SHI, R. ; ZHAO, P. ; XIA, Q.: CRISPR/Cas9 mediated multiplex genome editing and heritable mutagenesis of BmKu70 in *Bombyx mori*. *Scientific Reports* 4 (2014), P. 4489

[Maeso et al. 2012]   MAESO, I. ; IRIMIA, M. ; TENA, J. J. ; GONZÁLEZ-PÉREZ, E. ; TRAN, D. ; RAVI, V. ; VENKATESH, B. ; CAMPUZANO, S. ; GÓMEZ-SKARMETA, J. L. ; GARCIA-FERNÁNDEZ, J.: An ancient genomic regulatory block conserved across bilaterians and its dismantling in tetrapods by retrogene replacement. *Genome Research* 22 (2012), Nr. 4, P. 642–655

[Makarova et al. 2015]   MAKAROVA, K. S. ; WOLF, Y. I. ; ALKHNBASHI, O. S. ; COSTA, F. ; SHAH, S. A. ; SAUNDERS, S. J. ; BARRANGOU, R. ; BROUNS, S. J. ; CHARPENTIER, E. ; HAFT, D. H. ; HORVATH, P. ; MOINEAU, S. ; MOJICA, F. J. ; TERNS, R. M. ; TERNS, M. P. ; WHITE, M. F. ; YAKUNIN, A. F. ; GARRETT, R. A. ; OOST, J. van der ; BACKOFEN, R. ; KOONIN, E. V.: An updated evolutionary classification of CRISPR-Cas systems. *Nature Reviews Microbiology* 13 (2015), Nr. 11, P. 722–736

[Mali et al. 2013]   MALI, P. ; YANG, L. ; ESVELT, K. M. ; AACH, J. ; GUELL, M. ; DICARLO, J. E. ; NORVILLE, J. E. ; CHURCH, G. M.: RNA-guided human genome engineering via Cas9. *Science* 339 (2013), Nr. 6121, P. 823–826

[Mann and Morata 2000]   MANN, RS ; MORATA, G: The developmental and molecular biology of genes that subdivide the body of *Drosophila*. *Annual review of cell and developmental biology* 16 (2000), P. 243–271

[Mans et al. 2015]   MANS, R. ; ROSSUM, H. M. van ; WIJSMAN, M. ; BACKX, A. ; KUIJPERS, N. G. ; BROEK, M. van den ; DARAN-LAPUJADE, P. ; PRONK, J. T. ; MARIS, A. J. A. van ; DARAN, J. G.: CRISPR/Cas9: a molecular Swiss army knife for simultaneous introduction of multiple genetic modifications in *Saccharomyces cerevisiae*. *FEMS Yeast Research* 15 (2015), Nr. 2

[Martin et al. 2016]   MARTIN, A. ; SERANO, J. M. ; JARVIS, E. ; BRUCE, H. S. ; WANG, J. ; RAY, S. ; BARKER, C. A. ; O` CONNELL, L. C. ; PATEL, N. H.: CRISPR/Cas9 mutagenesis reveals versatile roles of Hox genes in crustacean limb specification and evolution. *Current Biology* 26 (2016), Nr. 1, P. 14–26

[Matz et al. 1999]   MATZ, M. V. ; FRADKOV, A. F. ; LABAS, Y. A. ; SAVITSKY, A. P. ; ZARAISKY, A. G. ; MARKELOV, M. L. ; LUKYANOV, S. A.: Fluorescent proteins from nonbioluminescent Anthozoa species. *Nature Biotechnology* 17 (1999), Nr. 10, P. 969–973

[Medioni et al. 2009]   MEDIONI, C. ; SENATORE, S. ; SALMAND, P. ; LALEVEE, N. ; PERRIN, L. ; SEMERIVA, M.: The fabulous destiny of the *Drosophila* heart. *Current Opinion in Genetics & Development* 19 (2009), Nr. 5, P. 518–525

[Mehta and Haber 2014]   MEHTA, A. ; HABER, J. E.: Sources of DNA double-strand breaks and models of recombinational DNA repair. *Cold Spring Harbor Perspectives in Biology* 6 (2014), Nr. 9, P. a016428

[Meister and Tuschl 2004]   MEISTER, G. ; TUSCHL, T.: Mechanisms of gene silencing by double-stranded RNA. *Nature* 431 (2004), Nr. 7006, P. 343–349

[Mello and Conte 2004]   MELLO, C. C. ; CONTE, D.: Revealing the world of RNA interference. *Nature* 431 (2004), Nr. 7006, P. 338–342

[Moehle et al. 2007]   MOEHLE, E. A. ; MOEHLE, E. A. ; ROCK, J. M. ; ROCK, J. M. ; LEE, Y. L. ; LEE, Y. L. ; JOUVENOT, Y. ; JOUVENOT, Y. ; DEKELVER, R. C. ; DEKELVER, R. C. ; GREGORY, P. D. ; GREGORY, P. D. ; URNOV, F. D. ; URNOV, F. D. ; HOLMES, M. C. ; HOLMES, M. C.: Targeted gene addition into a specified location in the human genome using designed zinc finger nucleases. *Proc. Natl. Acad. Sci. U.S.A.* 104 (2007), Nr. 9, P. 3055–3060

[Mojica et al. 2009]   MOJICA, F. J. M. ; DÍEZ-VILLASENOR, C. ; GARCÍA-MARTÍNEZ, J. ; ALMENDROS, C.: Short motif sequences determine the targets of the prokaryotic CRISPR defence system. *Microbiology* 155 (2009), Nr. 3, P. 733–740

[Mojica et al. 2005]   MOJICA, F. J. M. ; DÍEZ-VILLASENOR, C. ; GARCÍA-MARTÍNEZ, J. ; SORIA, E.: Intervening sequences of regularly spaced prokaryotic repeats derive from foreign genetic elements. *Journal of Molecular Evolution* 60 (2005), Nr. 2, P. 174–182

[Nakamoto et al. 2015]   NAKAMOTO, A. ; HESTER, S. D. ; CONSTANTINOU, S. J. ; BLAINE, W. G. ; TEWKSBURY, A. B. ; MATEI, M. T. ; NAGY, L. M. ; WILLIAMS, T. A.: Changing cell behaviours during beetle embryogenesis correlates with slowing of segmentation. *Nature Communications* 6 (2015), P. 6635

[Nakanishi et al. 2014]   NAKANISHI, T. ; KATO, Y. ; MATSUURA, T. ; WATANABE, H.: CRISPR/Cas-mediated targeted mutagenesis in *Daphnia magna*. *PLOS ONE* 9 (2014), Nr. 5, P. 1–7

[Nishimasu et al. 2014]   NISHIMASU, H. ; RAN, F. A. ; HSU, P. D. ; KONERMANN, S. ; SHEHATA, S. I. ; DOHMAE, N. ; ISHITANI, R. ; ZHANG, F. ; NUREKI, O.: Crystal structure of Cas9 in complex with guide RNA and target DNA. *Cell* 156 (2014), Nr. 5, P. 935–949

[Nunes da Fonseca et al. 2008]   NUNES DA FONSECA, R. ; LEVETZOW, C. von ; KAISCHEUER, P. ; BASAL, A. ; ZEE, M. van der ; ROTH, S.: Self-regulatory circuits in dorsoventral axis formation of the short-germ beetle *Tribolium castaneum*. *Developmental Cell* 14 (2008), Nr. 4, P. 605–615

[Nunes da Fonseca et al. 2010]   Nunes da Fonseca, R. ; Zee, M. van der ; Roth, S.: Evolution of extracellular Dpp modulators in insects: The roles of *tolloid* and *twisted-gastrulation* in dorsoventral patterning of the *Tribolium* embryo. *Developmental Biology* 345 (2010), Nr. 1, P. 80–93

[Ober and Jockusch 2006]   Ober, K. A. ; Jockusch, E. L.: The roles of *wingless* and *decapentaplegic* in axis and appendage development in the red flour beetle, *Tribolium castaneum. Developmental Biology* 294 (2006), Nr. 2, P. 391–405

[van der Oost et al. 2014]   Oost, J. van der ; Westra, E. R. ; Jackson, R. N. ; Wiedenheft, B.: Unravelling the structural and mechanistic basis of CRISPR-Cas systems. *Nature reviews microbiology* 12 (2014), Nr. 7, P. 479–492

[Oros et al. 2010]   Oros, S. M. ; Tare, M. ; Kango-Singh, M. ; Singh, A.: Dorsal eye selector *pannier* (*pnr*) suppresses the eye fate to define dorsal margin of the *Drosophila* eye. *Developmental Biology* 346 (2010), Nr. 2, P. 258–271

[Panfilio 2008]   Panfilio, K. A.: Extraembryonic development in insects and the acrobatics of blastokinesis. *Developmental Biology* 313 (2008), Nr. 2, P. 471–491

[Panfilio et al. 2013]   Panfilio, K. A. ; Oberhofer, G. ; Roth, S.: High plasticity in epithelial morphogenesis during insect dorsal closure. *Biology Open* 2 (2013), Nr. 11, P. 1108–1118

[Pawluk et al. 2014]   Pawluk, A. ; Bondy-Denomy, J. ; Cheung, V. H. W. ; Maxwell, K. L. ; Davidson, A. R.: A new group of phage anti-CRISPR genes inhibits the type I-E CRISPR-Cas system of *Pseudomonas aeruginosa. mBio* 5 (2014), Nr. 2, P. e00896

[Peng et al. 2015]   Peng, R. ; Lin, G. ; Li, J.: Potential pitfalls of CRISPR/Cas9-mediated genome editing. *FEBS Journal* 283 (2015), Nr. 7, P. 1218–1231

[Pfander et al. 2011]   Pfander, C. ; Anar, B. ; Schwach, F. ; Otto, T. D. ; Brochet, M. ; Volkmann, K. ; Quail, M. A. ; Pain, A. ; Rosen, B. ; Skarnes, W. ; Rayner, J. C. ; Billker, O.: A scalable pipeline for highly effective genetic modification of a malaria parasite. *Nature Methods* 8 (2011), Nr. 12, P. 1078–1082

[Posnien et al. 2010]   Posnien, N. ; Schinko, J. B. ; Kittelmann, S. ; Bucher, G.: Genetics, development and composition of the insect head – A beetles view. *Arthropod Structure & Development* 39 (2010), Nr. 6, P. 399–410

[Pourcel et al. 2005]   Pourcel, C. ; Salvignol, G. ; Vergnaud, G.: CRISPR elements in *Yersinia pestis* acquire new repeats by preferential uptake of bacteriophage DNA, and provide additional tools for evolutionary studies. *Microbiology* 151 (2005), Nr. 3, P. 653–663

[Rafiqi et al. 2008]   Rafiqi, A.M. ; Lemke, S. ; Ferguson, S. ; Stauber, M. ; Schmidt-Ott, U.: Evolutionary origin of the amnioserosa in cyclorrhaphan flies

correlates with spatial and temporal expression changes of *zen*. *Proc. Natl. Acad. Sci. U.S.A.* 105 (2008), Nr. 1, P. 234–239

[Ramain et al. 1993]   RAMAIN, P. ; HEITZLER, P. ; HAENLIN, M. ; SIMPSON, P.: *pannier*, a negative regulator of *achaete and scute* in *Drosophila*, encodes a zinc finger protein with homology to the vertebrate transcription factor *GATA-1*. *Development* 119 (1993), Nr. 4, P. 1277–1291

[Ran et al. 2013]   RAN, F. A. ; HSU, P. D. ; LIN, C. Y. ; GOOTENBERG, J. S. ; KON-ERMANN, S. ; TREVINO, A. E. ; SCOTT, D. A. ; INOUE, A. ; MATOBA, S. ; ZHANG, Y. ; ZHANG, F.: Double nicking by RNA-guided CRISPR Cas9 for enhanced genome editing specificity. *Cell* 154 (2013), Nr. 6, P. 1380–1389

[Rath et al. 2015]   RATH, D. ; AMLINGER, L. ; RATH, A. ; LUNDGREN, M.: The CRISPR-Cas immune system: Biology, mechanisms and applications. *Biochimie* 117 (2015), P. 119–128

[Reim and Frasch 2005]   REIM, I. ; FRASCH, M.: The *Dorsocross* T-box genes are key components of the regulatory network controlling early cardiogenesis in *Drosophila*. *Development* 132 (2005), Nr. 22, P. 4911–4925

[Richards et al. 2008]   RICHARDS, S. ; GIBBS, R. A. ; WEINSTOCK, G. M. ; BROWN, S. J. ; DENELL, R. ; BEEMAN, R. W.: The genome of the model beetle and pest *Tribolium castaneum*. *Nature* 452 (2008), Nr. 7190, P. 949–955

[Ricos et al. 1999]   RICOS, M.G. ; HARDEN, N. ; SEM, K.P. ; LIM, L. ; CHIA, W.: *Dcdc42* acts in TGF-beta signaling during *Drosophila* morphogenesis: distinct roles for the Drac1/JNK and Dcdc42/TGF-beta cascades in cytoskeletal regulation. *Journal of Cell Science* 112 (1999), Nr. 8, P. 1225–1235

[Riesgo-Escovar and Hafen 1997]   RIESGO-ESCOVAR, J R. ; HAFEN, E: *Drosophila* Jun kinase regulates expression of *decapentaplegic* via the ETS-domain protein Aop and the AP-1 transcription factor *DJun* during dorsal closure. *Genes & Development* 11 (1997), Nr. 13, P. 1717–1727

[Roth and Hartenstein 2008]   ROTH, S. ; HARTENSTEIN, V.: Development of *Tribolium castaneum*. *Development Genes and Evolution* 218 (2008), Nr. 3-4, P. 115–118

[Rugendorff et al. 1994]   RUGENDORFF, A. ; YOUNOSSI-HARTENSTEIN, A. ; HARTEN-STEIN, V.: Embryonic origin and differentiation of the *Drosophila* heart. *Roux's archives of developmental biology* 203 (1994), Nr. 5, P. 266–280

[Sanchez-Salazar et al. 1996]   SANCHEZ-SALAZAR, J. ; PLETCHER, M. T. ; BENNETT, R. L. ; BROWN, S. J. ; DANDAMUDI, T. J. ; DENELL, R. E. ; DOCTOR, J. S.: The *Tribolium decapentaplegic* gene is similar in sequence, structure, and expression to the *Drosophila dpp* gene. *Development Genes and Evolution* 206 (1996), Nr. 4, P. 237–246

[Sarrazin et al. 2012]   Sarrazin, A. F. ; Peel, A. D. ; Averof, M.: A segmentation clock with two-segment periodicity in insects. *Science* 336 (2012), Nr. 6079, P. 338–341

[Savard et al. 2006]   Savard, J. ; Tautz, D. ; Richards, S. ; Weinstock, G. M. ; Gibbs, R. A. ; Werren, J. H. ; Tettelin, H. ; Lercher, M. J.: Phylogenomic analysis reveals bees and wasps (Hymenoptera) at the base of the radiation of Holometabolous insects. *Genome Research* 16 (2006), Nr. 11, P. 1334–1338

[Schinko et al. 2008]   Schinko, J. B. ; Kreuzer, N. ; Offen, N. ; Posnien, N. ; Wimmer, E. A. ; Bucher, G.: Divergent functions of *orthodenticle*, *empty spiracles* and *buttonhead* in early head patterning of the beetle *Tribolium castaneum* (Coleoptera). *Developmental Biology* 317 (2008), Nr. 2, P. 600–613

[Schmidt-Ott and Kwan 2016]   Schmidt-Ott, U. ; Kwan, C. W.: Morphogenetic functions of extraembryonic membranes in insects. *Current Opinion in Insect Science* 13 (2016), P. 86–92

[Schneider et al. 2012]   Schneider, C. A. ; Rasband, W. S. ; Eliceiri, K. W.: NIH Image to ImageJ: 25 years of image analysis. *Nature Methods* 9 (2012), Nr. 7, P. 671–675

[Schröder et al. 2008]   Schröder, A. ; Wittkopp, N. ; Lutz, R.: From development to biodiversity—*Tribolium castaneum*, an insect model organism for short germband development. *Development Genes and Evolution* 218 (2008), Nr. 3, P. 119–126

[Scuderi and Letsou 2005]   Scuderi, A. ; Letsou, A.: Amnioserosa is required for dorsal closure in *Drosophila*. *Developmental Dynamics* 232 (2005), Nr. 3, P. 791–800

[Seed et al. 2013]   Seed, K. D. ; Lazinski, D. W. ; Calderwood, S. B. ; Camilli, A.: A bacteriophage encodes its own CRISPR/Cas adaptive response to evade host innate immunity. *Nature* 494 (2013), Nr. 7438, P. 489–491

[Shaner et al. 2005]   Shaner, N. C. ; Steinbach, P. A. ; Tsien, R. Y.: A guide to choosing fluorescent proteins. *Nature Methods* 2 (2005), Nr. 12, P. 905–909

[Sharma et al. 2013a]   Sharma, R. ; Beermann, A. ; Schroder, R.: The dynamic expression of extraembryonic marker genes in the beetle *Tribolium castaneum* reveals the complexity of serosa and amnion formation in a short germ insect. *Gene Expression Patterns* 13 (2013), Nr. 8, P. 362–371

[Sharma et al. 2013b]   Sharma, R. ; Beermann, A. ; Schröder, R.: FGF signalling controls anterior extraembryonic and embryonic fate in the beetle *Tribolium*. *Developmental Biology* 381 (2013), Nr. 1, P. 121–133

[Shen 2016]   Shen, H.: How to design homologous recombination template for CRISPR. *http://blog.benchling.com/how-to-design-homologous-recombination-template-for-crispr/* (2016). – last access: 13.10.2016

[Sheng et al. 1997]   SHENG, G. ; THOUVENOT, E. ; SCHMUCKER, D. ; WILSON, D. S. ; DESPLAN, C.: Direct regulation of *rhodopsin 1* by *Pax-6/eyeless* in *Drosophila*: evidence for a conserved function in photoreceptors. *Genes & Development* 11 (1997), Nr. 9, P. 1122–1131

[Singh et al. 2012]   SINGH, A. ; TARE, M. ; PULI, O. R. ; KANGO-SINGH, M.: A glimpse into dorso-ventral patterning of the *Drosophila* eye. *Developmental Dynamics* 241 (2012), Nr. 1, P. 69–84

[Stappert et al. 2016]   STAPPERT, D. ; FREY, N. ; LEVETZOW, C. von ; ROTH, S.: Genome-wide identification of *Tribolium* dorsoventral patterning genes. *Development* 143 (2016), Nr. 13, P. 2443–2454

[Sternberg et al. 2014]   STERNBERG, S. H. ; REDDING, S. ; JINEK, M. ; GREENE, E. C. ; DOUDNA, J. A.: DNA interrogation by the CRISPR RNA-guided endonuclease Cas9. *Nature* 507 (2014), Nr. 7490, P. 62–67

[Strobl and Stelzer 2014]   STROBL, F. ; STELZER, E. H.: Non-invasive long-term fluorescence live imaging of *Tribolium castaneum* embryos. *Development* 141 (2014), Nr. 11, P. 2331–2338

[Tao and Schulz 2007]   TAO, Y. ; SCHULZ, R. A.: Heart development in *Drosophila* . *Seminars in Cell & Developmental Biology* 18 (2007), Nr. 1, P. 3–15

[Terskikh et al. 2002]   TERSKIKH, A. V. ; FRADKOV, A. F. ; ZARAISKY, A. G. ; KAJAVA, A. V. ; ANGRES, B.: Analysis of DsRed mutants: Space around the fluorophore accelerates fluorescence development. *Journal of Biological Chemistry* 277 (2002), Nr. 10, P. 7633–7636

[Tietze 2009]   TIETZE, N.: *Studies on Efficiency and Toxicity of in vivo Delivery Systems for siRNA and plasmid DNA*. Februar 2009

[Trauner et al. 2009]   TRAUNER, J. ; SCHINKO, J. ; LORENZEN, M. D. ; SHIPPY, T. D. ; WIMMER, E. A. ; BEEMAN, R. W. ; KLINGLER, M. ; BUCHER, G. ; BROWN, S. J.: Large-scale insertional mutagenesis of a coleopteran stored grain pest, the red flour beetle *Tribolium castaneum*, identifies embryonic lethal mutations and enhancer traps. *BMC Biology* 7 (2009), P. 73

[Wada et al. 2007]   WADA, A. ; KATO, K. ; UWO, M. F. ; YONEMURA, S. ; HAYASHI, S.: Specialized extraembryonic cells connect embryonic and extraembryonic epidermis in response to Dpp during dorsal closure in *Drosophila*. *Developmental Biology* 301 (2007), Nr. 2, P. 340–349

[Wei-Ti et al. 2016]   WEI-TI, K. ; H., Hong-Yi ; H., Yi-You: Intracellular trafficking, metabolism and toxicity of current gene carriers. *Current Drug Metabolism* 10 (2016), Nr. 8, P. 885–894

[Winick et al. 1993]   WINICK, J. ; ABEL, T. ; LEONARD, M.W. ; MICHELSON, A.M. ; CHARDON-LORIAUX, I. ; HOLMGREN, R.A. ; MANIATIS, T. ; ENGEL, J.D.:   A GATA family transcription factor is expressed along the embryonic dorsoventral axis in *Drosophila melanogaster*. *Development* 119 (1993), Nr. 4, P. 1055–1065

[Witte et al. 2015]   WITTE, H. ; MORENO, E. ; RÄDELSPERGER, C. ; KIM, J. ; KIM, J. ; STREIT, A. ; SOMMER, R. J.: Gene inactivation using the CRISPR/Cas9 system in the nematode *Pristionchus pacificus*. *Development Genes and Evolution* 225 (2015), Nr. 1, P. 55–62

[Wotton et al. 2014]   WOTTON, K. R. ; JIMÉNEZ-GURI, E. ; GARCÍA MATHEU, B. ; JAEGER, J.: A staging scheme for the development of the scuttle fly *Megaselia abdita*. *PLOS ONE* 9 (2014), Nr. 1, P. e84421

[Xue et al. 2014]   XUE, Z. ; REN, M. ; WU, M. ; DAI, J. ; RONG, Y. S. ; GAO, G.: Efficient gene knock-out and knock-in with transgenic Cas9 in *Drosophila*. *G3-Genes Genomes Genetics* 4 (2014), Nr. 5, P. 925–929

[Yanushevich et al. 2002]   YANUSHEVICH, Y. G. ; STAROVEROV, D. B. ; SAVITSKY, A. P. ; FRADKOV, A. F. ; GURSKAYA, N. G. ; BULINA, M. E. ; LUKYANOV, K. A. ; LUKYANOV, S. A.: A strategy for the generation of non-aggregating mutants of Anthozoa fluorescent proteins. *FEBS Letters* 511 (2002), Nr. 1-3, P. 11–14

[Yonemura et al. 2013]   YONEMURA, N. ; TAMURA, T. ; UCHINO, K. ; KOBAYASHI, I. ; TATEMATSU, K. ; IIZUKA, T. ; TSUBOTA, T. ; SEZUTSU, H. ; MUTHULAKSHMI, M. ; NAGARAJU, J. ; KUSAKABE, T.: phiC31-integrase-mediated, site-specific integration of transgenes in the silkworm, *Bombyx mori* (Lepidoptera: Bombycidae). *Applied Entomology and Zoology* 48 (2013), Nr. 3, P. 265–273

[van der Zee et al. 2005]   ZEE, M. van der ; BERNS, N. ; ROTH, S.: Distinct functions of the *Tribolium zerknüllt* genes in serosa specification and dorsal closure. *Current Biology* 15 (2005), Nr. 7, P. 624–636

[van der Zee et al. 2006]   ZEE, M. van der ; STOCKHAMMER, O. ; VON LEVETSOW, C. ; NUNES DA FONSECA, R. ; ROTH, S.: *Sog/chordin* is required for ventral-to-dorsal Dpp/BMP transport and head formation in a short germ insect. *Proc. Natl. Acad. Sci. U.S.A.* 103 (2006), Nr. 44, P. 16307–16312

[Zhou et al. 2014]   ZHOU, J. ; WANG, J. ; SHEN, B. ; CHEN, L. ; SU, Y. ; YANG, J. ; ZHANG, W. ; TIAN, X. ; HUANG, X.: Dual sgRNAs facilitate CRISPR/Cas9-mediated mouse genome targeting. *FEBS Journal* 281 (2014), Nr. 7, P. 1717–1725

Chapter 6

Supplements

6.1 ImageJ plugin to process data generated by multiple-labeling imaging

The ImageJ plugin 'DVfiles2MIP.ijm', used for processing DeltaVision^{TM} multiple-color imaging files (see 2.7), is included on the DVD.

6.2 EGFP expression in the legs of embryos of the G04609 line is lost after *Tc-pnr* fragment 2 parental RNAi

Although pRNAi with dsRNA from the *Tc-pnr* fragment 2 did not show any other phenotype than pRNAi with the original *Tc-pnr* dsRNA, it has been observed that EGFP expression in the legs of a *Tc-pnr* fragment 2 knock down embryo of the G04609 line is lost (Figure 6.1). This is in difference to the knock down induced with the original *Tc-pnr* dsRNA, where it has been not observed that this expression is lost. However and due to experimental limitations, this has been observed only in a single embryo. Therefore, this finding needs further confirmation.
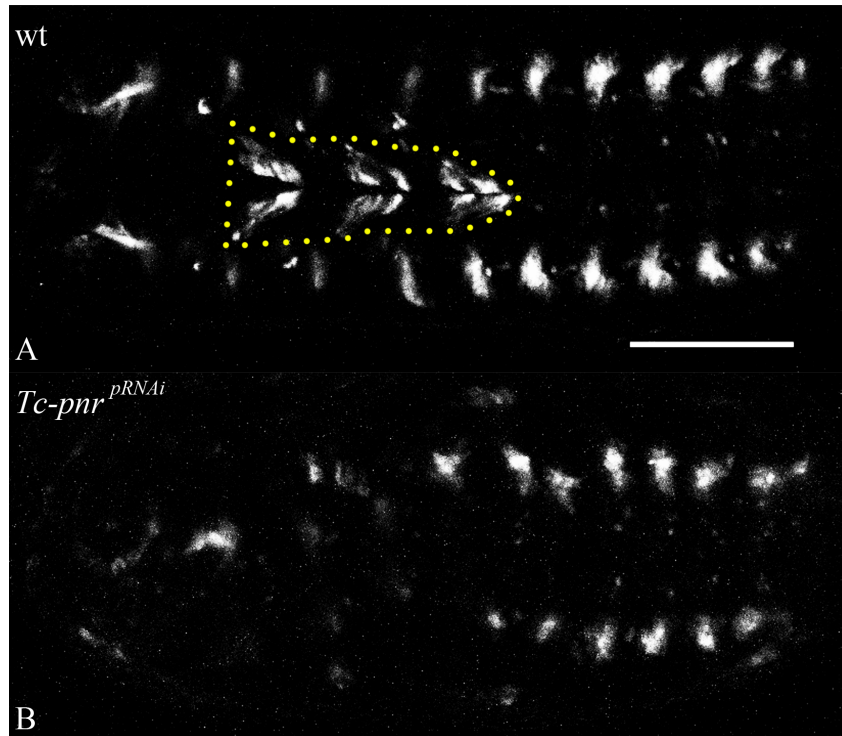
Figure 6.1: **Loss of EGFP expression in the legs of the G04609 line after *Tc-pnr* fragment 2 pRNAi**. (**A**) Wild type embryo of the G04609 line, in which EGFP is expressed in the tip of all three legs (encompassed by dashed yellow line; for a description of other expression domains, see Figure 3.25). (**B**) In the knock down, EGFP expression is absent in the legs, whereas its expression persists in all other domains (note that the anterior part of the embryo is slightly turned, so that not all expression domains in this area are at the same location or in view, compared to the wild type). Both embryos are ventral views. Scale bar is 100 μm.

6.3 *Tc-dpp* is expressed in the dorsal most ectoderm
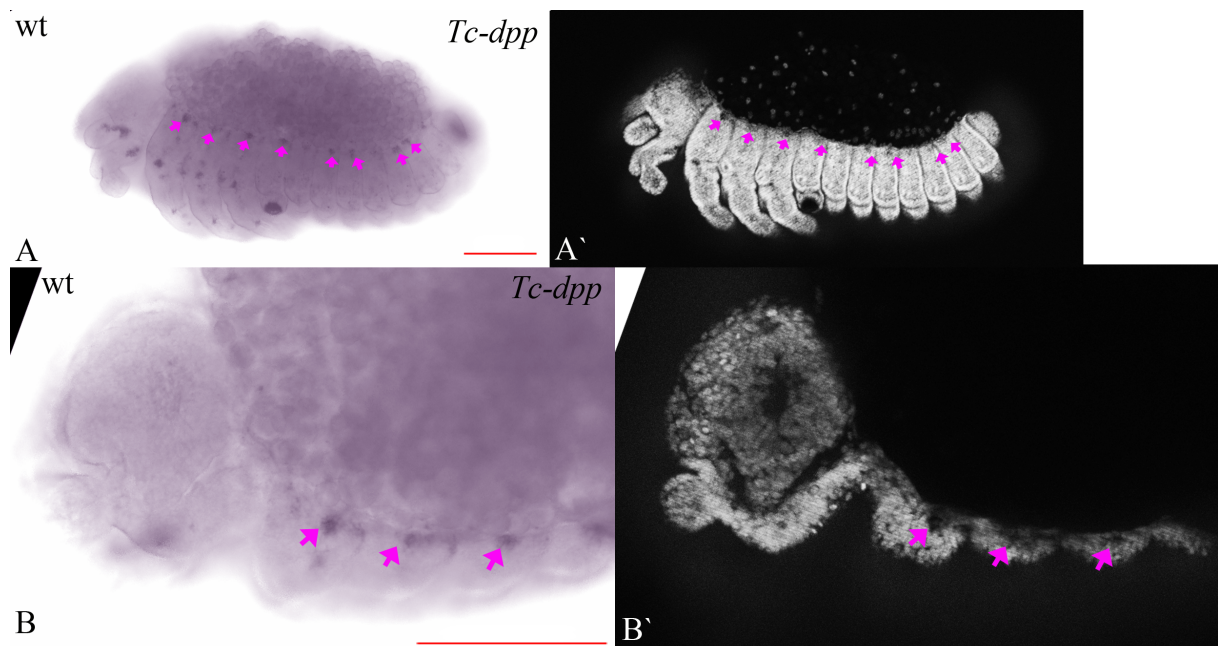
Figure 6.2A shows *Tc-dpp* expression in an embryo prior to the onset of dorsal closure. Figure 6.2B is an high magnification single section of the projection in Figure 6.2A, focusing on the dorsal most ectoderm. In both embryos, the purple arrows mark some of the point-like *Tc-dpp* expression in ectodermal cells.

Figure 6.2: ***Tc-dpp* expression in the dorsal most ectoderm**. (**A, B**) Wild type embryo stained for *Tc-dpp* via *in situ* hybridization. (**A`, B`**) Respective DAPI counterstain. **B** is a single section of the embryo in **A**, focusing on the dorsal most ectoderm, with a higher magnification. Purple arrows point to some of the *Tc-dpp* expression in cells of the dorsal most ectoderm. Both embryos are lateral views. Scale bars are 100 μm.

6.4 *Tc-pnr* parental RNAi impairs normal bristle pattern

In *Drosophila* it is known that loss of *Tc-pnr* expression effects the pattern of the sensory bristles in adult flies [Heitzler et al., 1996]. To check if the bristel pattern of *Tribolium* embryos/larvae are affected as well, cuticle preparations (see 2.3) have been performed.

Dorsal to the tracheal openings in a wild type larvae, three macrochaetes are located on the A1-A8 segments. Two are forming a pair just adjacent to a tracheal opening, while the third one is located separately more dorsally. This third machrochaete is absent in *Tc-pnr* knock down embryos (the *Tc-pnr* knock down embryos do not hatch, due to the failure in dorsal closure; still, a cuticle with a distinct bristle pattern is secreted everywhere but in the dorsal hole; data not shown). Additionally, the most dorsally located microchaetes seem to be missing as well (data not shown). These findings are based on dark field microscopy only. Even though these results need further validation, they are in accordance with the assumption that *Tc-pnr* may be important for establishing dorsal fates, acting as a DV selector gene.

6.5 Expression pattern of *Tc-iro* throughout *Tribolium* development

The homeodomain transcription factor *Tc-iro* [Kerner et al., 2009] is expressed in the presumptive anterior amniotic fold during the onset of differentiation of the blastoderm [Sharma et al., 2013a]. This expression made it an interesting target for a deeper investigation, in respect to be a potential candidate gene involved in amnion formation (see also 3.2.5).

The expression pattern of *Tc-iro* during embryogenesis is already published to a certain degree [Nunes da Fonseca et al., 2008, 2010; Sharma et al., 2013b] and especially its early expression from early nuclear divisions until the progression of the posterior fold was investigated in great detail [Sharma et al., 2013a]. Therefore, recapitulation of the expression pattern of *Tc-iro* will be done in a condensed fashion.

Figure 6.3 shows the expression of *Tc-iro* from the late undifferentiated blastoderm on until the beginning of the serosal window stage and Figure 6.4 shows its expression in an extending embryo until full germ band retraction.

wt   *Tc-iro*

A   A`

wt   *Tc-iro*

B   B`

wt   *Tc-iro*

C   C`

wt   *Tc-iro*

D   D`

wt   *Tc-iro*

E   E`

wt   *Tc-iro*
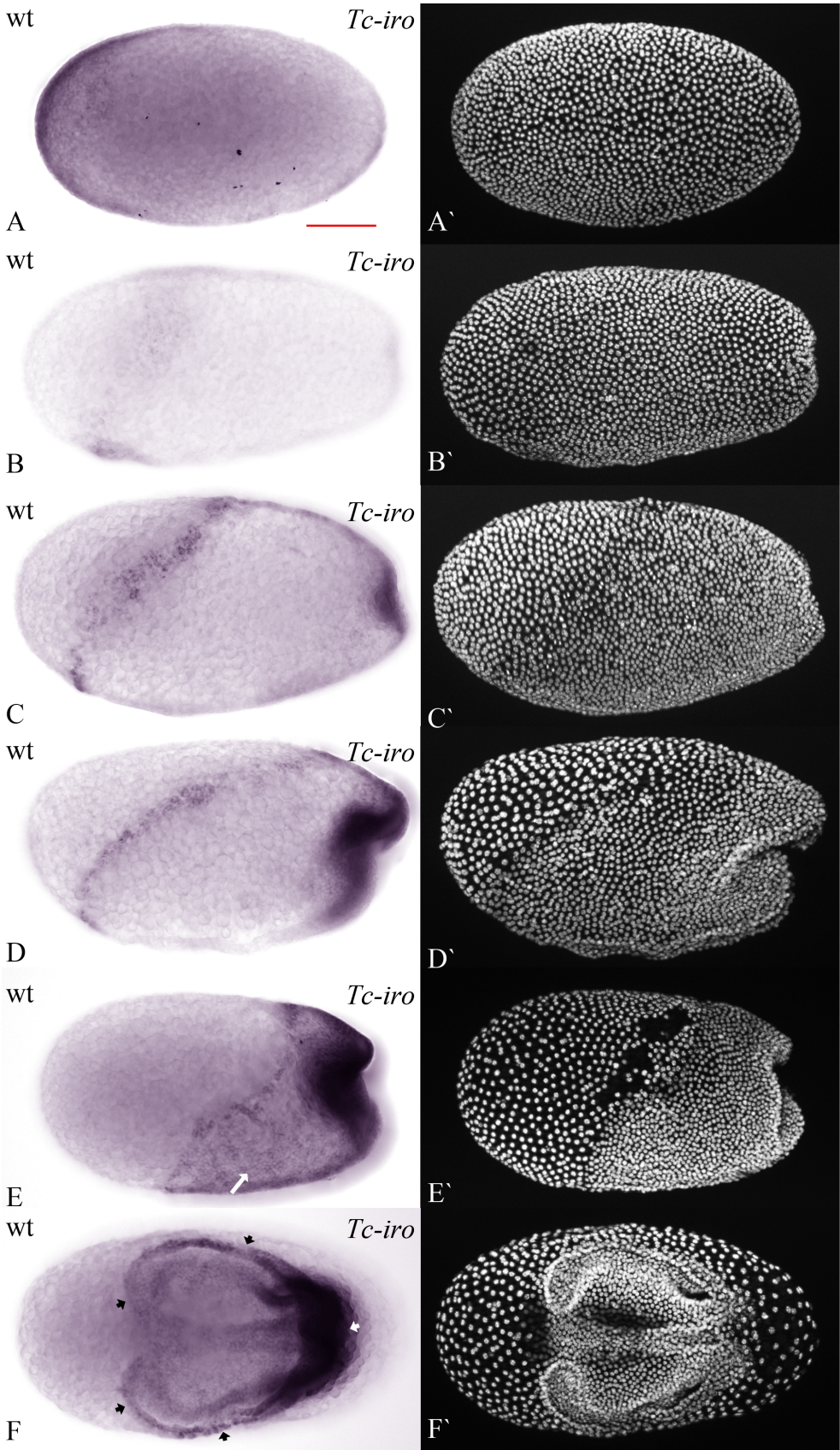
F   F`

Figure 6.3: ***Tc-iro* expression in different domains during early embryogenesis**. (**A-F**) Embryos stained for *Tc-iro* via *in situ* hybridization. (**A`-F`**) Respective DAPI counterstain. (**A**) During the late undifferentiated blastoderm stage, *Tc-iro* is expressed in an anterior domain. (**B**) When the primitive pit is forming, this expression shifts towards the posterior, forming a ring like and tilted domain. (**C**) At the onset of blastoderm differentiation, the ring like *Tc-iro* expression domain refines into a small stripe of expression along the presumptive anterior amniotic fold and *Tc-iro* expression in the dorsal amnion and around the primitive pit arises. (**D**) These expression domains persist when the posterior fold progresses. (**E**) Around that time, *Tc-iro* expression arises in embryonic tissue, which is not yet covered by the serosa (this expression is marked by the white arrow). (**F**) When the serosal window has formed, *Tc-iro* is expressed in its margins (black arrows), in different and distinct domains within the embryo and in the amnion covering the segment addition zone (white arrow). The angle of **A** is unknown, **B-E** are lateral views and **F** is a ventral view. Scale bar is 100 μm.

During late undifferentiated blastoderm stages, *Tc-iro* is expressed in an anterior domain (Figure 6.3A and A`), which will give rise to the serosa later on [Sharma et al., 2013a]. This expression domain is shifted towards the posterior shortly before the onset of blastoderm differentiation (Figure 6.3B and B`) and refines to a small stripe of expression in the presumptive anterior amniotic fold (Figure 6.3C and C`). It is then that *Tc-iro* expression arises in and around the primitive pit and in the dorsal amnion (Figure 6.3C and C`). When involution of the embryo has started and the posterior fold has progressed, these expression domains persist (Figure 6.3D-E and D`-E`). Expression in the posterior fold becomes very intense at this developmental time and in difference to reports in other publications [Nunes da Fonseca et al., 2008, 2010; Sharma et al., 2013b], *Tc-iro* is not only expressed in the dorsal ectoderm but in the whole embryonic tissue 'in between' its expression in the posterior fold and in the anterior amniotic fold (Figure 6.3E and E`; the white arrow in Figure 6.3E marks this expression). When the serosal window has formed, *Tc-iro* is expressed in its margins, in distinct domains in the embryo and in the amnion covering the segment addition zone.

During extension of the germ band, *Tc-iro* is expressed in segmentally repeated stripes in the embryo and it is expressed in the head (Figure 6.4A-C and A`-C`) and in the amnion (black arrows in Figure 6.4B). When the embryo has fully extended its germ band, an additional expression domain in two broad lateral domains arises, which persists until full germ band retraction (see black arrowheads in Figure 6.4C-E). At the time of full germ band extension, the segmentally repeated expression is not forming a continuous
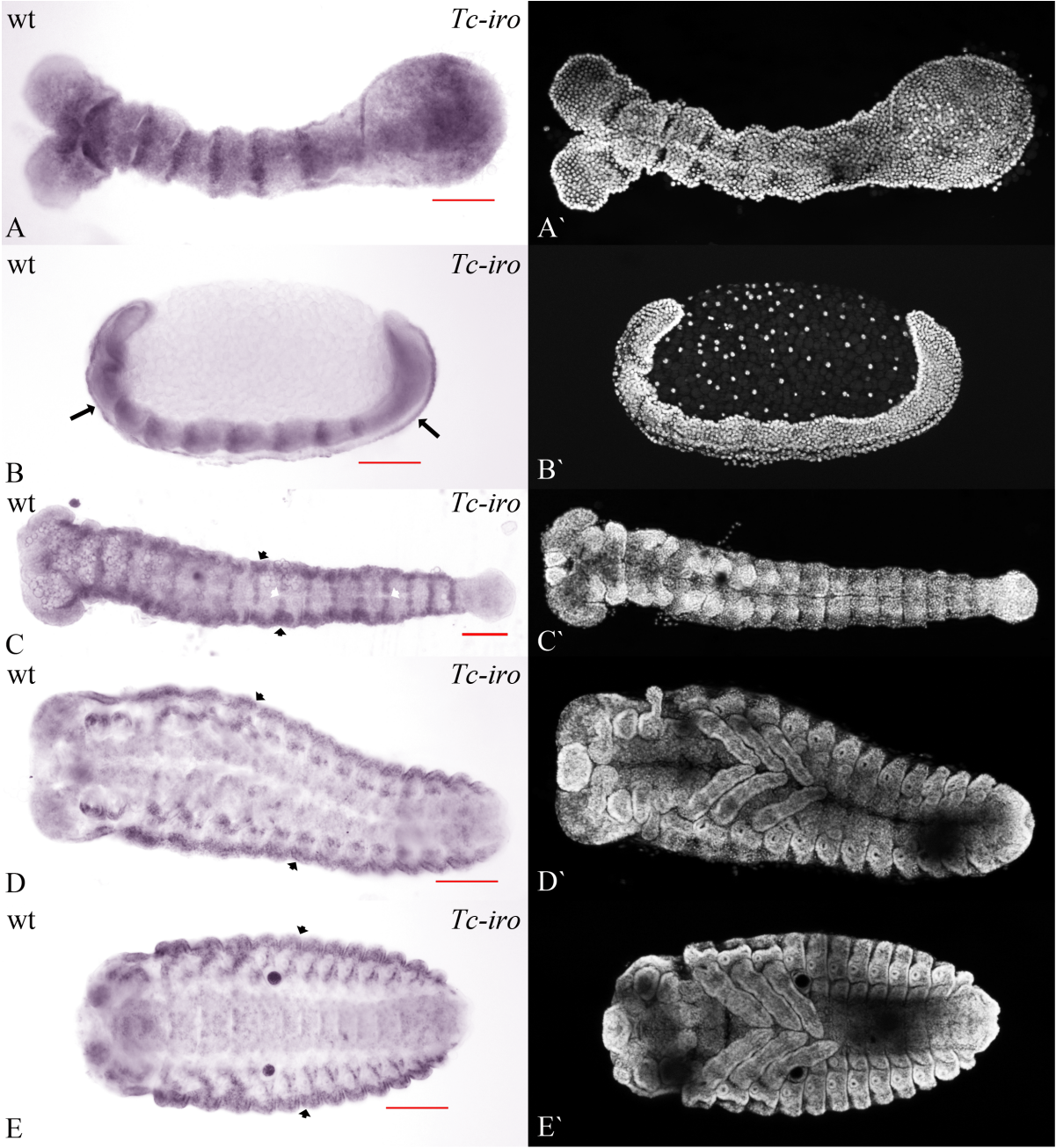
Figure 6.4: ***Tc-iro* expression throughout extension and retraction of the germ band**. (**A-E**) Embryos stained for *Tc-iro* via *in situ* hybridization. (**A`-E`**) Respective DAPI counterstain. (**A**) During extension of the germ band, *Tc-iro* is expressed in segmentally repeated stripes within the embryo, in the head and in the segment addition zone. (**B**) Additionally, *Tc-iro* is expressed in the whole amnion (black arrows). (**C**) When the embryo has fully extended, *Tc-iro* expression arises in two broad lateral domains (black arrowheads), while gaps of expression within some of the segmentally repeated stripes appear (white arrows point to two of these gaps). (**D**). During germ band retraction, *Tc-iro* expression arises in small segmentally repeated expression domains ventral to the two broad lateral expression domains. Distinct *Tc-iro* expression in different head structures arises as well. All of these expression domains persist in the fully retracted germ band embryo in **E**. **A** and **C-E** are ventral views of flat mounted embryos and **B** is a lateral view. Scale bars are 100 μm.

stripe anymore but gaps become visible in the middle of most of the stripes (Figure 6.4C and C`; the white arrowheads in Figure 6.4 point to two of these gaps). At least until the embryo has fully retracted, distinct and segmentally repeated expression domains more ventral to the initial two broad lateral expression domains persist, as well as expression in several distinct head domains (Figure 6.4C-E and D`-E`).

6.6 Bioinformatic analysis and gene expression of the genes of the Iroquois complex in *Oncopeltus fasciatus*

In the course of annotating the newly assembled genome of the milkweed bug *Oncopeltus fasciatus* (Hemiptera) (see `https://i5k.nal.usda.gov/Oncopeltus_fasciatus`), which is one of the species within the i5K project for sequencing 5000 arthropod genomes [i5K Consortium, 2013], its genome was searched in order to identify the coding sequences of the three genes *Oncopeltus fasciatus iro* (*Of-iro*), *Of-mirr* and *Of-pnr*.

The transcription factor *araucan* (*ara*), *caupolican* (*caup*) and *mirr* belong to the TALE superclass of homeodomain proteins [Burglin, 1997] and form the Iroquois complex (Iro-C) in *Drosophila* [Gomez-Skarmeta et al., 1996; Gomez-Skarmeta and Modolell, 2002], what is a unique property of the Drosophilids in general [Irimia et al., 2008]. It is already known that in this lineage *ara* and *caup* arose due to a tandem duplication of the gene *iro* [Cavodeassi et al., 2001], which together with *mirr* forms the Iro-C cluster, ancestral to crustaceans and insects. In vertebrates, one can find two to four of the Irx (vertebrate

equivalent of Iro) clusters, with up to three genes per cluster. More basal branching metazoans like cnidarians or the placozoans but also nematodes, which are much closer to insects, have only a single Irx gene [Kerner et al., 2009]. These examples show the high degree of conservation of the Iro/Irx cluster throughout the animal kingdom. Therefore, identification of the cluster in *Oncopeltus* may be as well used to assay the quality of its assembled genome.

The search for *Of-iro* and *Of-mirr* in *Oncopeltus* revealed its conserved synteny. Like in *Drosophila* and *Tribolium* (data not shown), *Of-iro* is transcriptionally upstream of *Of-mirr* and on the same scaffold (scaffold 82) in the genome assembly. Phylogenetic analyses of the Iro-C protein sequences from representative species within the insects (Figure 6.5), confirmed the expected branching of *Of*-Iro with other Iro proteins from different species (Figure 6.6). The same is true for *Of*-Mirr. By expansion of the analysis towards other predicted gene models of hemipteran species within the i5K project, namely the bed bug *Cimex lectularius* and the brown marmorated stink bug *Halyomorpha halys*, *iro* and *mirr* were identified on the scaffolds 47 and scaffold 1096 with conserved synteny, respectively.

This synteny can in most bilaterians but not in vertebrates, extended to the ankyrin

Figure 6.5: **Cladogram with the species used for the analyses of the Iro-C cluster**. All species, except the nematode *Trichinella spiralis*, which served as an outgroup (Irx cluster outgroup), are insect species. *Oncopeltus fasciatus* belongs to the basally branching Hemiptera, whereas the other species encompass the four major insect clades, namely Hymenoptera, Coleoptera, Lepidoptera and Diptera (from top to bottom; see also [Savard et al., 2006]).
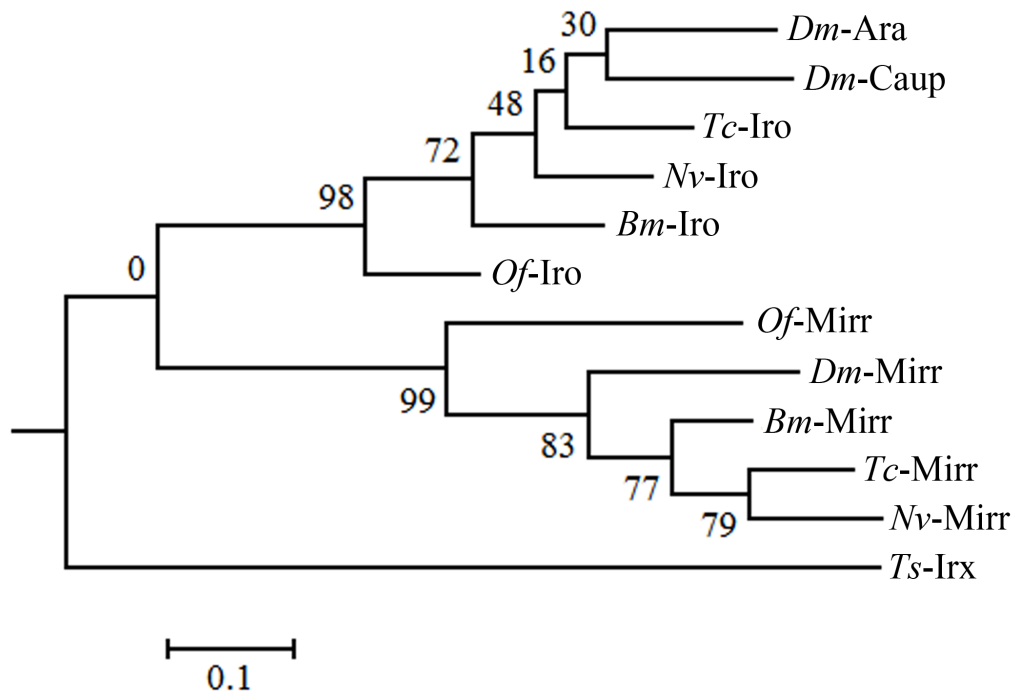
Figure 6.6: **Phylogenetic analysis of the Iro-C cluster in *Oncopeltus*.** *Of*-Iro and *Iro*-Mirr group together with the respective proteins of the other insect species, strengthening the assumption that the curated gene models in the *Oncopeltus* genome assembly actually present the respective gene. *Ts*-Irx served as an outgroup. Species abbreviations are according to Figure 6.5. Note that the support values on the Iro branch starting with *Nv-iro*, are very low (under 50) and that the support value separating the Iro and the Mirr branch is 0, which is probably due to the comparison with the outgroup. The scale bar represents the evolutionary change over time (counted in nucleotide substitutions per site that is the number of changes or substitutions divided by the length of the sequence (the number of changes per 100 nucleotide sites)).

repeat-containing gene *sosondowah* (*sowah*), which is known to be associated with the Iro-C [Irimia et al., 2008; Maeso et al., 2012]. In all investigated insect, *sowah* is located 5`to the Iro-C and has an opposite reading direction [Kerner et al., 2009].

In the *Oncopeltus* genome assembly, *Of-sowah* was found on scaffold 1078, so it is unclear if the synteny is conserved. However, an indirect hint provided the gene *Of ceramide transfer protein* (*Of-cerf*), which was found in the same reading direction on scaffold 1078. In *Drosophila*, *Dm-cert* is located on chromosome 3L, together with *Dm-sowah* and all three genes of the *Drosophila* Iro-C. That both *Of-sowah* and *Of-cert* were found to have the same reading direction and the same transcriptional orientation in *Oncopeltus*, compared to *Drosophila*, might indicate conserved synteny for *Of-sowah* as well.
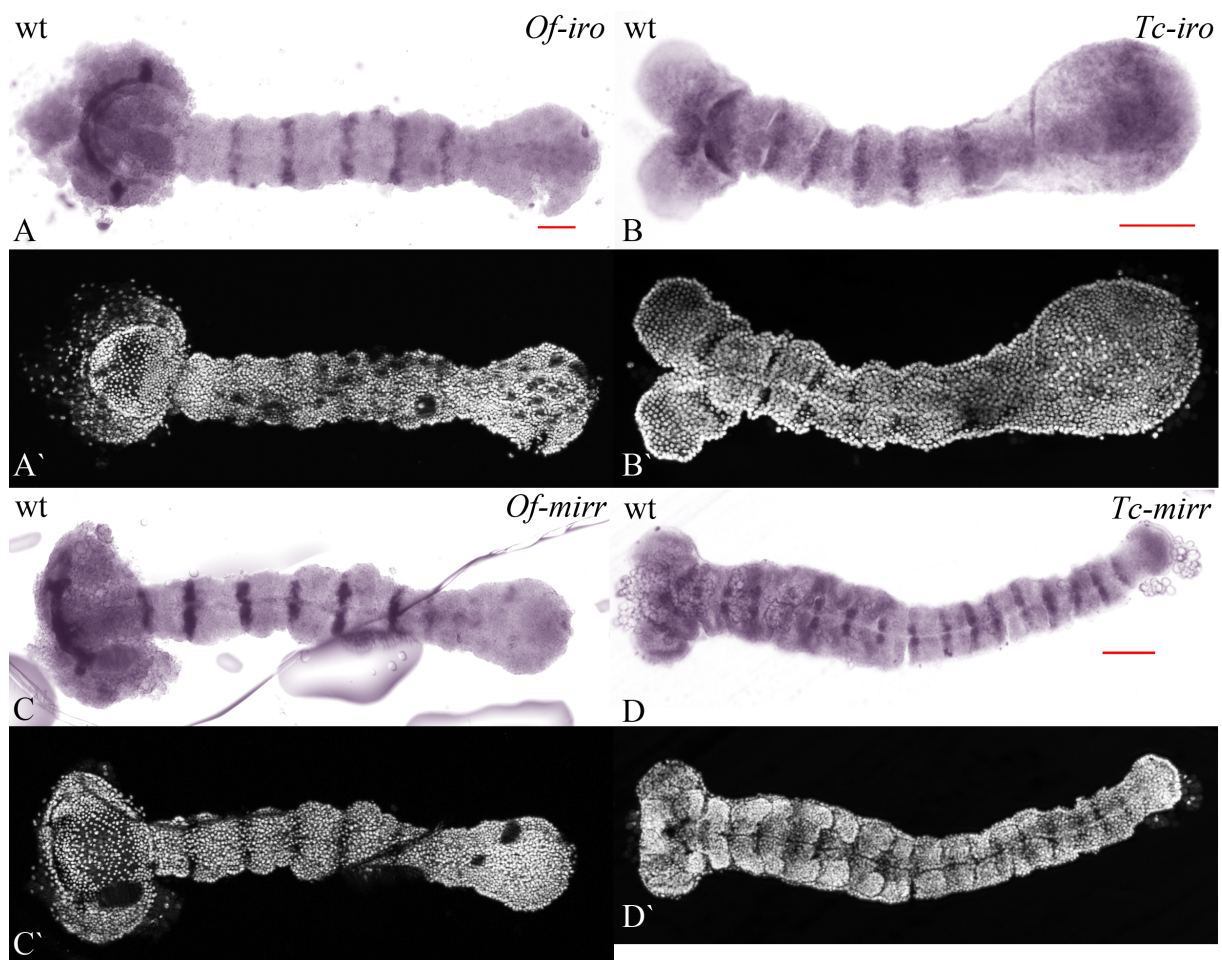
Initial experiments, investigating the gene expression pattern of *Of-iro* and *Of-mirr* via *in situ* hybridization, showed a similar gene expression pattern during extension of

Figure 6.7: **Expression pattern of *iro* and *mirr* in *Oncopeltus* and *Tribolium* during germband extension**. (**A-D**) Embryos stained for *iro* (**A** and **B**) and *mirr* (**C** and **D**) via *in situ* hybridization. (**A`-D`**) Respective DAPI counterstain. *Of-iro* (**A**) and *Of-mirr* (**C**) are similarly expressed in the head and in segmentally repeated stripes. This expression pattern is similarly found in *Tribolium* (**B** and **D**, respectively), whereat *Tc-iro* is also expressed in the segment addition zone. All embryos are ventral views. Scale bars are 100 μm.

the germband in relation to their respective homologs in *Tribolium* (Figure 6.7).

These analyses show that both *Of-iro* and *Of-mirr* were found in the assembled genome and based on the reported high degree of conservation of the Iro-C and its associated genes, they strengthen the quality of the *Oncopeltus* genome assembly in general.

When searching for the *Of-pnr* sequence, only its two zinc finger DNA binding domains were potentially identified on scaffold 2229. A manually curated gene model using the two domains as the starting point, was used to design a set of primers for making a probe for *in situ* hybridization. Unfortunately, the product size of this probe was only 464 bp long and did not result in any specific staining in an initially performed experiment. This is most likely due to the incomplete gene model, which does not provide enough sequence information for the design of a distinct *Of-pnr* primer pair to be used for *in situ* hybridization.

6.6.1 Material & Methods: Iro/Irx protein sequences and phylogenetic analyses

Iro-C and Irx protein sequences were retrieved using TBLASTN and BLASTP algorithms on the corresponding databases/genome browsers listed in Table 6.1. The sequences of the three Iro-C genes in *Drosophila melanogaster* was used as the query for all other species. Predicted gene models within the *Oncopeltus fasciatus* genome assembly were manually curated (see `https://i5k.nal.usda.gov/content/rules-web-apollo-annotation-i5k\` `-pilot-project` and `https://i5k.nal.usda.gov/manual-curation-example`) to obtain the full sequence.

The phylogeny shown in Figure 6.5 was first obtained via NCBI's taxonomy browser (see `https://www.ncbi.nlm.nih.gov/Taxonomy/CommonTree/wwwcmt.cgi`), refined with findings from Savard et al. 2006 and rebuilt and edited with the free software INKSCAPE (version 0.91). The protein phylogeny Figure 6.6 was build with the free software MEGA

Table 6.1: Protein sequences used for phylogenetic analyses

Species	database	Ara/Caup ID	Iro ID	Mirr ID
Bombyx mori	NCBI	-	XP_004929820.1	XP_004929953.1
Drosophila melanogaster	NCBI	AAF49896.1/AAF49895.1	-	AGB94471.1
Nasonia vitripennis	NCBI	-	XP_008216675.1	XP_001604937.1
Oncopeltus fasciatus	i5K	-	iroquois	mirror
Tribolium castaneum	Beetle Base	-	TC003632	TC003634
Trichinella spiralis	NCBI	-	XP_003372666.1	-

6 (Build#6140226), using ClustalW for the alignment and Maximum Likelihood for phylogenetic tree construction. For the analyses preferences the default settings were used, except the number of bootstrap replications, which was set to 1.000.

6.6.2 Material & Methods: *Oncopeltus fasciatus* husbandry, egg collection and egg fixation

The bugs were kept in large boxes at 25 °C and supplied with de-hulled sunflower seeds and water. Detailed husbandry conditions are described in Liu and Kaufman 2009.

The females laid their eggs in pre-supplied cotton wool (100% viscose), from where the eggs could be collected into 1.5 ml tubes filled with distilled water prior to fixation. Subsequently, the eggs were boiled for 3 min in water and immediately transferred onto ice for 5 min. The distilled water was removed and each 600 μl heptane and fix solution (FIX-S; 4% formaldehyde in 1 x PBS) was added for pre-fixation. After shaking for 5 min, the lower FIX-S phase was removed and 1 ml methanol was added. This washing with methanol was performed several times, thereby cracking the chorion and the vitelline membrane, which are tightly connected in *Oncopeltus*. Subsequently, residual methanol was removed and the eggs were fixed for 1 h in 1 ml FIX-S. Fixed eggs were stored in methanol at -20 °C.

6.6.3 Material & Methods: Protocol for *in situ* hybridization in *Oncopeltus fasciatus*

Embryos were collected and fixed as described in 6.6.2 and the subsequently performed *in situ* hybridization (probes were synthesized according to 2.4.1, using the primers listed in Table 6.2; note that the listed primer pair for *Ofas-pnr* did not result in a specific stain but is listed for the sake of completeness) was mainly following the protocol described in Liu and Kaufman 2004. A different antibody blocking solution was used (2% blocking reagent (Invitrogen), 1% BSA and 10% NGS in PBT (with 1% Tween®20), the NBT/BCIP stock solution (Roche) was diluted in fresh prepared AP-buffer (0.1 M Tris-HCl, 50 mM MgCl$_2$, 100 mM NaCl, pH 9.5) and levamisole hydrochloride (Cat#31742, Sigma) was added to the AP-buffer (final concentration is 1mM) to reduce the background. Coloration was developed at RT in the dark for up to two days.

Table 6.2: Gene specific primers used for *in situ* hybridization performed in *Oncopeltus*

common name	fwd sequence (5' → 3')	rev sequence (5' → 3')
Ofas-iro	CAGGCGACACTAGACACCAA	ACACAACCATGAACGAACGA
Ofas-mirr	GAAGAATGCCACAAGGGAAA	GTCGTATTTCGGCTGGATGT
Ofas-pnr	GGACTACCAGGCTCACCAGA	TCGTCTGGATACCGTCCTTC

6.7 List of movies included on the DVD

The in Table 6.3 listed movies are included on the DVD.

Table 6.3: Movies included on the DVD

ID	Reference	Comment
Movie 1	3.1.3	WT embryo of the #W13 rHC079 line
Movie 2A	3.1.4	Separate visualization of DsRed2 (amnion) and EGFP (serosa) channel
Movie 2B	3.1.4	Merge of DsRed2 and EGFP channel
Movie 3A	3.2.3	Development of a WT embryo (nGFP)
Movie 3B	3.2.3	Development of a *Tc-pnr* knock down embryo (nGFP)
Movie 4A	3.2.5	WT embryo (nGFP)
Movie 4B	3.2.5	Mildly affected *Tc-iro* knock down embryo (nGFP)
Movie 4C	3.2.5	Severely affected *Tc-iro* knock down embryo (nGFP)
Movie 5A	3.2.6	*Tc-pnr* knock down embryo; slow amnion withdrawal
Movie 5B	3.2.6	*Tc-pnr* knock down embryo; holes in the amnion
Movie 5C	3.2.6	*Tc-pnr* knock down embryo; ectopic amniotic rupture
Movie 5D	3.2.6	*Tc-pnr* knock down embryo; two sites of rupture
Movie 5E	3.2.6	*Tc-pnr* knock down embryo; disturbed organization of the amnion
Movie 6A	3.2.6	WT embryo of the G04910 line
Movie 6B	3.2.6	WT embryo of the G04923 line
Movie 7	3.2.8	*Tc-pnr* knock down embryo exhibiting ectopic amniotic rupture
Movie 8A	3.2.9	WT embryo of the G04609 line
Movie 8B	3.2.9	Mildly affected *Tc-pnr* knock down embryo (G04609 line)
Movie 8C	3.2.9	Severely affected *Tc-pnr* knock down embryo (G04609 line)
Movie 9	3.2.10	*Tc-pnr* knock down embryo used for the tracking of cardioblasts

Zusammenfassung

Die Embryogenese des Käfers *Tribolium castaneum* ist auf die gestaltgebenden Bewegungen der beiden extraembryonalen Membranen, Amnion und Serosa, angewießen. Durch deren Funktion und einer aufeinander abgestimmten Entwicklung, ist es dem Embryo möglich zu überleben und als voll ausgebildeter Organismus aus dem Ei zu schlüpfen. Bemerkenswerterweiße tragen die beiden Membranen letztendlich nicht zur Bildung des Embryo selbst bei. Für die Ausbildung der Membranen müssen diese erst expandieren, mit sich selbst fusionieren und abschließend voneinander trennen. Danach umgibt das Amnion den Embryo ventral und lateral, wodurch der Amnion-Hohlraum geformt wird. Das Serosa hingegen umschließt sowohl das Amnion, als auch den Embryo und den Eidotter. Somit schützt es den Embryo vor dem Austrocknen und trägt zu seiner Immunabwehr bei. Im Laufe der späteren Embryogenese ermöglichen die Membranen dem Embryo seinen Rücken zu schließen, indem sie sich koordiniert zurückziehen und degenerieren. Während sich das Serosa zurückzieht und bevor sich der Rücken schließen kann, wird der Eidotter kurzfristig vom Amnion bedeckt. In Embryos die kein Serosa besitzen, kompensiert das Amnion dessen Verlust, indem es die Funktion des Serosa übernimmt und den Eidotter bereits von Beginn an bedeckt. Dadurch kann sich der Embryo normal entwickeln und überleben.

Um nun mehr über das Amnion zu erfahren, wurde der Transkriptionsfaktor *Tc pannier* (*Tc-pnr*) untersucht, welcher zur Zeit der Differenzierung des Blastoderm im Amnion exprimiert ist. Mittels in-situ-Hybridisierung wurde das Expressionsmuster von *Tc-pnr* komplettiert und durch gezieltes Ausschalten der Genexpression mittels parentaler RNA Interferenz, Rückschlüsse auf seine Funktion gezogen. Embryos die kein *Tc-pnr* mehr exprimieren, weißen ein Loch in der dorsalen Kutikula auf und biegen sich zur dorsalen Seite hin. Dieser spezifische Phänotyp resultiert aus einem Defekt beim Schließen des embryonalen Rückens. Zur dieser Zeit ist *Tc-pnr* normalerweiße im dorsalen Ektoderm

und im Kopf des Embryos exprimiert. In der Fliege *Drosophila melanogaster* entsteht das dorsale Loch dadurch, dass die Expression von *Tc decapentaplegic* (*Tc-dpp*) im dorsalen Ektoderm gehemmt wird. Darauf aufbauend konnte in *Tribolium* gezeigt werden, dass *Tc-pnr* und *Tc-dpp* in überlappenden Bereichen im dorsalen Ektoderm exprimiert sind und *Tc-dpp* dort von *Tc-pnr* reguliert wird. Das deutet darauf hin, dass *Tc-pnr* am Schließen des embryonalen Rückens beteiligt ist und dies in *Tribolium* und *Drosophila* konserviert ist. Auch die Funktion von *Tc-pnr* während der Entwicklung des Herzens scheint in beiden Spezies konserviert zu sein. Hier führt der Verlust der *Tc-pnr* Expression in der kardialen Herzreihe dazu, dass sich diese nicht formieren kann und zur Inhibition des Gens *Tc midline*. Ist die späte Expression von *Tc-pnr* im Amnion inhibiert, treten eine Vielzahl von Defekten im Amnion auf. Besonders interessant dabei ist, dass das Amnion ektopisch reißt und sich offenbar nicht mehr zusammen mit dem Serosa zurückzieht, wenn der Embryo versucht seinen Rücken zu schließen. Das ist im Widerspruch zu einem vor Kurzem veröffentlichten Bericht in dem beschrieben wird, dass beide Membranen zu dieser Zeit miteinander verbunden sind. Deswegen wird vermutet, dass *Tc-pnr* für diese Adhäsion verantwortlich ist und das Serosa und Amnion nach der Inhibition von *Tc-pnr* nicht mehr verbunden sind. Damit dieser Defekt im Detail untersucht werden kann, wurde eine transgene *Tribolium* Linie derart verändert, dass sie nicht mehr EGFP im Amnion exprimiert, sondern DsRed2. Dazu wurde das CRISPR/Cas9 System in Verbindung mit dem Homologie gelenkten Reparaturmechanismus benutzt. Die neue Linie exprimiert nun DsRed2 im Amnion und kann mit einer weiteren transgenen Linie gekreuzt werden, die EGFP im Serosa exprimiert, wodurch der Nachwuchs beide Fluorophore exprimiert. Somit können beide Membranen im selben Embryo getrennt voneinander visualisiert werden und die Analyse der gefundenen Defekte im Amnion in Relation zum Serosa abgeschlossen werden.

Zusammengefasst deuten die Resultate darauf hin, dass *Tc-pnr* auf vielfältige Art und Weiße die Entwicklung der embryonalen und extraembryonalen Membranen zur der Zeit beeinflusst, wenn der Embryo versucht seinen Rücken zu schliessen. Da dieser Prozess in *Tribolium* ein Dreikomponentensystem ist (Amnion, Serosa und Embryo), wird die getrennte Betrachtung der regulatorischen Effekte von *Tc-pnr* dazu beitragen, die Interaktionen der zwei extraembryonalen Membranen untereinander und gegenüber dem Embryo, besser zu verstehen.

Danksagung

First, I wish to thank my supervisor Dr. Kristen A. Panfilio for the opportunity to work in her lab, with my now two favorite insect species, *Tribolium castaneum* and *Oncopeltus fasciatus*. Thanks for your availability around the clock, for the discussions and for answering all the not really short questions.

Danke ebenso an Herrn Prof. Dr. Siegfried Roth, der von Anfang an bereit war mich zu unterstützen, sei es durch interessante Fragen und Anregungen in den zahlreichen Seminaren oder durch die Begleitung meiner Doktorarbeit als Mitglied des Prüfungskomitees.

In this regard, special thanks to Dr. Juliette de Meaux, who accepted to be the chair of my disputation on short notice.

Vielen vielen Dank auch an Herrn Dr. Thorsten Horn, ohne den meine Doktorarbeit nicht in dieser Form vorliegen könnte, geschweige denn würde! Danke das Du immer Zeit hattest und alles mitgemacht hast, vom dritten, bis in den zweiten Stock! Danke, Meister!

Vielen Dank auch an Herrn Stefan Koelzer, der immer wusste wo ich alles finde und dafür das Du auch schon vor dem Feierabend Käse erzählt hast!

Dank auch an Herrn Oliver Karst von der AG Roth, der Mann der alles organisieren konnte, inklusive dem leckersten Honig!

Ein besonderes Dankeschön auch an Herrn Dr. Waldemar Wojciech, der den Beisitz in meiner Disputation übernommen hat und sich die Zeit genommen hat, die Dissertation aufwendig zu korrigieren.

Special thanks also to Dr. Anna Gilles and Prof. Dr. Toshiki Tamura, who provided me with the initial plasmids for the transgenesis project.

Thanks also to Dr. Maarten Hilbrant and Dr. Iris Vargas Jentzsch from the AG Panfilio, as well as Dr. Yen-Ta Chen, Dr. Matthias Pechmann, Nadine Frey and Dr. Matt Benton from the AG Roth for helping me during the time of my Ph.D.

I also wish to thank those people, who taught me that one should separate work and

private life. Thanks for this, it prepared me a lot for the future!

Ein besonderer Dank geht auch an Herrn Dionysos, dessen regelmäßige Besuche mich an einigen und noch ein paar mehr Feierabenden wieder zur Ruhe gebracht haben.

An dieser Stelle dürfen auch meine lieben Eltern, Marliese und Kurt und mein Hund Moni (und auch Ares, an den ich häufig gedacht habe) nicht fehlen, die mich durch die gesamte Doktorarbeit hindurch unterstützt haben, jeder auf seine Art und Weise.

Zum Ende, wenn auch eigentlich am Anfang, gehört der größte Dank meiner Freundin Karolina. Ohne Dich hätte ich die letzten vier Jahre nicht durchgestanden! Danke das Du mich immer wieder aufgebaut hast, mir in den Hintern getreten hast und vor allem für die unzähligen, unvergesslichen gemeinsamen Abende und Tage in den letzten neun Jahren, die ich zusammen mit Dir verbringen durfte! Diese Arbeit gehört Dir, denn ohne Dich hätte ich es nicht geschafft! In Liebe, Dein Jan.

Erklärung

Ich versichere, dass ich die von mir vorgelegte Dissertation selbständig angefertigt, die benutzten Quellen und Hilfsmittel vollständig angegeben und die Stellen der Arbeit - einschließlich Tabellen, Karten und Abbildungen -, die anderen Werken im Wortlaut oder dem Sinn nach entnommen sind, in jedem Einzelfall als Entlehnung kenntlich gemacht habe; dass diese Dissertation noch keiner anderen Fakultät oder Universität zur Prüfung vorgelegen hat; dass sie - abgesehen von unten angegebenen Teilpublikationen - noch nicht veröffentlicht worden ist sowie, dass ich eine solche Veröffentlichung vor Abschluss des Promotionsverfahrens nicht vornehmen werde. Die Bestimmungen der Promotionsordnung sind mir bekannt. Die von mir vorgelegte Dissertation ist von Frau Dr. Kristen Panfilio betreut worden.

....

(Ort, Datum)   (Jan Seibert)

Lebenslauf

Name:	Jan Seibert
Geburtsdatum und -ort:	25.03.1985, Speyer
Staatsangehörigkeit:	deutsch

Schulische Ausbildung:

1991-1995	Ritter-von-Weingarten-Schule in Weingarten
1995-2004	Friedrich-Magnus-Schwerd-Gymnasium in Speyer
	Abschluss: Allgemeine Hochschulreife im März 2004

Studienverlauf:

2004-2012	Studium der Biosystemtechnik an der Otto-von-Guericke Universität in Magdeburg
	Abschluss: Diplomingenieur im Mai 2012
	Titel der Diplomarbeit: Bestimmung der relativen Expressionsstärke lichtregulierter Gene in Abhängigkeit der Gendosis
seit 2012	Promotion am Institut für Entwicklungsbiologie an der Universität zu Köln, betreut durch Frau Dr. Kristen A. Panfilio
	Titel der Doktorarbeit: Characterizing multiple roles of *pannier* during embryogenesis, as revealed with an augmented fluorescent live imaging toolkit, in the beetle *Tribolium castaneum*

....
(Ort, Datum)

....
(Jan Seibert)